University of Bath

PHD

Unravelling the photochemistry of organometallic N-heterocyclic carbene complexes

Martin, Tom

Award date:
2011

Awarding institution:
University of Bath

Link to publication

Alternative formats
If you require this document in an alternative format, please contact:
openaccess@bath.ac.uk

Copyright of this thesis rests with the author. Access is subject to the above licence, if given. If no licence is specified above, original content in this thesis is licensed under the terms of the Creative Commons Attribution-NonCommercial 4.0 International (CC BY-NC-ND 4.0) Licence (https://creativecommons.org/licenses/by-nc-nd/4.0/). Any third-party copyright material present remains the property of its respective owner(s) and is licensed under its existing terms.

Take down policy
If you consider content within Bath's Research Portal to be in breach of UK law, please contact: openaccess@bath.ac.uk with the details. Your claim will be investigated and, where appropriate, the item will be removed from public view as soon as possible.

Download date: 05. May. 2023

Unravelling the photochemistry of organometallic *N*-heterocyclic carbene complexes

Thomas Antony Martin

A thesis submitted in partial fulfilment of the requirements for the degree of

Doctor of Philosophy

UNIVERSITY OF BATH

University of Bath

Department of Chemistry

September 2011

Attention is drawn to the fact that copyright of this thesis rests with the author. This copy of the thesis has been supplied on condition that anyone who consults it is understood to recognise that its copyright rests with its author and that no quotation from the thesis and no information derived from it may be published without the prior written consent of the author.

This thesis may be made available for consultation within the University Library and may be photocopied or lent to other libraries for the purposes of consultation.

Acknowledgements

Firstly, I would like to thank Dr. Michael ‘Gepetto’ Whittlesey for his unending support throughout my PhD. I’m sure there were many times it seemed elastic bands alone wouldn’t hold it all together anymore, but nonetheless we made it through and I certainly couldn’t have done it without Mike’s guidance. Thank you! I would also like to thank my collaborators at the University of Nottingham, particularly Madeeha Batool, who was always on the end of the phone and a real trooper throughout the project.

There are so many people at the University of Bath who made my time there both enjoyable and fruitful. Those who suffered through my ‘ideas’ deserve special mention, including Dr. Simon Brayshaw, Dr. Mark Warren and Tom Pugh. It was very helpful to have so many knowledgeable and enthusiastic people to discuss chemistry with.

Many thanks to Dr. John Lowe and Dr. Mary Mahon, John ‘the magnet’ for having saintly patience and the knack for making the most complex of NMR experiments seem like a walk in the park and Mary for her most excellent banter and for not kicking me off the course for photoshopping her face into an [insert brand name here] coffee advert and leaving it at the front of the lecture theatre! Oh, and the odd crystal structure too I guess…

To all the members of the Whittlesey group, past and present, it has been a real pleasure working with you all, although perhaps the best part were the times spent outside the lab and in close proximity to the local drinking establishments… Good times!

Last, but certainly not least, I would like to thank my family for all their enthusiasm and Charlotte for everything! Being there for me throughout the thesis, inspiring me to keep going through the hard times, whilst also making the easier parts much more fun! I don’t know how you’ve put up with me over all these years, but I’m so very glad you have!

Foreword

This thesis is a result of the EPSRC funded grant 'Unravelling the photochemistry of organometallic *N*-heterocyclic carbene complexes' (EP/F003285/1) 2007-2011. The grant was awarded as a joint project between the University of Bath (Dr. Michael K. Whittlesey) and the University of Nottingham (Prof. Michael W. George).

Synthesis, characterisation and analysis were carried out by Tom Martin at the University of Bath. Time-resolved infrared and UV/Vis absorption and emission experiments on compounds **5** and **6** were carried out at the University of Nottingham by Madeeha Batool and Tom Martin during collaborative visits. However, the majority of the time-resolved infrared spectroscopy, UV/Vis absorption and emission experiments (compounds **1**-**4** and **9**-**10**) were carried out at the University of Nottingham by Madeeha Batool.

Abstract

This thesis describes the synthesis, characterisation and reactivity of new manganese and rhenium(I) NHC complexes, which have been investigated both thermally and photochemically and the results contrasted with existing phosphine analogues in the literature.

Cp'$Mn(CO)_2$(NHC) (NHC = IEt_2Me_2 **1**, IMes **2**, $I^iPr_2Me_2$ **3** and IPr **4**) were synthesised and investigated by TRIR spectroscopy. Loss of CO was observed after 355 nm irradiation to form agostically stabilised intermediates, which reformed the parent species by recombination with CO on the nanosecond timescale. Loss of NHC was not observed, in contrast to Cp'$Mn(CO)_2(PPh_3)$ which lost both CO and PPh_3 upon photolysis.

$[Re(NHC)(Bpy)(CO)_3]BAr_4^F$ (NHC = IEt_2Me_2 **5**, IMes **6**) were synthesised and investigated by TRIR spectroscopy and UV/Vis absorption and emission spectrometry. Inclusion of an NHC altered the excited state manifold of the complexes, favouring population of the ^{3}MLCT over the ^{3}IL excited state. The lowest energy excited state for both **5** and **6** proved to be a ^{3}MLCT excited state at 298 and 77 K. In contrast, $[Re(PPh_3)(Bpy)(CO)_3]BAr_4^F$ exhibited ^{3}MLCT at 298 K, but ^{3}IL at 77 K.

A series of complexes, $M(NHC)(CO)_4X$ and $M(NHC)_2(CO)_3X$ (M = Re, X = Cl; M = Mn, X = Br) formed upon reaction of the corresponding $M(CO)_5X$ species and free NHC. The substitution pattern was dictated by the steric bulk of the NHC. Generation of the corresponding cations by halide abstraction was investigated. $M(NHC)_2(CO)_3X$ was found to form agostic stabilised species upon halide abstraction by $NaBAr_4^F$ in CH_2Cl_2. Under the same conditions, $Re(IPr)(CO)_4Cl$ was found to form the dichloromethane complex, $[Re(IPr)(CO)_4(\eta^1\text{-}CH_2Cl_2)]BAr_4^F$. In C_6H_5F solution under an atmosphere of dihydrogen, the CH_2Cl_2 ligand could be displaced by H_2 to form the dihydrogen species, $[Re(IPr)(CO)_4(H_2)]BAr_4^F$.

Contents

Abbreviations

Spectroscopic

TRIR	Time-resolved infrared spectroscopy
FTIR	Fourier transform infrared spectroscopy
UV/Vis	Ultraviolet and/or visible
NMR	Nuclear magnetic resonance
δ	NMR chemical shift
$^{n}J_{YZ}$	Coupling constant of Y to Z through n bonds
HMQC	Heteronuclear multiple quantum coherence
HMBC	Heteronuclear multiple bond correlation
NOESY	Nuclear overhauser effect spectroscopy
COSY	Correlation spectroscopy
V.T.	Variable temperature
s	Singlet
d	Doublet
t	Triplet
q	Quartet
sept	Septet
m	Multiplet
br	Broad
IR	Infrared
$\nu_{(L)}$	IR shift of ligand L

Units

h	Hour
min	Minute
s	Second
K	Kelvin
°	Degree
ppm	Parts per million
MHz	Megahertz
cm^{-1}	Wavenumber
Å	Angstrom

nm	Nanometre
g	Gram
mg	Milligram
mL	Millilitre
M	Mole per decimetre
mol	Mole
mmol	Millimol

Chemical

NHC	*N*-heterocyclic carbene
M	Metal
L	Ligand
μ-L	Bridging ligand
η^n-L	Ligand hapticity (of number, n)
X	Halide or heteroatom
R	Alkyl or aryl group
Ar	Aryl
Me	Methyl
Et	Ethyl
^{i}Pr	Isopropyl
^{t}Bu	*tert*-Butyl
Mes	Mesityl (2,4,6-trimethylphenyl)
Ph	Phenyl
i-	*Ipso*
o-	*Ortho*
m-	*Meta*
p-	*Para*
THF	Tetrahydrofuran
DCE	Dichloroethane
ODB	*o*-dichlorobenzene
IEt_2Me_2	1,3-diethyl-4,5-dimethyl-imidazol-2-ylidene
$I^iPr_2Me_2$	1,3-diisopropyl-4,5-dimethyl-imidazol-2-ylidene
I^iPr_2	1,3-*bis*(isopropyl)imidazol-2-ylidene
IPr	1,3-*bis*(2,6-diisopropylphenyl)imidazol-2-ylidene

IMes	1,3-*bis*(2,4,6-trimethylphenyl)imidazol-2-ylidene
IMe_4	1,3-dimethyl-4,5-dimethylimidazol-2-ylidene
SIH	Imidazolidin-2-ylidene
$NaBAr_4^F$	$[Na][B(3,5\text{-}(CF_3)_2C_6H_3)_4]$
DPPP	1,3-bis(diphenylphosphino)propane
AgOTf	Silver triflate
Dppz	dipyrido[3,2-a:2',3'-c]phenazine
Bpy	2,2-bipyridine
COD	*cis*-cyclooctadiene

Chapter 1 - General Introduction

1.1 *N*-Heterocyclic carbenes (NHCs) and phosphines in transition metal complexes.

The use of tertiary phosphines, often with bulky R groups, to stabilise transition metal complexes has been ubiquitous within organometallic chemistry for many years. This has led to a rich and diverse assortment of M-PR_3 complexes which have been phenomenally valuable in homogeneous catalysis and other areas. In recent years, primarily since the isolation of a stable free NHC by Arduengo in 1991, there has been a huge amount of research into the use of *N*-heterocyclic carbenes (NHCs) as replacements for phosphine ligands.[1] The reasons for this are numerous and shall be discussed here. A generalised NHC is compared to a phosphine in Figure 1, which also describes nomenclature for NHCs.

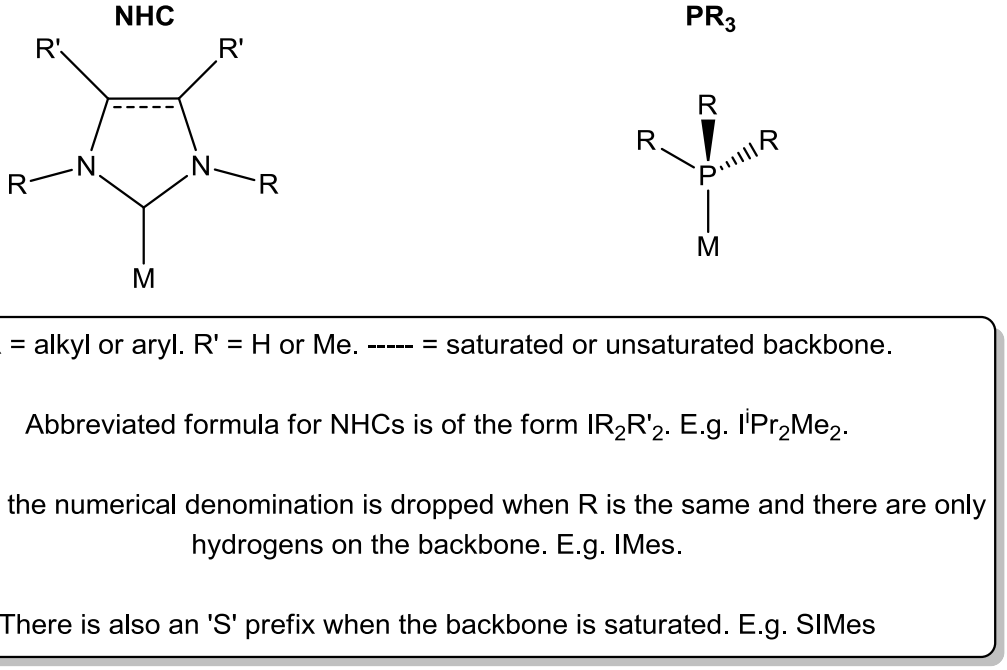

Figure 1: Illustration of an NHC vs. tertiary phosphine ligand binding to a metal.

NHCs are nucleophilic singlet carbenes stabilised by nitrogen atoms in the 1 and 3 positions of the ring. Although metal-carbenes are normally synonymous with high reactivity, in comparison, the chemistry of organometallic NHC complexes is much more subtle. In fact, NHCs are often thought of as spectator ligands, drawing their first similarity to phosphines. NHCs have been used as replacements to phosphines in a large number of modern homogeneous catalysis applications and this interest in NHC chemistry has led to some becoming commercially available reagents.[2] The M-L bond for NHCs is more thermally stable than phosphines, yet both have been shown to be excellent σ-donors with limited π-acceptor ability, although NHCs have proven to be much more donating then even the most basic phosphines.[3] Consequently, NHCs readily form bonds to transition metals in high or low oxidations states and even main group elements such as beryllium, sulphur and iodine.

NHCs can often increase the reactivity and stability of the metal complexes produced when compared to the phosphine analogues, which has proven highly beneficial in catalytic systems. For example, 2nd generation Grubbs catalysts, used for alkene metathesis, demonstrate a much higher activity and stability than their 1st generation predecessors (Figure 2).

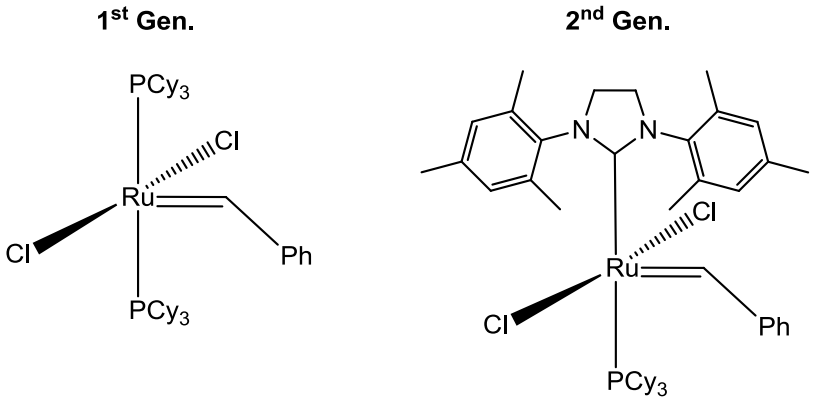

Figure 2: 1st *vs.* 2nd Generation Grubbs catalysts for alkene metathesis.

The reasons for NHCs improving catalysts are not necessarily generic, yet closer examination of the example from Grubbs is enlightening. Firstly, in order for either catalyst to partake in the alkene metathesis cycle it must first lose a

ligand to create a vacant site. It was initially assumed that the strong *trans* effect of the NHC means the PCy_3 is lost more easily in the 2nd generation than the 1st generation catalyst, which in turn led to higher reactivity with olefin substrates. However, detailed mechanistic studies confirmed that the rate of formation of the 14 e^- species for the NHC systems was actually 10^2 times slower than the phosphine counterpart.[4] The increase in rate of reaction for the NHC systems was in fact due to their greater reactivity towards the π acidic olefin substrates relative to other σ-donors in the reaction.[5] With respect to the increased stability of the NHC systems, the greater strength of the M-NHC bond means it is much less likely to dissociate, this helps to maintain the integrity of the catalyst by resisting further dissociation reactions and subsequent degradation.

The steric profiles of phosphines and NHCs can both be tuned systematically, by careful selection of the R groups used, to produce gradual trends in steric demand from both classes of ligand. However, due to the inherent differences in geometry, the steric profiles of phosphines and NHCs differ significantly.[6] It has long been realised that profiling the steric requirements of phosphines, is key to understanding the chemistry of the metal complexes formed, a principle which is likely to equally apply to NHCs. The Tolman cone angle is a concept that deals with this requirement for phosphines.[7] It is best described as the angle defined by the outer edge of the substituents at phosphorus and the metal centre of a space-filling model (Figure 3(b)).

In the case of NHCs it is worth noting that instead of the R groups pointing away from the metal centre they are in fact pointing towards it. However, in many cases these R groups can be arranged perpendicular to the plane of the ring, thus alleviating unfavourable steric interactions with the metal centre.

One of the consequences of the inherent geometrical differences between NHCs and phosphines is that the concept of Tolman cone angle cannot easily be applied to the former, which has led to the development of a new model based on the 'wingspan' of the ligand. This model looks at the wingspan angle, running from the closest carbon substituents on the NHC to the metal centre with a fixed M-C distance of 2 Å. A sphere of radius 3 Å is then centred on the

metal, allowing the volume of the sphere occupied by the NHC ligand to be determined (Figure 3(a)). This is then expressed as a percentage of the sphere, which is known as the buried volume of the NHC concerned. This model has been shown to be effective in predicting trends in bond dissociation energies for the M-C bond in nickel carbonyl NHC complexes.[3] The buried volume model can also be applied to phosphines, allowing direct comparison between the steric profiles of phosphines and NHCs.[8]

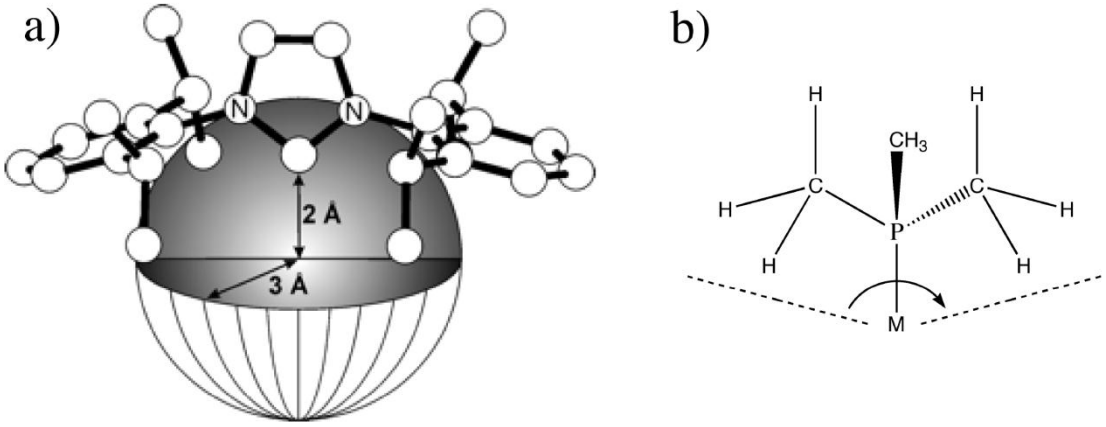

Figure 3: Illustration of a) Buried volume model for NHCs and b) Tolman cone angle for phosphines.

Unlike phosphines NHCs also exhibit several unusual coordination modes with late transition metal centres. The novel effects observed thus far in these complexes range from abnormal C-5(4) binding to agostic stabilisation or oxidative addition *via* C-H bond activation of aryl and alkyl side-arm substituents (Figure 4).[9,10]

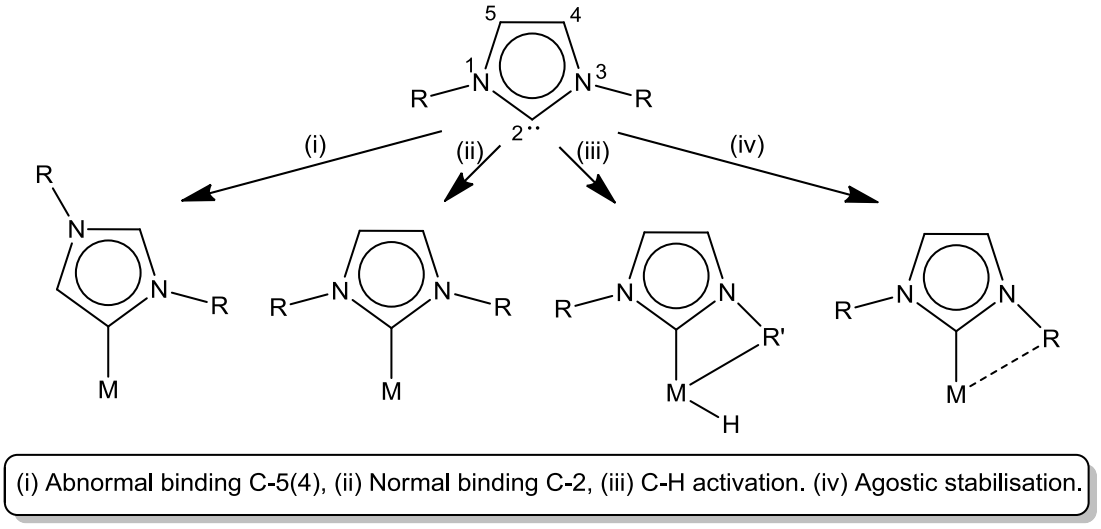

Figure 4: Illustration of different binding modes of NHC ligands to metal centres.

During the infancy of organometallic *N*-heterocyclic carbene (NHC) chemistry it was often postulated that NHCs were simply 'phosphine mimics'. This idea has come under increasing scrutiny, as alluded to above, largely due to increasing numbers of research papers describing stoichiometric and catalytic reactions of organometallic NHC complexes, many of which indicate a more complex and subtle chemistry than was previously imagined. There remain many researchers interested in this area and it seems certain that a greater understanding of the nuances of organometallic NHC complexes and the similarities to phosphines will become clear with time. However, to date the vast majority of studies are all focussed on thermal processes. It has been proposed that NHCs could exhibit interactions between the filled π and empty π^* orbitals of the heterocyclic ring with the metal d-orbitals, whereby, depending on the electron density of the metal centre, electrons are either donated ($\pi \rightarrow$ d) or accepted (d $\rightarrow \pi^*$) by the NHC ligand.[11] However, in light of such suggestions, it remains widely accepted that even in the most extreme cases NHCs have very limited π accepting or donating ability, and for thermal chemistry, the contribution to M-L bonding is generally insignificant. With respect to the photochemistry of NHCs, this π interaction can become a much more important factor.

The photochemistry of NHC complexes is implicitly hugely dependant on the symmetry and energy levels of the metal and ligand orbitals involved. Excitation

of electrons into higher energy orbitals can populate anti-bonding orbitals such as the empty π^* localised on the NHC (d → π^* Metal to Ligand Charge Transfer (MLCT)) or induce electron transfer from the NHC to the metal (π → d, Ligand to Metal Charge Transfer (LMCT)). By choosing suitable metals, Ni(0) (electron rich, full d-orbital) and Ti(IV) (electron poor, empty d-orbital), both MLCT (Ni(0)) and LMCT (Ti(IV)) functions have recently been confirmed in work by Vogler and Kunkely.[12] There are in fact a myriad of possibilities, even when considering only ligand centred transitions, π → π^*, σ → σ^* and σ → π^* (Intraligand (IL)). Exactly how coordination of NHCs to different transition metal centres will impact on photochemical processes has not been determined to any significant extent yet. This seems quite surprising when considering the parallels drawn between phosphines and NHCs in other parts of the literature and the rich photochemistry associated with phosphine stabilised metal dihydride, carbonyl and alkene complexes.[13,14,15,16]

There are a few papers addressing photochemical behaviour of organometallic NHC complexes. Xue *et al* reported synthesis, characterisation and photochemical behaviour of rhenium (I) NHC complexes with various diimine ligands attached ([Re(SIH)(diimine)$(CO)_3$][ClO_4] diimine = see Figure 5).[17] In this instance, the NHCs acted more as spectator ligands, with molecular orbital calculations determining only minor character present in the frontier orbitals. The HOMO of the complex was shown to be predominantly non-bonding d(Re) in nature and the LUMO mainly π*(diimine) with partial p_z(NHC) character. The photophysics of these species remained relatively unchanged from the phosphine substituted analogues with excitation chiefly d(Re) → π*(diimine) in nature and emission from ^{3}MLCT.

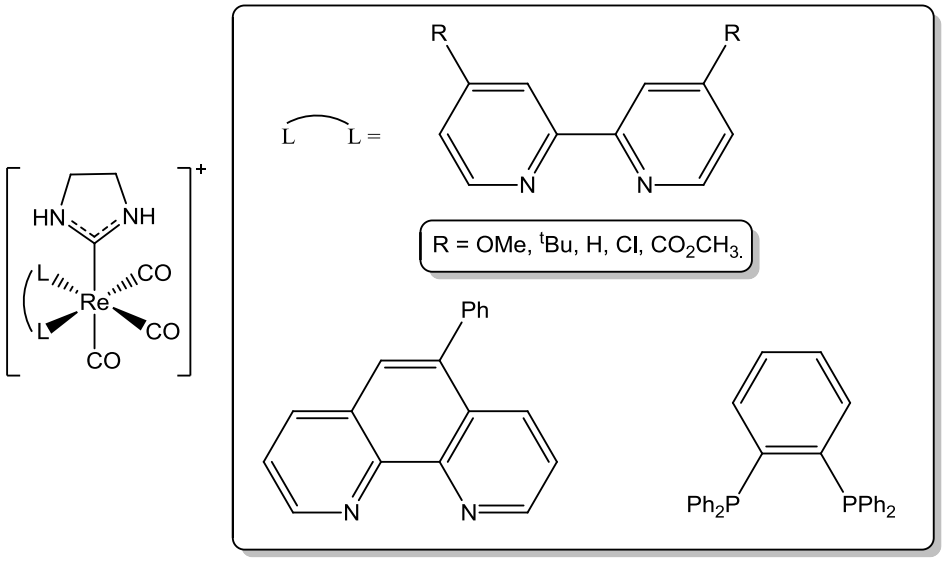

Figure 5: A schematic of the complexes synthesised and analysed by Xue *et al*.

A further study by Kunkely and Vogler, which investigated the excited state properties of $[Pd(NHC)(quinone)]_2$ (NHC = IMes, quinone = 1,4-naphthoquinone), detected two absorptions at 312 and 399 nm.[18] These were assigned to LLCT (NHC → quinone) and MLCT (d(Pd) → quinone) transitions respectively, providing another example of NHCs playing a more direct role in organometallic photochemistry. The MLCT state was unreactive, although emission at 564 nm was detected at 77 K. At room temperature the compound degrades under photolysis *via* photoredox decomposition which is initiated from the LLCT state.

One of the first reports of organometallic NHC photochemistry was published by the Whittlesey group and demonstrated that M-NHCs exhibit photochemistry which can be significantly different to that of the analogous phosphine systems.[19] Steady state irradiation (λ >285 nm) of $Ru(IEt_2Me_2)(PPh_3)_2(CO)(H)_2$ **(a)** at 223 K in d_8-toluene resulted in loss of either H_2 or PPh_3 and isomerisation of the 16 e^- fragments, which upon quenching with either H_2 or PPh_3 yielded the photoisomers **(b)**, **(c)** and a C-H activation product **(d)** (Figure 6).

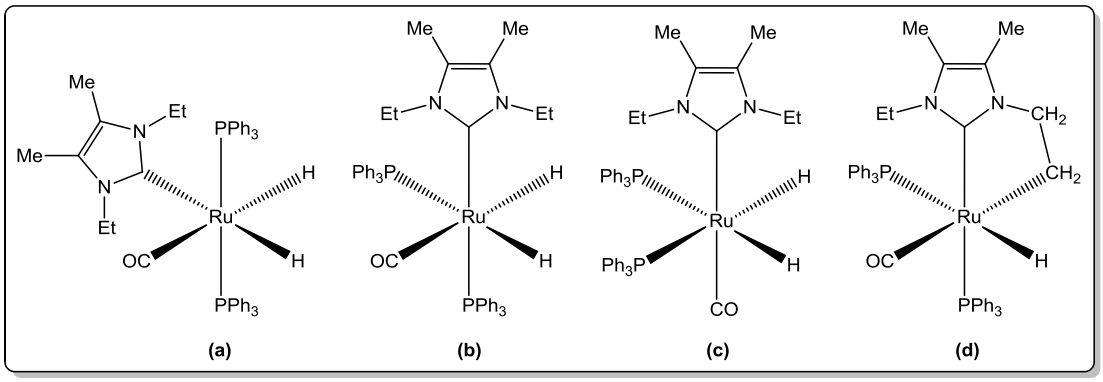

Figure 6: $Ru(IEt_2Me_2)(PPh_3)_2(CO)(H)_2$ (a) and associated photoproducts (b), (c) and (d).

This is markedly different to the results observed for $Ru(PPh_3)_3(CO)(H)_2$ which dissociates only H_2 upon irradiation before decomposing to form what are believed to be dimeric species.[20,21]

There are some more recent publications concerning organometallic NHC photochemistry involving advanced computational modelling, efficient blue emitting Iridium complexes suitable for use in OLEDs and even photoprecursors for catalytic applications.[22,23,24,25,26] However, the area remains relatively unexplored. The aim of this work is to synthesise simple NHC analogues of known photoactive organometallic phosphine systems to allow fundamental photochemical investigation. The chosen area for this research is manganese and rhenium (I) carbonyl complexes and derivatives. This is for several reasons, the d^6 configuration of the metal centres exhibit a number of interesting photochemical and photophysical properties and have been extensively characterised in the literature, often including phosphine derivatives. There are also relatively few manganese and rhenium NHC complexes in the literature, particularly those in low oxidation states.[27]

1.2 Photochemistry of transition metal carbonyls.

Some of the earliest reports of photochemical investigations into organotransition metal compounds involved metal carbonyls, as very early on it was observed that the substitution reactions of the CO ligand were often

accelerated in the presence of sunlight.[28] There have since been various other photoreactions of organometallic carbonyl compounds identified, most have involved either monomeric (e.g. $Cr(CO)_6$), dimeric (e.g. $Re_2(CO)_{10}$) or multimetallic cluster (e.g. $Ru_3(CO)_{12}$) carbonyl complexes, all of which are quite distinct in their reactivity.[29] More current research in this area has been focussed heavily on understanding the different types of photoreactions involved in order to achieve selective synthesis of new and novel compounds. The aim of such research feeds into homogeneous catalyst design; it would be of great benefit to be able to photolytically generate unsaturated and very reactive transient species, which could then function as *in situ* homogeneous catalysts. It is hoped that research in this vein could help to discover useful photocatalytic systems, which would have a number of benefits. For example, once generated, transient species could potentially undergo a large number of turnovers before the parent compound is regenerated. Such a process would be very energy efficient by yielding large amounts of product per photon absorbed by the system.[28]

The photochemistry of monomeric carbonyl compounds is relatively simple, which means they are ideal candidates for a fundamental study of their NHC substituted derivatives. The general photochemical reaction of such systems is ejection of a carbonyl group, which can be substituted for another ligand or induce aggregation of the monomeric carbonyls into dimeric or even higher nuclearity carbonyl clusters. A classic example of this behaviour is illustrated by the reactions of $Fe(CO)_5$. Upon irradiation, dissociation of a CO molecule occurs, $Fe(CO)_5 \rightarrow Fe(CO)_4 + CO$. The reactive fragment produced can then either react with a ligand, e.g. PPh_3 to form $Fe(CO)_3(PPh_3)_2$ by a further CO substitution, or with the parent compound to make $Fe_2(CO)_9$.[30,31] There are key differences between the photochemistry of substituted metal carbonyls and simple binary metal carbonyls. The former present additional pathways for photoactivity, for example, it must be considered whether dissociation is likely to occur at the carbonyl ligand or the substituted ligand. Further to this, when dissociation still occurs at the carbonyl ligand, the substitution can cause inequivalence of the remaining carbonyls, and therefore the selectivity of the photoreactions can also be affected.

Tertiary phosphines form stable complexes with metal carbonyls, as their increased electron donation enhances the π-back bonding to the remaining carbonyls, strengthening the M-CO bonds. Complexes of this type are less studied than might be expected, as phosphines do not have any major structural or electronic features that are likely to result in localisation of any excited states produced by photolysis. However, phosphine dissociation can be induced photochemically to produce reactive species. The wide scope of steric and electronic variation makes phosphines an ideal class of ligands for subtly modifying the chemical reactivity of either an initial photoproduct or the photolytic dissociation step itself.

An example of the chemical control exerted by phosphine substitution of metal carbonyls is shown by contrasting the photochemistry of $Mn_2(CO)_{10}$ and $Mn_2(CO)_8(PR_3)_2$ (PR_3 = PMe_3, P(*n*-Bu)$_3$ and P(^{i}Pr)$_3$) when reacting with Sn-H and Si-H bonds. In all cases photolysis results in CO loss and oxidative addition of a Sn-H / Si-H bond.[32,33,34] However, the rate of oxidative addition decreases as the steric requirements of the phosphine increases. Similarly the excited state properties of Re(I) complexes ($ReX(CO)_4(L)$, X = halogen L = CO, PPh_3, piperidine) can be tuned depending on the nature of the ligand L.[35]

1.3 Manganese and rhenium(I) carbonyl photochemistry.

The first half of this thesis covers the synthesis, characterisation and photochemistry of Cp'$Mn(CO)_2$(NHC) (Chapter 2) and [Re(NHC)(diimine)$(CO)_3$]BAr_4^F complexes (Chapter 3).

1.3.1 Photochemistry and photophysics of rhenium(I) diimine carbonyl complexes.

The photochemistry of rhenium is incredibly diverse and as such is one of the most investigated of the transition elements. Photoactive compounds have been studied across all eight oxidation states of rhenium, from Re(0) to Re(VII), and

their reactivity differs greatly. Bis and tricarbonyl complexes of rhenium(I) containing diimine or polypyridine donor ligands remain an area of great interest. The reasons for this are numerous. Metals with d^6 electronic configuration have demonstrated a multitude of photochemical and photophysical reactions that are rare in transition metal chemistry. The tricarbonyl Re(I) diimine systems are typically very stable and ultimately produce long-lived, emissive ^{3}MLCT excited states upon irradiation. Such triplet excited states are solvatochromic, exhibiting high sensitivity to their environment. This high sensitivity combined with the long life-times and stability of the Re(I) diimine tricarbonyl systems makes them ideal candidates for organometallic photosensors or probes. Studies have also shown that by reaction with a suitable electron source the ^{3}MLCT excited state can be reduced to form the anionic and highly reducing 'one-electron reduced' species, which has been harnessed in the photocatalytic reduction of CO_2 to CO.[36] Cyclic voltammetry (CV) of the parent Re(I) diimine complexes shows formation of very stable radicals at reducing potentials, which reversibly reform the parent when the potential is increased, indicating similar species to those observed from photolysis.[37] The budding applications of Re(I) diimine tricarbonyl complexes, which display a breadth of photo- and electrochemical reactivity, are as widespread as DNA probing/cleavage, sensors, light emitting diodes, dye-sensitised solar cells, electron-hole transport and photo- or electrocatalytic reduction of CO_2.

When under irradiation diimine ligands like 2,2-bipyridine absorb high energy UV light which causes intraligand ($\pi \rightarrow \pi^*$) excitation within the molecule and can lead to emission. However, once ligated to a metal centre, the relative energies of the orbital manifold and thus the photochemistry of the system can completely change. In Re(I) diimine tricarbonyl complexes, the MLCT absorption band tends to lie at slightly lower energy on the shoulder of the $\pi \rightarrow \pi^*$ intraligand transition. This can lead to population of both the ^{1}MLCT and ^{1}IL states upon excitation. These excited states then undergo non-radiative decay to their respective triplet states, either ^{3}MLCT or ^{3}IL, before radiative decay back to the ground state. As such, emission spectra are often observed around 500 nm with strong vibronic coupling when the contribution from the ^{3}IL state is

large, or around 600 nm exhibiting the broad, structure-less pattern typical of decay from a ^{3}MLCT state.

Coordination of the diimine to the metal centre changes both absorption and emission to higher wavelengths than the free ligand. Often a combination of ^{3}MLCT and ^{3}IL character is required to explain the emission behaviour of Re(I) diimine tricarbonyl species as there are many factors that affect the relative energies of these excited states and their subsequent population.[38] For example, electron density at the metal centre, degree of conjugation in the diimine and electron donating or withdrawing nature of the diimine, can all subtly shift the energies of the orbitals in these structures. Their emission behaviour is also temperature dependent. At very low temperatures, 77 K in a frozen solvent/glass matrix, the energy of the ^{3}MLCT state can rise above that of the ^{3}IL state for some systems, leading to intraligand emission dominating the spectra observed.[39]

Computational modelling of Re(I) diimine tricarbonyls have recently shed further light on the photophysical processes involved in the excitation of these complexes using density functional theory (DFT) and time-dependent density functional theory (TDDFT).[40] The orbital manifolds for $Re(Bpy)(CO)_3Cl$ and $[Re(Bpy)(CO)_3(Py)]^+$ were computed. In both cases, the highest occupied molecular orbital (HOMO) was shown to contain 50% or greater Re d-orbital character, with ca. 20% contribution from both CO and Cl for $Re(Bpy)(CO)_3Cl$, and ca. 20% CO character for $[Re(Bpy)(CO)_3(Py)]^+$. The lowest unoccupied molecular orbital (LUMO) was shown to be comprised of >80% π^* character and localised almost solely on the diimine ligand.[41] This has led to a refinement of the previously proposed mechanism, indicating that the initial transition is in fact better described as metal-ligand to ligand charge transfer (MLLCT) in nature (Figure 7).

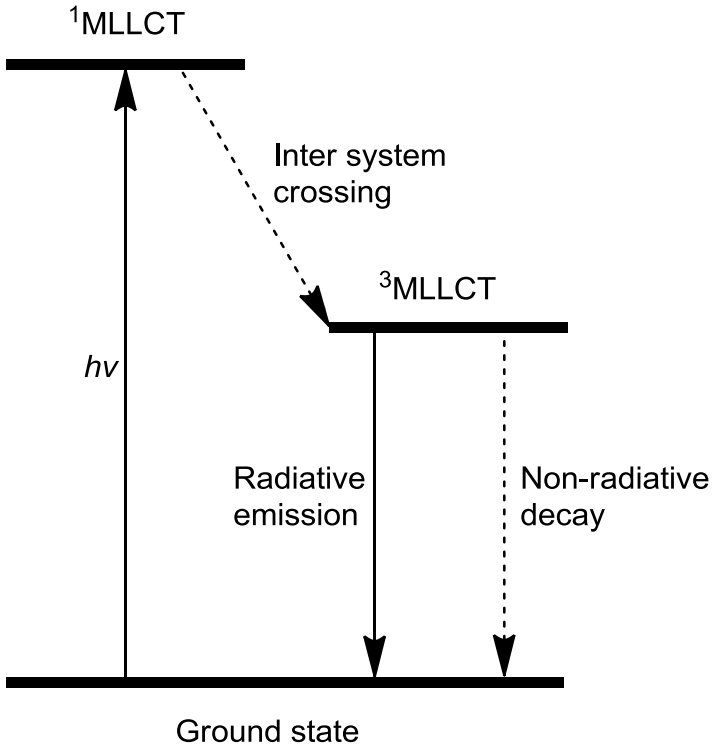

Figure 7: Jablonski energy diagram depicting MLLCT excitation in Re(I) diimine complexes.

Quite recently it was shown that the ^{3}MLCT excited state for Re(I) diimine tricarbonyls is not always photostable. Whilst the ^{3}MLCT excited states present in complexes with weak field ligands like chloride and pyridine remain relatively stable to prolonged irradiation of the ^{3}MLCT state, efficient photosubstitution is observed for a variety of $[Re(BpyX_2)(CO)_3(PR_3)]^+$ compounds yielding CO loss trans to PR_3 ($BpyX_2$ = 4,4'-X_2-2,2'-Bpy; X = H, CF_3, OEt or Ph; PR_3 = various phosphines or phosphites).[42]

The *cis* dicarbonyl species produced by the substitution process react with a variety of ligands such as, chloride, pyridine, acetonitrile and phosphines or phosphites, with isolated yields from ca. 50-95%. The mechanism for this photosubstitution reaction was examined in a later study.[43] A range of PR_3 compounds were photolysed in acetonitrile to yield the solvated complexes. The temperature dependence of these species' emission yields and lifetimes was interpreted as evidence for thermal transition from the ^{3}MLLCT state to a dissociative ligand field (^{3}LF) state (Figure 8).

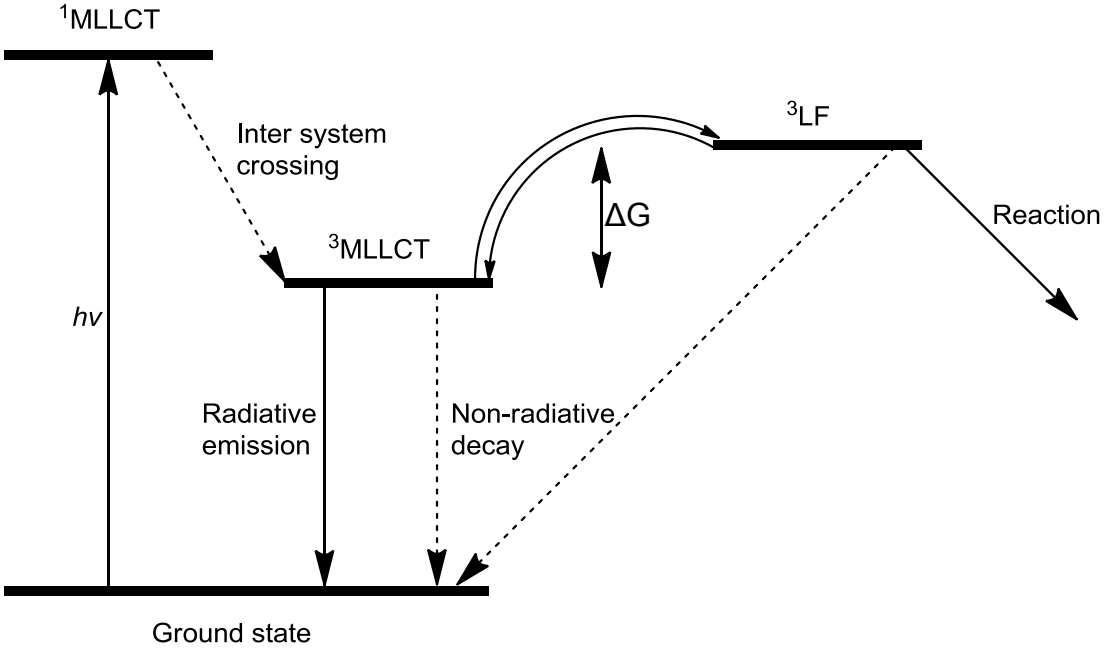

Figure 8: Jablonski energy diagram depicting ^{3}MLLCT excitation leading to thermal population of dissociative ^{3}LF states in Re(I) diimine complexes.

Labelling studies using ^{13}CO confirmed that the CO *trans* to PR_3 was indeed labilised.[43] The results obtained were consistent with a dissociative mechanism and an associated enhancement of the *trans* effect for the PR_3 ligand in the excited state. However, in the case of $Re(Bpy)(CO)_3Cl$, $[Re(Bpy)(CO)_3(Py)]^+$ and other weak field ligand species, it is proposed that their apparent stability to this substitution mechanism is not due to a larger thermal barrier for the ^{3}MLCT to ^{3}LF conversion, but a reduced kinetic trans effect from the weak field ligands.

Inclusion of phosphines or phosphites into Re(I) diimine tricarbonyls also subtly changes the system's photophysics. The emission and absorption energies in these systems shift slightly depending on the nature of the phosphine or phosphite used. This has been used to create species with different coloured emissions and even favour certain emissive excited states over others in some diimine systems (e.g. moving ^{3}MLCT to lower energy than ^{3}IL).[44,45] These principles have been harnessed successfully in a number of the areas of application for these compounds. For example, different coloured LEDs for electronic purposes, light harvesting dyes that absorb at different wavelengths,

DNA probes which favour ^{3}MLCT emission and formation of, to date, the most efficient photocatalyst for reduction of CO_2 to CO.[46,47,48] However, there remains a lot of room for improvement in all of these systems and the applications for the photo- and electrochemical properties of Re(I) diimine tricarbonyls continues to grow.

1.3.2 Alkane and small molecule coordination.

C-H activation of alkanes by metal complexes is immensely interesting from an academic perspective and potentially world changing from an industrial and economic perspective. If it can be achieved both catalytically and selectively, then many new processes could be developed to aid conversion of one of the most abundant and environmentally damaging waste materials, methane, into the next generation of chemical feedstocks. However, coordinating and breaking the very inert and strong bonds found in alkanes is non-trivial, particularly when selectivity and catalytic activity are required. One of the areas of research aimed at further understanding C-H activation reactions is alkane complexation. There is a lot of interest in researching the σ-complexation of alkanes to metal centres as they are often proposed as intermediates in C-H activation reactions.[49] Many compounds have been prepared which show different extents of σ-complexation, which demonstrate the course of a reaction from σ-complexation to true oxidative addition. This is best exemplified by studying the heavier homologues, silanes. There are now many examples of the activation of Si-H σ bonds by transition metal centres.[50,51,52] These investigations have shown that the bonding in silane σ-complexes corresponds to the later stages of oxidative addition to the metal centre. The ^{1}H NMR coupling constants and elongation of σ(Si-H) interatomic distances provide a good measure of the extent of oxidative addition in the complexes involved. These results indicate a pathway proceeding from σ-complexation through to oxidative addition (Figure 9).

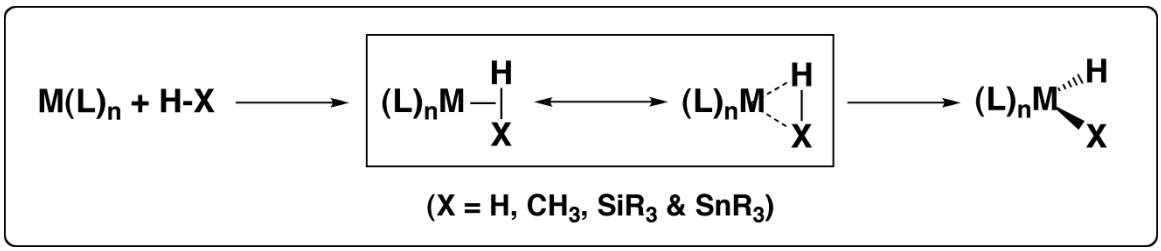

Figure 9: General reaction scheme for the reaction of a σ-coordinating ligand with a transition metal centre proceeding through complexation to oxidative addition.

There are far fewer complexes that can activate alkanes yet also have detectable σ-alkane complex intermediates, none of which have been fully characterised at every stage of the reaction. This is mainly due to the relatively low M-(alkane) bond strengths encountered (25-70 kJ mol^{-1}), which means they are typically very short lived transient species with low thermal stability.[53,54] Currently, the only room temperature stable complexes with σ-alkane complexation are structures with agostic interactions, where the chelate effect imparts enhanced stability to the compound. One of the main goals of research in this area is to produce an alkane σ-complex that is stable at room temperature, allowing this important intermediate to be subjected to routine characterisation techniques. This has been approached by trying to modify the steric and electronic properties of carbonyl metal centres by thermal or photochemical substitution of CO for new ligands, such as PR_3, pyridines, halides, hydrides, alkyls, nitrosyl and diimines. This has proven successful in many ways with a wide variety of new alkane complexes being discovered. Of particular note is $CpRe(CO)_2(PF_3)$, which loses CO upon photolysis and forms an alkane complex with cyclopentane that has the longest lifetime observed to date. In fact, the complex is so stable that at low temperatures it exists long enough for NMR studies.[55]

Unsurprisingly, the interaction of some of the highly reactive photogenerated species, discussed above with alkanes and silanes, is also mirrored by their reaction with many small molecules, such as H_2, N_2 and CO_2. A good example of this is the photolysis of $Cp'Mn(CO)_3$ (Cp' = C_5H_4Me), which under pressures of N_2 or H_2 undergoes CO loss with formation of the corresponding dinitrogen

and dihydrogen complexes.[56,57] Similarly, photolysis in super critical CO_2 leads to the formation of Cp'Mn$(CO)_2(CO_2)$.[58] Typically, the compounds formed with small molecules are much more stable than the corresponding alkane complexes, although for Cp'Mn$(CO)_3$ the photolysis products are frequently detected with spectroscopic techniques as they are often difficult to isolate. There remain many characterised H_2, N_2 and CO_2 compounds in the literature.[59,60,61]

As well as the academic interest in investigating and characterising challenging or unusual intermediates, there has been a lot of research trying to harness transition metal complexes that can interact with and activate small molecules for a variety of economic and environmental reasons. These include CO_2 sequestration, photocatalytic CO_2 reduction, catalytic activation and functionalisation of methane or other alkanes.[62,63,64,65] In order to work towards these applications, much more must be learnt about the nature of small molecule activation at transition metal centres.

The formation of a vacant site is a prerequisite for almost all catalytic processes. This is usually obtained by ligand dissociation from a saturated metal centre, which is induced either thermally or photochemically. Considering the increasing importance of transition metal NHC compounds in modern homogeneous catalysis, a fundamental study of their photochemistry is crucial if such species are to be utilised successfully as photocatalysts in the future.

TRIR studies show that photolysis of Cp'Mn$(CO)_3$ in heptane or cyclopentane at room temperature results in photolytic loss of CO and formation of the corresponding alkane complexes, Cp'Mn$(CO)_2$(alkane).[66] The lifetimes of the alkane complexes are very short at room temperature and have been best observed using laser induced photo dissociation coupled with TRIR spectroscopy. TRIR is the primary technique used to investigate the photochemistry of the new NHC species produced for this study. It has proven to be a hugely powerful technique for examining short lived photo-generated species, and is often ideally suited to the study of organometallic complexes. Typically, the cyclopentadienyl ligand is an ideal spectator ligand and does not

become involved in reactions. Under UV irradiation, CO loss is observed and the transient metal carbonyl fragments produced are highly reactive. Photogenerated species such as [Cp'Mn$(CO)_2$] and [CpRe$(CO)_2$] have been shown to induce bond activation reactions or coordinate solvent molecules as diverse as alkyl bromides, methanol, CF_2Cl_2 and even non-polar solvents like cyclohexane and noble gases.[67,68,69,70,71,72]

Photochemical CO loss from the parent cyclopentadienyl tricarbonyls of rhenium and manganese can be used synthetically to allow the introduction of many neutral donor ligands. For example, Cp'Mn$(CO)_2(PPh_3)$ has been synthesised *via* this method, with the photochemistry of the compound subsequently probed using step-scan FTIR.[56] As discussed, photochemistry of substituted metal carbonyls is normally more complicated (Chapter 1, section 1.2); in this case there are now two primary photoprocesses. Cp'Mn$(CO)_2(PPh_3)$ can lose either CO or PPh_3 photolytically. When this reaction is carried out under N_2, Cp'Mn$(CO)_2(N_2)$ is observed, but Cp'Mn$(CO)(PPh_3)(N_2)$ is not. However, when the bulk of the phosphine ligand is reduced (L= PMe_3), the monocarbonyl dinitrogen complex Cp'Mn$(CO)(L)(N_2)$ is seen as the major photoproduct. The behaviour of this simple system was immediately promising, not only as means of forming M-NHC species, but for a fundamental comparison of photoactive M-PR_3 with M-NHC compounds.

1.3.3 The use of TRIR to observe transient organometallic species.

Transient excited-state organometallic species are of great interest for their high reactivity and also the part they often play in the elucidation of reaction mechanisms and pathways. However, they are often so reactive that their observation becomes a challenge in itself. Consequently there has been a lot of research into applicable methods for identifying such species over the years. To begin with *indirect* methods were often used, for example, combining resonance Raman spectra of complexes in their ground states with either Frank-Condon analysis or time-dependent formulation could give information about excited states.[73,74] However, as the transient species were never actually observed

using the above techniques, there are clear limitations and this has led to the development of new *direct* observation methods, preferably in real time.

The most commonly used *direct* observation method in solution is UV/Vis transient absorption (TA) spectroscopy. This is an extension of UV/Vis absorption spectroscopy, where an absorbance at a particular frequency, or range of frequencies, is measured with time after excitation of the system by a pulse of light. Typically, for fast processes, a pulsed laser is used to initiate the reaction and a white light source to measure the absorbance. However, there is a fundamental issue with TA, often the absorption bands of excited metal complexes are broad and featureless, and as such may provide very little structural information.

Time-resolved vibrational spectroscopy can also be used to detect transient species and often the bands exhibited by the excited states retain their structural information, making such techniques a very a powerful tool in this area of research.[75] Probably the most widely used method of this type is time-resolved resonance Raman (TR^3) spectroscopy. Typically TR^3 makes use of the pump-probe methodology, where a pulsed laser is used both to initiate the reaction (pump) and to monitor the absorbance (probe). This pump-probe principle is recurrent in many transient spectroscopic techniques. The detection system for TR^3 filters out the laser's excitation wavelength and collects photons produced by inelastic scattering (Stokes and Anti-Stokes). This technique retains structural information and can also detect 'dark' states; it has been put to excellent use in the literature. For example, TR^3 studies on $[Ru^{II}(bpy)_3]^{2+}$ (bpy = 2,2'-bipyridine) managed to characterise the lowest ^{3}MLCT excited state as $[Ru^{III}(bpy)_2(bpy^-)]^{2+}$.[76]

Whilst this demonstrates the power of TR^3, it is also easy to imagine some limitations of the technique. The selection rules for resonance Raman spectroscopy (non-zero polarisability) mean that only totally symmetrical vibrations will be enhanced enough for observation. This clearly restricts the variety of complexes that are suitable for analysis *via* TR^3. The selection rules for infrared spectroscopy (non-zero dipole) are often more appropriate for

organometallic species, and are in fact complementary to TR[3]. IR is often particularly suited to analysis of certain functional groups, such as ν(CO) bands in metal carbonyl complexes.

Time-resolved infrared spectroscopy (TRIR) is a combination of UV/Vis flash photolysis and fast infrared detection (Figure 10). Again TRIR makes use of the pump-probe methodology, but often a frequency doubler is used to provide pulsed UV/Vis (pump) and IR (probe) from the same laser. The UV/Vis pulse initiates a photochemical reaction, which can be monitored by fast IR.

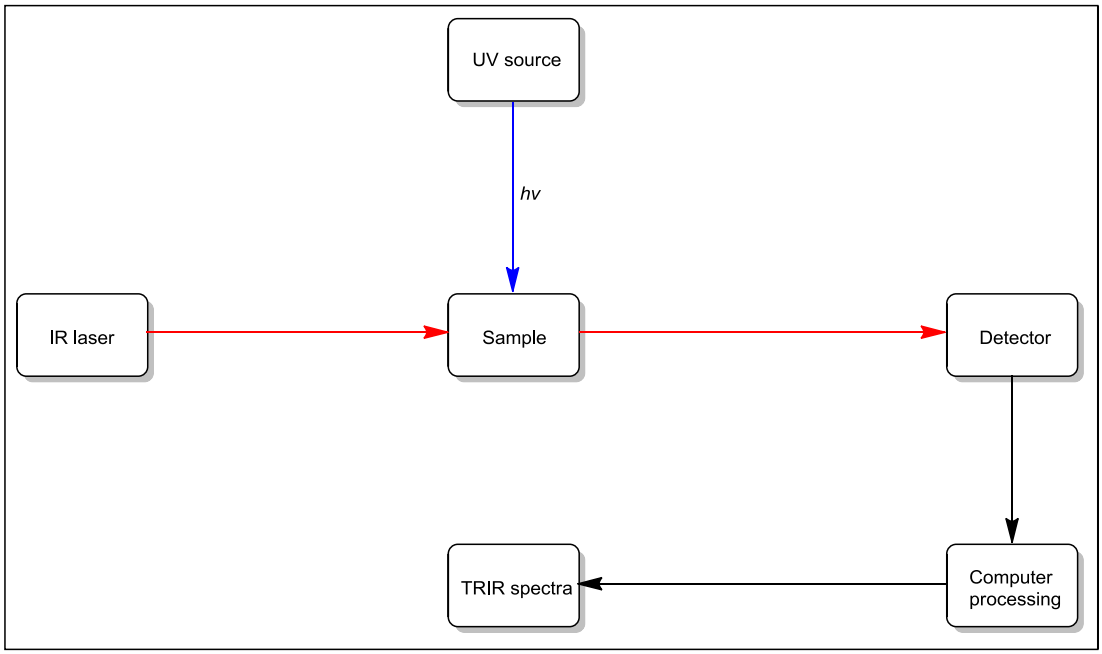

Figure 10: Schematic illustrating the operation of a TRIR spectrometer.

Metal complexes containing ν(CO) bands are highly suitable for this technique as their vibrational modes have high IR extinction coefficients and are ideal 'sensors' for changes in the electron density at the metal centre. For example, TRIR studies on $Re(CO)_3(bpy)Cl$ allowed observation of the ν(CO) bands for the ^{3}MLCT excited state and the shift of the bands to higher frequency showed the change in electron density at the metal centre following electron transfer from Re to Bpy.[77]

There are different ways of acquiring TRIR data, which are still being developed. As mentioned, the most commonly used is a pump-probe approach where an IR source is coupled with a fast IR detector to measure the changes in IR absorption with time following a short intense UV/Vis pulse. A background spectrum of the sample is taken in the ground state, prior to the UV/Vis pulse, which then allows production of a difference spectrum with the data collected after the pulse. Initially a point-by-point approach was used to measure the absorption changes, where after the UV/Vis flash the changing intensity of only one frequency was monitored. The IR frequency would then be changed and the measurements repeated as many times as required to build up a 'point-by-point' TRIR difference spectrum of the relevant species. This is obviously an arduous experiment to undertake, with a large number of runs required to collect the data for one spectrum whilst maintaining a significant frequency range and resolution. It may also be further complicated if the photochemical reaction is irreversible, forcing the use of flow cells to keep sample homogeneity.

More recent advances in IR data collection have made it possible to capture all the TRIR data points required for a spectrum from a single laser pulse by the use of spectral multiplexing and FTIR technology. FTIR techniques require the photochemical event to be highly reversible, at risk of creating artefacts in the spectrum; fortunately, this can also be avoided by the use of flow cells. A combination of 'point-by-point' TRIR and FT-TRIR have been used in this work.

1.4 References.

(1) Arduengo, A. J.; Harlow, R. L.; Kline, M.; *J. Am. Chem. Soc.* **1991**, *113*, 361-363.

(2) Herrmann, W. A.; *Angew. Chem. Int. Ed.* **2002**, *41*, 1290-1309.

(3) Scott, N. M.; Nolan, S. P.; *Eur. J. Inorg. Chem.* **2005**, *2005*, 1815-1828.

(4) Sanford, M. S.; Ulman, M.; Grubbs, R. H.; *J. Am. Chem. Soc.* **2001**, *123*, 749-750.

(5) Grubbs, R. H.; *Tetrahedron* **2004**, *60*, 7117-7140.

(6) Huang, J.; Schanz, H.-J.; Stevens, E. D.; Nolan, S. P.; *Organometallics* **1999**, *18*, 2370-2375.

(7) Tolman, C. A.; *Chem. Rev.* **1977**, *77*, 313-348.

(8) Clavier, H.; Nolan, S. P.; *Chem. Commun.* **2010**, *46*, 841.

(9) Crudden, C. M.; Allen, D. P.; *Coord. Chem. Rev.* **2004**, *248*, 2247-2273.

(10) Arnold, P. L.; Pearson, S.; *Coord. Chem. Rev.* **2007**, *251*, 596-609.

(11) Hu, X.; Tang, Y.; Gantzel, P.; Meyer, K.; *Organometallics* **2003**, *22*, 612-614.

(12) Kunkely, H.; Vogler, A.; *J. Organomet. Chem.* **2003**, *684*, 113-116.

(13) Janowicz, A. H.; Bergman, R. G.; *J. Am. Chem. Soc.* **1982**, *104*, 352-354.

(14) Bergman, R. G.; *Science* **1984**, *223*, 902 -908.

(15) Jones, W. D.; Feher, F. J.; *J. Am. Chem. Soc.* **1984**, *106*, 1650-1663.

(16) Hoyano, J. K.; Graham, W. A. G.; *J. Am. Chem. Soc.* **1982**, *104*, 3723-3725.

(17) Xue, W.-M.; Chan, M. C.-W.; Su, Z.-M.; Cheung, K.-K.; Liu, S.-T.; Che, C.-M. *Organometallics* **1998**, *17*, 1622-1630.

(18) Kunkely, H.; Vogler, A.; *J. Organomet. Chem.* **2005**, *690*, 6051-6053.

(19) Ampt, K. A. M.; Burling, S.; Donald, S. M. A.; Douglas, S.; Duckett, S. B.; Macgregor, S. A.; Perutz, R. N.; Whittlesey, M. K.; *J. Am. Chem. Soc.* **2006**, *128*, 7452-7453.

(20) Geoffroy, G. L.; Bradley, M. G.; *Inorg. Chem.* **1977**, *16*, 744-748.

(21) Colombo, M. W.; George, M. N.; Moore, J. I.; Pattison, D. N.; Perutz, R. G.; Virrels, I.; Ye, T.-Q.; *J. Chem. Soc., Dalton Trans.* **1997**, 2857-2860.

(22) Wang, D.; Wurst, K.; Buchmeiser, M. R.; *Chem. Eur. J.* **2010**, *16*, 12928-12934.

(23) Liu, T.; Xia, B.-H.; Zheng, Q.-C.; Zhou, X.; Pan, Q.-J.; Zhang, H.-X.; *J. Comput. Chem.* **2010**, *31*, 628-638.

(24) Au, V. K.-M.; Wong, K. M.-C.; Zhu, N.; Yam, V. W.-W.; *J. Am. Chem. Soc.* **2009**, *131*, 9076-9085.

(25) Chang, C.; Cheng, Y.; Chi, Y.; Chiu, Y.; Lin, C.; Lee, G.; Chou, P.; Chen, C.; Chang, C.; Wu, C.; *Angew. Chem. Int. Ed.* **2008**, *47*, 4542-4545.

(26) Sajoto, T.; Djurovich, P. I.; Tamayo, A.; Yousufuddin, M.; Bau, R.; Thompson, M. E.; Holmes, R. J.; Forrest, S. R.; *Inorg. Chem.* **2005**, *44*, 7992-8003.

(27) Braband, H.; Kuckmann, T. I.; Abram, U.; *J. Organomet. Chem.* **2005**, *690*, 5421-5429.

(28) Roundhill, D. M.; *Photochemistry and Photophysics of Metal Complexes*; 1st ed. Springer, **1994**.

(29) Wrighton, M.; *Chem. Rev.* **1974**, *74*, 401-430.

(30) Chong, C. V. Y.; Redfern, J. P.; Salmon, J. E.; Kent, P. W.; Wood, K. R.; Ferraro, J. J.; Kaye, I. A.; Weiss, U.; Matthews, R. S.; Scala, A. A.; Purohit, D. N.; Sogani, N. C.; Dunlop, J. H.; Gillard, R. D.; Clark-Lewis, J. W.; Singh, R. P.; Lewis, J.; Nytholm, R. S.; Sandhu, S. S.; Stiddard, M. H. B.; Nayar, V. S. V.; Peacock, R. D.; Russell, D. W.; Davis, M.; Cullis, C. F.; Yates, J. G.; Wilkinson, G.; Harris, D. M.; Fowles, G. W. A.; Walton, R. A.; Feenan, K.; Cort, L. A.; Manders, R. G.; Parlett, G. R.; Gee, W.; Shaw, R. A.; Smith, B. C.; Buck, K. W.; Foster, A. B.; Labib, A.; Webber, J. M.; *J. Chem. Soc.* **1964**, 2811-2848.

(31) Dewar, J.; Jones, H. O.; *Proceedings of the Royal Society of London. Series A* **1905**, *76*, 558 -577.

(32) Sullivan, R. J.; Brown, T. L.; *J. Am. Chem. Soc.* **1991**, *113*, 9162-9169.

(33) Sullivan, R. J.; Brown, T. L.; *J. Am. Chem. Soc.* **1991**, *113*, 9155-9161.

(34) Yasufuku, K.; Hiraga, N.; Ichimura, K.; Kobayashi, T.; *Coord. Chem. Rev.* **1990**, *97*, 167-178.

(35) Glezen, M. M.; Lees, A. J.; *J. Am. Chem. Soc.* **1988**, *110*, 3892-3897.

(36) Hori, H. P. A.; Johnson, F.; Koike, K.; Takeuchi, K.; Ibusuki, T.; Ishitani, O.; *J. Chem. Soc., Dalton Trans.* **1997**, 1019-1024.

(37) Johnson, F. P. A.; George, M. W.; Hartl, F.; Turner, J. J.; *Organometallics* **1996**, *15*, 3374-3387.

(38) Kirgan, R.; Sullivan, B.; Rillema, D.; *Photochemistry and Photophysics of Coordination Compounds II*; Topics in Current Chemistry; Springer Berlin / Heidelberg, **2007**; Vol. 281, pp. 45-100.

(39) Pomestchenko, I. E.; Polyansky, D. E.; Castellano, F. N.; *Inorg. Chem.* **2005**, *44*, 3412-3421.

(40) Villegas, J. M.; Stoyanov, S. R.; Huang, W.; Rillema, D. P.; *Dalton Trans.* **2005**, 1042-1051.

(41) Villegas, J. M.; Stoyanov, S. R.; Huang, W.; Rillema, D. P.; *Inorg. Chem.* **2005**, *44*, 2297-2309.

(42) Koike, K.; Tanabe, J.; Toyama, S.; Tsubaki, H.; Sakamoto, K.; Westwell, J. R.; Johnson, F. P. A.; Hori, H.; Saitoh, H.; Ishitani, O.; *Inorg. Chem.* **2000**, *39*, 2777-2783.

(43) Koike, K.; Okoshi, N.; Hori, H.; Takeuchi, K.; Ishitani, O.; Tsubaki, H.; Clark, I. P.; George, M. W.; Johnson, F. P. A.; Turner, J. J.; *J. Am. Chem. Soc.* **2002**, *124*, 11448-11455.

(44) Tsubaki, H.; Tohyama, S.; Koike, K.; Saitoh, H.; Ishitani, O.; *Dalton Trans.* **2005**, 385-395.

(45) Tsubaki, H.; Sekine, A.; Ohashi, Y.; Koike, K.; Takeda, H.; Ishitani, O.; *J. Am. Chem. Soc.* **2005**, *127*, 15544-15555.

(46) Hori, H.; Johnson, F. P. A.; Koike, K.; Ishitani, O.; Ibusuki, T.; *J. Photoch. Photobiol. A.* **1996**, *96*, 171-174.

(47) Takeda, H.; Koike, K.; Inoue, H.; Ishitani, O.; *J. Am. Chem. Soc.* **2008**, *130*, 2023-2031.

(48) Stoeffler, H. D.; Thornton, N. B.; Temkin, S. L.; Schanze, K. S.; *J. Am. Chem. Soc.* **1995**, *117*, 7119-7128.

(49) Bengali, A. A.; Schultz, R. H.; Moore, C. B.; Bergman, R. G.; *J. Am. Chem. Soc.* **1994**, *116*, 9585-9589.

(50) Graham, W. A. G.; *J. Organomet. Chem.* **1986**, *300*, 81-91.

(51) Schubert, U.; *Academic Press*, **1990**; *30*, 151-187.

(52) Rabaa, H.; Saillard, J.-Y.; Schubert, U.; *J. Organomet. Chem.* **1987**, *330*, 397-413.

(53) Morse, J. M.; Parker, G. H.; Burkey, T. J.; *Organometallics* **1989**, *8*, 2471-2474.

(54) Leu G. L.; Burkey, T. J.; *J. Coord. Chem.* **1995**, *34*, 87-97.

(55) Ball, G. E.; Brookes, C. M.; Cowan, A. J.; Darwish, T. A.; George, M. W.; Kawanami, H. K.; Portius, P.; Rourke, J. P.; *Proc. Nat. Acad. Sci. USA* **2007**, *104*, 6927 -6932.

(56) Banister, J. A.; George, M. W.; Grubert, S.; Howdle, S. M.; Jobling, M.; Johnson, F. P. A.; Morrison, S. L.; Poliakoff, M.; Schubert, U.; Westwell, J. R.; *J. Organomet. Chem.* **1994**, *484*, 129-135.

(57) Howdle S. M.; Jobling M.; Poliakoff M.; *Supercritical Fluid Technology*; ACS Symposium Series; American Chemical Society, **1992**; Vol. 488, pp. 121-131.

(58) George, M. W.; Grills, D. C.; Sun, X.-Z.; Poliakoff, M.; In *Advances in Chemical Conversions for Mitigating Carbon Dioxide, Proceedings of the Fourth International Conference on Carbon Dioxide Utilization*; Elsevier, **1998**; Vol. Volume 114, pp. 255-260.

(59) Kubas, G. J.; *Chem. Rev.* **2007**, *107*, 4152-4205.

(60) Gibson, D. H.; *Chem. Rev.* **1996**, *96*, 2063-2096.

(61) Leigh, G. J.; *Transition Met Chem* **1986**, *11*, 118-120.

(62) Kolomnikov, I. S.; Grigoryan, M. K.; *Russ. Chem. Rev.* **1978**, *47*, 334.

(63) Sakakura, T.; Choi, J.-C.; Yasuda, H.; *Chem. Rev.* **2007**, *107*, 2365-2387.

(64) Labinger, J. A.; Bercaw, J. E.; *Nature* **2002**, *417*, 507-514.

(65) Díaz-Requejo, M. M.; Pérez, P. J.; *Chem. Rev.* **2008**, *108*, 3379-3394.

(66) Creaven, B. S.; Dixon, A. J.; Kelly, J. M.; Long, C.; Poliakoff, M.; *Organometallics* **1987**, *6*, 2600-2605.

(67) O'Driscoll, E.; Simon, J. D.; *J. Am. Chem. Soc.* **1990**, *112*, 6580-6584.

(68) Simon, J. D.; Xie, X.; *J. Phys. Chem.* **1986**, *90*, 6751-6753.

(69) Joly, A. G.; Nelson, K. A.; *J. Phys. Chem.* **1989**, *93*, 2876-2878.

(70) Lee, M.; Harris, C. B.; *J. Am. Chem. Soc.* **1989**, *111*, 8963-8965.

(71) Wells, J. R.; Weitz, E.; *J. Am. Chem. Soc.* **1992**, *114*, 2783-2787.

(72) Bogdan, P. L.; Wells, J. R.; Weitz, E.; *J. Am. Chem. Soc.* **1991**, *113*, 1294-1299.

(73) Clark, R. J. H.; Dines, T. J.; *Angew. Chem. Int. Ed. Engl.* **1986**, *25*, 131-158.

(74) Zhang, J. Z.; Heller, E. J.; Huber, D.; Imre, D. G.; *J. Phys. Chem.* **1991**, *95*, 6129-6141.

(75) Schoonover, J.; *Comments Inorg. Chem.* **1996**, *18*, 77-100.

(76) Bradley, P. G.; Kress, N.; Hornberger, B. A.; Dallinger, R. F.; Woodruff, W. H.; *J. Am. Chem. Soc.* **1981**, *103*, 7441-7446.

(77) George, M. W.; Johnson, F. P. A.; Westwell, J. R.; Hodges, P. M.; Turner, J. J.; *J. Chem. Soc., Dalton Trans.* **1993**, 2977-2979.

Chapter 2

2.1 Contrasts between the photochemistry of organometallic NHC and phosphine complexes: An investigation using TRIR spectroscopy.

An examination into the accessibility of $Cp'Mn(CO)_{3-n}(NHC)_n$ ($Cp' = C_5H_4Me$) species will form the primary focus of this chapter, ideally those which have previously studied phosphine analogues, allowing for close comparison. TRIR studies were conducted at Nottingham University in collaboration with Prof. Michael W. George and Madeeha Batool, where the reactivity and lifetime of photo-generated transients with alkane solvents and small molecules was examined under different conditions.

2.2 Synthesis of $Cp'Mn(CO)_2(IEt_2Me_2)$ (1).

For the preliminary TRIR studies in Nottingham samples of $Cp'Mn(CO)_2(PPh_3)$ were synthesised in Bath.[1] Initial efforts employed $Cp'Mn(CO)_2(PPh_3)$ as a starting point for the synthesis of the NHC analogue, **1**. Unfortunately, even in the presence of 3 equivalents of IEt_2Me_2 in refluxing toluene, no thermal substitution of PPh_3 for IEt_2Me_2 was observed. However, photolysis (300 W Xenon arc lamp) of a THF solution of $Cp'Mn(CO)_2(PPh_3)$ with a threefold excess of free carbene in an NMR tube, resulted in generation of free PPh_3 and formation of **1** in *ca*. 25% yield after 1 hour as observed by NMR. After a further 2 hours of irradiation, NMR analysis showed only a modest increase in conversion to *ca*. 50%, indicating that this method was insufficient to drive the reaction to completion. Further to this, separation of the desired product from the residual starting material proved impossible. Direct photolysis of 3 equivalents of IEt_2Me_2 with $Cp'Mn(CO)_3$ in THF yielded **1**, almost quantitatively according to the IR spectra recorded, although this was always formed along with an unknown insoluble red precipitate. The red precipitate by-product could be obtained in larger amounts by leaving a solution of **1** to stand in ambient light

for several days. Thus far the precipitate has resisted all attempts at characterisation, due to high sensitivity and intractability.

The photochemical reaction of Cp'Mn(CO)$_3$ with IEt$_2$Me$_2$ was further optimised to allow facile isolation of **1** from the reaction mixture and scale up. During the reaction work up it became apparent that **1** was soluble in hexane, which is typically used to aid separation and remove any unreacted free NHC or Cp'Mn(CO)$_3$ after reaction. However, **1** remains less soluble in hexane than the other reagents used in the synthesis and reduction of the number of equivalents of NHC used to a 1:1 ratio allowed the product to be isolated from hexane, after concentration and recrystallization of the reaction mixture. Large scale preparation of **1** was performed in hexane solution using an immersion well (100 mL) and a 150 W mercury arc lamp (Figure 11). A constant stream of argon was maintained throughout the reaction to ensure removal of the photogenerated CO.

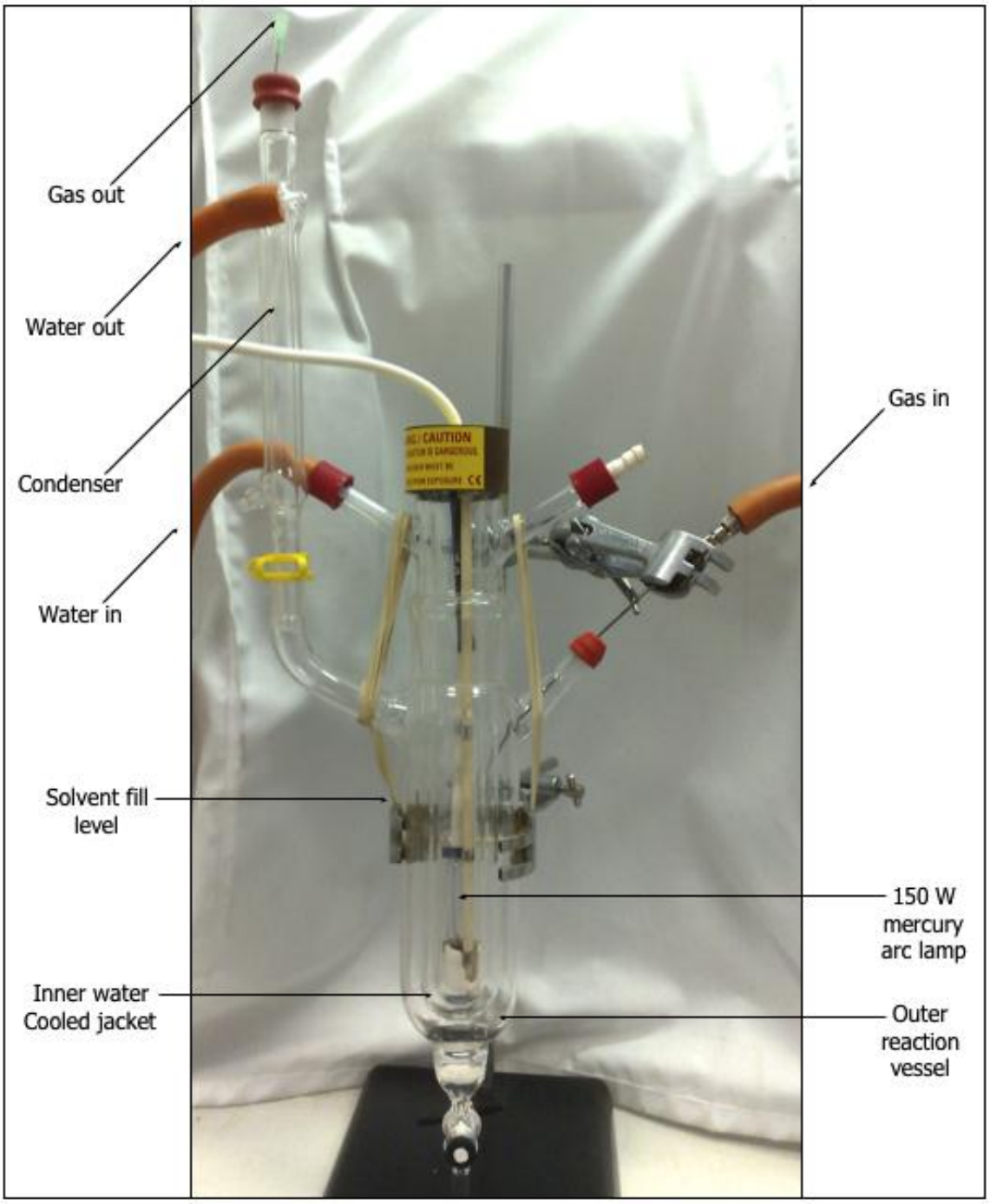

Figure 11: Photochemical reactor setup.

The progress of the photoreaction was monitored by periodic removal of samples for analysis with IR spectroscopy. The samples were removed by syringe, evaporated to dryness and redissolved in CH_2Cl_2 (Figure 12).

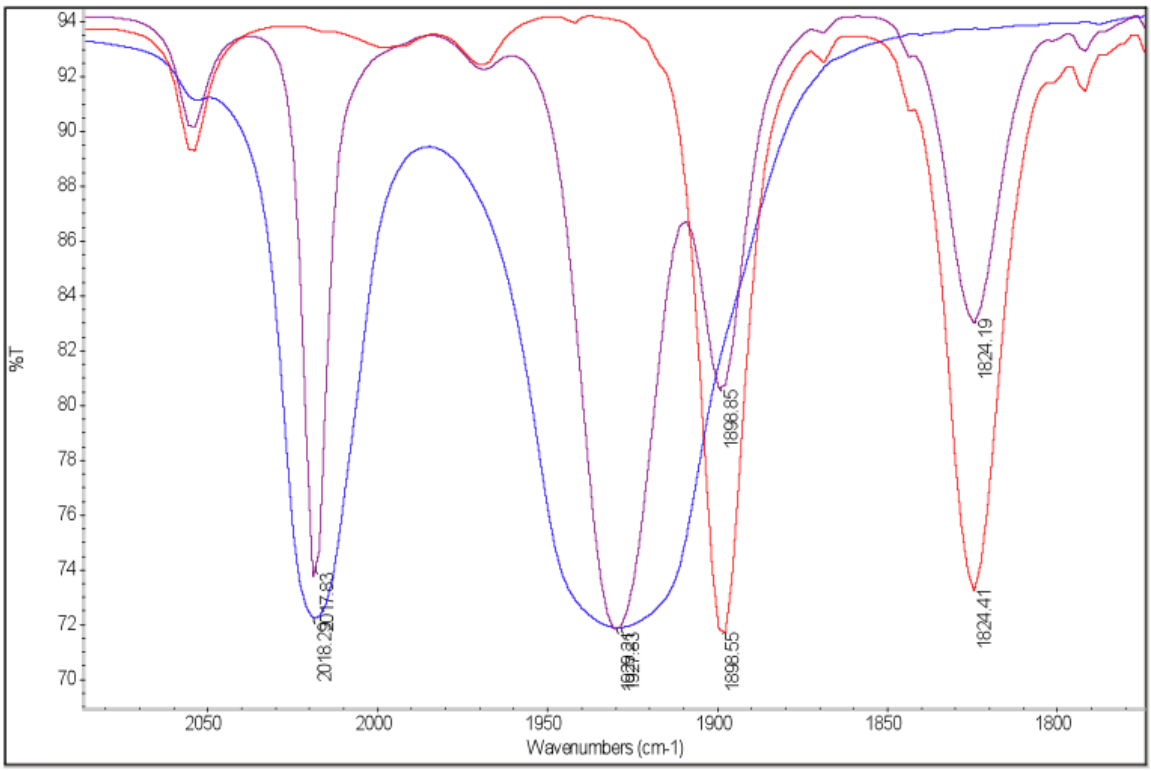

Figure 12: Overlayed FTIR spectra showing the reaction progression for photolysis of $Cp'Mn(CO)_3$ + IEt_2Me_2 in hexane (0 mins = blue, 15 mins = purple, 30 mins = red, IR solvent = CH_2Cl_2).

The reaction was judged to have finished once the high frequency carbonyl bands for the starting material (2018 and 1928 cm^{-1}, blue line) were no longer apparent and the lower frequency carbonyl bands from the product (1898, 1824 cm^{-1}, red line) indicated it as the major species; this typically took *ca*. 40 min of irradiation. The shift too much lower frequency for the product is consistent with the replacement of CO, a strong π acceptor, with IEt_2Me_2, a strong σ donor. The ^{1}H NMR spectrum of **1** was collected in d_8-THF at 298 K. Three signals were found for the carbene; the backbone methyl groups (δ 2.13) and two resonances for the the N-Et groups (δ 4.42 and 1.29). The Cp' ring was observed as a series of peaks which integrated to a 2:2:3 ratio. The $^{13}C\{^1H\}$ NMR spectrum showed one CO (δ 235.6) and one carbenic carbon (δ 196.3)

After reaction, the hexane solution was passed through a pad of celite, to remove the red precipitate. Concentrating the hexane solution and allowing it to stand at room temperature gave crystals suitable for X-ray diffraction in a 37%

yield. The crystal structure of **1** confirmed the expected half-sandwich piano stool geometry (Figure 13).

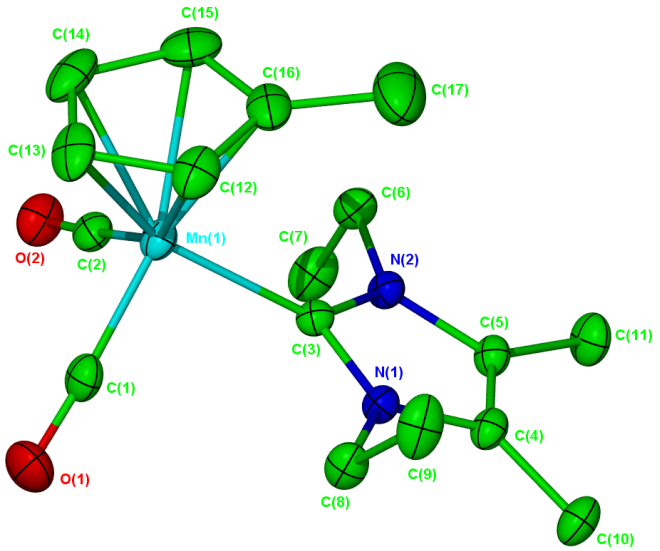

Figure 13: X-ray crystal structure of Cp'Mn(CO)$_2$(IEt$_2$Me$_2$) (1), ellipsoids shown at 30% and hydrogen atoms omitted for clarity.

The metal-CO bond distances of 1.748(3) (Mn(1)-C(2)) and 1.757(4) Å (Mn(1)-C(1)) are the same as those in Cp'Mn(CO)$_2$(PPh$_3$) (1.76(1) and 1.77(1) Å).[2] This is surprising considering the shift (*ca*. 30 cm^{-1}) of the ν(CO) bands observed by IR for **1** to lower frequency than for Cp'Mn(CO)$_2$(PPh$_3$), indicating significantly higher electron density on the metal centre. This would increase the degree of back bonding, thus strengthening and shortening the Mn-CO bonds. It could be that the error associated with the bond lengths for Cp'Mn(CO)$_2$(PPh$_3$) is too high to allow accurate comparison between the structures. The Mn-NHC bond distance is 2.014(3) Å, much shorter than the Mn-PPh$_3$ bond (2.232(2) Å) in Cp'Mn(CO)$_2$(PPh$_3$), which would signify a much stronger bond to the NHC in a 'like for like' system. However, the radius of phosphorous is significantly larger than carbon, as such these lengths are difficult to compare accurately. The central C-Mn-C angles show the change caused by exchange of CO for the bulkier NHC which has compacted the C(1)-Mn(1)-C(2) angle (89.63(15)°), and increased the C(1)-Mn(1)-C(3) (94.33(13)°) and C(2)-Mn(1)-C(3) (97.97(12)°) angles away from 90°. The steric demands of IEt$_2$Me$_2$ appear small enough to allow the Me group of the Cp' ring to point directly towards the NHC over the

Mn(1)-C(3) vector. This is not the case for Cp'$Mn(CO)_2(PPh_3)$ where the methyl group is *trans* to PPh_3.[2]

2.3 Synthesis of Cp'$Mn(CO)_2$(IMes) (2).

The N-aryl carbene complex **2** was prepared using an analogous approach, a 1:1 ratio of starting materials irradiated in hexane for *ca*. 40 min. There was noticeably less red precipitate by-product formed in this reaction. The infrared spectrum of **2** in CH_2Cl_2 exhibited bands at 1905 and 1832 cm^{-1}, very similar to those obtained for **1**, although perhaps suggestive of IMes being slightly less donating that IEt_2Me_2. The ^1H NMR spectrum of **2** was collected in C_6D_6 at 298 K. The carbene showed four resonances; the aryl protons (δ 7.00), the backbone protons (δ 6.19) and the *para* (δ 2.15) and *ortho* (δ 2.09) CH_3 groups. The Cp' ring was observed as a series of peaks which integrated to a 2:2:3 ratio. As for **1**, the $^{13}C\{^1H\}$ NMR spectrum showed one CO (δ 234.7) and one carbenic carbon resonance (δ 205.8).

Crystals suitable for X-ray diffraction were obtained *via* precipitation from a concentrated solution of hexane in 42% yield (Figure 14). Whilst a similar half-sandwich piano stool geometry is seen for **2**, the unit cell showed a much longer c axis (33.1360 Å for IMes, 14.0950 Å for IEt_2Me_2) and volume (10011.51 $Å^3$ for IMes, 1685.47 $Å^3$ for IEt_2Me_2). This change in volume was explained by the unit cell content, which was found to consist of four molecules in the asymmetric unit, each slightly different to one another (Table 1, page 39). The metal-CO bond distances ranged from 1.756(2) Å to 1.769(2) Å, and the Mn-NHC bond lengths varied from 1.998(2) Å to 2.007(2) Å. The central OC-Mn-CO angles were again compacted by the NHC with angles ranging from 87.05(10)° to 89.50(11)°. There was also a corresponding expansion of the NHC-Mn-CO angles, which varied from 93.10(9)° to 98.09(9)°.

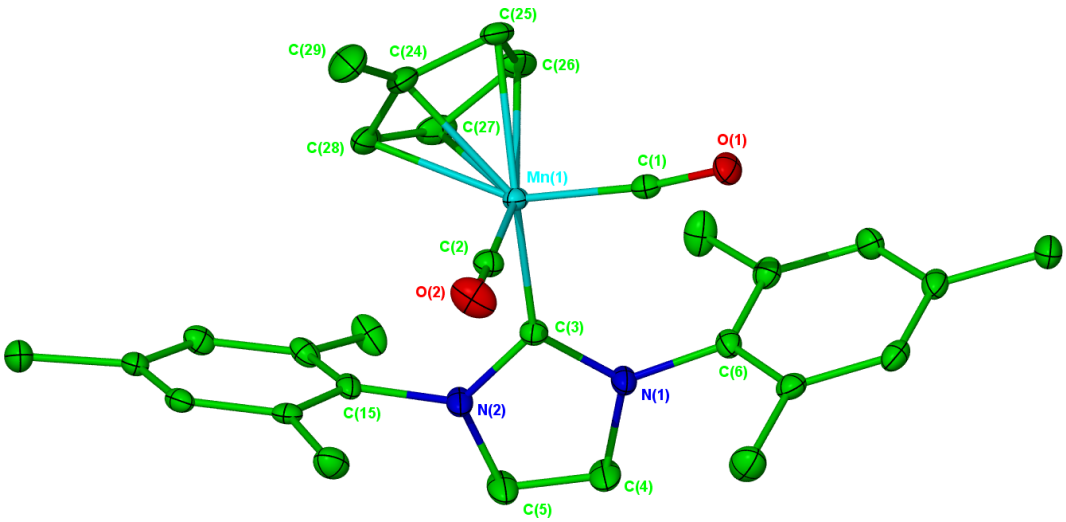

Figure 14: X-ray crystal structure of one of the four molecules of Cp'Mn(CO)$_2$(IMes) (2) in the unit cell, ellipsoids shown at 30% and hydrogen atoms omitted for clarity.

	Mn(1)	Mn(2)	Mn(3)	Mn(4)
M-CO	1.756(2) 1.765(2)	1.762(2) 1.766(2)	1.761(3) 1.769(2)	1.756(2) 1.763(2)
M-NHC	1.998(2)	2.002(2)	2.007(2)	2.002(2)
OC-Mn-CO	87.05(10)	87.55(10)	88.72(10)	89.50(11)
NHC-Mn-CO	93.21(10) 97.22(9)	98.09(9) 93.10(9)	93.44(10) 97.72(9)	94.87(9) 97.04(10)

Table 1: Selected bond lengths (Å) and angles (°) for the 4 molecules of Cp'Mn(CO)$_2$(IMes) in the unit cell.

2.4 Synthesis of Cp'Mn(CO)$_2$(I^{i}Pr$_2$Me$_2$) (3).

Synthesis of **3** proved to be more problematic than for either of the previous two compounds, as large amounts of red precipitate were produced during

photolysis under argon, which prevented high conversion to **3**. Replacement of the argon purge through the system with a slow flow of CO minimised the formation of the red precipitate and allowed isolation of **3** from hexane as crystals in a 51% yield (Figure 15).

The infrared spectrum of **3** in CH_2Cl_2 exhibited bands at 1898 and 1824 cm^{-1}, identical to those obtained for **1**, indicating very little difference in donor ability between the two N-alkyl carbenes. The ^1H NMR spectrum of **3** was collected in d_3-MeCN at 298 K (Figure 18). The signals for the carbene were observed as 3 resonances; isopropyl CH (δ 6.02), backbone CH_3 (δ 2.20) and isopropyl CH_3 (δ 1.42). The Cp' ring was observed as a series of peaks integrating in a 2:2:3 ratio. The $^{13}C\{^1H\}$ NMR spectrum showed one CO (δ 235.0) and one carbenic carbon resonance (δ 194.6).

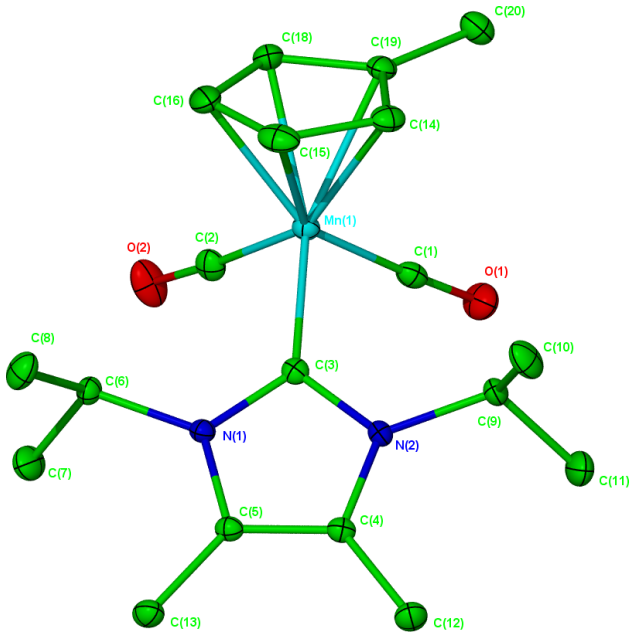

Figure 15: X-ray crystal structure of Cp'Mn(CO)$_2$(I^{i}Pr$_2$Me$_2$) (3), ellipsoids shown at 30% and hydrogen atoms removed for clarity.

The familiar half-sandwich piano stool geometry is seen for **3**. The Mn-CO and Mn-NHC distances, as well as the OC-Mn-CO angles, are comparable to those in both **1** and **2** (as shown in Table 2, page 46). As in **2**, the methyl group on the Cp' ring points away from the NHC ligand.

It was possible to characterise the red precipitate by-product formed during the formation of **3** by IR and ESI-MS analysis. The IR data showed a very strong and broad absorption at 1712 cm^{-1}, which was indicative of bridging carbonyl groups. This suggested the possibility of dimeric products forming during photolysis. There is some precedent for such a reaction in the literature. During the photolysis of Cp'Mn$(CO)_3$, Poliakoff *et al.* observed a highly sensitive red precipitate and proposed a dimeric structure with bridging carbonyls.[5] This was believed to arise from reaction of the intermediate, Cp'Mn$(CO)_2$(solvent), with the starting tricarbonyl complex (Figure 16). An alternative process could be anticipated, where instead Cp'Mn(CO)(NHC)(solvent) participates in the reaction to yield a closely related species.

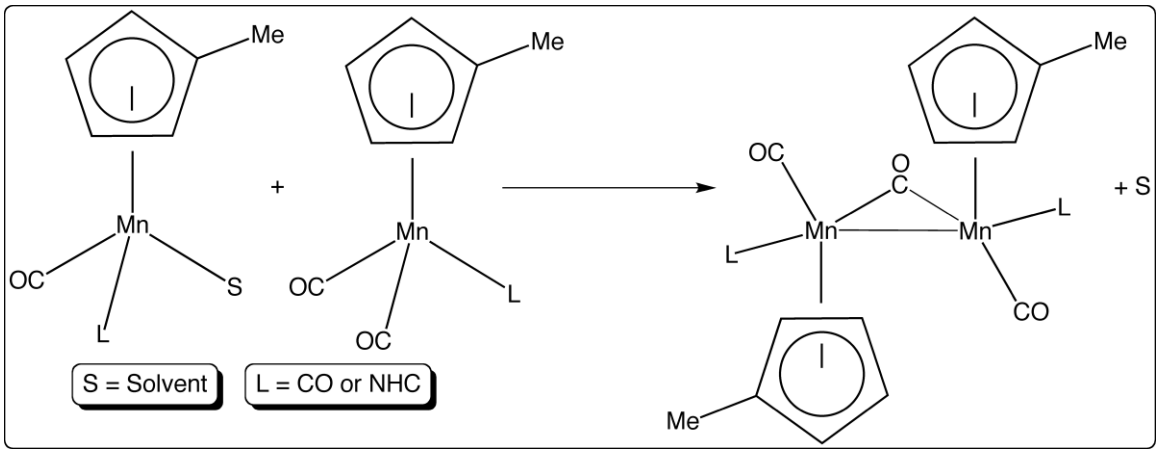

Figure 16: Proposed route for formation of dimeric by-product.

Such a pathway is understandable, as generally, the concentration of [Cp'Mn$(CO)_2$] / [Cp'Mn(CO)(NHC)] and thus any potentially reactive solvated or otherwise stabilised species is low, implying a very low probability of any reaction process involving two intermediates. Consequently, the reaction should follow pseudo first order kinetics, due to the concentration of the parent compound greatly exceeding that of the photogenerated species. The ESI-MS data showed evidence of a dimeric product having formed, but the molecular ion mass and fragmentation pattern did not match up with the dimer proposed by Poliakoff *et al*. It suggested another intriguing possibility (Figure 17) ($[M+Na]^+$, m/z = 707.3465, $C_{36}H_{54}Mn_2N_4O_2Na$, I = 100%) ($[M]^+$, m/z = 684.2033, $C_{36}H_{54}Mn_2N_4O_2$, I = 45%).

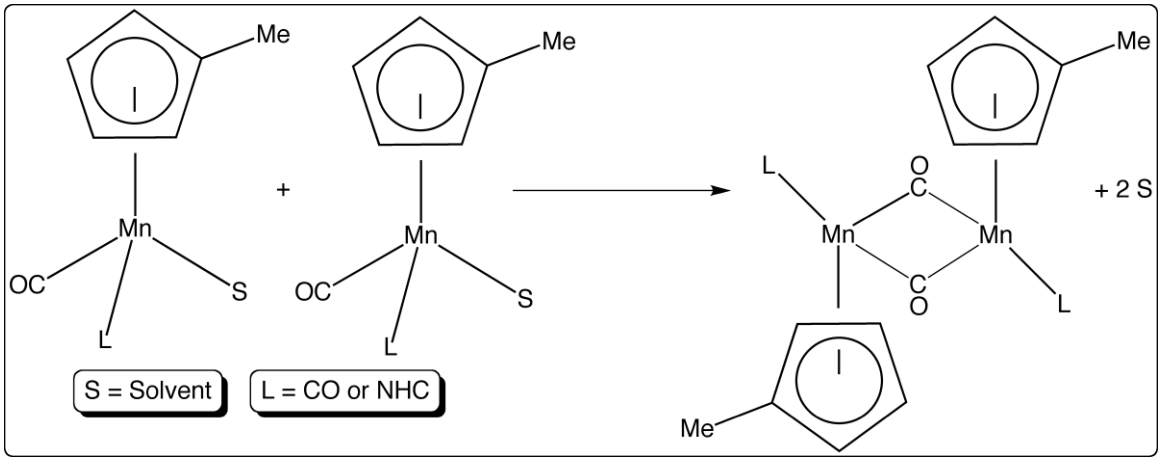

Figure 17: Dimeric species indicated by ESI-MS analysis.

Admittedly this dimer would be a 16 electron species, unless further stabilised by metal-metal or agostic interactions from the NHC, yet this could go some way towards explaining the compound's incredibly high sensitivity, and why similar species have gone uncharacterised for many years.

The increased bulk of the 2° NHC ($I^iPr_2Me_2$) over the 1° (IEt_2Me_2) may have imparted a higher stability to the dimeric species, or made it more able to participate in agostic stabilisation, and explain why noticeably larger amounts of the red by-product was produced during the synthesis of $Cp'Mn(CO)_2(I^iPr_2Me_2)$. It is also interesting that one of the most obvious routes to formation of this dimer is *via* combination of two CO loss intermediates, presumably then eliminating two solvent molecules to produce the dimer.

This would indicate a bimolecular second order reaction, which as mentioned previously, remains highly unlikely since the concentration of the transient species should be too low for the reaction to occur under diffusion control, even with the very high quantum yields of these systems.[5] Thus, it is likely that an unanticipated reaction pathway could be responsible for the dimer formation, perhaps proceeding *via* monomeric agostic intermediates.

Whilst this reactivity is worthy of note, it remains undesirable for our purposes in trying to cleanly produce **3**. However, if the dimer is considered as an unsaturated organometallic fragment, then conceptually, the addition of two

molecules of CO should break it apart and regenerate **3**. Thus, whilst it might be counter intuitive to increase the amount of CO present in the reaction, as the photolysis is designed to eject CO in order for it to be substituted, in fact it had the desired effect by reducing the amount of the red dimeric precipitate formed.

As mentioned previously, substituting the argon flow through the photoreactor with CO and carrying out all subsequent manipulations under the same atmosphere, allowed **3** to be isolated. This is presumably because the rate of photolytic CO dissociation is very fast (high quantum yield), therefore the increased CO pressure does not slow the formation of **3** unduly, but it does allow for the dimer formation to be minimised, either by breaking apart the dimer to reform **3** or by competing for recombination with the [Cp'Mn(CO)($I^iPr_2Me_2$)] (**3-CO**) and [Cp'Mn$(CO)_2$] fragments, thus reducing the concentration of the species likely to be responsible for the dimer formation.

2.5 Synthesis of Cp'Mn$(CO)_2$(IPr) (4).

The N-aryl carbene complex **4** was prepared using the same approach as for **1** and **2**, namely combination of a 1:1 ratio of starting materials and *ca*. 40 minutes of irradiation in hexane with an argon purge. There was more red precipitate by-product formed from this reaction than for Cp'Mn$(CO)_2$(IMes), although it was not enough to impede isolation. The IR spectrum of **4** in CH_2Cl_2 exhibited bands at 1906 and 1834 cm^{-1}, comparable to those seen for **1**-**3**.

The ^{1}H NMR spectrum of **4** was collected in d_8-THF at 298 K (Figure 19). Six resonances were seen for the carbene; *para* CH (δ 7.43), *meta* CH (δ 7.32), backbone CH (δ 7.18), isopropyl CH (δ 2.87) and two sets of isopropyl CH_3 (δ 1.39 and δ 1.11), indicating restricted rotation about the bond from the *ortho* carbon to the isopropyl groups. Unlike the previous compounds **1**-**3**, the Cp' ring in **4** appeared as two multiplets exhibiting second order effects and a singlet for the methyl group integrating in a 2:2:3 ratio. This is best illustrated by comparison of Figures 18 and 19. One explanation for this change could be that the Cp' ring has developed a degree of inequivalence due to steric clashing

between the Cp-Me and isopropyl groups in **4**. The $^{13}C\{^{1}H\}$ NMR spectrum showed one CO (δ 234.5) and one carbenic carbon resonance (δ 207.9).

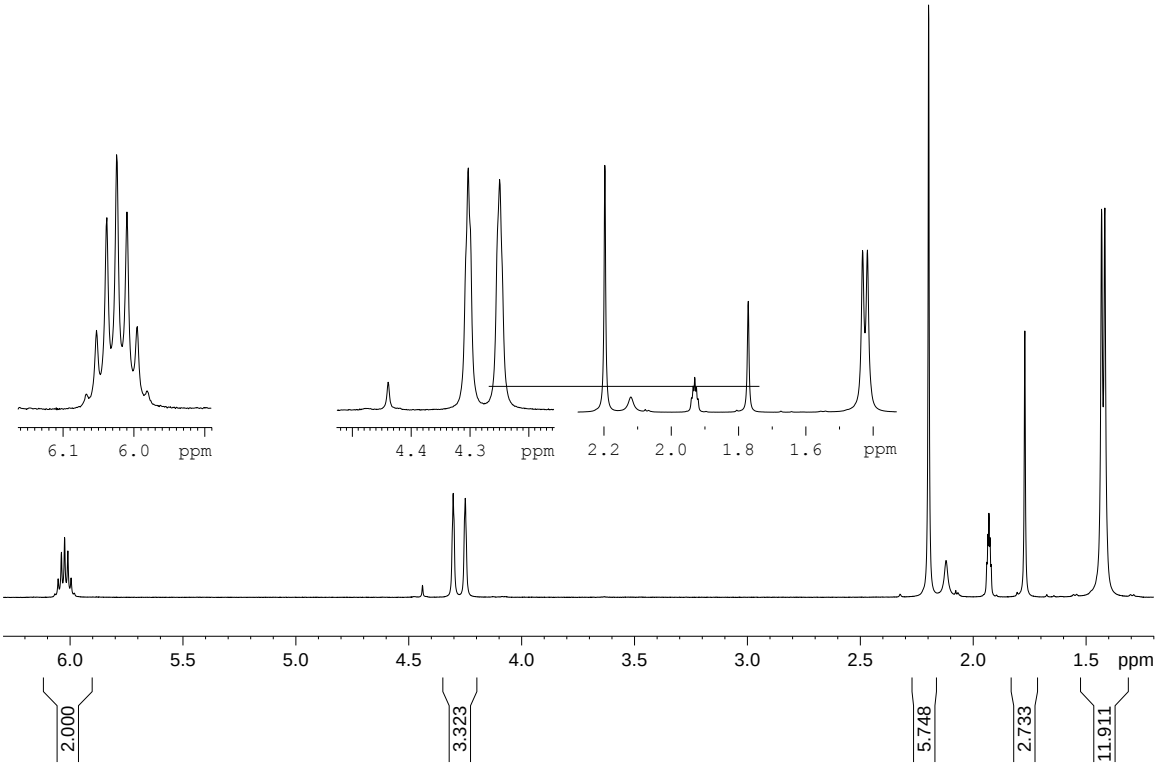

Figure 18: 500 MHz ^{1}H NMR spectrum of Cp'Mn(CO)$_2$(l^{i}Pr$_2$Me$_2$) (3) in d_3-MeCN at 298 K.

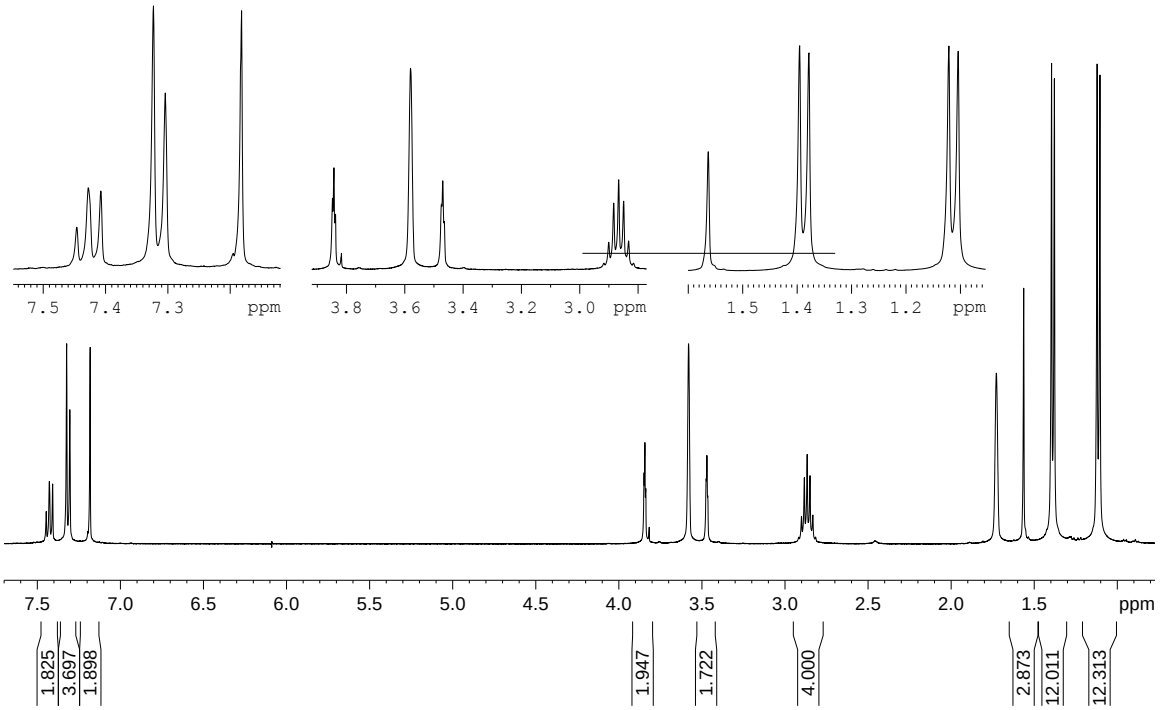

Figure 19: 500 MHz ^{1}H NMR spectrum of Cp'Mn(CO)$_2$(IPr) (4) in d_8-THF at 298 K.

Crystals suitable for X-ray diffraction were obtained *via* precipitation from a concentrated hexane solution in 47% yield (Figure 20). The structure also adopts the now familiar half-sandwich piano stool geometry as seen for **1**-**3**, with bond lengths and angles summarised in Table 2 (page 46). However, in the case of **4**, there is a significant structural change apparent. In compounds **1**-**3** the side arms of the NHC lay parallel to the CO groups. However, in the case of **4** the NHC has rotated almost 45° and lies parallel with the plane described by the C(1)-Mn(1)-C(3) angle. This may explain why the ^{i}Pr groups are in very close proximity to the Cp' ring, as evidenced in the ^{1}H NMR spectrum. Presumably this is due to the ^{i}Pr substituents on the phenyl ring interacting unfavourably with the CO groups if the NHC was to align itself in a parallel fashion. In the distorted configuration adopted by **4** it is possible that the rotation of the Cp' ring is prevented by steric clashing between the Me group on the Cp' ring and the ^{i}Pr groups on the NHC ligand.

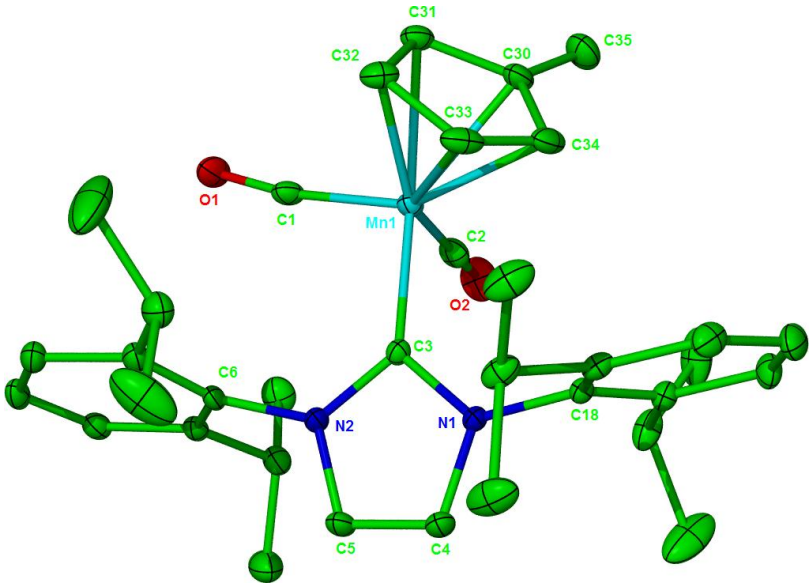

Figure 20: X-ray crystal structure of Cp'Mn(CO)$_2$(IPr) (4), ellipsoids at 30% and hydrogen atoms omitted for clarity.

	1	2*	3	4
Mn-NHC	2.014(3)	2.002(2)	2.018(3)	2.0013(18)
Mn-CO	1.748(3)	1.759(2)	1.758(3)	1.760(2)
	1.757(4)	1.766(2)	1.758(3)	1.762(2)
NHC-Mn-CO	97.97(12)	94.90(10)	95.36(12)	98.84(8)
	94.33(13)	96.27(9)	94.06(12)	89.45(9)
OC-Mn-CO	89.63(15)	88.21(10)	88.44(12)	89.35(10)

Table 2: Selected bond lengths (Å) and angles (°) in the manganese NHC complexes 1, 2, 3 and 4 (* average values from across the 4 asymmetric molecules in the unit cell).

2.6 FTIR and TRIR analysis of $Cp'Mn(CO)_2(IEt_2Me_2)$ *vs*. $Cp'Mn(CO)_2(PPh_3)$.

FTIR and TRIR studies were performed in Nottingham. In an initial study $Cp'Mn(CO)_2(PPh_3)$ (**PPh_3**) and $Cp'Mn(CO)_2(IEt_2Me_2)$ (**1**) were investigated using step-scan FTIR for comparison to previous work.

2.6.1 Photolysis of $Cp'Mn(CO)_2(PPh_3)$ / $Cp'Mn(CO)_2(IEt_2Me_2)$ in liquid C_2H_6 (1400 psi) under N_2 (200 psi) at room temperature monitored by difference FTIR.

The ν(CO) bands for **PPh_3** appear at 1944 cm^{-1} and 1886 cm^{-1} in liquid C_2H_6 (1400 psi). Photolysis (λ > 300 nm) of this solution under 200 psi of N_2 at 298 K, results in bleaching of the parent bands and the production of three new bands (Figure 21). The bands at 1979 cm^{-1} and 1928 cm^{-1} are ν(CO) bands and the band at 2168 cm^{-1} is from bound dinitrogen. Assignment of these bands is aided by comparison to previous work and they are attributed to formation of $Cp'Mn(CO)_2(N_2)$.[5] No $Cp'Mn(CO)(PPh_3)(N_2)$ was detected in this experiment. These results would suggest that predominantly PPh_3 is lost from the parent and that at this temperature and within the acquisition time frame, any CO loss products are not stable enough to be observed. This is consistent with previous studies,[5] although it remains curious that dinitrogen, which typically binds as a

weak π acceptor, appears not to bind the comparatively less electrophilic [Cp'Mn(CO)(PPh_3)] (**PPh_3-CO**) fragment.

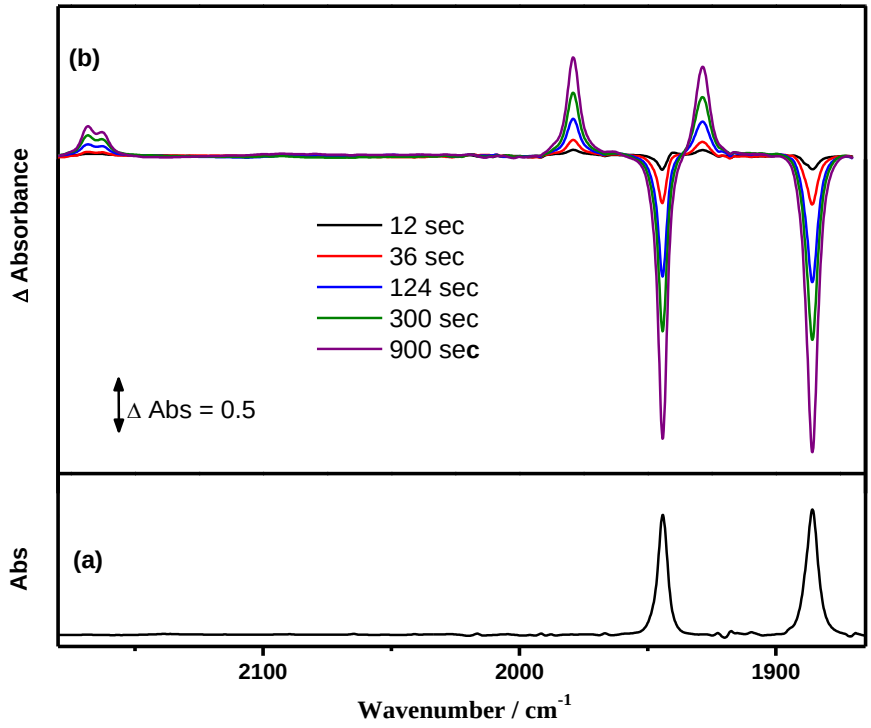

Figure 21: (a) FTIR spectrum of Cp′Mn(CO)$_2$(PPh_3) in liq.C_2H_6 (1400 psi) and N_2 (200 psi) at 298 K (b) FTIR difference spectra after broadband photolysis (>300 nm).

The ν(CO) bands for **1** in liquid C_2H_6 appear at 1919 cm^{-1} and 1855 cm^{-1}, significantly lower in frequency than for **PPh_3**, demonstrating increased electron density on the metal centre due to the stronger δ donor properties of the NHC ligand. Photolysis of a solution of **1** under the same conditions resulted solely in bleaching of the parent bands (Figure 22). There were no new species observed. However, there was evidence for formation of a red insoluble photoproduct, which we postulate is the same species encountered during the synthesis.

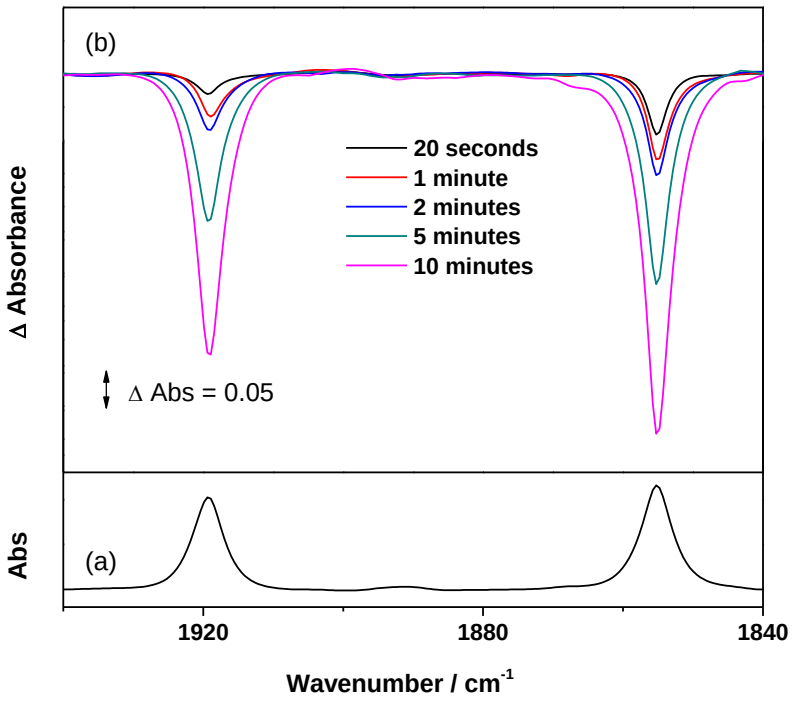

Figure 22: (a) FTIR spectrum of Cp′Mn(CO)$_2$(IEt$_2$Me$_2$) (1) in liq.C$_2$H$_6$ (1400 psi) and N$_2$ (200 psi) at 298 K (b) FTIR difference spectra after broadband photolysis (>300 nm).

There are a number of conclusions to be drawn from these observations. Firstly, IEt$_2$Me$_2$ is not lost from **1** upon photolysis, contrary to the observations for **PPh$_3$**, as if [Cp'Mn(CO)$_2$] were produced it would coordinate N$_2$ under the experimental conditions. However, the bleaching of the parent bands clearly shows the molecule is undergoing a photolytic process, which would indicate CO loss as the most probable pathway and therefore generation of [Cp'Mn(CO)(IEt$_2$Me$_2$)] (**1-CO**). However, as no new carbonyl species were observed in the FTIR spectra, it seems likely that decomposition to the insoluble by-product is favoured under these conditions. Yet again, considering that the proposed **1-CO** fragment is less electrophilic than the dicarbonyl or phosphine analogues, it is surprising that it does not bind N$_2$.

Two theories that could explain why Cp'Mn(CO)(IEt$_2$Me$_2$)(N$_2$) was not observed in this experiment are that the rate at which the insoluble photoproduct forms is much faster than dinitrogen coordination or that the expected product is simply unstable. Thus, to probe these hypotheses, the experiment was repeated under 200 psi of H$_2$. The increased electron density on **1-CO** could favour the

formation of manganese dihydrogen or hydride species, which may be expected to be more stable than Mn-N_2 species. However, when the experiment was performed under a hydrogen atmosphere, binding of H_2 was not observed and results very similar to those for N_2 were obtained, with just loss of the parent bands and no new product bands produced.

2.6.2 Fast TRIR analysis of Cp'Mn(CO)$_2$(PPh$_3$) / Cp'Mn(CO)$_2$(IEt$_2$Me$_2$) in *n*-heptane under 2 atmospheres of CO at 298 K.

In order to further investigate and elucidate the photochemistry of **PPh_3** and **1** the complexes were examined with fast TRIR. Previous work examining the photochemistry of related phosphine complexes has been limited to analysis with FTIR spectroscopy. However, the highly reactive photoproducts that are formed by irradiation of these species tend to be stabilised by solvation or other interactions so quickly that the 'naked' fragments are undetectable by even the fastest spectroscopic methods. The TRIR spectrum obtained 1 ns after 355 nm photolysis of **PPh_3** in *n*-heptane under 2 atm. of CO showed bleaching of the parent bands at 1940 and 1879 cm^{-1} and formation of three new ν(CO) bands at 1839, 1889 and 1956 cm^{-1} (Figure 23).

The spectrum obtained after a longer delay (1 μs) showed that the band at 1839 cm^{-1} had decayed and the parent bands partially reformed, while the bands at 1889 cm^{-1} and 1956 cm^{-1} remained. The bands at 1889 cm^{-1} and 1956 cm^{-1} had been previously assigned to the dicarbonyl alkane complex Cp'Mn(CO)$_2$(heptane).[6,7] By extension, the band at 1839 cm^{-1} was assigned initially to the monocarbonyl phosphine analogue, Cp'Mn(CO)(PPh_3)(heptane). The TRIR analysis confirmed that **PPh_3** undergoes two separate primary photolytic events, either loss of CO (**PPh_3-CO**) or loss of PPh_3 (**PPh_3-PPh_3**). The decay of the proposed Cp'Mn(CO)(PPh_3)(heptane) complex was measured by monitoring the reaction with CO (k_{obs} = 6 (± 0.2) x 10^6 s^{-1}), and occurs at the same rate as the parent reforms (k_{obs} = 5.5 (± 0.5) x 10^6 s^{-1}). If **PPh_3-CO** existed as a 'naked' fragment it would be expected to react with CO under diffusion control. However, the rate of decay for the band at 1839 cm^{-1} is roughly 1 μs slower than the diffusion limit, indicating that **PPh_3-CO** has been stabilised in

some way. This slower rate of reaction provides good evidence for assignment of the band to the alkane complex, Cp'Mn(CO)(PPh_3)(heptane). Cp'Mn$(CO)_2$(heptane) also decays by reaction with CO much more slowly, over *ca*. 25 μs to produce Cp'Mn$(CO)_3$, which has characteristic bands at 1945 cm^{-1} and 2021 cm^{-1} in *n*-heptane.

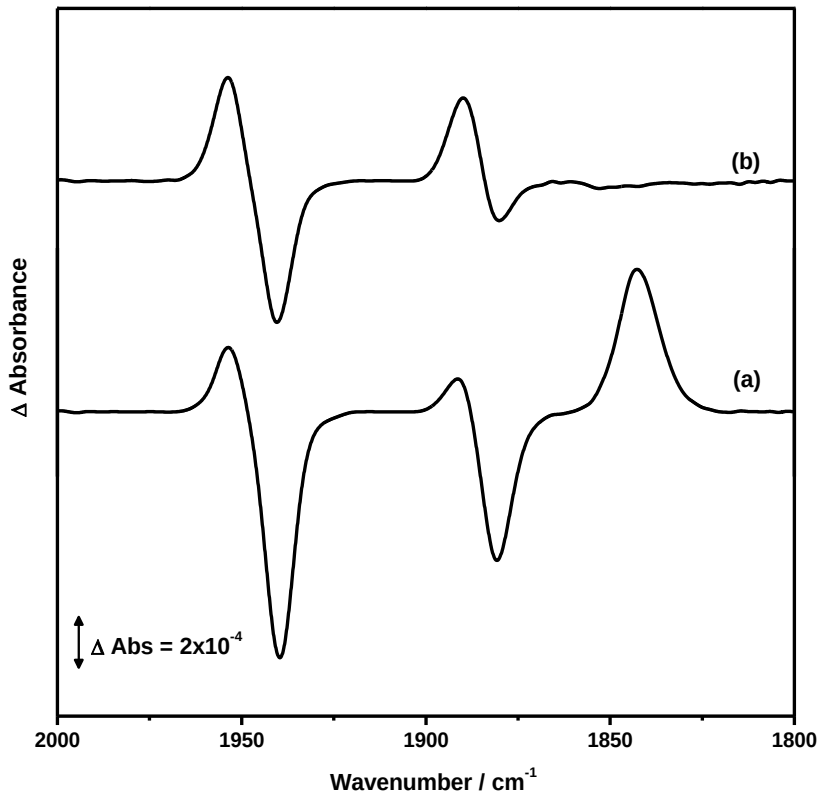

Figure 23: TRIR spectra obtained (a) 1 ns and (b) 1 μs after 355 nm photolysis of Cp′Mn$(CO)_2$(PPh_3) in *n*-heptane under 2 atm. of CO.

The TRIR spectrum of **1,** under analogous conditions, showed bleaching of the parent bands at 1914 cm^{-1} and 1849 cm^{-1} and formation of one new ν(CO) band at 1820 cm^{-1} (Figure 24). This new transient was initially assigned to the monocarbonyl alkane complex, Cp'Mn(CO)(IEt_2Me_2)(heptane), by comparison to the results obtained with **PPh_3**. Since this species is the sole detectable product it also indicates CO loss (**1-CO**) as the only primary photo process for Cp'Mn$(CO)_2$(IEt_2Me_2), consistent with the results obtained using step-scan FTIR in the presence of dinitrogen and dihydrogen. The ν(CO) band at 1820 cm^{-1} decayed fully by reaction with CO to reform the parent (k_{obs} = 7.9 x 10^6 s^{-1}) (Figure 25).

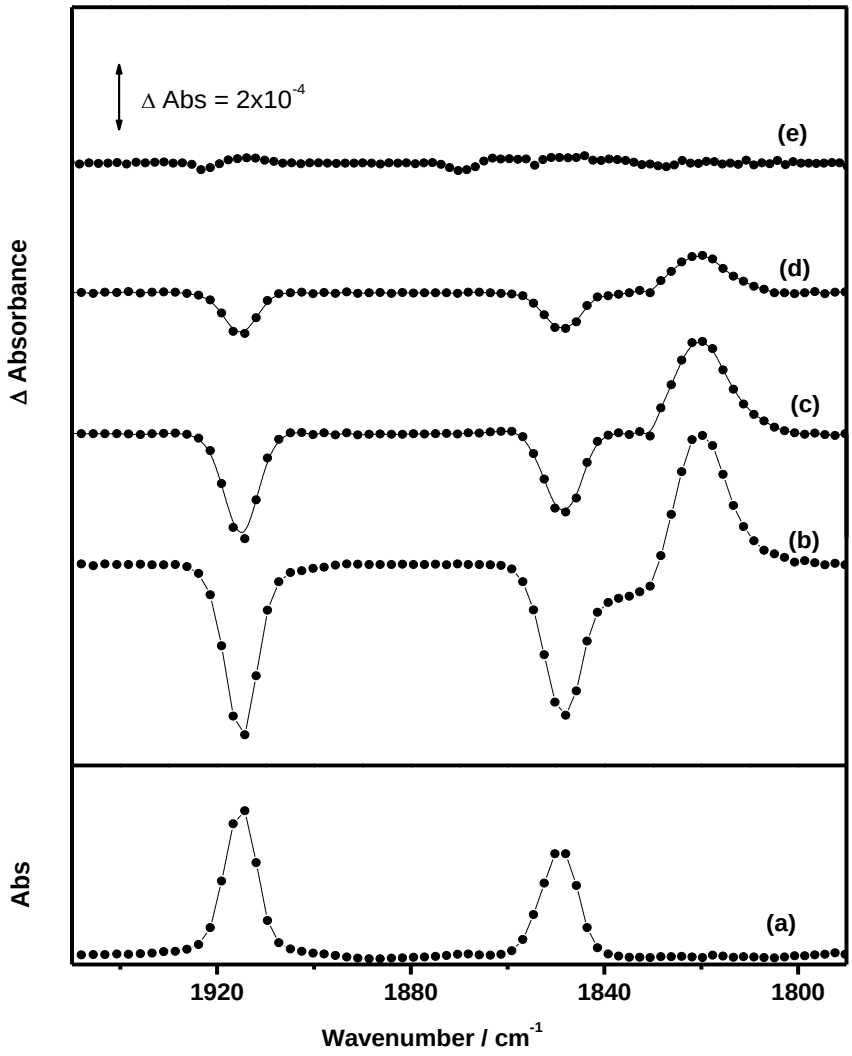

Figure 24: (a) FTIR ground state spectrum of Cp′Mn(CO)$_2$(IEt$_2$Me$_2$) (1) in *n*-heptane. TRIR spectra after 355 nm photolysis at 298 K, collected at various time delays after the laser pulse, (b) 5 ns, (c) 5 µs, (d) 10 µs and (e) 20 µs.

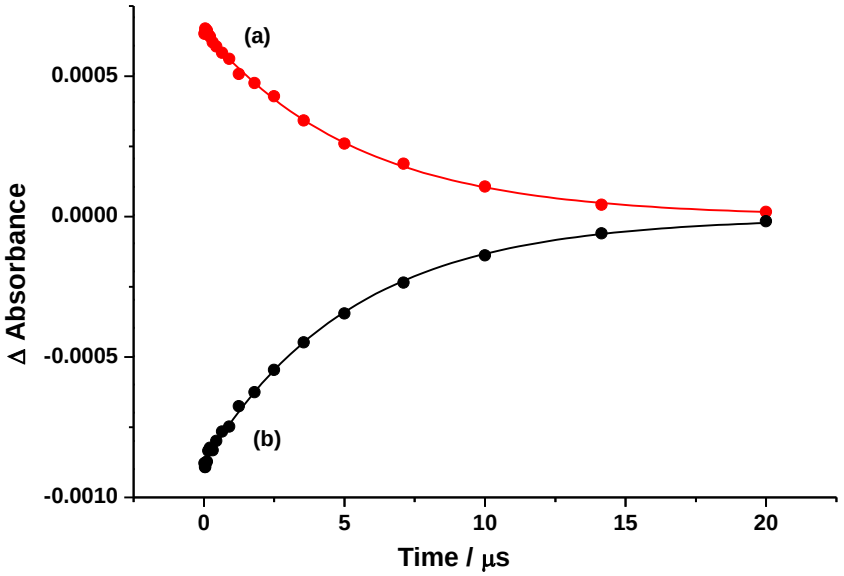

Figure 25: TRIR kinetic trace recorded following irradiation (355 nm) of Cp′Mn(CO)$_2$(IEt$_2$Me$_2$) (1) in *n*-heptane under 2 atm. of CO showing (a) the decay of the band at 1820 cm^{-1} and (b) full recovery of the parent complex.

2.6.3 Fast TRIR analysis of Cp'Mn(CO)$_2$(PPh$_3$) and 1 in *n*-heptane under N$_2$ at 298 K.

The same TRIR experiment was repeated under an atmosphere of N_2 to examine the fate of **1-CO** under such conditions. Along with the formation of the previously assigned complex, Cp'Mn(CO)(IEt$_2$Me$_2$)(heptane) at ν(CO) of 1820 cm^{-1}, an additional ν(CO) band at 1922 cm^{-1} is produced with a lifetime of 34 μs (Figure 26). The identity of this band is unclear although it is tempting to assign it to the terminal ν(CO) of a dimer akin in structure to that proposed by Poliakoff *et al*. However, there are two clear issues. There was no evidence for bridging ν(CO) at lower frequencies (*ca*. 1650 cm^{-1}) which would presumably also be present, but perhaps most importantly, the red by-product is known to be completely insoluble in *n*-hexane. Thus, it is possible that the band at 1922 cm^{-1} is from an intermediate on the way to dimer formation, although the exact nature of this species remains unknown.

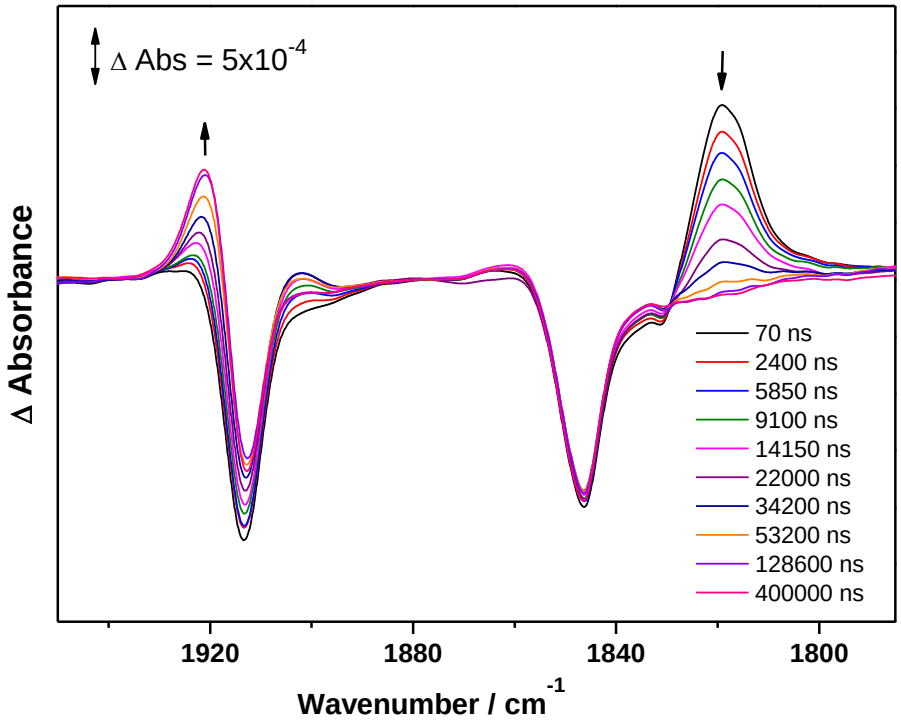

Figure 26: TRIR spectra of Cp′Mn(CO)$_2$(IEt$_2$Me$_2$) (1) recorded after 355 nm photolysis in *n*-heptane under 2 atm. of nitrogen at 298 K.

2.7 TRIR analysis of Cp'Mn(CO)$_2$(NHC) *vs*. Cp'Mn(CO)$_2$(PPh$_3$) in *n*-heptane and cyclopentane under various pressures of CO.

To enhance the comparison of **1** and **PPh$_3$** and probe the nature of the intermediates involved, TRIR measurements were performed on Cp'Mn(CO)$_2$(NHC) (NHC = IMes (**2**), I^{i}Pr$_2$Me$_2$ (**3**) and IPr (**4**)). In each case, photolysis in *n*-heptane solution gave formation of a single transient species, initially believed to be of the form Cp'Mn(CO)(NHC)(heptane), again by comparison to the results obtained with **PPh$_3$**. In order to further investigate the nature of these transients species, k_{obs} was measured as a function of CO concentration in both *n*-heptane and cyclopentane. A linear relationship was determined and fitted in Origin^{TM} with a polynomial expression. The second order rate constants were obtained from the gradient of the line (shown for **1** in Figure 27) and the errors were estimated based on the deviation of the data from the linear fit. The k_{CO} values obtained from the analysis of complexes **1**-**4** and **PPh$_3$** in both *n*-heptane and cyclopentane are shown in Table 3 (page 54).

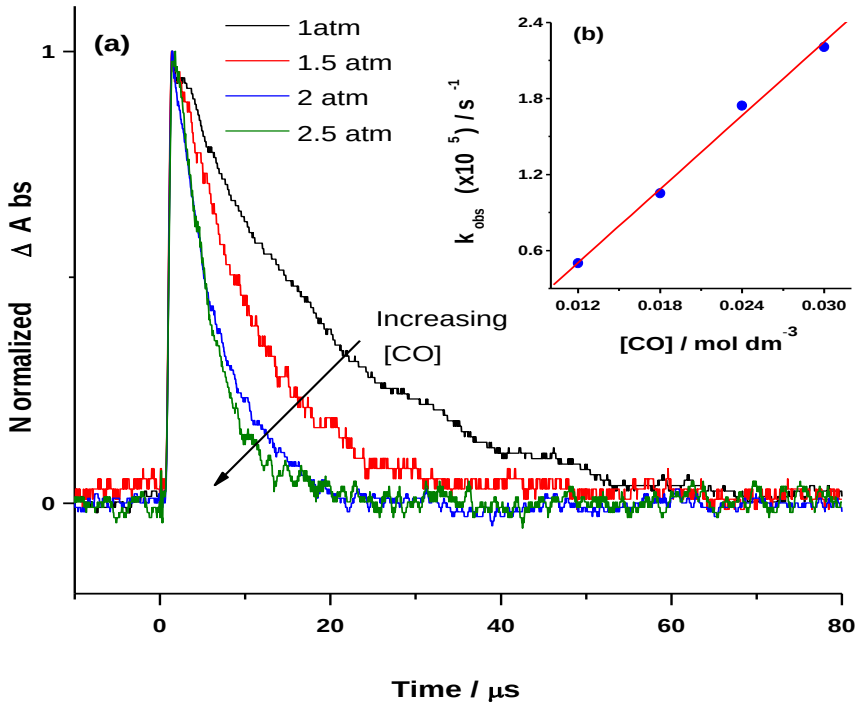

Figure 27: (a) TRIR kinetic traces showing the decay of the band at 1820 cm^{-1} for 1 in *n*-heptane and (b) plot of k_{obs} *vs*. [CO] at 298 K.

	k_{CO} $M^{-1}s^{-1}$	
Intermediate	***n*-heptane**	**cyclopentane**
[Cp′Mn(CO)$_2$] (**PPh$_3$-PPh$_3$**)	1.7 (± 0.3) x 10^6	9.4 (± 0.6) x 10^5
[Cp′Mn(CO)(PPh$_3$)] (**PPh$_3$-CO**)	3.3 (± 0.3) x 10^8	3.5 (± 0.6) x 10^8
[Cp′Mn(CO)(IEt$_2$Me$_2$)] (**1-CO**)	9.7 (± 0.5) x 10^6	9.7 (± 0.8) x 10^6
[Cp′Mn(CO)(IMes)] (**2-CO**)	5.6 (± 0.3) x 10^6	6.4 (± 0.7) x 10^6
[Cp′Mn(CO)(I^{i}Pr$_2$Me$_2$)] (**3-CO**)	8.1 (± 0.2) x 10^6	8.1 (± 0.7) x 10^6
[Cp′Mn(CO)(IPr)] (**4-CO**)	6.6 (± 0.3) x 10^6	7.2 (± 0.3) x 10^6

Table 3: The k_{CO} rate constants determined from TRIR analysis.

The results above (Table 3) immediately showed something unexpected. The lifetimes of the transients measured in *n*-heptane and cyclopentane for **PPh$_3$** and compounds **1**-**4** are within experimental error, effectively remaining unchanged between different alkanes. Metal alkane complexes typically vary significantly in stability and lifetime between different alkanes.[6,8,9] This can be verified simply by looking at the lifetime observed for Cp'Mn(CO)$_2$(alkane),

which changes by a factor of *ca*. two between *n*-heptane and cyclopentane (Table 3, page 54). Combined with the results from photolysis under dinitrogen and dihydrogen for **PPh_3** and complexes **1**-**4**, which revealed σ-coordination only to [Cp'Mn$(CO)_2$], this forced re-evaluation of the nature of the transient species observed. It was initially unclear what species could fit the experimental data until the possibility of agostic stabilised intermediates was revisited.

It was not possible to distinguish between Cp'Mn(CO)(NHC') (' = ligand involved in agostic bond) and Cp'Mn(CO)(NHC)(alkane), or the analogous phosphine species, using the TRIR data alone. As such, DFT calculations were undertaken in collaboration with Prof. Stuart Macgregor at Herriot-Watt University, who was able to model the potential agostic stabilised intermediates produced by photolysis of the compounds **PPh_3**, **1** and **2**.[#] These calculations revealed the putative agostic species to be of lower energy than the alkane complexes, and thus gives strong evidence for the formation of agostic stabilised species, Cp'Mn(CO)(NHC') and Cp'Mn(CO)(PPh_3'), upon photolysis of the parent compounds. This theory corroborates the solvent independence of the k_{CO} values obtained for the NHC and phosphine intermediates.

The DFT calculations showed that the agostic bonding was to an *ortho*-methyl group in **2-CO**, an *ortho*-C-H bond of one of the phenyl groups on the phosphine in **PPh_3-CO** and involved the ethyl substituent in **1-CO**. These interactions were characterised by short Mn···H contacts (**PPh_3-CO**: 1.88 Å, **2-CO**: 1.75 Å; **1-CO**: 1.79 Å) and elongation of the C-H bond interacting with the metal centre (**PPh_3-CO**: 1.13 Å, **2-CO**: 1.17 Å; **1-CO**: 1.15 Å). The optimised structures for the modelled agostic and cyclopentane species for **PPh_3** and **1** are shown in Figure 28. Initial inspection of the calculations seemed to suggest that the distances calculated for **PPh_3-CO** are indicative of a weaker agostic interaction than was found for the NHC analogues. However, it must also be kept in mind that the agostic interaction for **PPh_3-CO** involves an sp^2 hybridised carbon, whereas for **1-CO** and **2-CO** it is sp^3 hybridised, and as such may impact upon direct comparison of the bond lengths calculated here.

[#] See page 150 for experimental information.

Nonetheless, the proposed weaker agostic interaction for **PPh_3-CO** was confirmed by the experimental data obtained from the TRIR experiments, which found a significantly higher k_{CO} for **PPh_3-CO** than for either **1-CO** or **2-CO**.

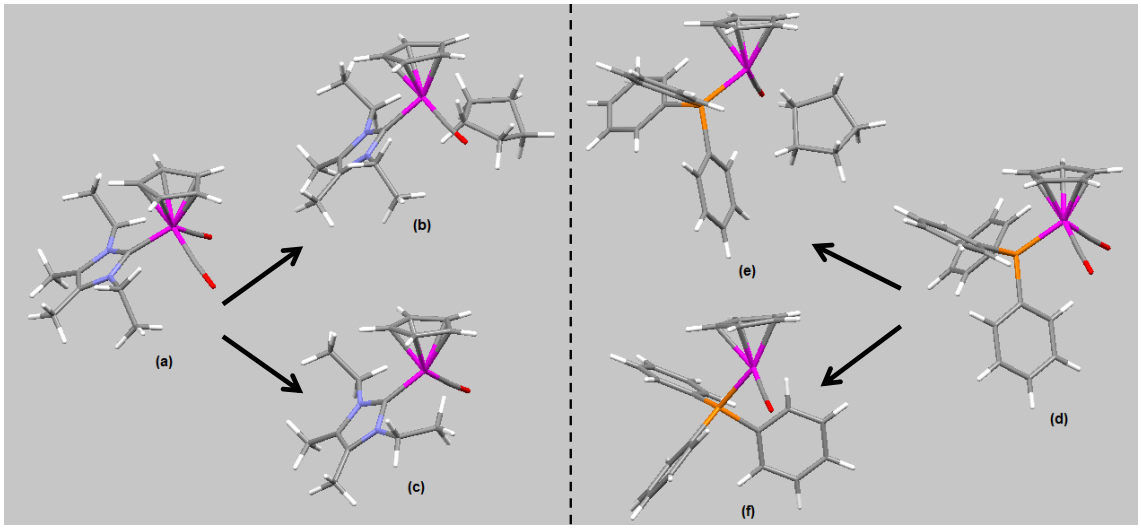

Figure 28: The optimised structures for the DFT modelled species, (a) 1, (b) 1-CO with cyclopentane, (c) 1-CO, (d) PPh_3, (e) PPh_3-CO with cyclopentane and (f) PPh_3-CO.

It is interesting to debate the steric and electronic effects that may cause the differences in structure and reactivity between the intermediates observed. Table 3 (page 54) shows that Cp'Mn$(CO)_2$(heptane) has by far the longest lifetime (22 μs). This complex can be regarded as the most electron deficient and least sterically shielded of the series, yet is also the only alkane complex present. At the other end of the spectrum is the weakest of the agostic stabilised species, Cp'Mn(CO)(PPh_3'), the lifetime of which is much shorter (170 ns), yet the electron density has increased and the steric shielding is much greater. The agostic intermediates for the NHC compounds **1**-**4** have lifetimes between these extremes, though the electron density has been significantly increased. However, there is also a slight steric variation observable as the lifetimes are shortest for the smallest NHCs and follow this trend; IEt_2Me_2 < $I^iPr_2Me_2$ < IPr ≤ IMes.

The reason an agostic stabilised intermediate should form over an alkane species in this case is difficult to rationalise purely from an electronic or steric perspective. However, the DFT calculations were extended to include the

interaction energies between [Cp'Mn(CO)$_2$], **PPh$_3$-CO** and **1-CO** with methane ([Cp'Mn(CO)$_2$]: -7.1 kcal mol^{-1}, **PPh$_3$-CO**: -1.9 kcal mol^{-1} and **1-CO**: +2.6 kcal mol^{-1}). It is clear from these values that alkane complexation appears to be disfavoured by phosphine substitution and further so by inclusion of NHC ligands. This is likely to be predominantly caused by an electronic effect as the electron density on the metal centre is increased following this order; [Cp'Mn(CO)$_2$] << [Cp'Mn(CO)(PPh$_3$)] < [Cp'Mn(CO)(NHC)]. Although clearly whether such species could form alkane complexes or not is precluded by the presence of ligands capable of agostic stabilisation in this case.

2.8 Efforts to prepare CpRe(CO)$_2$(NHC).

Having been able to synthesise, characterise and examine the photochemistry of this new family of manganese (I) NHC complexes, it was highly desirable to extend the investigation to the rhenium (I) analogues. As often the CpRe(CO)$_2$(L) systems are more stable, for example, they typically form much longer lived alkane complexes in comparison to their manganese analogues.[10] In fact, CpRe(CO)$_2$(PF$_3$) forms alkane complexes with cyclopentane and heptane which are so stable that their lifetimes at low temperature are sufficient for NMR studies.[11] It was possible to produce CpRe(CO)$_2$(IEt$_2$Me$_2$) in solution, as detected by IR (v(CO) in CH$_2$Cl$_2$: 1891 and 1817 cm^{-1}), using the same techniques for preparation of the manganese analogues. From this solution, a small number of serendipitous crystals were isolated (Figure 29). However, concentration and work up of the reaction mixture invariably led to a plethora of undetermined products from which the desired complex could not be isolated. This is clearly illustrated by the ^{1}H NMR spectrum of a sample following photolysis (Figure 30). Comparison of the IR spectrum obtained with the phosphine analogue CpRe(CO)$_2$(PPh$_3$) (v(CO) in CH$_2$Cl$_2$: 1925 and 1855 cm^{-1}) showed a similar reduction in wavenumber of the v(CO) bands for CpRe(CO)$_2$(IEt$_2$Me$_2$), as was seen for **1**-**4**.[12]

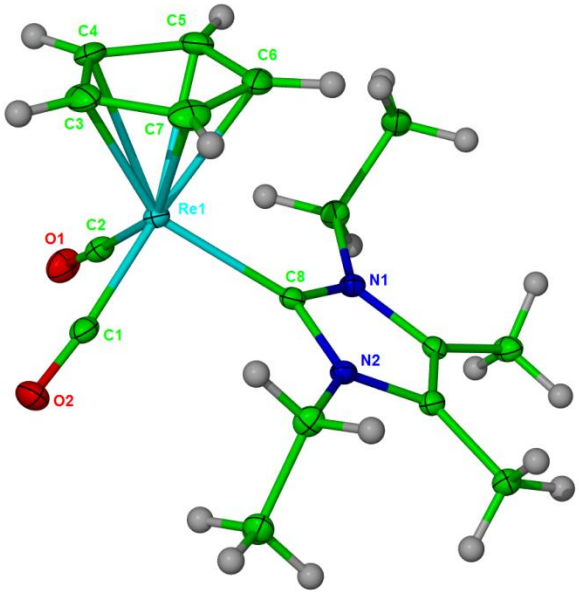

Figure 29: X-ray crystal structure of $CpRe(CO)_2(IEt_2Me_2)$, ellipsoids shown at 30%.

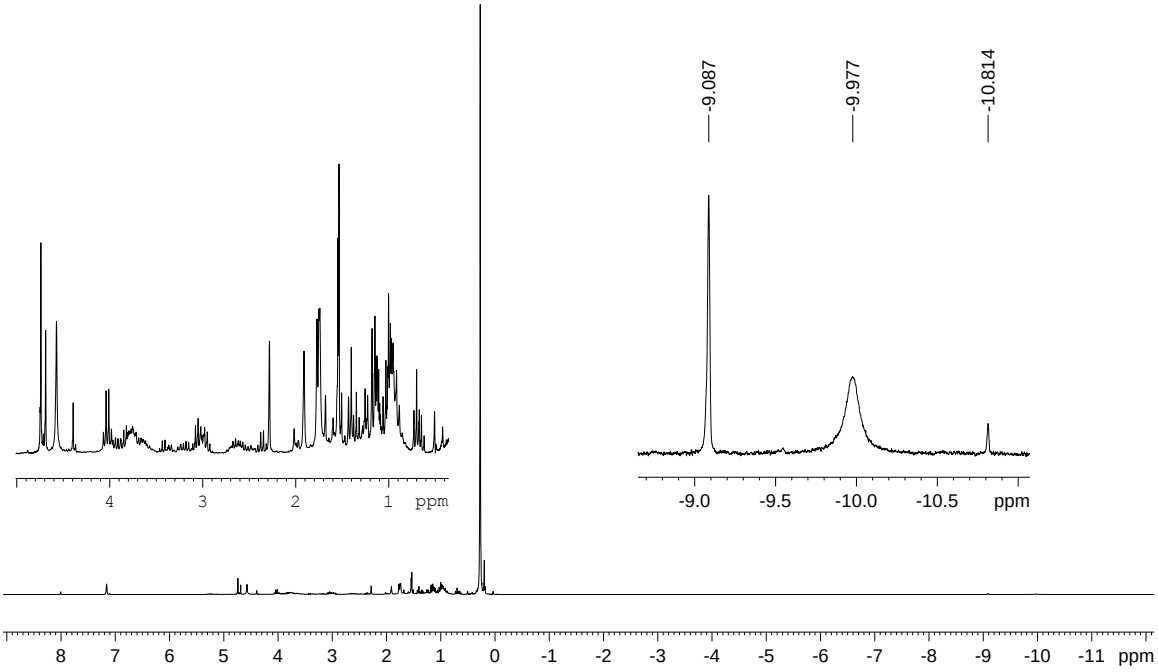

Figure 30: 500 MHz ^{1}H NMR spectrum after concentration and extraction of $CpRe(CO)_2(IEt_2Me_2)$ in C_6D_6 at 298 K.

It is not immediately obvious why $CpRe(CO)_2(IEt_2Me_2)$ should be so unstable in solution, particularly as it becomes more concentrated. However, the ^1H NMR (Figure 30) showed evidence for several low frequency signals which are typical of hydridic environments. It is possible that moving from manganese to rhenium has not only increased the compound's light sensitivity, but also the affinity of the CO loss product towards stabilisation from the NHC, although in the case of rhenium the interaction goes further than agostic binding and on to C-H activation of the NHC. Unfortunately, this remains speculation, although it could explain the presence of hydridic signals in the ^1H NMR and the highly challenging isolation of $CpRe(CO)_2(IEt_2Me_2)$ from solution.

2.9 Conclusions.

Several new photoactive NHC containing manganese complexes were synthesised and the photochemistry of $Cp'Mn(CO)_2(IEt_2Me_2)$ (**1**), $Cp'Mn(CO)_2(IMes)$ (**2**), $Cp'Mn(CO)_2(I^iPr_2Me_2)$ (**3**) and $Cp'Mn(CO)_2(IPr)$ (**4**) investigated and compared with the analogous phosphine complex, $Cp'Mn(CO)_2(PPh_3)$ (**PPh_3**). Throughout the photolysis experiments there has been no evidence for loss of an NHC ligand as a primary photoprocess in any of the complexes tested, all of which instead lose CO upon photolysis. This is in marked contrast to the phosphine analogues, which lose both PR_3 and CO. The implication that M-NHC bonds may be stable to irradiation is immediately apparent when compared to the growing use of NHCs in many thermal, homogeneous, transition metal catalysts. For some time now the improved thermal stability of M-NHC bonds have made NHCs desirable replacements to phosphines in well-known catalysts, in some cases resulting in new catalysts that can withstand much more arduous conditions and improving catalyst lifetimes and turnover numbers by being more resistant to degradation reactions.

A long-standing aim of organometallic photochemistry has been the photolytic generation of highly reactive transient species, which could potentially then be used as *in situ* homogeneous catalysts for a variety of thermal transformations. Such an application would require a very clean photolytic initiation step. Often

CO loss or H_2 elimination is used, but many potential catalyst precursors contain PR_3, which can also be removed under photolysis. This leads to complex and possibly unwanted reactions, as more than one reactive species can be generated during initiation.

Using NHCs in place of phosphines could yield much cleaner initiation steps for metal carbonyl or dihydrogen photocatalysts, as well as the subsequent benefits NHCs often bestow in homogeneous catalysis. From a catalyst design perspective it would be very useful to have M-NHC bonds that are effectively unbreakable both thermally and photolytically, potentially helping to maintain activity throughout the reaction and the wide range of conditions that modern catalysts are expected to be able to function under.

Previous FTIR spectroscopy studies on **PPh_3** were insufficient to fully elucidate the photochemistry of the compound. The TRIR spectroscopy results depicting the coincident lifetimes of the CO loss products of compounds **1**-**4** and **PPh_3** in both *n*-heptane and cyclopentane, combined with the results of the DFT studies, refute the possibility of these species being present in solution as alkane complexes. Whilst the TRIR studies are not a conclusive method to prove that these species truly exist as agostic stabilised complexes, the results of the DFT studies combined with literature comparison, demonstrate that it is a reasonable supposition. It would be very interesting indeed for any future work in this area to examine the photochemistry of complexes with phosphine or NHC ligands that have been designed to be incapable of forming agostic stabilised complexes upon loss of CO.

Above all else, the tentative, but most insightful implication of these results is that whilst NHCs and phosphines may have many strong similarities as ligands, there are a number of subtle and intriguing nuances to be found, and that for NHCs at least, they remain largely undetermined. This is particularly true in the realm of organometallic photochemistry. For further incentive, investigation of this area has already increased our understanding of established photoactive organometallic systems, such as $Cp'Mn(CO)_2(PPh_3)$. This work has only scratched the surface of organometallic NHC photochemistry, as evidenced by

the unexplained behaviour of $CpRe(CO)_2(IEt_2Me_2)$, and it can only be hoped that further work will be undertaken in this area, which should lead to an interesting future.

2.10 References.

(1) Burrows, A.; *Second year Inorganic Lab Manual*; University of Bath, **2000**.

(2) Zaworotko, M. J.; Shakir, R.; Atwood, J. L.; Sriyunyongwat, V.; Reynolds, S. D.; Albright, T. A.; *Acta Cryst. B* **1982**, *38*, 1572-1574.

(3) Creaven, B. S.; Dixon, A. J.; Kelly, J. M.; Long, C.; Poliakoff, M.; *Organometallics* **1987**, *6*, 2600-2605.

(4) Geoffroy, G. L.; Wrighton, M. S.; *Organometallic Photochemistry*; Academic Press Inc, **1980**.

(5) Banister, J. A.; George, M. W.; Grubert, S.; Howdle, S. M.; Jobling, M.; Johnson, F. P. A.; Morrison, S. L.; Poliakoff, M.; Schubert, U.; Westwell, J. R.; *J. Organomet. Chem.* **1994**, *484*, 129-135.

(6) Childs, G. I.; Colley, C. S.; Dyer, J.; Grills, D. C.; Sun, X.-Z., Yang, J.; George, M. W.; *J. Chem. Soc., Dalton Trans.* **2000**, 1901-1906.

(7) Childs, G. I.; Grills, D. C.; Sun, X. Z.; George, M. W.; *Pure. Appl. Chem.* **2001**, *73*, 443–448.

(8) Cowan, A. J.; George, M. W.; *Coord. Chem. Rev* **2008**, *252*, 2504-2511.

(9) Calladine, J. A.; Duckett, S. B.; George, M. W.; Matthews, S. L.; Perutz, R. N.; Torres, O.; Vuong, K. Q.; *J. Am. Chem. Soc.* **2011**, *133*, 2303-2310.

(10) Calladine, J. A.; Torres, O.; Anstey, M.; Ball, G. E.; Bergman, R. G.; Curley, J.; Duckett, S. B.; George, M. W.; Gilson, A. I.; Lawes, D. J.; Perutz, R. N.; Sun, X.-Z.; Vollhardt, K. P. C.; *Chem. Sci.* **2010**, *1*, 622.

(11) Ball, G. E.; Brookes, C. M.; Cowan, A. J.; Darwish, T. A.; George, M. W.; Kawanami, H. K.; Portius, P.; Rourke, J. P.; *Proc. Nat. Acad. Sci. USA.* **2007**, *104*, 6927 -6932.

(12) Yang, G. J.; Bergman, R. G.; *Organometallics*, **1985**, *4*, 129-138.

Chapter 3

3.1 NHC substituted rhenium (I) diimine tricarbonyl species: Exploring the influence of NHCs on photochemical and photophysical properties.

An active area in modern coordination chemistry is the utilisation of luminescent d^6 metal-diimine complexes, which typically have charge separated excited states, in a range of photo- or electrochemical applications.[1] The applications are numerous, spanning use as DNA, cell or imaging probes to dyes for light harvesting in solar cells and photocatalysts.[2,3,4] The vast majority of this research is based on the more prevalent ruthenium (II) diimine complexes, such as $[Ru(Bpy)_2(MeCN)_2]^{2+}$.[5,6,7] However, the rhenium (I) tricarbonyl diimines, such as $Re(Bpy)(CO)_3Cl$, have also been investigated and typically have simpler photochemistry, as only one diimine ligand is available for excited state charge localisation. As such, this research aims to expand upon the work started by Xue *et al* and synthesise a larger range of NHC substituted rhenium (I) tricarbonyl diimines.[8] The intention is then to study these species with TRIR spectroscopy.

3.2 Synthesis of $[Re(NHC)(Bpy)(CO)_3]X$.

Many phosphine analogues of the target compounds exist in the literature.[9] As such, substitution of phosphine for NHC in a literature synthesis was attempted as the first route to the synthesis of $[Re(NHC)(Bpy)(CO)_3]^+$ (Figure 31).

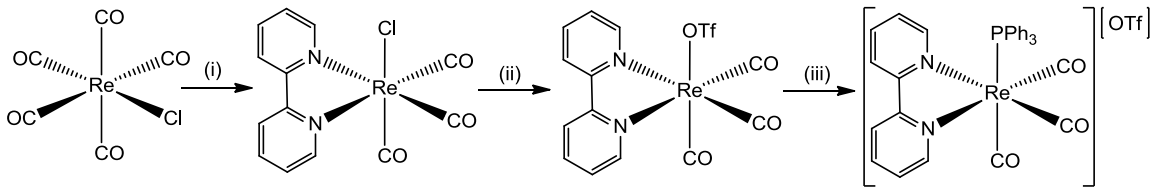

(i) 2 eq. Bpy, C_6H_6, 343 K, 2 h. (ii) AgOTf, CH_2Cl_2, RT, O/N (iii) 30 eq. PPh_3, CH_2Cl_2, 343 K, O/N

Figure 31: Literature preparation for $[Re(PPh_3)(Bpy)(CO)_3]OTf$.

Step (iii) is where the phosphine is introduced to the metal centre by displacement of the relatively weak Re triflate bond. However, as can be seen from Figure 31, this step requires rather forcing conditions and, in addition, is only low yielding. Nonetheless, addition of IEt_2Me_2 and $I^iPr_2Me_2$ was tried at this stage of the synthesis and resulted in immediate formation of deep red solutions. The ^1H NMR spectra showed in each case the presence of multiple NHC species, although the only Bpy signals observed corresponded to the free ligand, indicating no formation of NHC diimine species. As such, introduction of the NHC at step (ii) was tried, but again no formation of NHC diimine species was detected. Fortuitously, addition of the NHC at step (i) led directly to clean formation of Re (I) NHC species, as shown in Figure 32. The thermal chemistry of these complexes, their manganese analogues and further derivatives are described in depth in Chapter 5.

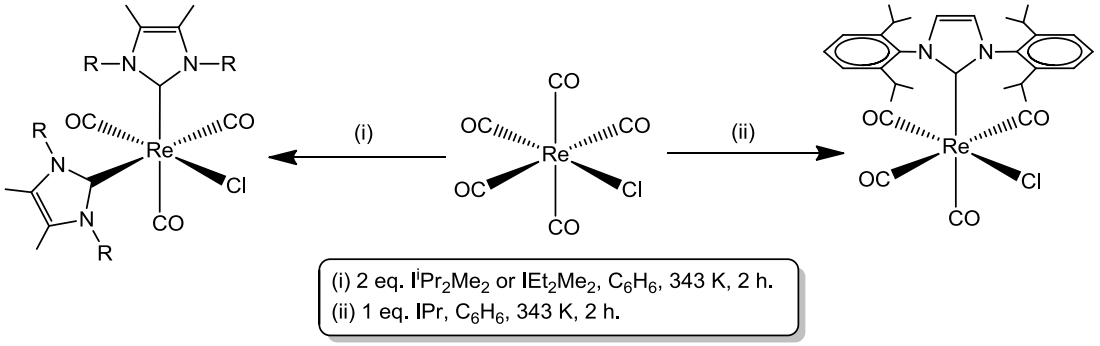

Figure 32: Preparation of $Re(NHC)_n(CO)_{5-n}Cl$.

It was hoped that these compounds would function as useful starting materials for the synthesis of the desired Re (I) diimine tricarbonyl species. Treatment of *cis,fac*-$Re(IEt_2Me_2)_2(CO)_3Cl$ and *cis,fac*-$Re(I^iPr_2Me_2)_2(CO)_3Cl$ with AgOTf in the presence of 2 eq. of Bpy in refluxing dichloromethane led to the formation of the corresponding cationic species *fac*-$[Re(NHC)(Bpy)(CO)_3]OTf$ (NHC = IEt_2Me_2, $I^iPr_2Me_2$) and imidazolium salt over 48 h. It is probable that this reaction occurs *via* displacement of triflate by Bpy, followed by subsequent ejection of the second NHC in the form of imidazolium, presumably aided by the chelation effect. The source of the imidazolium proton and corresponding anion is not immediately clear, although free NHCs are relatively basic and are known to form imidazolium chlorides upon exposure to dichloromethane.[10,11] The N-aryl NHC species *cis*-$Re(IPr)(CO)_4Cl$ did not form the desired

fac-[Re(IPr)(Bpy)$(CO)_3$]OTf under these conditions. However, its formation was possible by treatment of *cis*-Re(IPr)$(CO)_4$Cl with AgOTf in the presence of 2 eq. of Bpy in refluxing ODB at 393 K for 48 h. The higher temperature presumably helps to labilise the CO ligand that is lost.

An alternative method for synthesis of *fac*-[Re(NHC)(Bpy)$(CO)_3$]X involved reaction of Re(IPr)$(CO)_4$Cl with excess Bpy in the absence of any solvent at 423 K, which gave *fac*-[Re(IPr)(Bpy)$(CO)_3$]Cl in almost quantitative yield. This route proved to be unsuccessful for the preparation of *fac*-[Re(NHC)(Bpy)$(CO)_3$]X (NHC = IEt_2Me_2, $I^iPr_2Me_2$). The reaction schemes are depicted in Figures 33 and 34.

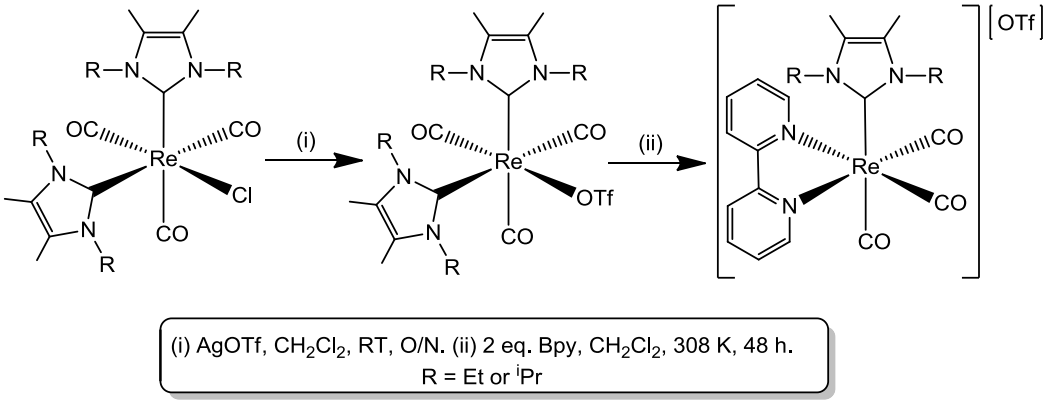

(i) AgOTf, CH_2Cl_2, RT, O/N. (ii) 2 eq. Bpy, CH_2Cl_2, 308 K, 48 h.
R = Et or ^{i}Pr

Figure 33: Formation of *fac*-[Re(NHC)(Bpy)$(CO)_3$]OTf (NHC = IEt_2Me_2, $I^iPr_2Me_2$).

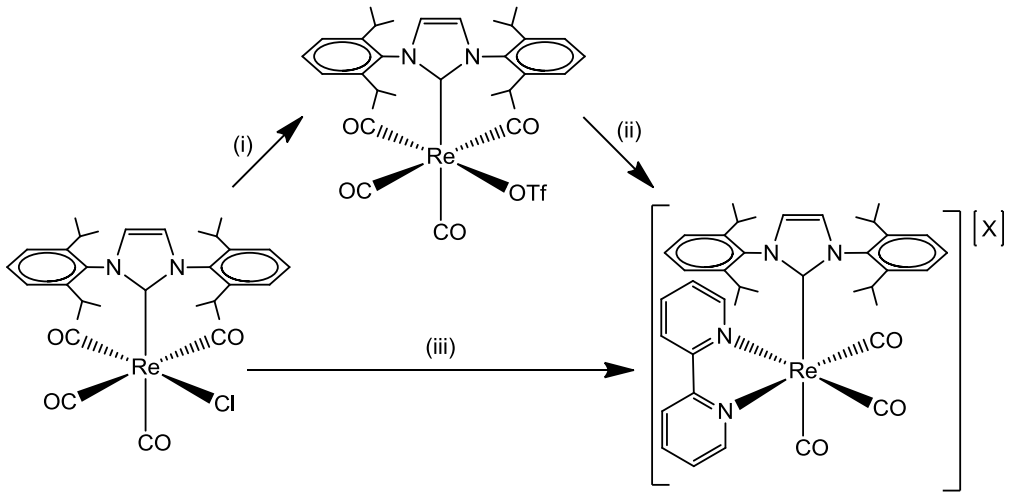

(i) AgOTf, ODB, RT, O/N. (ii) 2 eq. Bpy, ODB, 393 K, 48 h. (iii) 10 eq. Bpy, 423 K, 24 h.
X = OTf for (i)/(ii) and Cl for (iii).

Figure 34: Formation of *fac*-[Re(IPr)(Bpy)$(CO)_3$]X.

Despite the ease of synthesis of *fac*-[Re(NHC)(Bpy)$(CO)_3$]OTf (NHC = IEt_2Me_2, $I^iPr_2Me_2$), removal of the imidazolium salt was problematic. Slow recrystalisation from CH_2Cl_2/hexane afforded crystals of *fac*-[Re(IEt_2Me_2)(Bpy)$(CO)_3$]OTf, but alongside imidazolium, as shown by the corresponding ^{1}H NMR spectrum (Figure 35). As such, a number of other metal salts were tried for halide abstraction, including $NaBPh_4$, $AgBF_4$, KPF_6 and $NaBAr_4^F$.

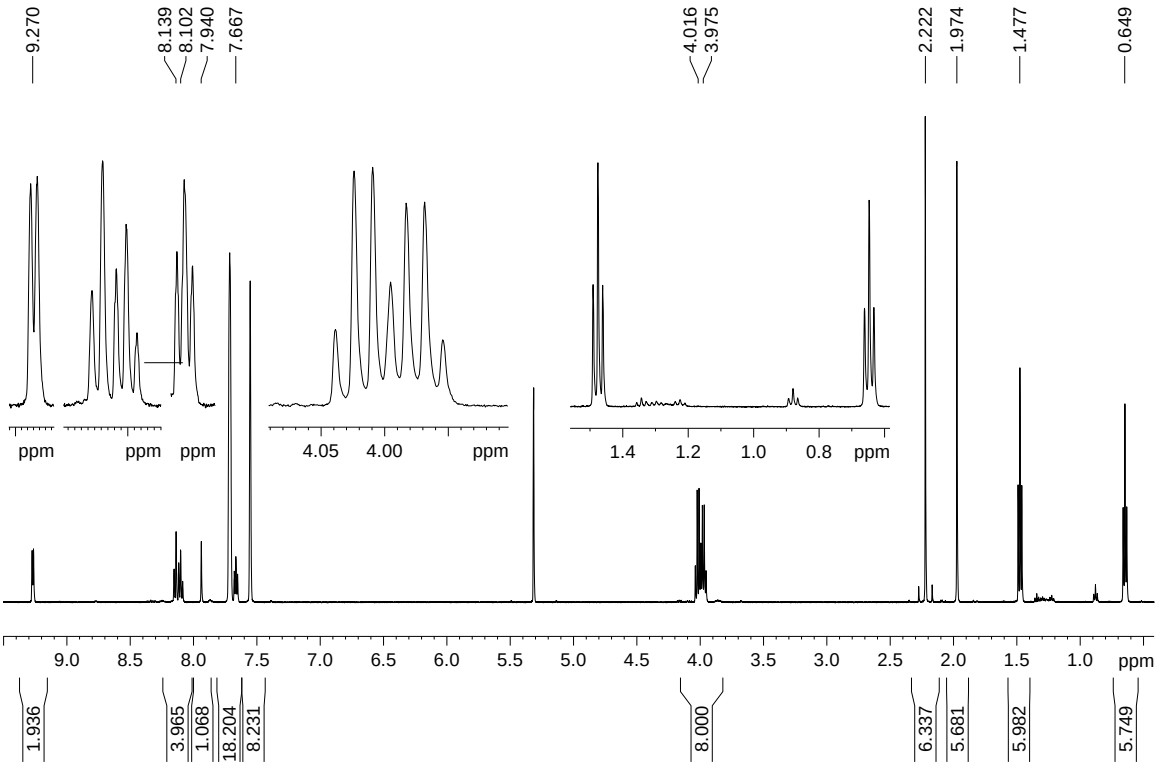

Figure 35: 500 MHz ^{1}H NMR spectrum of *fac*-[Re(IEt_2Me_2)(Bpy)$(CO)_3$]BAr_4^F (5) in CD_2Cl_2 at 298 K.

The silver and sodium salts appeared to result in halide abstraction from *cis*-Re$(NHC)_2(CO)_3Cl$ (NHC = IEt_2Me_2, $I^iPr_2Me_2$), but no reaction was observed with KPF_6. None of the successful halide abstraction reagents gave *fac*-[Re(NHC)(Bpy)$(CO)_3$]X (NHC = IEt_2Me_2, $I^iPr_2Me_2$) in particularly high yields or, crucially, without formation of >1 equiv. of imidazolium salt. The most promising of the halide abstraction reagents found was $NaBAr_4^F$ (Figure 36), which under the same conditions used for AgOTf gave the desired complex and one equivalent of imidazolium salt, in an almost quantitative yield according to ^{1}H NMR spectroscopy.

Products *fac*-[Re(IEt_2Me_2)(Bpy)$(CO)_3$]BAr_4^F (**5**) and *fac*-[Re($I^iPr_2Me_2$)(Bpy)$(CO)_3$]BAr_4^F (**6**) were separated using column chromatography and extracted from the 1st bright yellow band. After slow recrystallisation from CH_2Cl_2/hexane, yellow crystals of **5** (36% yield) and **6** (44% yield) suitable for X-ray crystallography were isolated (Figures 37 and 38).

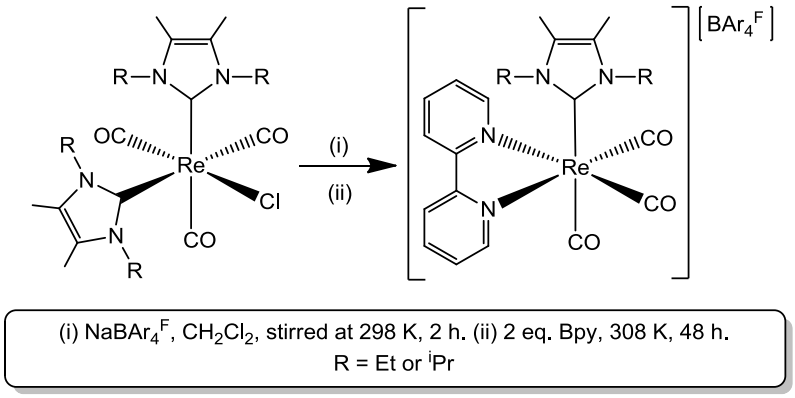

Figure 36: Formation of *fac*-[Re(NHC)(Bpy)$(CO)_3$]BAr_4^F (NHC = IEt_2Me_2, $I^iPr_2Me_2$).

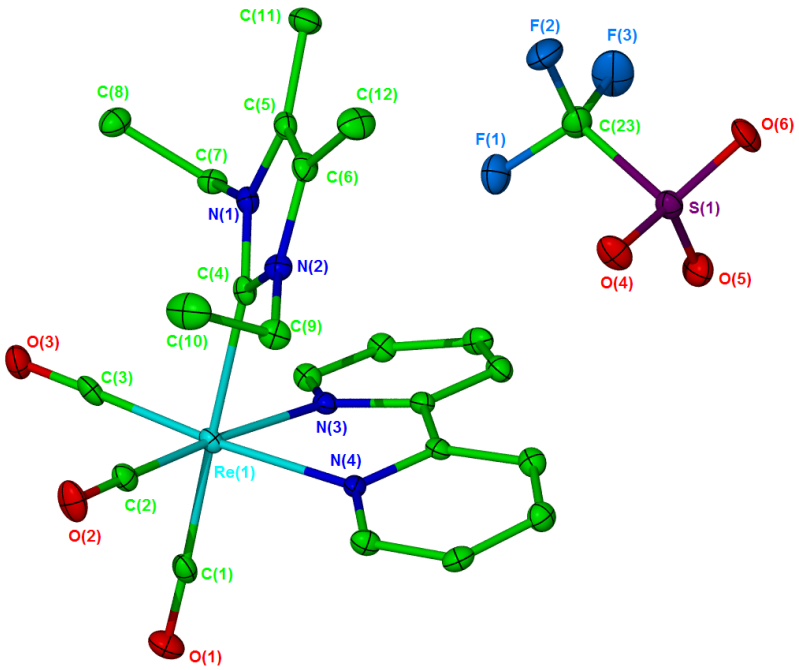

Figure 37: X-ray crystal structure of *fac*-[Re(IEt_2Me_2)(Bpy)$(CO)_3$]OTf. Hydrogen atoms omitted for clarity and ellipsoids shown at 30%.

The crystal structures of the triflate salt of *fac*-[Re(IEt_2Me_2)(Bpy)$(CO)_3$]$^+$ and the BAr_4^F salt of *fac*-[Re($I^iPr_2Me_2$)(Bpy)$(CO)_3$]$^+$ are very similar, with the most obvious perturbation being the deviation from 180° in the bipyridine ligand away from the more bulky $I^iPr_2Me_2$ NHC (18.5°) and towards the less bulky IEt_2Me_2 (15.7°). When viewed with the anion present in the unit cell it can be seen that this deviation is supported by the association between the ions. For *fac*-[Re(IEt_2Me_2)(Bpy)$(CO)_3$]OTf, the triflate anion nestles between the planes of the bipyridine and imidazol rings. In **6** the anion is too large to fill this void and resides away from the NHC between Bpy and CO. Selected bond lengths and angles for **5** and **6** are presented in Table 4 (page 68).

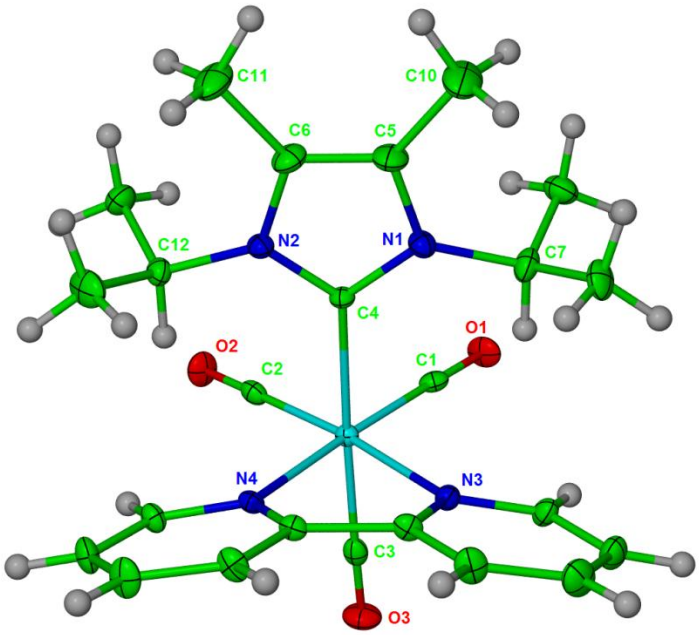

Figure 38: X-ray crystal structure of the cation in *fac*-[Re($I^iPr_2Me_2$)(Bpy)$(CO)_3$]BAr_4^F (6), ellipsoids shown at 30%.

	5	**6**	***fac*-[Re(SIH)(Bpy)(CO)$_3$]ClO$_4$**
Re-NHC	2.224(6)	2.231(4)	2.171(7)
Re-CO$_{trans\ to\ NHC}$	1.931(7)	1.946(5)	1.965(9)
Re-CO$_{trans\ to\ N}$	1.926(6)	1.916(5)	1.917(9)
	1.922(6)	1.909(5)	1.924(9)
Re-N	2.190(4)	2.189(3)	2.178(6)
	2.184(5)	2.194(4)	2.175(6)
NHC-Re-CO	177.6(2)	177.19(18)	178.6(3)
OC-Re-CO	89.0(2)	85.25(19)	89.1(4)
	88.4(2)	88.50(18)	88.4(3)
	85.5(2)	89.16(19)	90.5(3)

Table 4: Selected bond lengths (Å) and angles (°) for the rhenium NHC complexes 5 and 6, alongside those for *fac*-[Re(SIH)(Bpy)(CO)$_3$]ClO$_4$ which were taken from the literature.[8]

Comparison of the selected bond length and angle data illustrates few structural differences between **5** and **6**. The Re-NHC bond lengths are within error, as are the Re-Bpy lengths and OC-Re-CO angles. When contrasted with structural data obtained by Xue *et al*. for *fac*-[Re(SIH)(Bpy)(CO)$_3$]ClO$_4$ the Re-NHC bond length is slightly shorter than found in **5** and **6**.[8] The OC-Re-CO angles and Re-CO lengths are perhaps the most interesting features of these structures. The facial tricarbonyl fragment is slightly compacted for **5** and **6** with angles less than 90°. This not the case for *fac*-[Re(SIH)(Bpy)(CO)$_3$]ClO$_4$ where all the Re-CO angles are much closer to 90°. In **5** and **6**, the Re-CO *trans* to NHC is significantly longer than those *trans* to Bpy, an effect also observed in *fac*-[Re(SIH)(Bpy)(CO)$_3$]ClO$_4$.

The lengthening of the Re-NHC bond and compaction of the *fac*-Re-CO$_3$ fragment for **5** and **6**, relative to *fac*-[Re(SIH)(Bpy)(CO)$_3$]ClO$_4$, are likely to be due to the increased steric bulk of the NHC. The lengthening of the Re-CO bond *trans* to NHC is most pronounced for IiPr$_2$Me$_2$ and may indicate that the NHC ligand exhibits a strong *trans* effect in these complexes, which could influence their reactivity. To test the photostability of the Re NHC complex, **6** and 3 eq. of PPh$_3$ in CH$_2$Cl$_2$ was irradiated with broadband UV for several hours. The solution immediately darkened, changing from golden yellow to dark red within

an hour. The $^{31}P\{^{1}H\}$ NMR spectrum showed formation of a single new phosphine containing species at 24.2 ppm (Figure 39). After work up, dark red crystals of *trans*-Re($l^{i}Pr_2Me_2$)(PPh_3)(Bpy)$(CO)_2$]BAr_4^F (**7**) suitable for X-ray diffraction were obtained from CH_2Cl_2/hexane (Figure 40). Formation of **7** is good evidence for the labilisation of the CO *trans* to the NHC and a photolytic CO dissociation process.

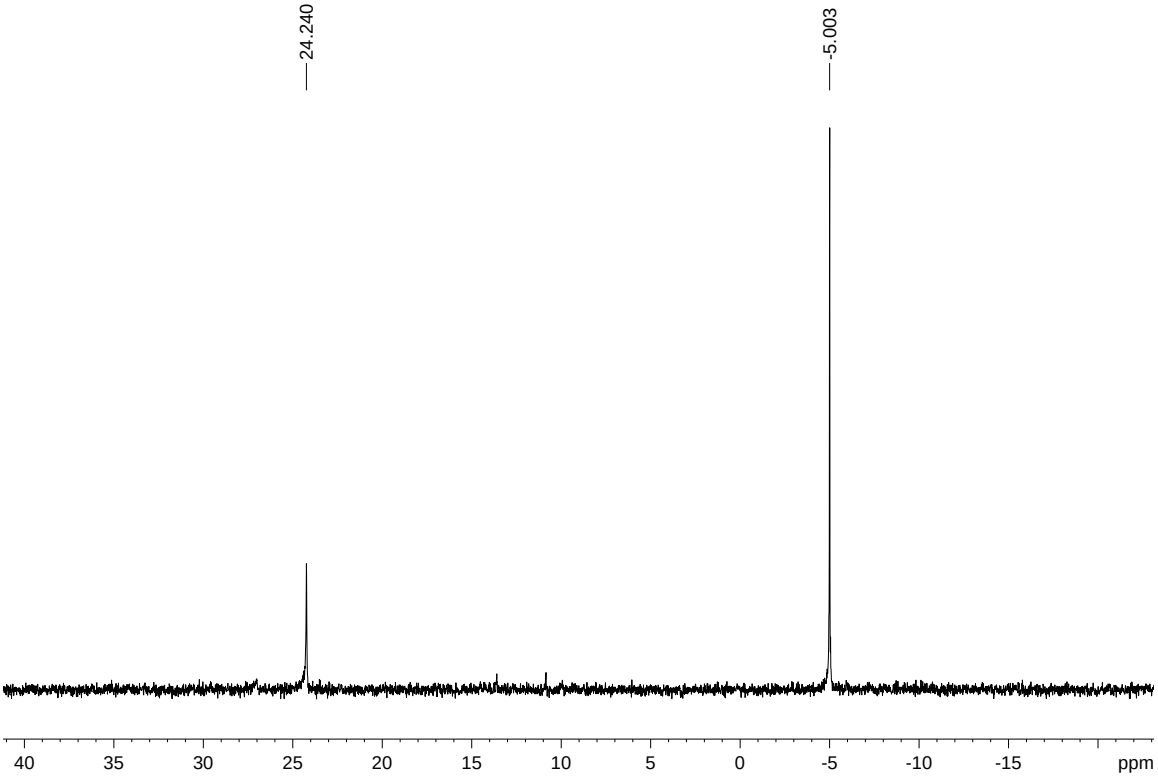

Figure 39: 162 MHz $^{31}P\{^{1}H\}$ NMR spectrum of *trans*-Re($l^{i}Pr_2Me_2$)(PPh_3)(Bpy)$(CO)_2$]BAr_4^F (7) in CD_2Cl_2 at 298 K.

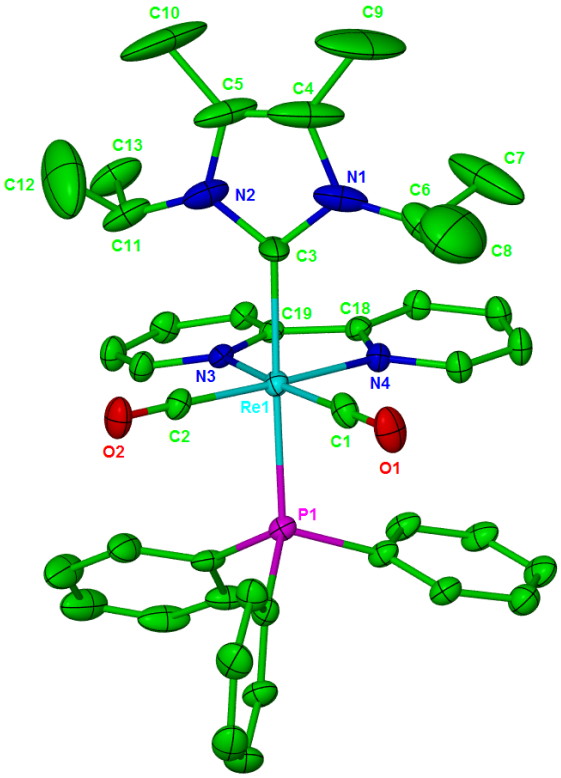

Figure 40: X-ray crystal structure of the cation in *trans*-Re(I^{i}Pr$_2$Me$_2$)(PPh$_3$)(Bpy)(CO)$_2$]BAr$_4^F$ (7). Hydrogen atoms are omitted for clarity and ellipsoids are shown at 30%.

	7	***fac*-[Re(PPh$_3$)(Bpy)(CO)$_3$]PF$_6$**
Re-NHC	2.215(7)	
Re-PPh$_3$	2.426(2)	2.508(3)
Re-CO*trans* to P		1.915(12)
Re-CO	1.899(7)	1.939(17)
	1.904(8)	1.939(15)
Re-N	2.169(6)	2.169(9)
	2.186(6)	2.191(10)
PPh$_3$-Re-NHC	178.4(2)	
PPh$_3$-Re-CO		176.0(3)

Table 5: Selected bond lengths (Å) and angles (°) for 7, alongside those for *fac*-[Re(PPh$_3$)(Bpy)(CO)$_3$]PF$_6$ which were taken from the literature.[12]

The molecular structure of **7** is very close to an ideal octahedral geometry. Table 5 above, shows comparison of the selected bond lengths and angles for **7**

and *fac*-[Re(PPh$_3$)(Bpy)(CO)$_3$]PF$_6$.[12] The Re-N and Re-CO bond lengths are within error between the structures. The Re-PPh$_3$ bond length is significantly shorter in **7**, perhaps contrary to expectation, which may indicate that there is also a degree of back bonding to the phosphine.

3.3 Ultraviolet absorption and emission characterisation of [Re(NHC)(Bpy)(CO)$_3$]BAr$_4^F$.

The neutral chloride complex, *fac*-Re(Bpy)(CO)$_3$Cl, and other d^6 metal Bpy compounds typically show broad, featureless absorption and subsequent emission bands in solution, consistent with decay from a ^{3}MLCT excited state as opposed to $^3\pi\pi^*$ which typically show structured emission.[13] For many years the ^{3}MLCT excited state in systems of this type was thought to be highly stable to subsequent ligand loss. Only very recently was it determined that *fac*-Re(Bpy)(CO)$_3$Cl can undergo photolytic CO loss when irradiated at 313 nm in MeCN to form the corresponding *cis* and *trans* solvated species Re(Bpy)(CO)$_2$(MeCN)Cl.[14] This is also true of complexes such as, *fac*-[Re(PPh$_3$)(Bpy)(CO)$_3$]BAr$_4^F$, although CO substitution *trans* to PR$_3$ has been known to occur in phosphine substituted systems for some time.[15] The mechanism and photophysical processes which allow CO dissociation to occur, from what appears to be predominantly MLCT excitation remain unclear, although it is postulated that thermal transition of the ^{3}MLCT state to a dissociative ligand field (^{3}LF) state may be responsible. This is discussed in more depth in Chapter 1, section 1.3.1. As demonstrated earlier, broadband irradiation of **6** also led to CO loss *trans* to the NHC and it was possible to trap this species by coordination of PPh$_3$. However, none of the excited states involved in this process have yet been characterised.

The UV/Vis absorption spectra of **5** and **6** were measured in CH$_2$Cl$_2$. There was a broad absorption centred at 407 nm for **5** and 409 nm for **6** with extinction coefficients of 1500 cm^{-1} M^{-1} and 1680 cm^{-1} M^{-1} respectively, which are typical for ^{3}MLCT. Exponential absorption began at <350 nm into the hard UV region. These measurements were repeated in acetonitrile, which is significantly more polar than dichloromethane. This changed the position of the absorption

maxima for both compounds to higher energy by *ca*. 20 nm (385 nm for **5** and 386 nm for **6**). Observing this solvatochromic effect is again indicative of a MLCT excited state, as a more polar solvent interacts differently with a charge separated excited state, thereby changing the energy of that state. These results are consistent with those reported previously by Xue *et al* for *fac*-[Re(SIH)(Bpy)(CO)$_3$]ClO$_4$.[8] A comparison of the spectra obtained for **5** in both CH_2Cl_2 and MeCN is shown in Figure 41 and absorption maxima and extinction coefficients for **5** and **6** in CH_2Cl_2 and MeCN are shown below in Table 6.

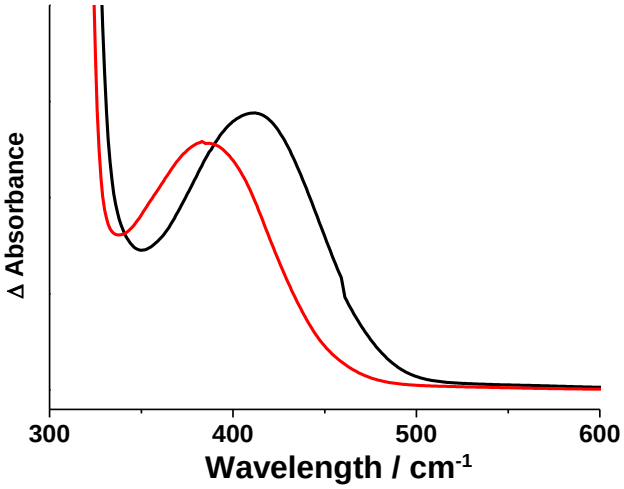

Figure 41: UV absorption spectra of 5 in CH_2Cl_2 (-) and MeCN (-).

Complex	CH_2Cl_2		CH_3CN	
	λ, nm	ε (x10^3) / cm^{-1}M^{-1}	λ, nm	ε (x10^3) / cm^{-1}M^{-1}
5	407	2.41	385	1.50
	320	5.19	319	4.59
	294	10.34	305	5.34
	279	16.23	278	14.50
	269	20.06	268	20.32
6	409	2.16	386	1.68
	321	6.14	320	5.02
	294	11.50	306	5.61
	279	17.47	278	13.28
	269	21.70	268	17.69

Table 6: UV/Vis absorption maxima and extinction coefficients for 5 and 6 in both CH_2Cl_2 and MeCN.

When the ^{3}MLCT manifold was irradiated at the respective wavelengths determined for **5** and **6** from the absorption experiments, broad, structureless emission was detected in CH_2Cl_2 for both complexes, confirming the assignment as ^{3}MLCT (610 nm for **5** and 580 nm for **6**) (Figure 42). These measurements were repeated in MeCN and a solvatochromic shift of the emission maxima to slightly higher energy was observed for **5**, yet **6** was shifted to lower energy (600 nm for **5** and 594 nm for **6**) (Table 7).

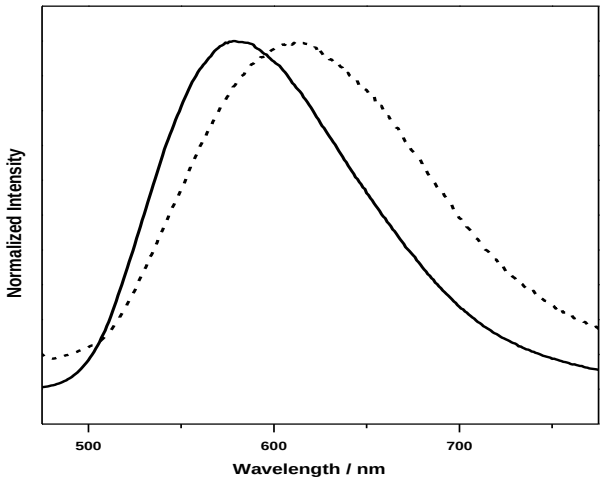

Figure 42: Emission spectra of 5 (···) and 6 (-) in CH_2Cl_2 (λ_{ex} = 410 nm).

The emission bands decayed monoexponentially (Figure 43) allowing lifetimes to be measured for both complexes (Table 7, page 75). For **6** the lifetimes of the ^{3}MLCT excited state (CH_2Cl_2: 900 ns, MeCN: 526 ns) were *ca*. 10x greater than observed for **5** (CH_2Cl_2: 74 ns, MeCN: 39 ns) in either solvent, although for both **5** and **6** the lifetimes in MeCN were *ca*. 2x smaller than those measured in CH_2Cl_2, which indicates a reduction in lifetime with increasing solvent polarity. Presumably the interaction with the more polar solvent accelerates the decay of the excited state, although if you examine the relative energy of the ^{3}MLCT states for both complexes in MeCN, only **6** is actually lowered in energy and **5** is in fact slightly higher. As such, changing the solvent may not be having a large effect on radiative decay, even though it does modify the energies of the orbital manifold, which suggests that perhaps non-radiative decay pathways are enhanced in the more polar solvent.

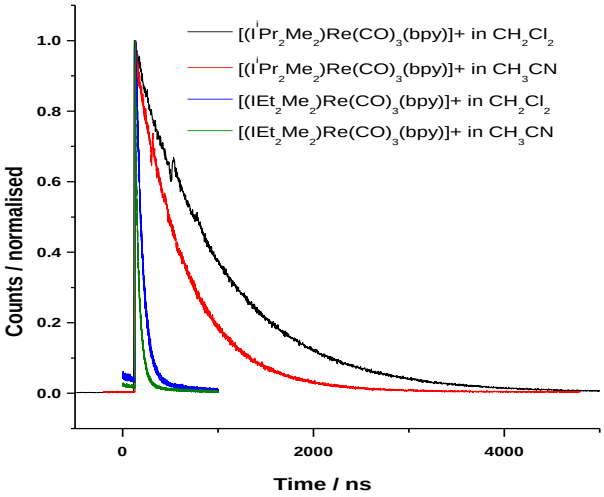

Figure 43: Emission decay for 5 and 6 in CH_2Cl_2 and MeCN at room temperature. The intensity of counts has been normalised.

In order to further investigate the effect of the medium on the photoluminescence, emission spectra were recorded at 77 K in frozen CH_3OH:C_2H_5OH (1:4) glass matrices of **5** and **6** (Figure 44). The 1:4 mixture of methanol and ethanol yields a medium with similar polarity to MeCN, but which possesses much greater hydrogen bonding capability. However, most significant for this experiment is the effect that lowering the temperature will have on the relative energies of the orbital manifold. In this case, for both **5** and **6**, the lowest energy excited state remained the same (^{3}MLCT) (Figure 44). However, the emission bands shifted to significantly higher energy (536 nm for **5** and 528 nm for **6**) with a coincident increase in the lifetimes observed, to >12 μs for **5** and >10 μs for **6**.

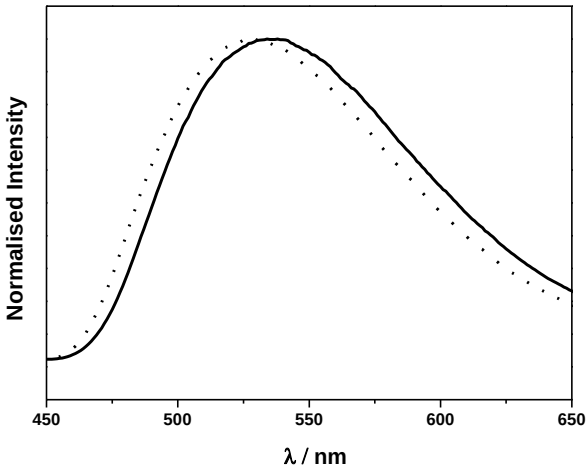

Figure 44: Steady state emission spectra of 5 (···) and 6 (-) at 77 K in CH_3OH:C_2H_5OH (1:4).

To place these results in context, the absorption and emission experiments were repeated, where literature reference was not available, with *fac*-[Re(PPh_3)(Bpy)$(CO)_3$]BAr_4^F under similar conditions (Table 7, page 76).[15] The room temperature measurements showed a ^{3}MLCT to be the lowest energy excited state for *fac*-[Re(PPh_3)(Bpy)$(CO)_3$]BAr_4^F. The absorption and emission bands for *fac*-[Re(PPh_3)(Bpy)$(CO)_3$]BAr_4^F (λ_{abs} = 367 nm, λ_{em} = 540 nm) were at higher energy than the corresponding bands for **5** and **6** (**5**: λ_{abs} = 407 nm, λ_{em} = 600 nm; **6**: λ_{abs} = 409 nm, λ_{em} = 594 nm). The emission lifetimes measured for *fac*-[Re(PPh_3)(Bpy)$(CO)_3$]BAr_4^F in both CH_2Cl_2 and MeCN (CH_2Cl_2: τ = 356 ns, MeCN: τ = 416 ns) are intermediate between those of **5** (CH_2Cl_2: τ = 74 ns, MeCN: τ = 39 ns) and **6** (CH_2Cl_2: τ = 900 ns, MeCN: τ = 526 ns), but show much less sensitivity to the change in solvent and thus polarity. However, the most striking difference is apparent in the behaviour of the lowest energy excited state for *fac*-[Re(PPh_3)(Bpy)$(CO)_3$]BAr_4^F, which changes from a ^{3}MLCT state at 298 K to a ^{3}IL state at 77 K (Figure 45).

***fac*-[Re(L)(CO)$_3$(bpy)]$^+$**	**CH_2Cl_2 (298 K)**			**CH_3CN (298 K)**			**CH_3OH:C_2H_5OH (77 K)**		
	λ_{ab}/nm	**λ_{em}/nm**	**τ/ns**	**λ_{ab}/nm**	**λ_{em} /nm**	**τ/ns**	**λ_{ab}/nm**	**λ_{em} /nm**	**τ/µs**
fac-[Re(I^{i}Pr$_2$Me$_2$)(CO)$_3$(bpy)]$^+$	409	580 MLCT	900	386	594 MLCT	526	376	528 MLCT	> 10
fac-[Re(IEt$_2$Me$_2$)(CO)$_3$(bpy)]$^+$	407	610 MLCT	74	386	600 MLCT	39	378	536 MLCT	> 12
fac-[Re(PPh$_3$)(CO)$_3$(bpy)]$^+$	367	528 MLCT	356	¥	540	416	356	450 482 508 519 IL π-π*	> 10

¥ *not reported*

Table 7: Experimentally determined UV absorption and emission maxima and emission lifetimes for 5, 6 and *fac*-[Re(PPh$_3$)(CO)$_3$(Bpy)]BAr$_4^F$.

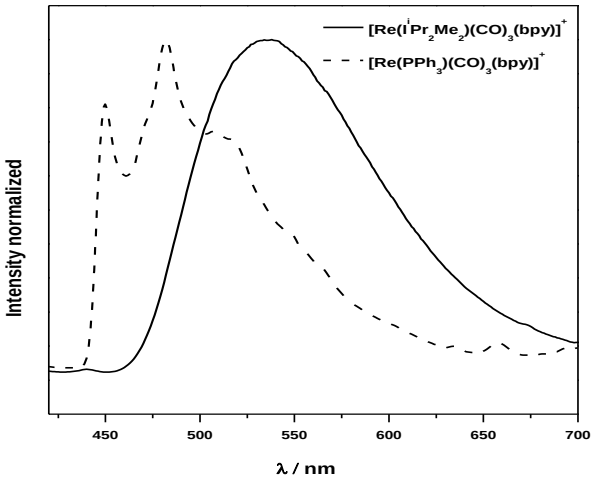

Figure 45: Emission spectra of 6 and *fac*-[Re(PPh$_3$)(Bpy)(CO)$_3$]BAr$_4^F$ in CH$_3$OH:C$_2$H$_5$OH (1:4) at 77 K.

It is not clear from the absorption and emission data alone precisely why these differences between the phosphine and NHC systems occur, although the data does suggest certain points. The ^{3}MLCT excited state for **5** and **6** is significantly lower in energy than for *fac*-[Re(PPh$_3$)(Bpy)(CO)$_3$]BAr$_4^F$, which is likely to be due to the increased electron donation to the metal centre from the NHC, as evidenced by the relative positions of the carbonyl bands in the IR spectra. Presumably this serves to make more electron density available for the metal to ligand charge transfer upon excitation. The absorption and emission measurements were shifted to slightly higher (*ca*. 10 nm) energies in the more polar solvent, apart from **5**, consistent with the report of Xue *et al.*[8] This behaviour is indicative of a polar ground state and a less polar excited state, the latter then being destabilised by a more polar solvent.

The ^{3}MLCT states for **5** and **6** are of lower energy (or more stable) than that of the phosphine analogue, yet the lifetimes measured are in the order **6** > PPh$_3$ >> **5**. This is difficult to rationalise electronically, yet it seems that the difference is too large for just steric factors to be responsible. Another point of interest concerning the lifetimes of all three species is that for **5** and **6** they were significantly reduced upon moving to a more polar solvent, whereas for the phosphine analogue, lifetimes are essentially invariant between solvents.

However, without a greater knowledge of the structure and character of the excited states concerned it is difficult to reconcile these findings. Perhaps the most interesting comparison to be made between **5**, **6** and the phosphine complex is that even at 77 K, the emission from the NHC complexes remains MLCT in nature. This shows that the introduction of a more strongly σ donating ligand has significantly changed the orbital manifold and stabilised the MLCT state, which could impact upon the design of new M-NHC based complexes for photoluminescence applications.

3.4 TRIR studies of $[Re(L)(Bpy)(CO)_3]BAr_4^F$ (L = PPh_3, NHC).

As described previously, *fac*-$[Re(PPh_3)(Bpy)(CO)_3]BAr_4^F$ and analogues can undergo photochemical loss of CO.[15] Similarly, during the synthesis of **6**, it was observed that broadband irradiation of **6** in the presence of excess PPh_3 led to the formation of **7**, presumably via a CO dissociation pathway. In order to characterise this process more completely, TRIR experiments were performed on **5** and **6**. The mechanism of photochemical CO substitution for *fac*-$[Re(PPh_3)(Bpy)(CO)_3]BAr_4^F$ in MeCN has been reported previously by the Ishitani group.[15] They determined that the ^{3}MLCT excited state renders the 'reduced' Bpy^- ligand a much stronger donor with a large *trans* effect, which in turn facilitates dissociation of an equatorial CO. The coordinatively unsaturated complex then rapidly rearranges, the axial CO moving to the vacant equatorial position prior to solvent co-ordination *trans* to PPh_3. Similar experiments on solutions of **5** and **6**, along with *fac*-$[Re(PPh_3)(Bpy)(CO)_3]BAr_4^F$, were performed in CH_2Cl_2 and followed with TRIR spectroscopy for comparison.

Following 355 nm laser irradiation of a CH_2Cl_2 solution of *fac*-$[Re(PPh_3)(Bpy)(CO)_3]BAr_4^F$ under argon, the transient solvent complex *trans*-$[Re(PPh_3)(CH_2Cl_2)(Bpy)(CO)_2]BAr_4^F$ is formed. The TRIR difference spectrum observed for this process is shown in Figure 46. The bands of the starting material at 1930, 1959 and 2042 cm^{-1} are bleached by irradiation and transient bands at 1970, 2002, and 2054 cm^{-1} are formed. These are shifted to higher frequency, indicative of reduced electron density on the metal centre, and are typical of a ^{3}MLCT excited state i.e Re(d) → Bpy(π*).[16] The ^{3}MLCT

state decays after ca. 1 ns with concomitant growth of two new bands at 1880 and 1948 cm^{-1}, consistent with the formation of a dicarbonyl species, presumably the solvent complex *trans*-$[Re(PPh_3)(CH_2Cl_2)(Bpy)(CO)_2]BAr_4^F$.

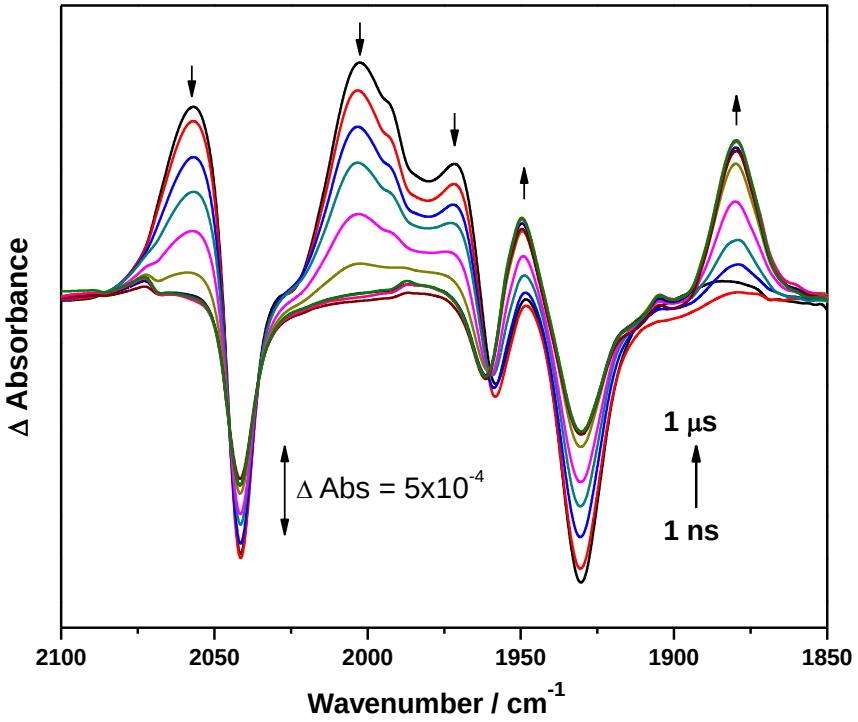

Figure 46: TRIR difference spectrum following 355 nm irradiation of *fac*-$[Re(PPh_3)(Bpy)(CO)_3]BAr_4^F$ in CH_2Cl_2 under argon at 298 K.

Figure 47 reveals that the rate of decay of the ^{3}MLCT state matches the rate of the formation of the solvated dicarbonyl intermediate, consistent with CO loss from the ^{3}MLCT excited state. However, this pathway for decay of the ^{3}MLCT excited state was not exclusive as partial recoordination with CO was also observed to reform the starting material (Figure 48).

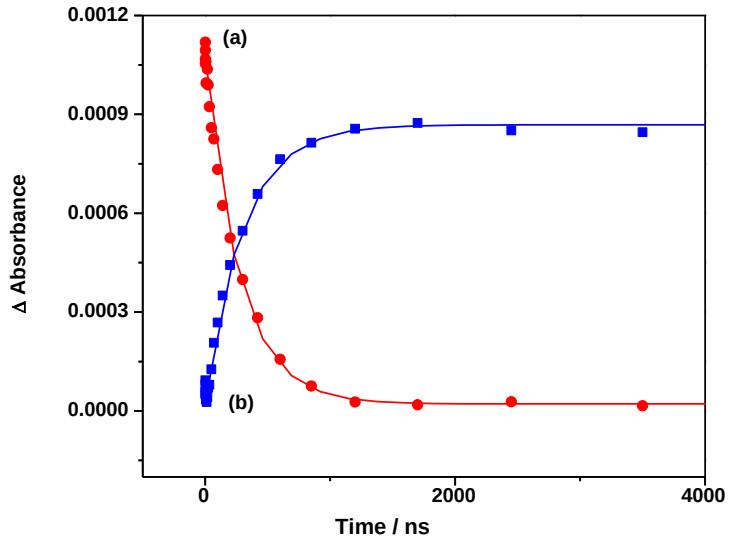

Figure 47: TRIR kinetic traces showing (a) the decay of ^{3}MLCT state at 2054 cm^{-1} and (b) the growth of *trans*-[Re(PPh$_3$)(CH$_2$Cl$_2$)(Bpy)(CO)$_2$]BAr$_4^F$. Solid lines are the monoexponential fit to the data points collected.

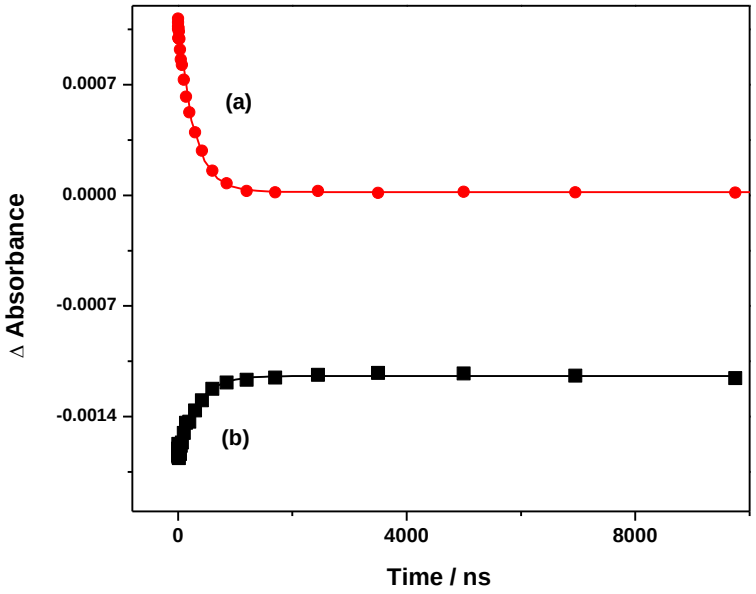

Figure 48: TRIR kinetic traces showing (a) the decay of ^{3}MLCT state at 2054 cm^{-1} and (b) the partial recovery of the parent at 2042 cm^{-1}. Solid lines are the monoexponential fit to the data points collected.

Very similar results were found upon changing the solvent from CH_2Cl_2 to MeCN. The data are summarised in Table 8 (page 81).

	CH_2Cl_2		CH_3CN	
	ν(CO) / cm^{-1}	**τ / ns**	**ν(CO) / cm^{-1}**	**τ / ns**
Parent bands	1930, 1959, 2042	366 (± 29)	1923, 1953, 2040.	376 (± 85)
^{3}MLCT bands	2054, 2002, 1970	286 (± 29)	1964, 2008, 2057.	198 (± 21)
Dicarbonyl species	1880, 1948	282 (± 11)	1863, 1923	212 (± 46)

Table 8: Experimentally determined ν(CO) band positions and lifetimes for *fac*-[Re(PPh$_3$)(Bpy)(CO)$_3$]BAr$_4^F$ and derivatives in CH_2Cl_2 and MeCN.

Complexes **5** and **6** were then examined under similar conditions. A CH_2Cl_2 solution (*ca*. 1.1 mM) of **5** was irradiated at 355 nm under argon (Figure 49). The parent bands at 2029, 1935 and 1915 cm^{-1} were bleached and one set of three transient bands at 2064, 1998 and 1948 cm^{-1} were formed, within the time resolution of the experiment (*ca*. 0.5 ps). As for the phosphine analogue, these were assigned to a ^{3}MLCT excited state. However, there was no evidence for the formation of a dicarbonyl species, the ^{3}MLCT excited state simply decayed in < 300 ns to fully reform the parent (Figure 50).

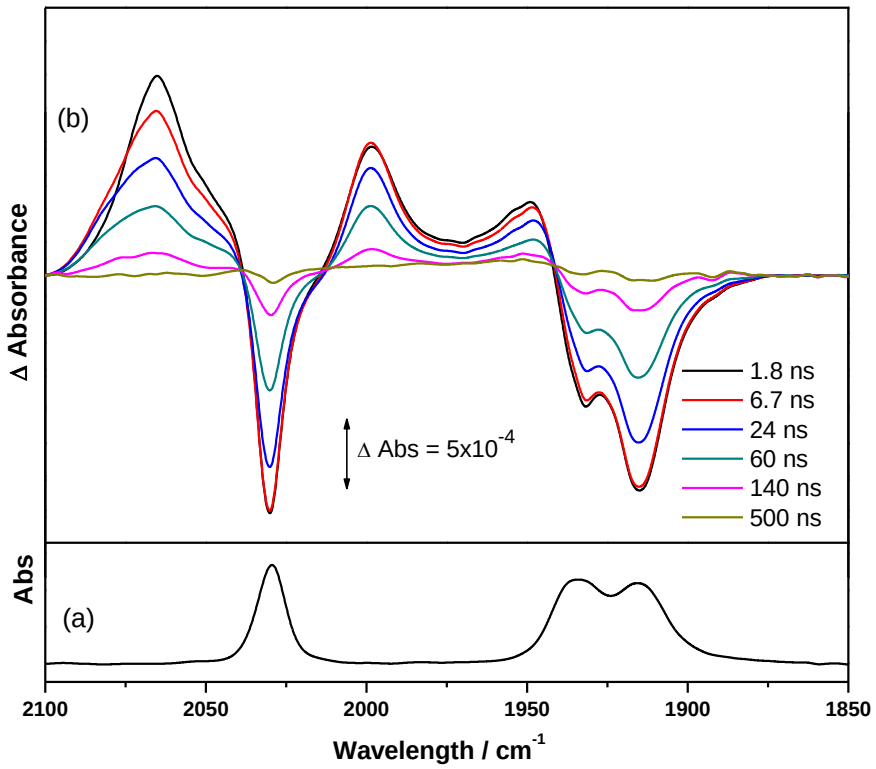

Figure 49: (a) FTIR ground state spectrum of 5 in CH_2Cl_2. (b) Series of ns-TRIR difference spectra of the same solution obtained after 355 nm UV laser photolysis under argon.

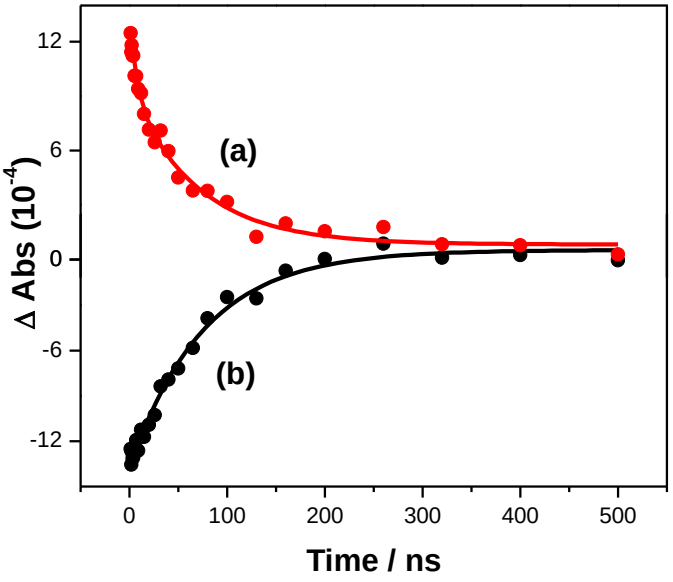

Figure 50: TRIR Kinetic trace recorded following irradiation (355 nm) of 5 in CH_2Cl_2 under argon showing the decay of (a) the ^{3}MLCT state and (b) the full recovery of parent. Solid lines are the monoexponential fit to the data.

Irradiation of **6** under similar conditions gave results analogous to **5**; formation of a ^{3}MLCT excited state with bands at 2062, 1992 and 1945 cm^{-1} (Figure 51).

The ^{3}MLCT state of **6** proved to be much longer lived and decayed with a lifetime of 800 (± 114) ns, again with complete recovery of the parent (Figure 52).

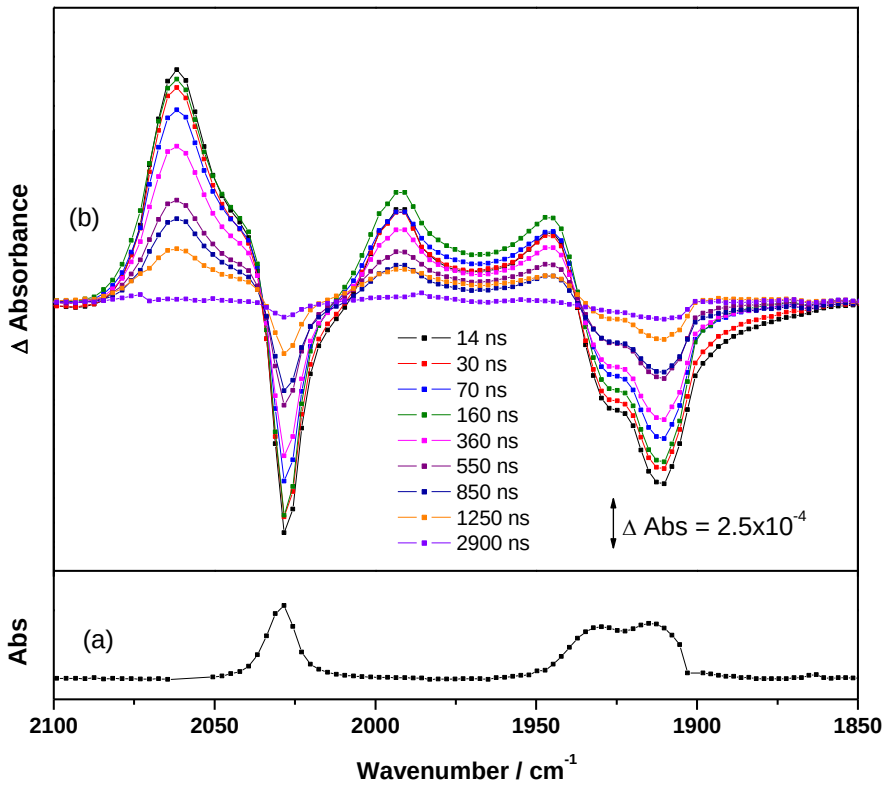

Figure 51: (a) FTIR spectrum before photolysis (b) TRIR difference spectra of 6 after 355 nm UV photolysis in CH_2Cl_2 under argon.

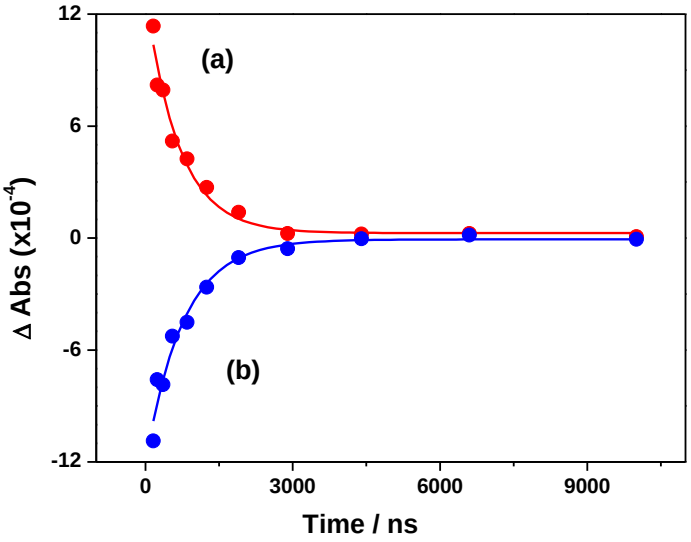

Figure 52: TRIR kinetic trace showing the decay of (a) ^{3}MLCT band at 2062 cm^{-1} and (b) full recovery of parent at 2028 cm^{-1}. Solid lines are the monoexponential fit to the data.

In analogy to the TRIR experiments, irradiation of **6** was repeated with hard UV photolysis (266 nm) and followed by FTIR to see if this treatment would engender CO loss. However, the parent bands fully recovered, indicating that CO loss is not initiated even with 266 nm photolysis. As CO loss had not been observed at either 355 or 266 nm, direct photolysis of **6** (without the use of filters) with a Hg-arc lamp for 1 minute in CH_2Cl_2 under argon was tried and monitored by FTIR, analogous to the conditions used to form **7**.

This resulted in loss of the parent bands and formation of two new bands at lower energy, 1889 and 1805 cm^{-1}, consistent with the formation of a dicarbonyl species (Figure 53). Repeating the experiment in MeCN also produced a photoproduct at lower energy, although slightly shifted compared to CH_2Cl_2, with two carbonyl bands at 1913 and 1837 cm^{-1} (Figure 54). This shift of the bands between solvents is suggestive of a solvent interaction with the complex, presumably forming $[Re(I^iPr_2Me_2)(CH_2Cl_2)(Bpy)(CO)_2]^+$ and $[Re(I^iPr_2Me_2)(MeCN)(Bpy)(CO)_2]^+$ respectively. These data confirm that irradiation of the NHC complexes can result in CO loss to form dicarbonyl species. However, the requirement for broadband irradiation may indicate that CO loss occurs much less readily than for their phosphine analogues. The absence of any dicarbonyl formation in the TRIR measurements suggests that the CO loss process may have a rather low quantum yield compared to the formation of the ^{3}MLCT excited state. The v(CO) band positions for all the NHC complexes and transients are shown in Table 9 (page 86).

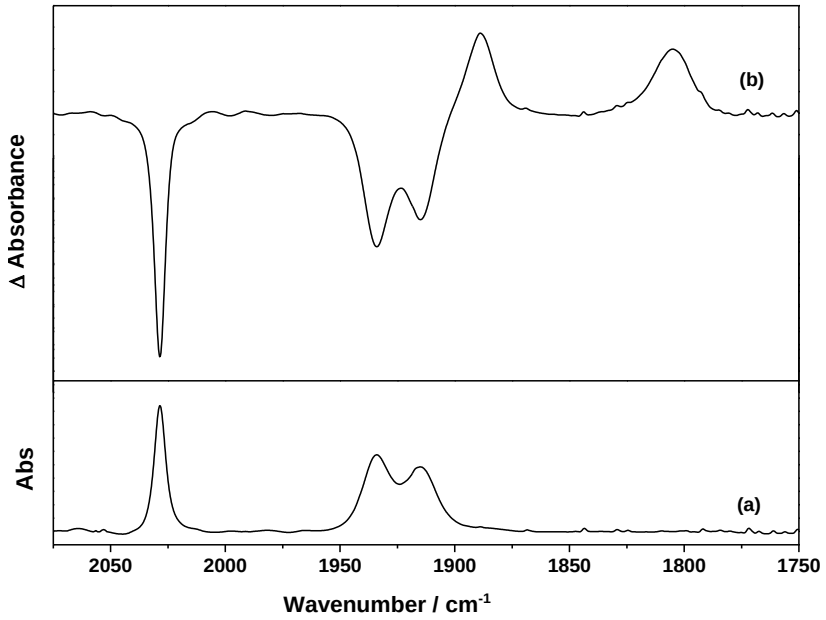

Figure 53: (a) FTIR spectrum before photolysis and (b) FTIR difference spectrum after 1 min UV photolysis of a solution of 6 in CH_2Cl_2 under argon at room temperature.

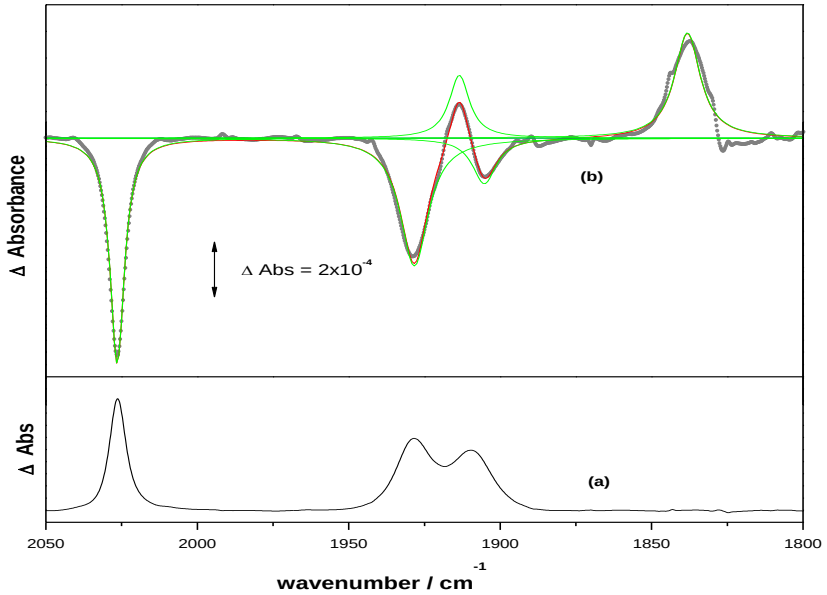

Figure 54: (a) FTIR spectrum before photolysis and (b) FTIR difference spectrum after 1 min UV photolysis of a solution of 6 in MeCN under argon at room temperature.

Complex	ν(CO) / cm^{-1}	Solvent
5	2029,1935, 1915	CH_2Cl_2
5 ^{3}MLCT	2064, 1998, 1948	CH_2Cl_2
6	2028,1931, 1915	CH_2Cl_2
6 ^{3}MLCT	2062,1992, 1945	CH_2Cl_2
5	2026,1928, 1910	CH_3CN
5-CO	1889, 1805	CH_2Cl_2
5-CO	1913, 1838	CH_3CN

Table 9: IR frequencies of the CO bands for the NHC complexes and their derivatives after irradiation.

3.5 Synthesis of $[Re(NHC)(Dppz\text{-}X)(CO)_3]BAr_4^F$.

An application of Re(I) diimine tricarbonyl species which was of particular interest to our collaborators in Nottingham was the use of Dppz substituted complexes as DNA probes.[17] Attempts to prepare analogues of **5** and **6** bearing Dppz in place of the Bpy ligand using the same methodology as for **5** and **6** resulted in some conversion to the desired products, but longer reaction times (> 48 h) were needed and led to increased amounts of imidazolium salt formation.

Substituting dichloromethane with dichloroethane (DCE) or *o*-dichlorobenzene (ODB) and heating the reaction at 358 K for 48 h led to formation of the Dppz substituted product and 1 equiv. of imidazolium. This procedure was used to synthesise a variety of Dppz substituted Re(I) NHC complexes as summarised in Figure 55. Removal of imidazolium salts from the reaction mixtures was often problematic. Chromatography through silica was employed and provided the most effective route to isolation of *fac*-$Re(IEt_2Me_2)(Dppz)(CO)_3]BAr_4^F$ (**8**), *fac*-$Re(I^iPr_2Me_2)(Dppz)(CO)_3]BAr_4^F$ (**9**) and

fac-Re(I^{i}Pr$_2$Me$_2$)(Dppz-F$_2$)(CO)$_3$]BAr$_4^F$ (**10**), but only after subsequent multiple fast recrystalisations from dichloromethane and hexane to remove traces of imidazolium salts not separated on the column. Unfortunately, *fac*-Re(I^{i}Pr$_2$Me$_2$)(Dppz-Me$_2$)(CO)$_3$]BAr$_4^F$ remained contaminated by imidazolium salt side product even after these procedures.

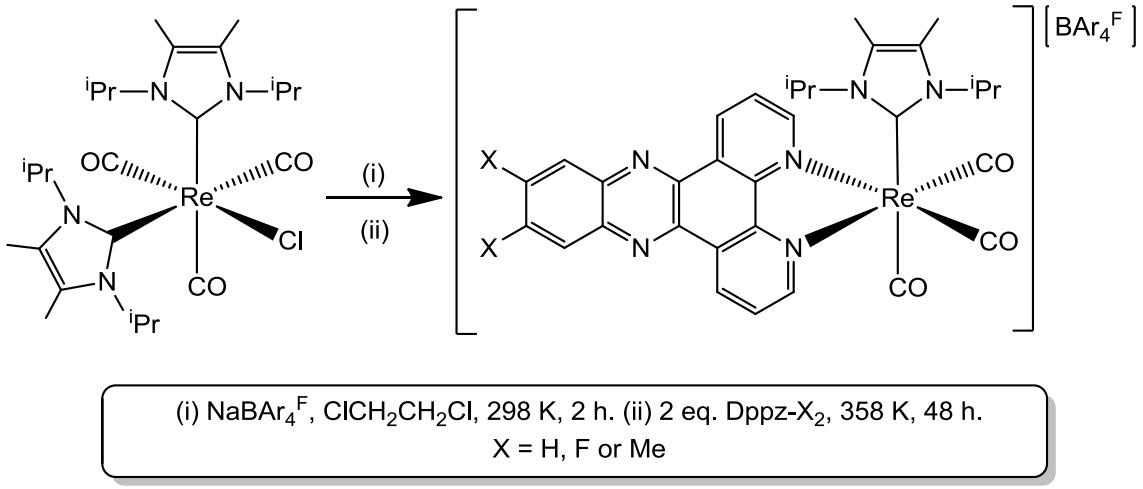

Figure 55: Formation of *fac*-[Re(NHC)(Dppz-X)(CO)$_3$]BAr$_4^F$.

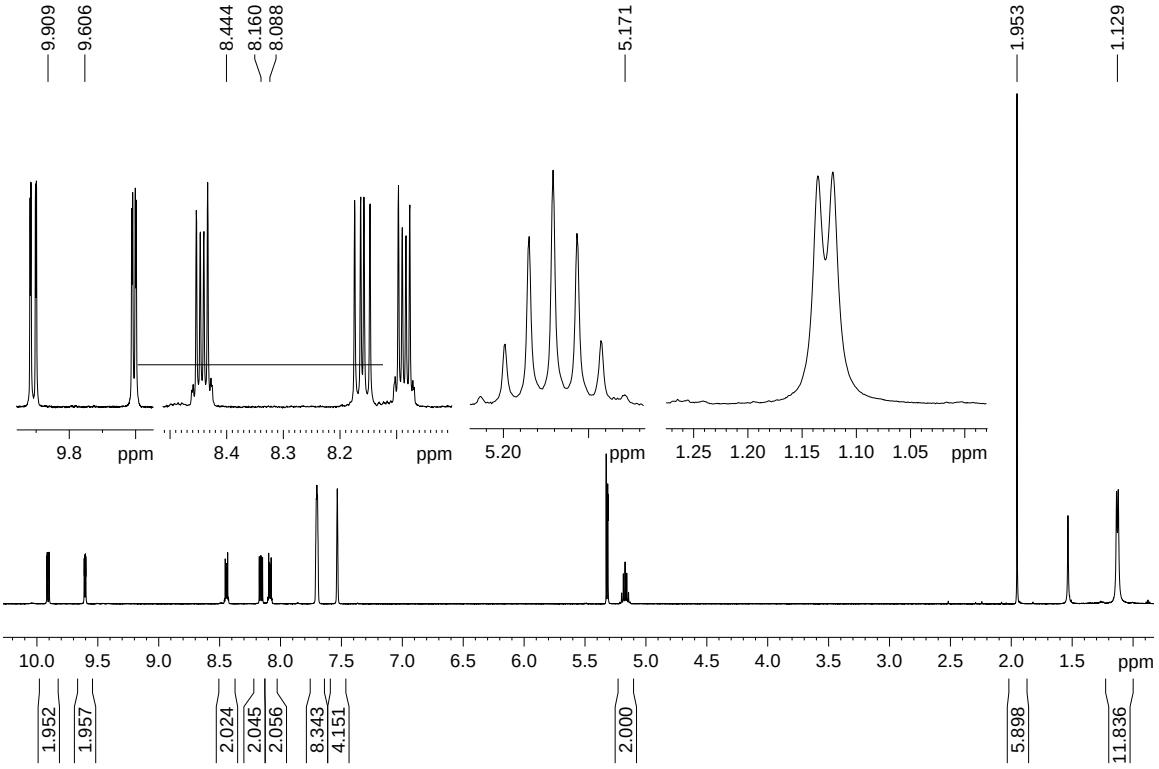

Figure 56: 500 MHz ^{1}H NMR spectrum of *fac*-Re(I^{i}Pr$_2$Me$_2$)(Dppz)(CO)$_3$]BAr$_4^F$ (9) in CD$_2$Cl$_2$ at 298 K.

The ^{1}H NMR spectrum of **9** is shown in Figure 56 as a representative example of this class of compounds. The Dppz ligand is observed as 5 multiplets between 10 and 8 ppm and the NHC signals as 3 equivalent environments, indicating free rotation about the M-NHC bond. The IR frequencies of the CO bands for **9** in CH_2Cl_2 are 2031, 1937 and 1918 cm^{-1}, which are shifted to slightly higher frequency than for the Bpy analogues **5** and **6**.

X-Ray quality crystals of **8**, **9** and **10** were obtained by slow diffusion of hexane into concentrated CH_2Cl_2 solutions of the complexes (Figures 57-59). All of the molecular structures are very similar, with fewer perturbations to the geometries than seen for the Bpy analogues, although again a lengthening of the M-CO bonds *trans* to NHC is observed. Selected bond lengths and angles for **8**, **9** and **10** are shown in Table 10 (page 90).

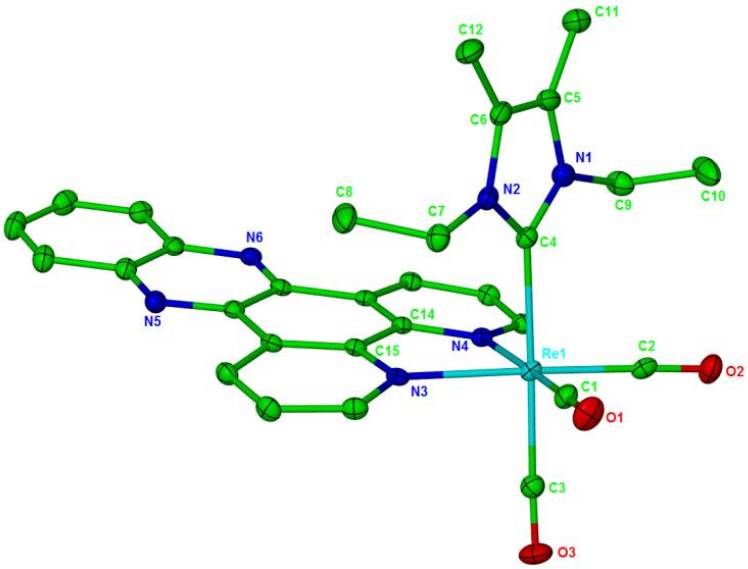

Figure 57: X-ray crystal structure of the cation in *fac*-[Re(IEt$_2$Me$_2$)(Dppz)(CO)$_3$]BAr$_4^F$ (8). Hydrogen atoms omitted for clarity and ellipsoids shown at 30%.

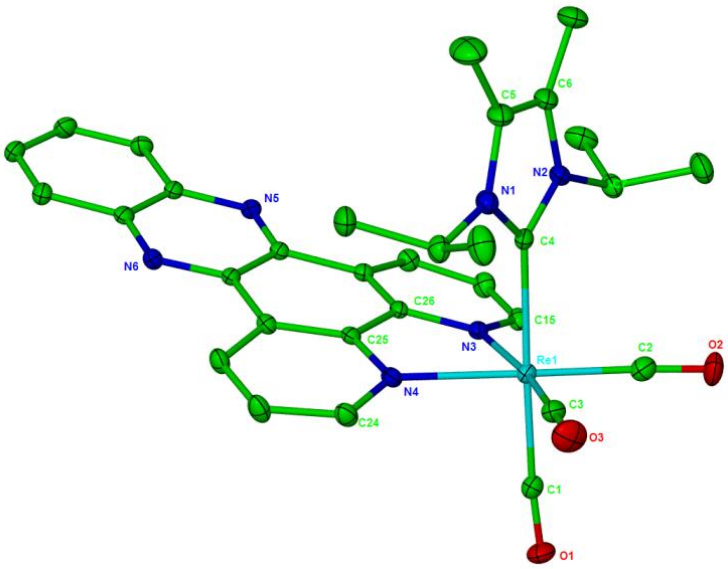

Figure 58: X-ray crystal structure of the cation in *fac*-[Re(l^iPr$_2$Me$_2$)(Dppz)(CO)$_3$]BAr$_4^F$ (9). Hydrogen atoms omitted for clarity and ellipsoids shown at 30% .

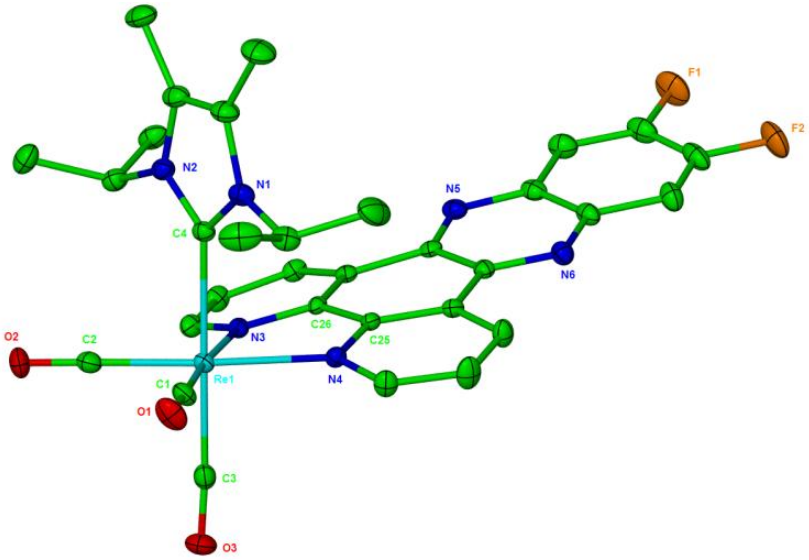

Figure 59: X-ray crystal structure of the cation in *fac*-[Re(l^iPr$_2$Me$_2$)(Dppz-F$_2$)(CO)$_3$]BAr$_4^F$ (10). Hydrogen atoms omitted for clarity and ellipsoids shown at 30%.

	8	9	10
Re-NHC	2.250(3)	2.235(4)	2.244(3)
Re-CO*trans* to NHC	1.951(4)	1.955(4)	1.951(4)
Re-CO*trans* to N	1.916(4)	1.923(4)	1.908(4)
	1.919(4)	1.927(4)	1.927(4)
Re-N	2.200(3)	2.203(3)	2.206(3)
	2.197(3)	2.194(3)	2.190(3)
NHC-Re-CO	177.70(14)	178.28(16)	179.55(14)
OC-Re-CO	85.94(17)	86.78(17)	85.78(16)
	86.94(16)	87.72(17)	89.25(15)
	88.40(16)	88.59(18)	88.78(15)

Table 10: Selected bond lengths (Å) and angles (°) for the rhenium NHC complexes 8, 9 and 10.

3.6 Ultraviolet absorption and emission characterisation of $[Re(l^{i}Pr_2Me_2)(Dppz\text{-}X_2)(CO)_3]BAr_4^F$ (X = H, F).

After the results observed for compounds **5** and **6**, which appeared to show introduction of the NHC favouring the MLCT excited state, it was hoped that a similar effect could be achieved with analogous Dppz complexes. An ideal property for a DNA probe is to have a MLCT transition as the lowest lying excited state, as the solvatochromism exhibited by MLCT excited states provides a highly sensitive probe of the surrounding environment. However, typically transition metal Dppz complexes exhibit intraligand ($\pi \rightarrow \pi^*$) excitation alongside MLCT ($M(d) \rightarrow \pi^*$) excitation.[18] NHC substitution, alongside more established modification processes such as modification of the Dppz backbone, may offer sufficient means to change the excited state manifold in favour of MLCT excitation.

Dppz complexes exhibit relatively complex photochemistry,[19,20,21] especially when contrasted to the Bpy complexes discussed earlier in this chapter. As mentioned previously, both MLCT and IL excited states are often observed. Further to this, Dppz can be considered to consist of two distinct ring systems within the molecule, each of which have their own π* acceptor orbitals. These

are referred to as the phenanthroline (3 rings closest to the metal) and phenazine (3 rings furthest from the metal) systems. It has been determined previously that both the phenanthroline (phen) and phenazine (phz) orbitals lie very close in energy, accounting for the complex behaviour upon irradiation. As such, there are four different excited states that are commonly observed, both MLCT and IL excitation either localised on the phenanthroline or phenazine system, i.e. π→π* ^{3}IL phenanthroline, π→π* ^{3}IL phenazine, Re(d)→π* ^{3}MLCT phenanthroline and Re(d)→π* ^{3}MLCT phenazine. Typically the ^{3}MLCT (phen) state is emissive in solution, whereas the ^{3}MLCT (phz) state is dark and non-emissive.[22] However, to add further complexity, the phen and phz states as well as the ^{3}IL and ^{3}MLCT states can interconvert or exist in equilibrium.[23]

Dppz complexes have been studied with UV/Vis absorption and emission spectroscopy previously,[24,25] which provides a reference point for this investigation and a means towards assignment of the excited states observed. The UV/Vis absorption spectrum of **9** in CH_2Cl_2 shows very strong absorption around 360-380 nm (Figure 60), indicative of ^{3}IL π→π* excitation.[26] However, there is also a weaker absorption at *ca*. 420 nm on the shoulder of the ^{3}IL band, which could be suggestive of ^{3}MLCT (phen) excitation. The absorption spectrum was taken in MeCN and gave very similar results, although the proposed ^{3}MLCT (phen) transition is less clear in the more polar solvent.

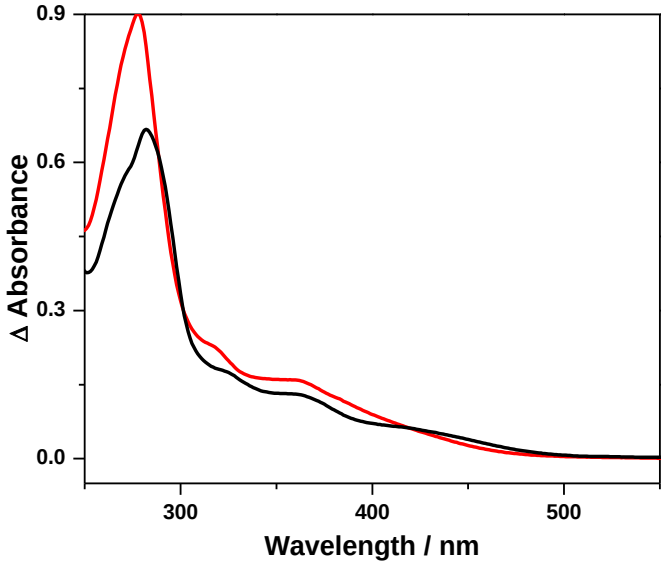

Figure 60: UV/Vis absorption spectra of 9 in CH_2Cl_2 (-) and MeCN (-) at 298 K.

Spectra were also collected of **10** under similar conditions for comparison (Figure 61). The results were largely the same between complexes **9** and **10**, although the potential ^{3}MLCT transition was slightly more apparent for **10** in both solvents. The absorption maxima and extinction coefficients for complexes **9** and **10** in CH_2Cl_2 and MeCN are shown below in Table 11.

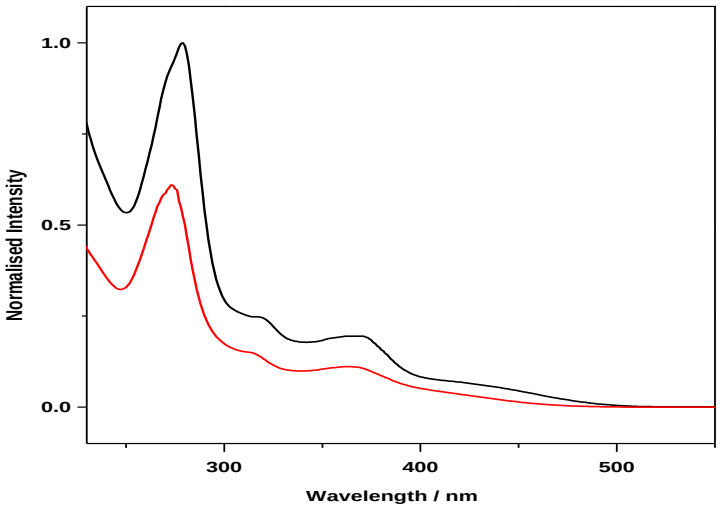

Figure 61: UV/Vis absorption spectra of 10 in CH_2Cl_2 (-) and MeCN (-) at 298 K.

Complex	CH_2Cl_2		CH_3CN
	λ, nm	ε (x10^3) / $cm^{-1}M^{-1}$	λ, nm
9	420	5.8	365
	360	13.2	320
	324	16.2	278
	280		
10	425	5.5	415
	371	15.2	365
	320	19.0	315
	279	73.2	275

Table 11: UV/Vis absorption maxima and extinction coefficients for 9 and 10 in CH_2Cl_2 and MeCN.

Using the irradiation wavelengths obtained from the UV/Vis absorption spectroscopy experiments, emission spectra of **9** and **10** were measured at 298 K. The spectra obtained for **9** in both CH_2Cl_2 and MeCN are shown in Figure 62. In CH_2Cl_2, a strong emission band at 560 nm with a shoulder at *ca.* 600 nm with a lifetime of *ca*. 9 μs was detected. This long emission time is characteristic of a π→π* transition indicating formation of a ^{3}IL excited state. However, in MeCN, the ^{3}IL emission is absent and instead a broad and much weaker emission at 640 nm is observed with a significantly shorter lifetime of 20 ns. Broad featureless emission and short lifetime suggest this band is ^{3}MLCT in nature. This suggests that not only are both ^{3}IL and ^{3}MLCT states present for **9**, but that changing the solvent polarity can effectively quench the strong ^{3}IL emission, yet leave the much weaker ^{3}MLCT emission still observable. Such an effect has been noted previously for other Dppz complexes and is similar to the 'light switch' effect,[22] whereby emission is shutdown in aqueous solution but enhanced when intercalated with DNA, a large factor in why Dppz complexes are so attractive as DNA probes.

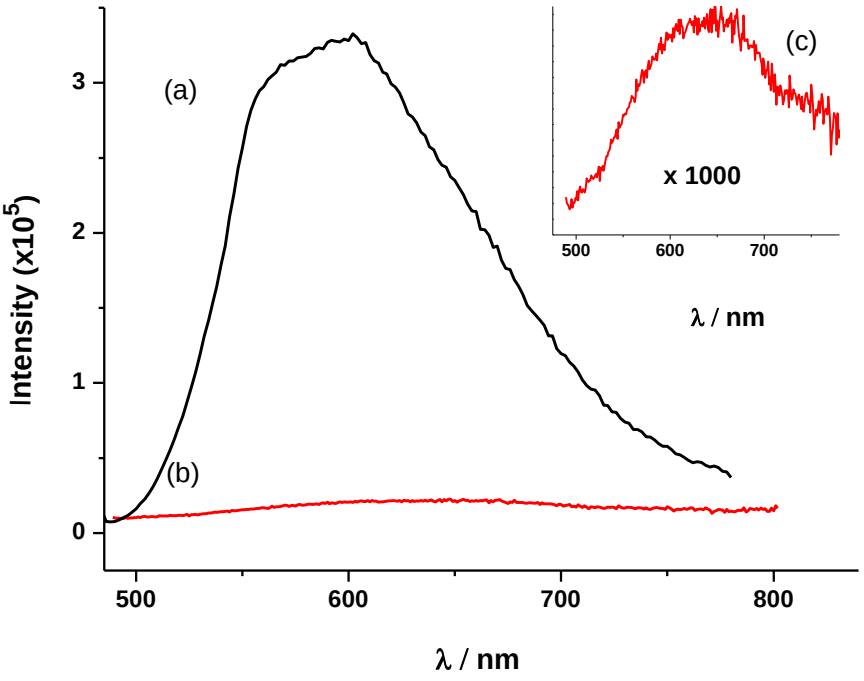

Figure 62: Steady state emission spectra of 9 (λ_{ex} = 420 nm, 10^{-5} M) in (a) CH_2Cl_2 (-) and (b) CH_3CN (-) at 298 K (c = 1000 x b).

The spectra obtained for **10** in CH_2Cl_2 and MeCN are shown in Figure 63. In CH_2Cl_2, a broad featureless emission band centred at 590 nm was observed with a lifetime of 866 ns, suggestive of ^{3}MLCT (phen) being the lowest energy emissive excited state. In MeCN, the emission from **9** is greatly reduced, presumably due to quenching by the more polar solvent as seen for **8**.

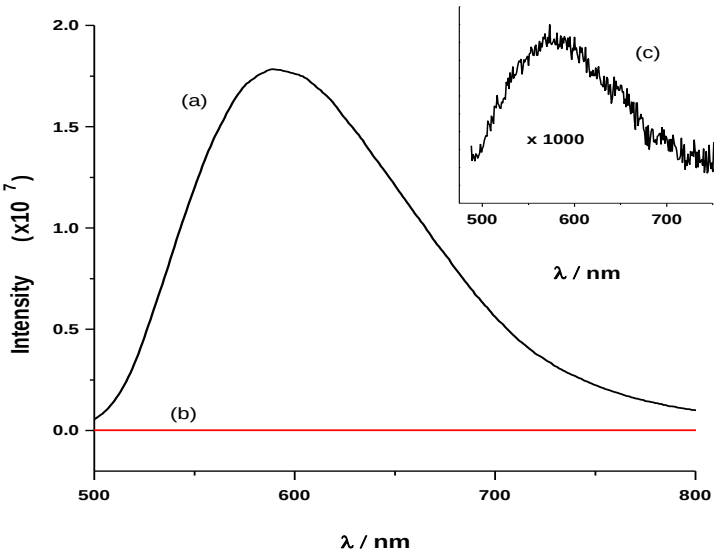

Figure 63: Steady state emission spectra of 10 (λ_{ex} = 420 nm, 10^{-5} M) in (a) CH_2Cl_2 (-) and (b) CH_3CN (-) at 298 K (c = 1000 x b).

	CH_2Cl_2 (298 K)		CH_3CN (298 K)		CH_3OH:C_2H_5OH (77 K)	
	λ_{em}/nm	τ/ns	*λ_{em}/nm	τ/ns	λ_{em}/nm	τ/µs
9	560, 600(sh) IL $\pi\pi^*$	9000	640	20	545, 561 (sh), 646 (sh), 612 (sh) 591 (sh) IL $\pi\pi^*$	> 50
10	590 MLCT	866	580	< 2 ns	521,534 (sh), 564 (sh), 580 (sh), 613 (sh) IL $\pi\pi^*$	> 50

**Very weak emission*

Table 12: UV/Vis absorption and emission maxima and lifetimes for 9 and 10 in CH_2Cl_2 and MeCN at 298 K and CH_3OH:C_2H_5OH (1:4) at 77 K.

In order to examine if any other excited states were close in energy to the lowest energy excited states, emission spectra were also measured in CH_3OH:C_2H_5OH (1:4) frozen glass matrices at 77 K. Under such conditions, the energy of a ^{3}MLCT excited state is typically increased, while the relative energy of any ^{3}IL $\pi \rightarrow \pi^*$ state remains unchanged.[27] The emission maxima and lifetimes detected for **9** and **10** in CH_2Cl_2 and MeCN at 298 K and CH_3OH:C_2H_5OH (1:4) at 77 K are shown in Table 12 (page 94). Both **9** and **10** showed structured emission bands at 77 K (shown for **9** in Figure 64) typical of ^{3}IL excited states. Comparison of the data for the two complexes, indicates that at 298 K the lowest energy excited state is ^{3}IL $\pi \rightarrow \pi^*$ for **9** and ^{3}MLCT for **10**, although the ^{3}MLCT and ^{3}IL $\pi \rightarrow \pi^*$ states respectively, are also close in energy. At 77 K only ^{3}IL $\pi \rightarrow \pi^*$ emissions are detected. Both **9** and **10** exhibited much longer lifetimes at 77 K than 298 K, an effect that has been noted previously for other Re(I) diimine complexes.[26,28]

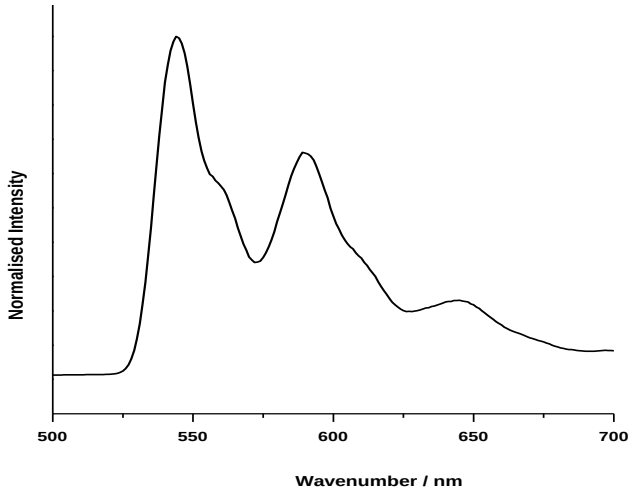

Figure 64: Emission spectrum of 9 (λ_{ex} = 365 nm) in CH_3OH:C_2H_5OH (1:4) at 77 K.

In summary, the aim to produce a Dppz complex that exhibits purely ^{3}MLCT character has in part been realised. At 298 K the lowest energy excited state for **10** is ^{3}MLCT (phen) in nature. It would appear that this has been achieved by the synergistic effect of both strong σ-donation from the NHC and introduction of electron withdrawing fluorine substituents on the backbone of the Dppz ligand. However, in order for tests to be carried out on the complex in the presence of DNA it must be water soluble, which is unfortunately not the case. It

was assumed that the reason for this was primarily the presence of the large greasy BAr_4^F anion. However, the complex remained insoluble in water even with a chloride anion. It is likely that modification of the NHC ligand would be required to favour water solubility, a task which was beyond the scope of this work.

3.7 TRIR studies of $[Re(I^iPr_2Me_2)(Dppz\text{-}X_2)(CO)_3]BAr_4^F$ (X = H, F).

The ps-TRIR spectra of **9** in CH_2Cl_2 at 298 K following 400 nm laser irradiation under argon is shown in Figure 65. The loss of the parent carbonyl bands at 2031, 1937 and 1918 cm^{-1} was accompanied by the appearance of two transient species. The first of these exhibited higher frequency ν(CO) bands at 2057, 1994 and 1947 cm^{-1}, consistent with population of a ^{3}MLCT excited state. The magnitude of the shift to higher wavenumber is *ca*. 30 cm^{-1}, which suggests formation of a ^{3}MLCT (phen) state by comparison with the literature.[16]

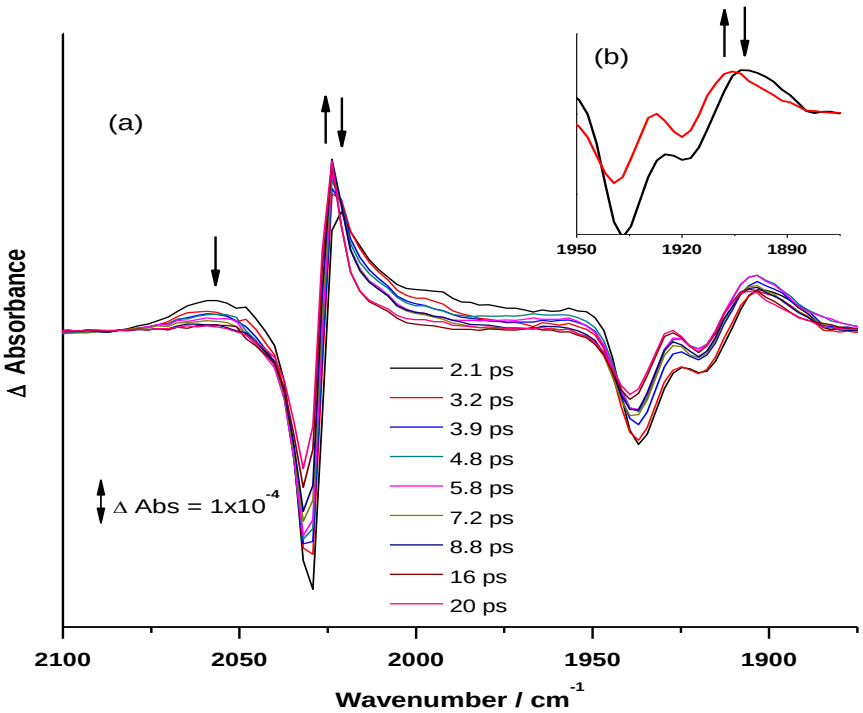

Figure 65: (a) ps-TRIR difference spectra of 9 after 400 nm photolysis in CH_2Cl_2 under argon, (b) the decay of ^{3}IL (phen) state and the growth of ^{3}IL (phz) state.

The second transient species exhibited two bands at 2020 and 1903 cm^{-1}, shifted slightly to lower frequency relative to the parent bands, consistent with

population of a ^{3}IL π→π* excited state. It is likely that a third band is also present, but may be hidden by coincidence with the parent bands. As the time after the laser pulse increases from 2 to 20 ps, these bands shift slightly to higher energy by 3 to 4 cm^{-1}. The resulting bands at 2026 and 1909 cm^{-1} were assigned to ^{3}IL (phz) by comparison with the literature,[29] which suggests internal conversion of an initially populated ^{3}IL (phen) state. The ^{3}IL (phen) band at 2020 cm^{-1} decayed with a lifetime of 5 (± 1.9) ps and the ^{3}IL (phz) band at 2026 cm^{-1} grew in with a lifetime of 1.8 (± 0.2) ps. Similarly, the ^{3}MLCT (phen) band at 2031 cm^{-1} decayed with a lifetime of 2.8 (± 0.3) ps. Recovery of the parent was also observed on the picosecond timescale, 12 (± 1) ps. The decay of the ^{3}MLCT (phen) and ^{3}IL (phen) states and growth of the ^{3}IL (phz) state is shown in Figure 66. At this stage it is difficult to conclude, from the ps-TRIR data alone, which states are converting to ^{3}IL (phz) and or decaying to the parent.

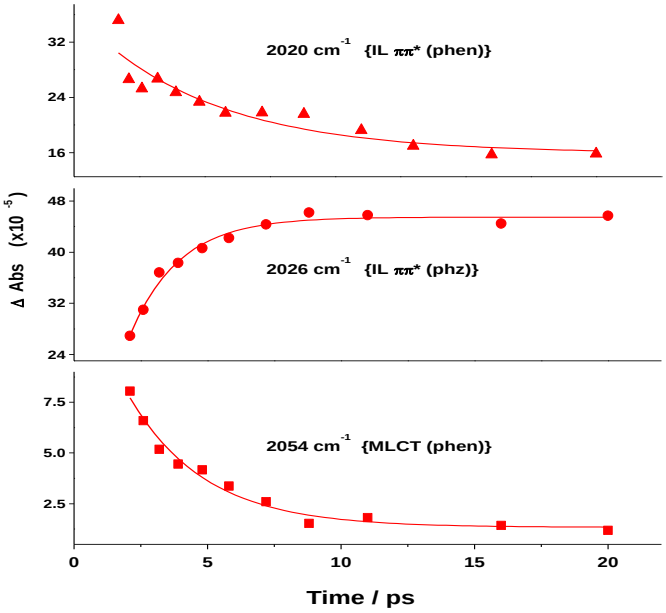

Figure 66: Kinetic trace showing the proposed conversion of ^{3}MLCT (phen) state into ^{3}IL (phz) state and ^{3}IL (phen) into IL (phz) state at ps time scale, obtained after 400 nm UV photolysis of 8 in CH_2Cl_2 under argon.

The ns-TRIR spectra of **9** in CH_2Cl_2 at 298 K following 400 nm laser irradiation under argon is shown in Figure 67. On the nanosecond timescale, only the ^{3}IL (phz) state was observed and decayed back to the parent with a lifetime of *ca*. 1.5 μs *via* a radiative pathway, as seen previously in the emission

measurements. However, the lifetimes detected from the TRIR experiments are much shorter than those from the emission spectroscopy, most likely because of a degree of self-quenching in the TRIR experiments which are run at significantly higher concentration (1 x 10^{-3} M) than the emission measurements (1 x 10^{-5} M).

The information obtained from both ps- and ns-TRIR, alongside the absorption and emission measurements, suggests rather complex photophysics in **9**. Excitation initially leads to population of both ^{1}IL (phen) and ^{1}MLCT (phen) states, which rapidly decay *via* inter system crossing to their respective triplet states. However, it seems that these triplet states are sufficiently close in energy for a degree of conversion to exist, suggested by the lifetimes determined from the ps-TRIR experiments. On the picosecond timescale rapid internal conversion of the initially populated ^{3}IL (phen) state to the emissive ^{3}IL (phz) state also occurs. There was some emission detected from the ^{3}MLCT (phen) state at 298 K although it is very weak compared to that detected from the ^{3}IL (phz) state. This suggests that most of the decay from the ^{3}MLCT (phen) state is non-radiative, presumably *via* internal conversion to form ^{3}IL (phen) and or ^{3}IL (phz) states.

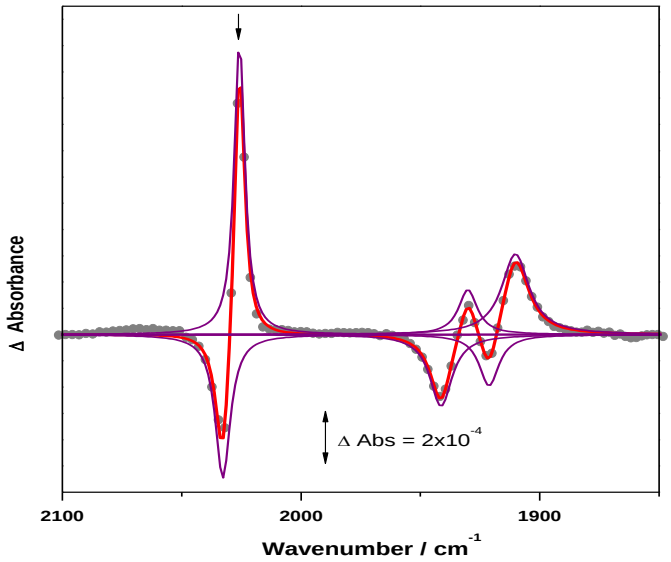

Figure 67: Lorentzian fitted ns-TRIR difference spectrum of 9 in CH_2Cl_2 following 355 nm UV photolysis under argon at 298 K, recorded at 10 ns showing the decay of ^{3}IL (phz) state to the parent.

Due to the closeness in energy of the three excited states for **9** in CH_2Cl_2, TRIR experiments were conducted in MeCN to see whether solvent polarity impacted on the excited state manifold.

As the ^{3}MLCT (phen) and ^{3}MLCT (phz) are charge separated states their energies are expected to shift with changes in solvent polarity, although conversely, ^{3}IL states should remain at approximately the same energy.[30] With excited states that are very close in energy, as in **9**, it is possible for the photophysics of the complex to be significantly altered by solvents of different polarity. The ps-TRIR spectra of **9** in MeCN following 400 nm laser irradiation under argon at 298 K is shown in Figure 68. The loss of the parent carbonyl bands at 2027, 1930, and 1913 cm^{-1} was accompanied by the appearance of two transient species. The first of these exhibited higher frequency v(CO) bands at 2064, 1996 and 1948 cm^{-1} is consistent with population of the ^{3}MLCT (phen) state and the second at 2021 and 1896 cm^{-1} suggests ^{3}IL $\pi \rightarrow \pi^*$ excitation. The latter bands again shift slightly as the time delay increases from 1 to 1200 ps, to give a new species at 2024 and 1903 cm^{-1} which is assigned as ^{3}IL (phz) by comparison with previous results and the literature.[30] The lifetimes detected for the two transients are 10 (± 1) ps for ^{3}IL (phen), which converts into the ^{3}IL (phz) state over a timescale of 14 (± 3) ps, and 26 (± 2) ps for the ^{3}MLCT (phen) state (Figure 69). However, on close inspection it becomes apparent that the ^{3}MLCT (phen) state does not decay fully and an equilibrium is established between ^{3}MLCT (phen) and ^{3}IL (phz) states. The parent recovers on a timescale of 18 (± 2) ps.

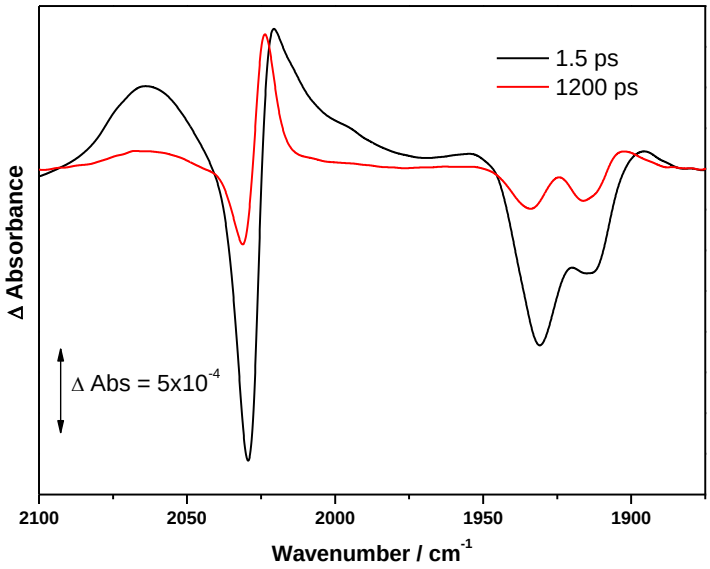

Figure 68: ps-TRIR difference spectra of 9 after irradiation at 400 nm in CH_3CN under argon.

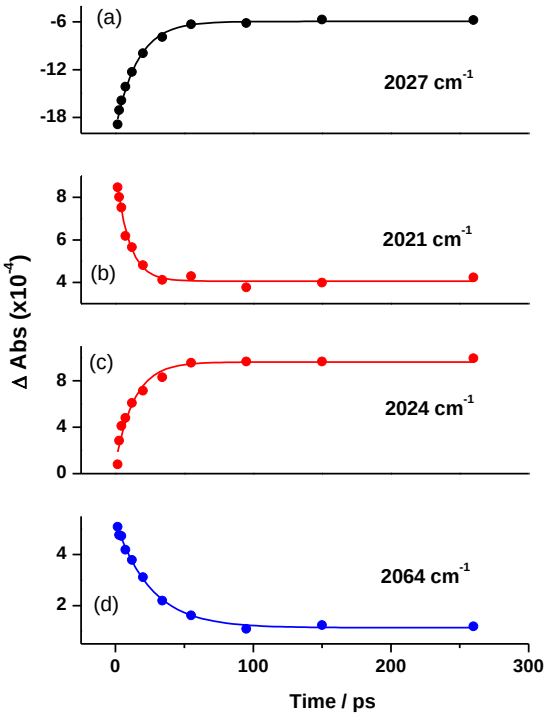

Figure 69: Kinetic traces of (a) Parent band (b) ^{3}IL (phen) state (c) ^{3}IL (phz) state (d) ^{3}MLCT (phen) state after irradiation of 8 at 400 nm in CH_3CN under argon.

The ns-TRIR of **9** in MeCN following laser irradiation at 355 nm under argon at 298 K shows formation of both ^{3}MLCT (phen) and ^{3}IL (phz) states (Figure 70). However, the lifetimes of both states are the same at *ca*. 27 ns and decay with

recovery of the parent (Figure 71), which suggests that these states are in equilibrium with each other and must be very close in energy.

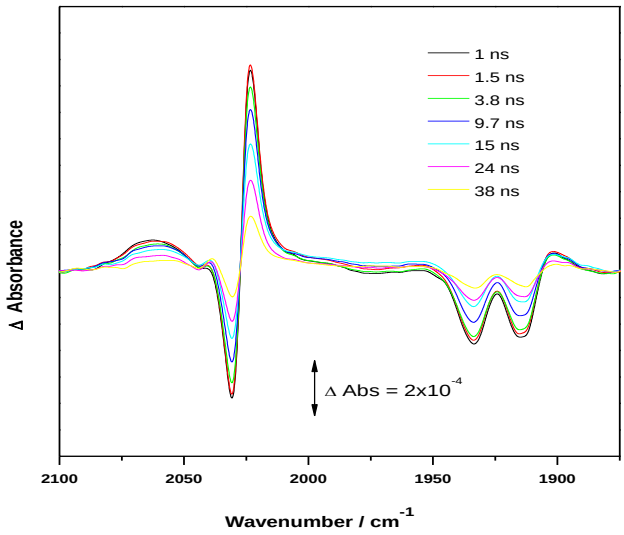

Figure 70: ns-TRIR difference spectra of 9 after irradiation at 355 nm in CH_3CN under argon.

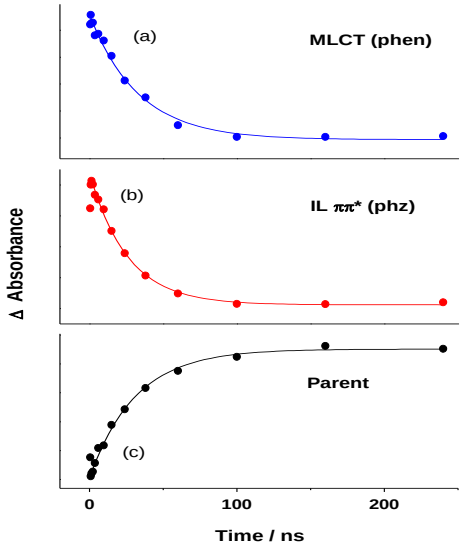

Figure 71: Kinetic traces of (a) ^{3}MLCT (phen) state at 2064 cm^{-1} (b) ^{3}IL (phz) state at 2024 cm^{-1} and (c) parent at 2027 cm^{-1} after irradiation of 9 at 355 nm in CH_3CN under argon.

Overall it appears that whilst the photophysics of **9** in both CH_2Cl_2 and MeCN are largely similar. There is a slight perturbation caused by the change in solvent to the excited state manifold, which is manifested in the emission spectroscopy as almost complete quenching of the ^{3}MLCT (phen) emission in MeCN. This is explained by the ps- and ns-TRIR data, which suggests that in

MeCN, conversion of the ^{3}MLCT (phen) state to the ^{3}IL (phz) state is so strongly favoured that no emission is seen from the ^{3}MLCT (phen) state at all. Figures 72 and 73 summarise the proposed photophysical pathways for **9** in both CH_2Cl_2 and MeCN.

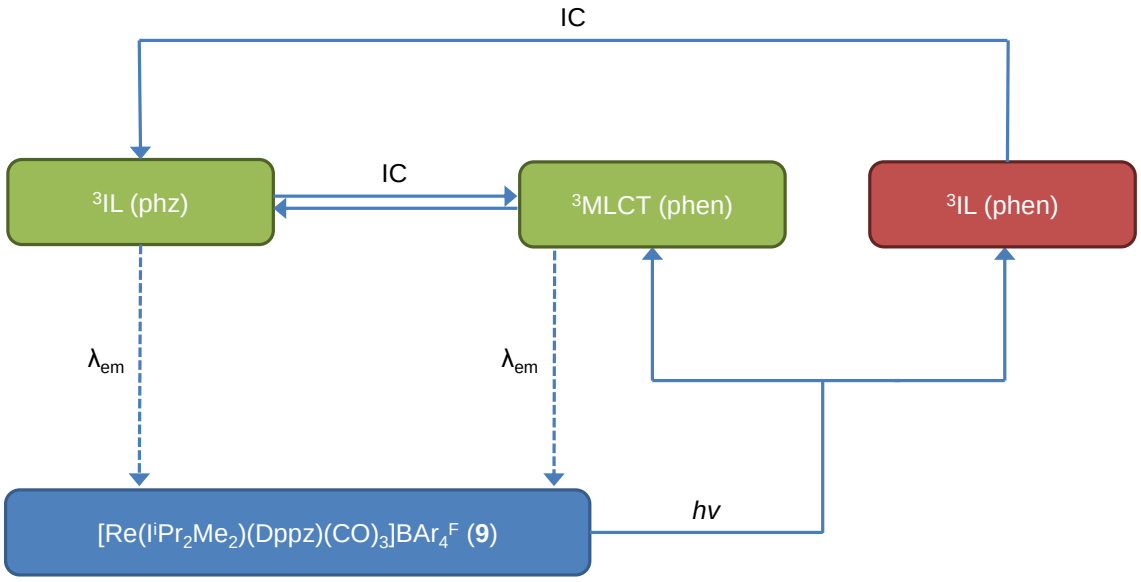

Figure 72: Schematic of the photophysical pathways observed for 9 in CH_2Cl_2 (blue = ground state, red = non-emissive excited state and green = emissive excited state).

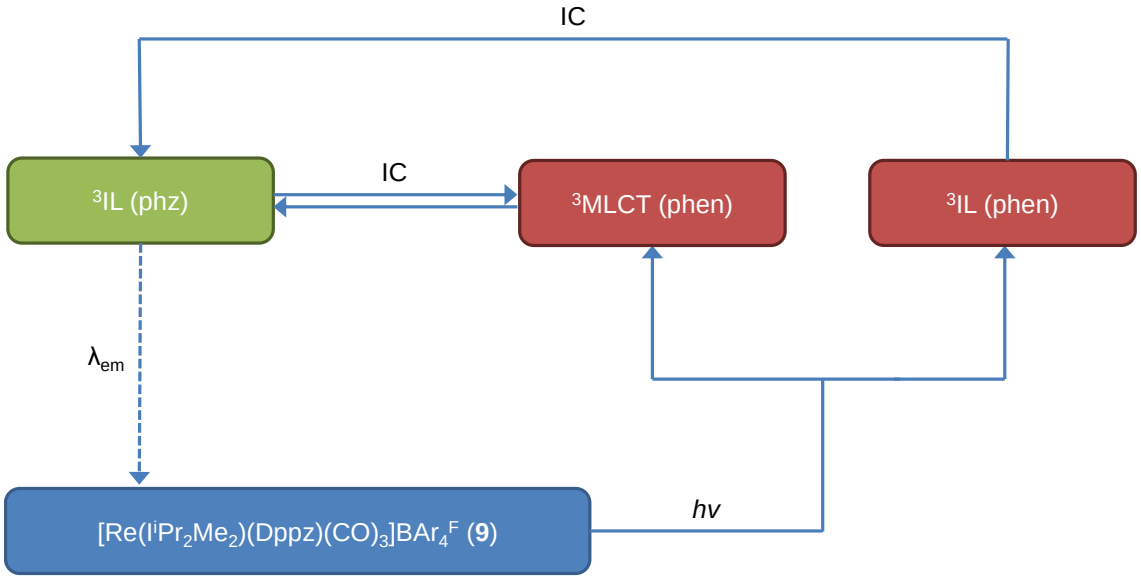

Figure 73: Schematic of the photophysical pathways observed for 9 in MeCN (blue = ground state, red = non-emissive excited state and green = emissive excited state).

At this stage it is worth pausing to compare the results obtained for **9** with the analogous and previously analysed phosphine complex,

fac-[Re(PPh$_3$)(Dppz)(CO)$_3$]$^+$, which is reported to have ^{3}IL π→π* as the lowest energy excited state when irradiated at 355 nm in MeCN at 298 K.[31] This is in contrast to the results obtained for **9**, where it is clear that a combination of ^{3}MLCT and ^{3}IL excited states are present under the same conditions. This suggests that incorporation of NHC in place of phosphine has brought down the energy of the ^{3}MLCT state sufficiently for it to be very close in energy to the ^{3}IL state. However, the effect was not great enough to favour ^{3}MLCT alone as the lowest energy excited state. As such, the backbone of the Dppz ligand was altered to include electron withdrawing fluorine atoms, which should further lower the energy of the ^{3}MLCT excited state.[30]

The photophysics of **10** were altered dramatically compared to **9** and produced quite complex TRIR data; the results in MeCN are clearer than those in CH_2Cl_2 and thus are presented first. The ps-TRIR spectra of **10** in MeCN following laser irradiation at 400 nm under argon at 298 K is shown in Figure 74. The ground state spectrum of **10** shows three v(CO) bands at 2027, 1929 and 1913 cm^{-1}. After irradiation, transient bands at 2056, 1996 and 1951 cm^{-1} were formed, indicating population of the ^{3}MLCT (phen) excited state. The ^{3}MLCT (phen) state grew in over a timescale of *ca*. 6 ps and decayed with a lifetime of *ca*. 0.6 ns to recover the parent. There was no evidence for ^{3}IL excitation.

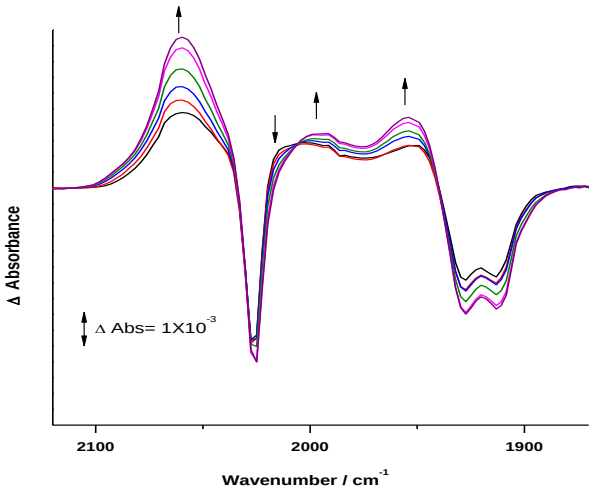

Figure 74: ps-TRIR difference spectra of 10 after irradiation at 400 nm in CH_3CN under argon from 0.7 to 30 ps.

The ps-TRIR spectra of **10** in CH_2Cl_2 following laser irradiation at 355 nm under argon at 298 K is shown in Figure 75. The ground state spectrum of **10** shows three v(CO) bands at 2031, 1934 and 1918 cm^{-1}. After irradiation, transient bands at 2065, 2000 and 1947 cm^{-1} were formed, indicating population of the ^{3}MLCT (phen) excited state, as seen in MeCN. The ^{3}MLCT (phen) state grew in over a timescale of 3.2 (± 0.3) ps and decayed to partially recover the parent. Once again there was no evidence for ^{3}IL excitation.

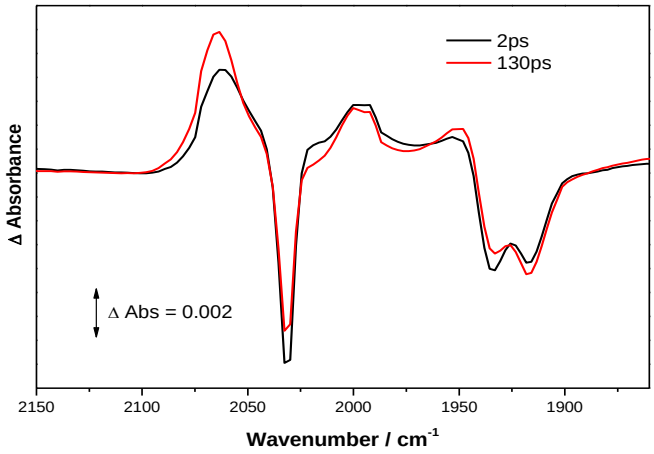

Figure 75: ps-TRIR difference spectra of 10 in CH_2Cl_2 after irradiation at 355 nm under argon at 298 K.

Unfortunately the data become more complex at this stage. As the timescale after the laser pulse increased throughout the experiment, the ^{3}MLCT (phen) bands began to shift slightly. It is possible that this is simply due to vibrational cooling, although the kinetic data for the ^{3}MLCT (phen) state was not always consistent when measured from different bands, which suggests there could be mixing of another state coincident with ^{3}MLCT (phen) on the picosecond timescale.

The ns-TRIR of **10** in CH_2Cl_2 showed population of the ^{3}MLCT (phen) state, which decayed back to fully reform the parent with a lifetime of 630 (± 30) ns (Figure 76).

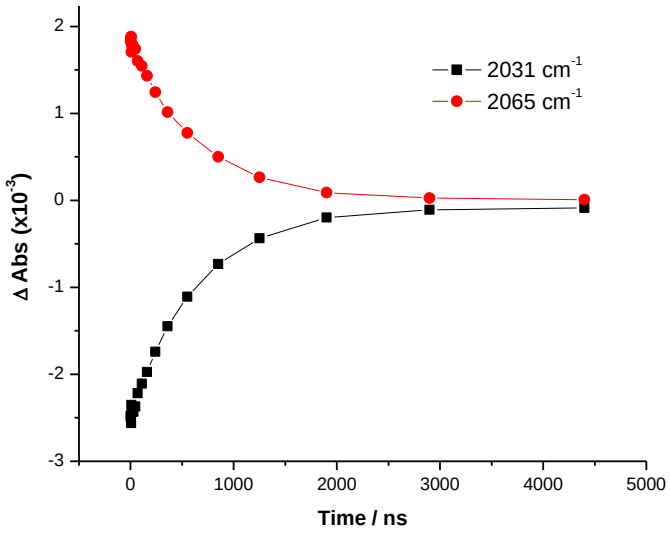

Figure 76: Kinetic traces showing the decay of the ^{3}MLCT (phen) band for 10 and full recovery of the parent.

In summary, the ps- and ns-TRIR data in both MeCN and CH_2Cl_2 is consistent with ^{3}MLCT (phen) as the lowest energy excited state for **10**, which decays *via* emission back to the ground state at 298 K. This is a dramatic change compared to **9**, which showed both ^{3}IL and ^{3}MLCT excitation and suggests that complex **10** may offer ideal properties for use as a DNA probe.

Figure 77 summarises the proposed photophysical pathways for **10** in both CH_2Cl_2 and MeCN. Table 13 (page 107) shows the frequencies of the carbonyl bands for **9** and **10**, alongside all the transients detected upon irradiation in MeCN and CH_2Cl_2.

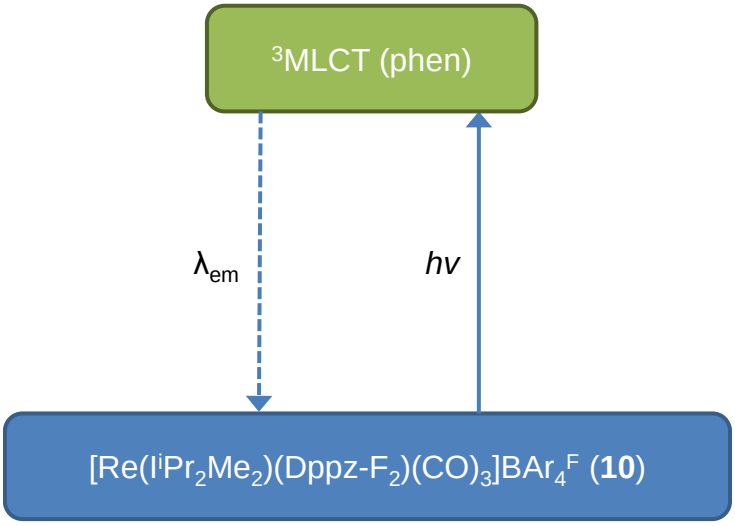

Figure 77: Schematic representing the photophysical pathways observed for 10 in both CH_2Cl_2 and MeCN (blue = ground state, red = non-emissive excited state and green = emissive excited state).

Complex	Solvent	[a]Parent ν(CO) / cm^{-1} bands	[c]Transient ν(CO) / cm^{-1} bands	Assignment
9	CH_2Cl_2	2031, 1937, 1918	2057, 1994, 1947	^{3}MLCT (phen)
			2020, 1903	^{3}IL (phen)
			[b]2026, 1909, 1930	^{3}IL (phz)
9	CH_3CN	2027, 1930, 1913	2064, 1996, 1948	^{3}MLCT (phen)
			2021, 1896	^{3}IL (phen)
			2024, 1903	^{3}IL (phz)
10	CH_2Cl_2	2031, 1934, 1918	[b]2065, 2000, 1947	^{3}MLCT (phen)
10	CH_3CN	2027, 1929, 1913	[b]2056, 1996, 1951	^{3}MLCT (phen)

** Band positions obtained by subtracting 2000 ps spectrum from 2 ps spectrum. Other values are [a]from FTIR ground state, [b]Lorentzian fitting or [c]peak position.*

Table 13: The IR frequencies of the carbonyl bands for 9 and 10, alongside transients formed upon irradiation in MeCN and CH_2Cl_2.

3.8 Conclusions.

A number of synthetic routes to NHC substituted Re(I) diimine tricarbonyl species have been developed and used to produce a series of new compounds, which have been analysed using UV/Vis absorption, emission and TRIR spectroscopy. These experiments have allowed determination of the photochemistry and photophysics of the Re NHC complexes, which has been contrasted to previous research on phosphine analogues. This has led to the identification of numerous similarities between the photochemistry of Re phosphine and NHC complexes, yet perhaps most interestingly, many differences too.

One of the first comparisons in this chapter was between *fac*-[Re(NHC)(Bpy)$(CO)_3$]BAr_4^F and *fac*-[Re(PPh_3)(Bpy)$(CO)_3$]BAr_4^F. In terms of the photochemistry, *fac*-[Re(PPh_3)(Bpy)$(CO)_3$]BAr_4^F eliminates CO at λ_{exc} = 355 nm to afford *trans* substituted products. In contrast, both of the NHC species **5** and **6** were resistant to photolytic dissociation of CO at λ_{exc} = 400, 355 and 266 nm, although broadband steady state irradiation did result in CO substitution and formation of *trans* substituted products. With regard to the photophysics of these systems, irradiation of *fac*-[Re(PPh_3)(Bpy)$(CO)_3$]BAr_4^F results in formation of an emissive ^{3}MLCT excited state at 298 K and a ^{3}IL excited state at 77 K. Under the same conditions **5** and **6** exhibit only a ^{3}MLCT state at both 298 and 77 K. This suggests that the greater donor strength of the NHC has lowered the energy of the ^{3}MLCT with respect to the ^{3}IL state, which raises the possibility of altering the excited state manifold in other such complexes. The ^{3}MLCT excited state for *fac*-[Re(NHC)(Bpy)$(CO)_3$]BAr_4^F proved to be very sensitive to changes in solvent polarity, affecting emission maxima as well as lifetime.

In the case of the Dppz species, *fac*-[Re(PPh_3)(Dppz)$(CO)_3]^+$ exhibits only ^{3}IL excitation and emission at 298 K, whereas *fac*-[Re($I^iPr_2Me_2$)(Dppz)$(CO)_3$]BAr_4^F (**9**) exhibits both ^{3}IL and ^{3}MLCT at 298 K. This again suggests a lowering in energy of the ^{3}MLCT excited state upon introduction of a NHC ligand. The excited state manifold can be further modified by introduction of electron withdrawing groups on the backbone of the Dppz ligand. Thus,

fac-[Re(l^iPr$_2$Me$_2$)(Dppz-F$_2$)(CO)$_3$]BAr$_4^F$ (**10**) exhibits only ^{3}MLCT excitation and emission at 298 K, although ^{3}IL emission is detected at 77 K. Changing the nature of the lowest lying excited state so significantly, but also gradually, by modification of the ligand sphere represents a significant result towards using *fac*-[Re(NHC)(Dppz-F$_2$)(CO)$_3$]BAr$_4^F$ derived complexes as potential DNA probes.

3.9 References.

(1) Vogler, A.; Kunkely, H.; *Coord. Chem. Rev.* **2002**, *230*, 243-251.

(2) Balzani, V.; *Photochem. Photobiol. Sci.* **2003**, *2*, 459-476.

(3) Balzani, V.; Bergamini, G.; Ceroni, P.; *Coord. Chem. Rev.* **2008**, *252*, 2456-2469.

(4) Wagenknecht, P. S.; Ford, P. C.; *Coord. Chem. Rev.* **2011**, *255*, 591-616.

(5) Gafney, H. D.; Adamson, A. W.; *J. Am. Chem. Soc.* **1972**, *94*, 8238-8239.

(6) Creutz, C.; Sutin, N.; *Proc. Nat. Acad. Sci.* **1975**, *72*, 2858 -2862.

(7) Navon, G.; Sutin, N.; *Inorg. Chem.* **1974**, *13*, 2159-2164.

(8) Xue, W.-M.; Chan, M. C.-W.; Su, Z.-M.; Cheung, K.-K.; Liu, S.-T.; Che, C.-M.; *Organometallics* **1998**, *17*, 1622-1630.

(9) Hori, H.; Koike, K.; Ishizuka, M.; Takeuchi, K.; Ibusuki, T.; Ishitani, O.; *J. Organomet. Chem.* **1997**, *530*, 169-176.

(10) McGuinness, D. S.; Saendig, N.; Yates, B. F.; Cavell, K. J.; *J. Am. Chem. Soc.* **2001**, *123*, 4029-4040.

(11) Herrmann, W. A.; Elison, M.; Fischer, J.; K\öcher, C.; Artus, G. R. J.; *Chem. Eur. J.* **1996**, *2*, 772–780.

(12) Tsubaki, H.; Tohyama, S.; Koike, K.; Saitoh, H.; Ishitani, O.; *J. Chem. Soc., Dalton Trans.* **2005**, 385-395.

(13) Schanze, K. S.; Brent MacQueen, D.; Perkins, T. A.; Cabana, L. A.; *Coord. Chem. Rev.* **1993**, *122*, 63-89.

(14) Sato, S.; Sekine, A.; Ohashi, Y.; Ishitani, O.; Blanco-Rodríguez, A. M.; Vlček; Unno, T.; Koike, K.; *Inorg. Chem.* **2007**, *46*, 3531-3540.

(15) Koike, K.; Okoshi, N.; Hori, H.; Takeuchi, K.; Ishitani, O.; Tsubaki, H.; Clark, I. P.; George, M. W.; Johnson, F. P. A.; Turner, J. J.; *J. Am. Chem. Soc.* **2002**, *124*, 11448-11455.

(16) Butler, J. M.; George, M. W.; Schoonover, J. R.; Dattelbaum, D. M.; Meyer, T. J. *Coord. Chem. Rev.* **2007**, *251*, 492-514.

(17) Metcalfe, C.; Thomas, J. A.; *Chem. Soc. Rev.* **2003**, *32*, 215-224.

(18) Dyer, J.; Grills, D. C.; Matousek, P.; Parker, A. W.; Towrie, M.; Weinstein, J. A.; George, M. W.; *Chem. Commun.* **2002**, 872-873.

(19) Olson, E. J. C.; Hu, D.; Hörmann, A.; Jonkman, A. M.; Arkin, M. R.; Stemp, E. D. A.; Barton, J. K.; Barbara, P. F.; *J. Am. Chem. Soc.* **1997**, *119*, 11458-11467.

(20) Hiort, C.; Lincoln, P.; Norden, B.; *J. Am. Chem. Soc.* **1993**, *115*, 3448-3454.

(21) Nair, R. B.; Cullum, B. M.; Murphy, C. J.; *Inorg. Chem.* **1997**, *36*, 962-965.

(22) Fees, J.; Kaim, W.; Moscherosch, M.; Matheis, W.; Klima, J.; Krejcik, M.; Zalis, S.; *Inorg. Chem.* **1993**, *32*, 166-174.

(23) Dyer, J.; Blau, W. J.; Coates, C. G.; Creely, C. M.; Gavey, J. D.; George, M. W.; Grills, D. C.; Hudson, S.; Kelly, J. M.; Matousek, P.; McGarvey, J. J.; McMaster, J.; Parker, A. W.; Towrie, M.; Weinstein, J. A.; *Photochem. Photobiol. Sci.* **2003**, *2*, 542-554.

(24) Fees, J.; Ketterle, M.; Klein, A.; Fiedler, J.; Kaim, W.; *J. Chem. Soc., Dalton Trans.* **1999**, 2595-2600.

(25) Stoeffler, H. D.; Thornton, N. B.; Temkin, S.; L.; Schanze, K. S.; *J. Am. Chem. Soc.* **1995**, *117*, 7119-7128.

(26) Sacksteder, L.; Zipp, A. P.; Brown, E. A.; Streich, J.; Demas, J. N.; DeGraff, B. A.; *Inorg. Chem.* **1990**, *29*, 4335-4340.

(27) Wrighton, M.; Morse, D. L.; *J. Am. Chem. Soc.* **1974**, *96*, 998-1003.

(28) Sacksteder, L.; Lee, M.; Demas, J. N.; DeGraff, B. A.; *J. Am. Chem. Soc.* **1993**, *115*, 8230-8238.

(29) Kuimova, M. K.; Alsindi, W. Z.; Dyer, J.; Grills, D. C.; Jina, O. S.; Matousek, P.; Parker, A. W.; Portius, P.; Zhong Sun, X.; Towrie, M.; Wilson, C.; Yang, J.; George, M. W.; *J. Chem. Soc.,Dalton Trans.* **2003**, 3996-4006.

(30) Kuimova, M. K.; Alsindi, W. Z.; Blake, A. J.; Davies, E. S.; Lampus, D. J.; Matousek, P.; McMaster, J.; Parker, A. W.; Towrie, M.; Sun, X.-Z.; Wilson, C.; George, M. W.; *Inorg. Chem.* **2008**, *47*, 9857-9869.

(31) Schoonover, J. R.; Bates, W. D.; Meyer, T. J.; *Inorg. Chem.* **1995**, *34*, 6421-6422.

Chapter 4 - Introduction

4.1 NHC complexes of manganese and rhenium.

The number of manganese and rhenium NHC complexes in the literature is limited in comparison to other mid/late transition elements. Most of the complexes that have been studied are in high oxidation states.[1] There are remarkably few manganese or rhenium(I) NHC complexes. This is rather unusual as there are lots of Mn/Re(I) phosphine substituted complexes with interesting reactivity. During the course of the synthesis of the compounds in Chapter 3, many new Mn/Re(I) NHC complexes were prepared. Whilst some of these compounds were subjected to photochemical investigations where appropriate, most of the reactivity that will be discussed in Chapter 5 involves thermal transformations, primarily due to the relative scarcity of similar compounds in the literature and the interesting nature of their reactivity.

Angelici *et al* prepared a range of manganese and rhenium(I) phosphine and phosphite complexes, almost 50 years ago, from the simple $M(CO)_5X$ precursors (X = Br, Cl) (Figure 78).[2]

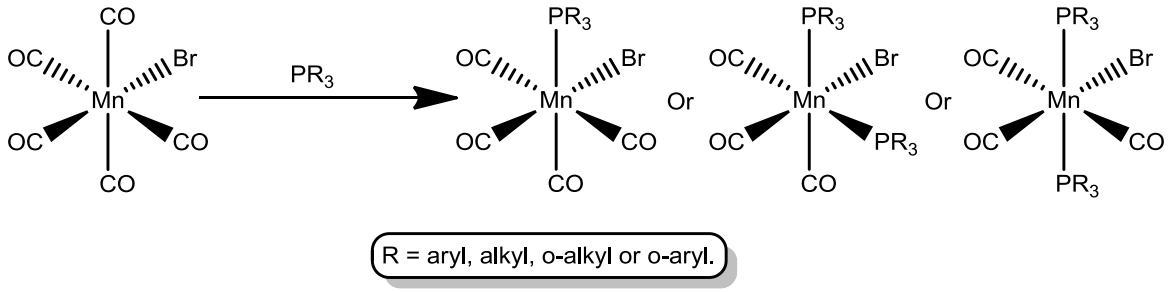

Figure 78: Schematic summary of the complexes produced by Angelici *et al*.

Forming NHC analogues of these compounds provided an excellent starting point for expanding the number of known manganese and rhenium(I) NHC complexes and a suitable point of reference for literature comparison. When $Mn(CO)_5Br$ was reacted with $P(OC_6H_5)_3$ at 310 K in chloroform for 12 hours the disubstituted *cis,fac*-$Mn(P(OC_6H_5)_3)_2(CO)_3Br$ compound is produced. However,

when the same reagents were reacted at 328 K *trans,mer*-$Mn(P(OC_6H_5)_3)_2(CO)_3Br$ was obtained. Similarly, PPh_3 was found not to react with $Mn(CO)_5Br$ at low temperature, but at higher temperature, *trans,mer*-$Mn(PPh_3)_2(CO)_3Br$ is formed. These observations indicated that at low temperature the reaction with PR_3 proceeds *via* kinetic control, but at higher temperatures under thermodynamic control where the less sterically frustrated *trans* isomer is favoured. Kinetic experiments to observe this isomerisation between 323 and 343 K found that the rate of reaction was first order, with respect to the manganese complex, zero order with respect to additional PR_3 ligand and almost independent of the solvent used. The activation energy for the isomerisation increased with the steric bulk of the PR_3 ligand.

In a follow up study Angelici *et al.* determined the rate and mechanism for the initial reaction of $Mn(CO)_5X$ (X = Cl, Br or I) with L (L = PR_3 and AsR_3).[3] A dissociative mechanism was inferred, with CO loss as the rate-determining step, due to the rate constants of reaction being independent of the entering ligand, dependent on the strength of the M-C bond and matching the rate of CO exchange. Bulkier entering ligands halted reaction at the monosubstituted product, but smaller, more flexible ligands progressed to disubstitution. In all cases initial formation of the *cis*-$Mn(CO)_4(L)X$ species was observed, presumably favoured by the greater degree of back bonding to the carbonyl *trans* to the halide. Reaction with $Mn(CO)_5X$ depended mainly on the σ donor strength of the entering ligand rather than the π acceptor properties. This trend was also reflected in the IR spectra of the compounds where the most π accepting ligands yielded complexes with the highest carbonyl stretching frequencies.

The rate of reaction of *cis*-$Mn(CO)_4(L)X$ with L' (L' = $P(OR)_3$ or $PRCl_2$) was also studied.[4] Similarly, the rate of reaction was zero order with respect to the entering ligand and first order with respect to the complex, with minor solvent effects, indicating a dissociative mechanism with CO loss as the rate determining process. In all cases the *cis,fac*-$Mn(CO)_3(L)(L')X$ species formed initially, although with some of the bulkier ligands subsequent isomerisation to *trans,fac*-$Mn(CO)_3(L)(L')X$ was seen. Interestingly, the rate of reaction was

dependent on the nature of L. Complexes with bulky L ligands favoured CO loss and increased the rate of substitution for L'.

Kubas *et al* revisited this area in 1998.[5] Upon protonation of the methyl group in *cis*-$Re(Me)(CO)_4(PPh_3)$ with $[H(Et_2O)_2]BAr_4^F$ in diethylether, the solvated salt $[Re(CO)_4(PPh_3)(OEt_2)]BAr_4^F$ was produced. The analogous reaction of *cis*-$Re(Me)(CO)_4(PPh_3)$ with $[Ph_3C]BAr_4^F$ in CH_2Cl_2, led to abstraction of the methyl group and formation of $[Re(CO)_4(PPh_3)(CH_2Cl_2)]BAr_4^F$ (Figure 79).

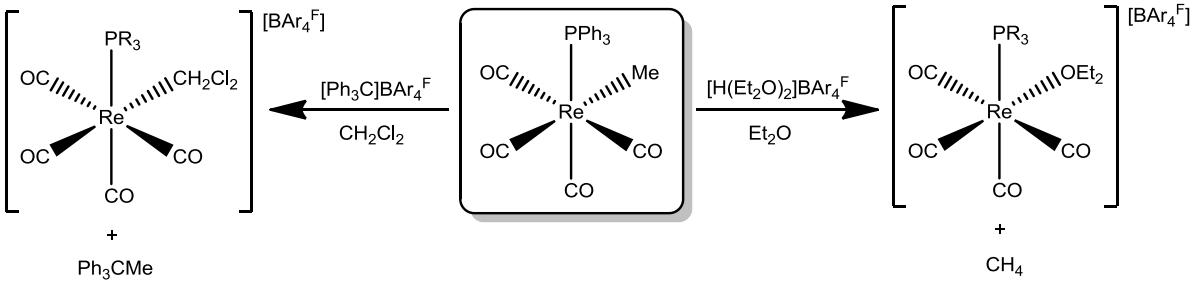

Figure 79: Schematic illustrating the solvato complexes prepared by Kubas *et al*.

This was one of the first organometallic dichloromethane complexes ever to be isolated and crystallographically characterised, which indicated unique binding properties for the metal centre. Interaction with very weak bases, such as dichloromethane that are typically associated with poor ligation properties, is intriguing, but this complex also provided a useful source of the corresponding 16 e^- metal fragment due to the high lability of the CH_2Cl_2 ligand in solution. This was demonstrated by dissolving $[Re(CO)_4(PPh_3)(CH_2Cl_2)]BAr_4^F$ in non-coordinating C_6H_5F under an atmosphere of H_2 which produced the dihydrogen complex, $[Re(CO)_4(PPh_3)(H_2)]BAr_4^F$. Measurement of the longitudinal relaxation time (T_1) of this species at different temperatures produced a very short T_1 minimum of *ca*. 13 ms, confirming the identity as a metal dihydrogen species. The coordination properties of highly electrophilic cationic metal fragments had been examined previously, but the combination of careful solvent selection to avoid polar, coordinating species and the use of large non-coordinating anions has subsequently allowed isolation of these interesting solvent and small molecule complexes.

A similar experiment by Heinekey demonstrated that when $Re(PR_3)_2(CO)_3(R')$ (R = Ph, Cy or ^iPr, R' = H or Me) was protonated with $[H(Et_2O)_2]BAr_4^F$ under H_2 the dihydrogen complex $[Re(CO)_3(PR_3)_2(H_2)]BAr_4^F$ formed (Figure 80).[6]

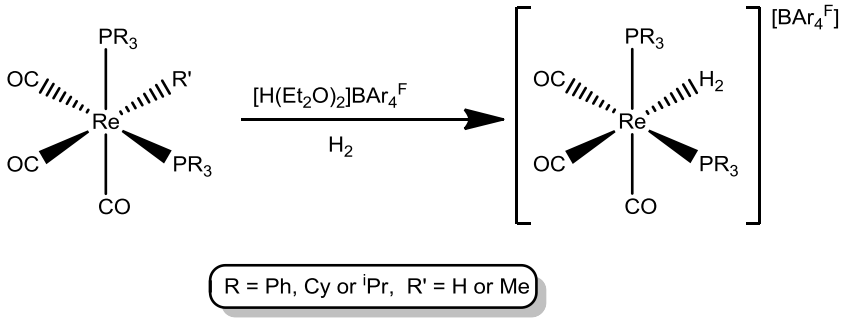

Figure 80: Schematic illustrating the dihydrogen complex observed by Heinekey *et al*.

However, upon attempted isolation, the dihydrogen complex was not observed. Instead an agostic species, $[Re(CO)_3(PPh_3)_2]BAr_4^F$, with an interaction from the PR_3 ligand to the metal centre was obtained. The binding of H_2 in these complexes is typically highly reversible unless a base is added which can deprotonate the heterolytically activated and relatively acidic bound dihydrogen. Comparable reactivity was observed for the manganese analogue. Toupadakis reacted $Mn(PCy_3)_2(CO)_3Br$ with $NaBAr_4^F$ in dichloromethane and produced the agostic stabilised green salt, $[Mn(PCy_3)_2(CO)_3]BAr_4^F$.[7] When placed under an atmosphere of dihydrogen this compound turns light yellow as it coordinates H_2. At room temperature, the bound dihydrogen is very labile and is present in equilibrium with the agostic compound, but no coordinated dichloromethane complex is observed. The dihydrogen product can be favoured by lowering the temperature and at 195 K under <1 atm. of H_2 it is the only product observed. Intriguingly, other small molecules, such as N_2 and ethene, were unable to coordinate in place of dihydrogen in this system. This can be explained by examining the electrophilicity of the metal centre, which appears to play an important role in the stability of complexes of this type. For example, whilst $[Mn(CO)(Ph_2PC_2H_4PPh_2)_2(N_2)]^+$ is known to exist, the analogous dinitrogen complexes for $[M(PR_3)(CO)_4]^+$ and $[M(PR_3)_2(CO)_3]^+$ do not. Due to the nature of N_2 binding to metal centres, which is dominated by back bonding from the

metal, this observation can be explained by the tetra- and tricarbonyls' much higher degree of electrophilicity, which prevents the necessary degree of back bonding from the metal. Toupadakis *et al* commented that dihydrogen appeared to be a very versatile ligand for complexes of this type, and in general, its coordination to a metal centre can be stabilised by both σ-complexation and donation to the metal (electrophilic metals) and back bonding from the metal to the ligand (nucleophilic metals). In fact, most metal dihydrogen complexes exhibit degrees of both binding modes, which is perhaps the rational for the versatility of H_2 as a coordinating small molecule, allowing coordination to a variety of both electrophilic and nucleophilic metal centres.

Shortly after this Kubas *et al* published two clever follow up studies. The first of these examined the reactivity of the highly electrophilic, unsaturated fragments, $[Re(PPh_3)(CO)_4]X$ (X = BAr_4^F or $MeB(C_6F_5)_3$), by combining the corresponding dichloromethane solvated species with dihydrogen, silanes and alkenes.[8] Both dihydrogen and $HSiEt_3$ formed the expected σ complexes at low temperature, but upon warming to room temperature underwent intramolecular heterolytic cleavage, initially eliminating a proton or $^+SiEt_3$ to give the corresponding neutral metal hydrides. These go on to rapidly combine with residual solvated species forming cationic metal-metal bonded, bridged hydride containing products $[(Re(PPh_3)(CO)_4)_2(\mu\text{-}H)]MeB(C_6F_5)$ (plus methane/Et_3SiMe) and $[(Re(PPh_3)(CO)_4)_2(\mu\text{-}H)]BAr_4^F$ (plus $Et_3SiOSiEt_3$/Et_3SiF/1,3-$(CF_3)_2(C_6H_4)$), depending on the nature of the small molecule that is introduced and the anion present in the reaction (Figure 81).

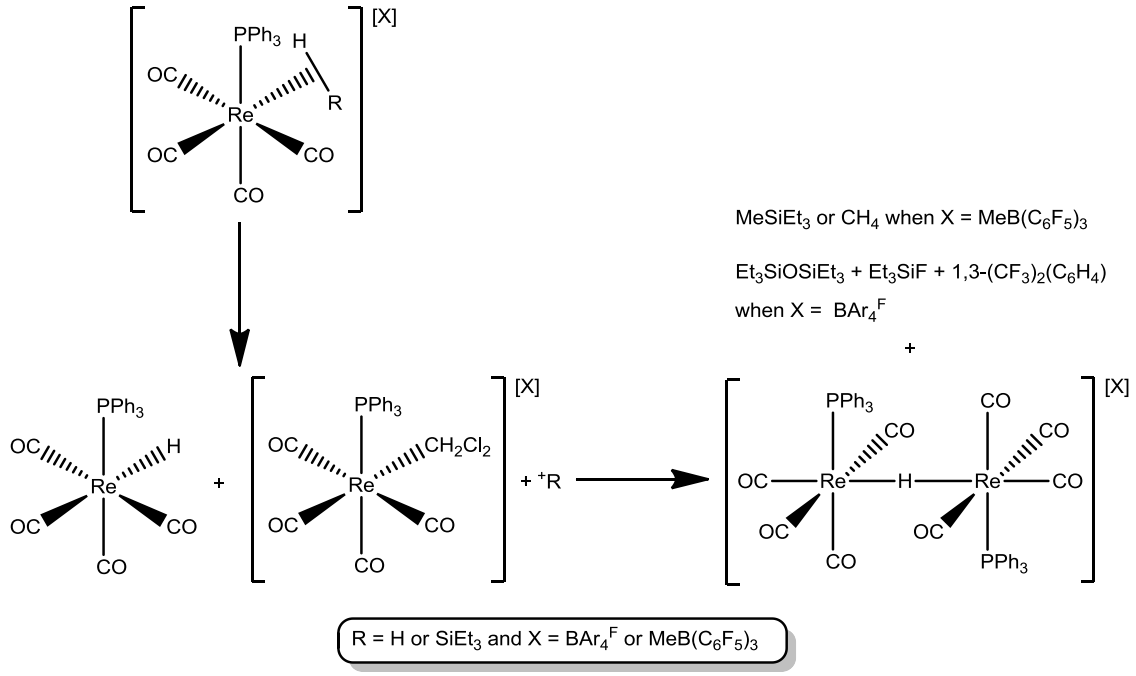

Figure 81: Schematic illustrating the degradation of $[Re(PPh_3)(CO)_4(H\text{-}R)][X]$ as observed by Kubas et al.

Addition of alkenes to $[Re(CO)_4(PPh_3)(CH_2Cl_2)]X$ led to good yields of the coordinated alkene complexes, which remained able to rotate around the metal-alkene bond even at very low temperatures, indicating that binding is predominantly σ donating in nature; these compounds were stable at room temperature.

In the second study by Kubas *et al* tied-back phosphites, incapable of forming agostic interactions, were used to synthesise both $M(CO)_3(P(OR)_3)_2(Me)$ and $M(CO)_4(P(OR)_3)(Me)$ (M = Mn or Re and $P(OR)_3$ = $P(OCH_2)_3CMe$)) (Figure 82).[9,10]

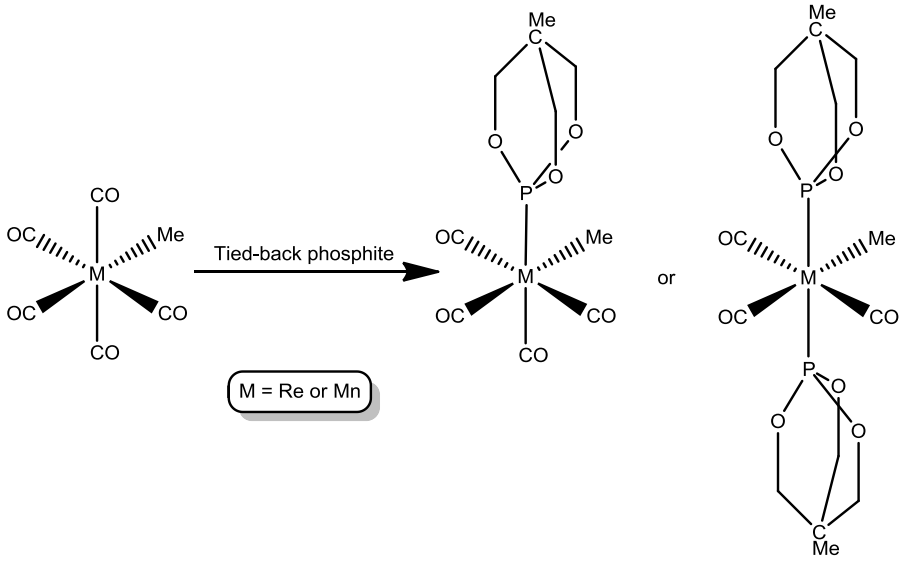

Figure 82: Schematic illustrating the tied-back phosphite complexes produced by Kubas *et al*.

This produced a series of compounds which were not only incapable of agostic stabilisation, but even more electrophilic than their phosphine analogues. When these precursors were reacted with $[Ph_3C]BAr_4^F$ in dichloromethane, all produced the anticipated solvated compounds, which were also highly labile in solution yet, at least for the Re(I) species, coordinated strongly enough in the solid state that they could not be removed under high vacuum. These dichloromethane compounds were also subjected to further experiments with small molecules. Reaction of *mer*-$Mn(CO)_3(P(OCH_2)_3CMe)_2(Me)$ with $[Ph_3C]BAr_4^F$ under dihydrogen at low temperature formed an equilibrium between the expected H_2 complex and starting material.

Upon warming the dihydrogen species were also subject to heterolytic cleavage, albeit to a lesser extent than seen for $[Re(PPh_3)(CO)_4(\eta^2\text{-}H_2)]X$ (X = $MeB(C_6F_5)$ or BAr_4^F). When used in the presence of $HSiEt_3$ and phenol, [*mer*-$Mn(CO)_3(P(OCH_2)_3CMe)_2(\eta^1\text{-}CH_2Cl_2)]BAr_4^F$ is a highly effective catalyst for production of Et_3SiOPh and H_2. Reaction of both the solvated rhenium dichloromethane species with Et_2O, Et_3SiH and COD displaced the dichloromethane to form the ether, η^2-$HSiEt_3$ and COD complexes. All were room temperature stable apart from the $[Re(P(OCH_2)_3CMe)(CO)_4(\eta^2\text{-}HSiEt_3)]BAr_4^F$ complex which decomposed *via* heterolytic cleavage of the Si-H

bond. The $[Re(P(OCH_2)_3CMe)_2(CO)_3(\eta^2\text{-}HSiEt_3)]BAr_4^F$ complex is a very rare example of a stable, cationic η^2-silane complex.

Understanding the interaction of small molecules such as silanes and dihydrogen, with transition metal centres is imperative to the modern goals of organometallic chemistry and homogeneous catalysis. These include complexation and catalytic functionalisation of alkanes, capture and fixation of CO_2, hydrogen storage and release and catalytic organic transformations using syngas ($CO + H_2$) or other waste gas materials. The rhenium and manganese(I) complexes discussed here, particularly their cationic derivatives, could prove to be a fruitful area of study for furthering the present understanding of organometallic small molecule and solvent complexes.

4.2 References.

(1) Braband, H.; Kuckmann, T. I.; Abram, U.; *J. Organomet. Chem.* **2005**, *690*, 5421-5429.

(2) Angelici, R. J.; Basolo, F.; Poe, A. J.; *Nature* **1962**, *195*, 993-994.

(3) Angelici, R. J.; Basolo, F.; *J. Am. Chem. Soc.* **1962**, *84*, 2495-2499.

(4) Angelici, R. J.; Basolo, F.; *Inorg. Chem.* **1963**, *2*, 728-731.

(5) Huhmann-Vincent, J.; Scott, B. L.; Kubas, G. J.; *J. Am. Chem. Soc.* **1998**, *120*, 6808-6809.

(6) Heinekey, D. M.; Radzewich, C. E.; Voges, M. H.; Schomber, B. M.; *J. Am. Chem. Soc.* **1997**, *119*, 4172-4181.

(7) Toupadakis, A.; Kubas, G. J.; King, W. A.; Scott, B. L.; Huhmann-Vincent, J.; *Organometallics* **1998**, *17*, 5315-5323.

(8) Huhmann-Vincent, J.; Scott, B. L.; Kubas, G. J.; *Inorg. Chim. Acta.* **1999**, *294*, 240-254.

(9) Fang, X.; Huhmann-Vincent, J.; Scott, B. L.; Kubas, G. J.; *J. Organomet. Chem.* **2000**, *609*, 95-103.

(10) Fang, X.; Scott, B. L.; John, K. D.; Kubas, G. J.; *Organometallics* **2000**, *19*, 4141-4149.

Chapter 5

5.1 Neutral and cationic NHC complexes of manganese (I) and rhenium (I) derived from carbonyl halide precursors.

During the course of the synthesis required for the compounds in Chapter 3, a number of novel manganese and rhenium(I) NHC complexes were produced. As mentioned previously, there are very few examples of such compounds in the literature.[1] This chapter investigates the reactivity of species formed upon abstraction of the halide ligand with $NaBAr_4^F$, which resulted in a number of new compounds stabilised by solvent, small molecule coordination and agostic binding from the NHC ligands.

5.2 Synthesis of $M(I^iPr_2Me_2)_2(CO)_3X$ (M = Mn, X = Br; M = Re, X = Cl).

During the synthesis for $[Re(NHC)(diimine)(CO)_3]X$ it was found that adaption of the literature preparation for the PPh_3 analogue (Figure 31) by introducing NHC in place of PPh_3 did not result in formation of the desired product. As such, the NHC had to be introduced much earlier in the synthesis and direct reaction of NHCs with $M(CO)_5(X)$ was investigated. A brief look at the literature showed that in 1977 Lappert had tried to react $Mn(CO)_5X$ (X = Br, Me) and $Mn_2(CO)_{10}$ with the dimers of the saturated carbenes 1,3-dimethyl- and 1,3-diethyl-imidazolidin-2-ylidene, but observed no reaction.[2] Substitution of phosphine for NHC was possible in $Mn(PPh_3)_2(CO)_3Br$, although the resulting complex, *fac*-$Mn(SIMe)_2(CO)_3Br$, was produced in only 5% yield. This is surprising behaviour for a highly electrophilic metal centre, where CO substitution for the strongly donating NHC may be expected to yield stable species. Substitution of CO for NHC should increase the electron density available for back bonding to the remaining CO groups, thus strengthening the M-C bonds as is seen for phosphine analogues.[3] This led to the belief that the dimer used by Lappert may not be a good source of the NHC ligand in this case.

Addition of 2 equiv. of the free carbene $I^iPr_2Me_2$ to a benzene solution of $Mn(CO)_5Br$ at room temperature resulted in the instantaneous evolution of CO and formation of the bis-carbene complex $Mn(I^iPr_2Me_2)_2(CO)_3Br$ (**11**), which was isolated as an orange solid in *ca*. 50% yield. The rhenium counterpart $Re(I^iPr_2Me_2)_2(CO)_3Cl$ (**12**) was prepared from $Re(CO)_5Cl$ under more forcing conditions (343 K, 2 hours) and was isolated in 80% yield as a white solid (Figure 83). This process was investigated with other free NHCs and appeared to be quite generic, although ligand bulk plays an important part in the structures obtained; more details are given later in the chapter. Importantly at this stage, suitable starting materials for the synthesis of the target complexes in Chapter 3 had now been obtained. However, these compounds were also excellent candidates for a comparative study with phosphine analogues, especially considering the interest paid to species of the general formula $M(PR_3)_n(CO)_{(5-n)}X$ (M = Mn or Re; X = Cl, Br or I; n = 1, 2) and the ability of the corresponding cations $[M(PR_3)_n(CO)_{(5-n)}]^+$ to form σ-complexes.[4,5,6,7,8,9] As such, further investigation of the substitution chemistry of $M(CO)_5X$ (M = Re, X = Cl; M = Mn, X = Br) with free N-alkyl and N-aryl NHCs was undertaken, with a view towards the possibility of forming analogous cationic species *via* halide abstraction.

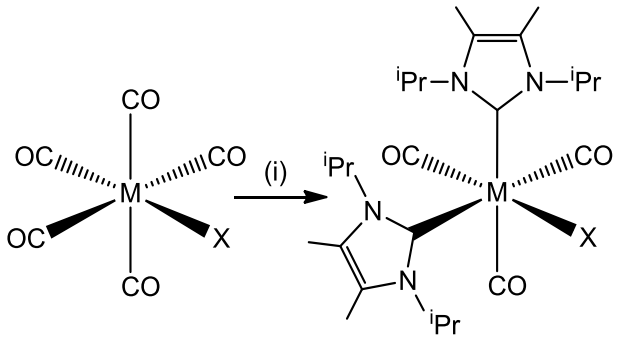

M = Mn, X = Br (**11**)
M = Re, X = Cl (**12**)

(i) 2 eq $I^iPr_2Me_2$, C_6H_6, (Mn: 298 K; Re: 343 K).

Figure 83: Reaction scheme for the formation of $M(I^iPr_2Me_2)_2(CO)_3X$ (M = Mn, X = Br; M = Re, X = Cl).

Both **11** and **12** were characterized as facial isomers by a combination of IR and NMR spectroscopy, as well as by X-ray crystallography. Three strong carbonyl bands were observed for **11** at 2004, 1926 and 1864 cm^{-1} and for **12** at 2009, 1911 and 1857 cm^{-1}. The frequencies for **12** are close to those reported for $Re(I^iPr_2)_2(CO)_3Br$.[10] The appearance of four methine proton septets in the ^1H NMR spectra (Figure 84) of both **11** (δ 6.89, 6.03, 5.23, 5.15) and **12 (**δ 6.57, 6.04, 5.50, 5.26) reveals the presence of restricted rotation about the M-C_{NHC} bonds and thus, as seen for $Re(I^iPr_2)_2(CO)_3Br$, chemical inequivalence throughout both molecules.[11] Similarly, two $^{13}C\{^1H\}$ carbene resonances were observed, with those for manganese at δ 191.1 and 190.0 being higher in frequency than the two signals for the rhenium analogue which were at δ 180.5 and 179.2. A similar variation has been observed previously by Kaufold *et al* in complexes of group VII metals containing macrocyclic NHC ligands.[12]

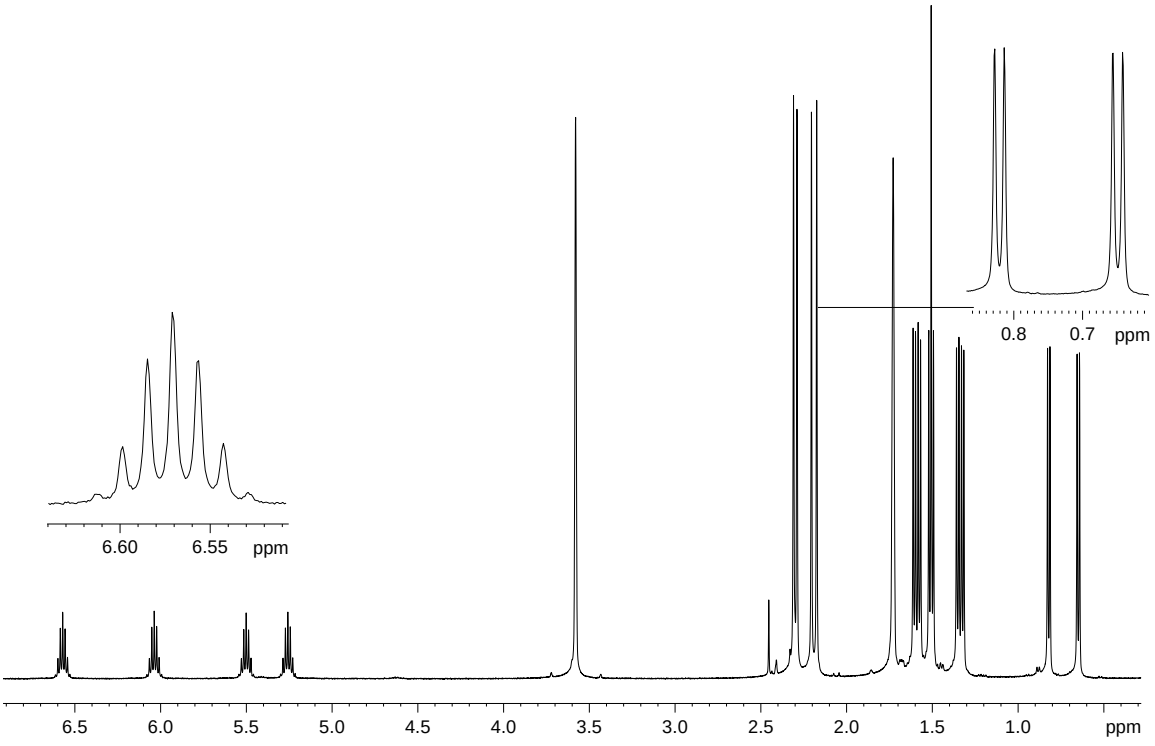

Figure 84: 500 MHz ^1H NMR spectrum of $Re(I^iPr_2Me_2)_2(CO)_3Cl$ (12) in d_8-THF at 298 K.

The X-ray crystal structures of the two complexes are shown in Figure 85, with selected bond lengths and angles shown in Tables 14 and 15 (pages 145 and 146). In both cases, the structures contain a mirror plane rendering the two *trans* OC-M-$I^iPr_2Me_2$ crystallographically identical. As expected, the Mn-C_{NHC}

distance in **11** (2.093(4) Å) is shorter than the Re-C_{NHC} bond length in **12** (2.224(4) Å), the latter being the same as that found in the I^iPr_2 analogue.[11] In both cases the NHCs are oriented such that the isopropyl groups nest approximately midway between pairs of the remaining ligands. This serves to minimize steric repulsions between the *cis* $I^iPr_2Me_2$ moieties. Angles between the least square planes of the imidazole rings are 68.9 and 68.5° in **11** and **12**, respectively.

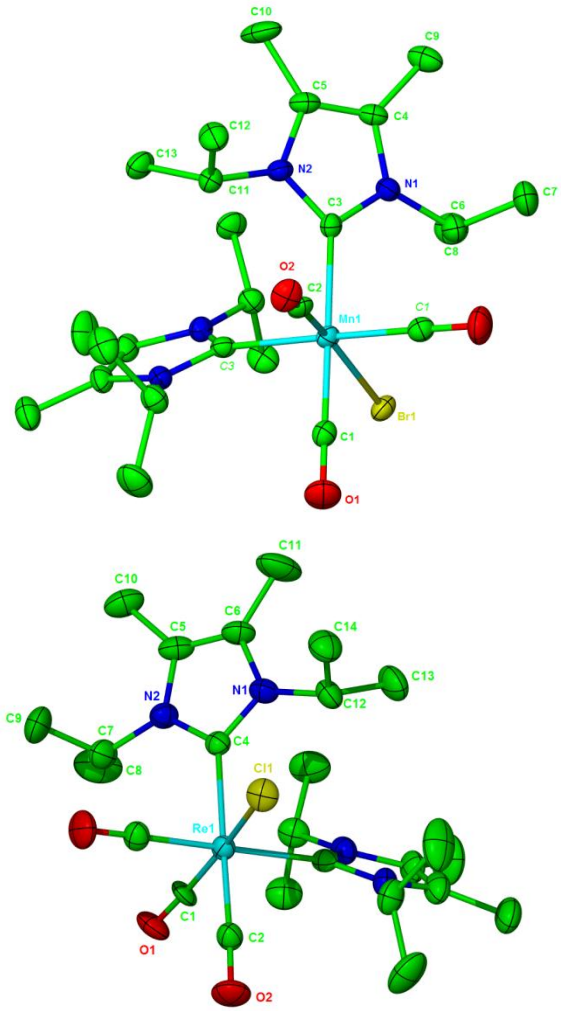

Figure 85: X-ray crystal structures of (top) 11 and (bottom) 12. Thermal ellipsoids shown at 30% level with all hydrogen atoms and minor disordered components omitted for clarity.

To purify $Re(I^iPr_2Me_2)_2(CO)_3Cl$ it was washed with dry EtOH, to remove any free NHC or $Re(CO)_5Cl$, prior to recrystallisation. When $Mn(I^iPr_2Me_2)_2(CO)_3Br$ was washed with EtOH, there was an immediate colour change from an orange to

yellow solution with formation of a small amount of vivid green precipitate. The green solid was removed *via* filtration and found to contain a hydride species by ^{1}H NMR spectroscopy, the identity of which will be discussed later. The yellow filtrate was dried under vacuum and recrystallised from CH_2Cl_2 / hexane to afford light yellow crystals suitable for X-ray diffraction.

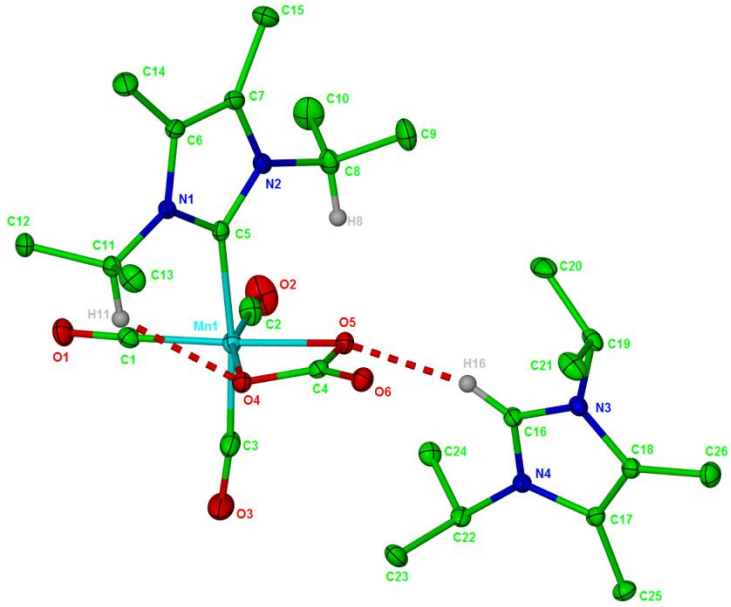

Figure 86: X-ray crystal structure of [Mn(I^{i}Pr$_2$Me$_2$)(O$_2$CO)(CO)$_3$]I^{i}Pr$_2$Me$_2$-H. Thermal ellipsoids shown at 30% level with all hydrogen atoms, other than those involved in close contacts, omitted for clarity.

The molecular structure obtained (Figure 86) indicated formation of a novel charged bidentate carbonato species, [Mn(I^{i}Pr$_2$Me$_2$)(O$_2$CO)(CO)$_3$]I^{i}Pr$_2$Me$_2$-H (**13**), with a strong intermolecular hydrogen bond from an oxygen on the carbonate to the proton on the imidazolium cation. Unfortunately, it was not possible to isolate enough of this compound from the free imidazolium salt, and other products formed in the reaction, in order for full characterisation to be obtained. Nonetheless, the intriguing nature of this species and the characterisation that was acquired are well worth discussing. The ^{1}H NMR spectrum of **13** is shown in Figure 87 and the ^{13}C-^{1}H HMBC spectrum in Figure 88. The HMBC is rather interesting as it shows a correlation between the imidazolium proton on the counter ion with the carbonato carbon, i.e. J-coupling through the hydrogen bond.[13,14] Whilst this is not unheard of for strong

hydrogen bonds in protein chemistry, it is quite unusual for organometallic species, particularly a carbon hydrogen correlation.

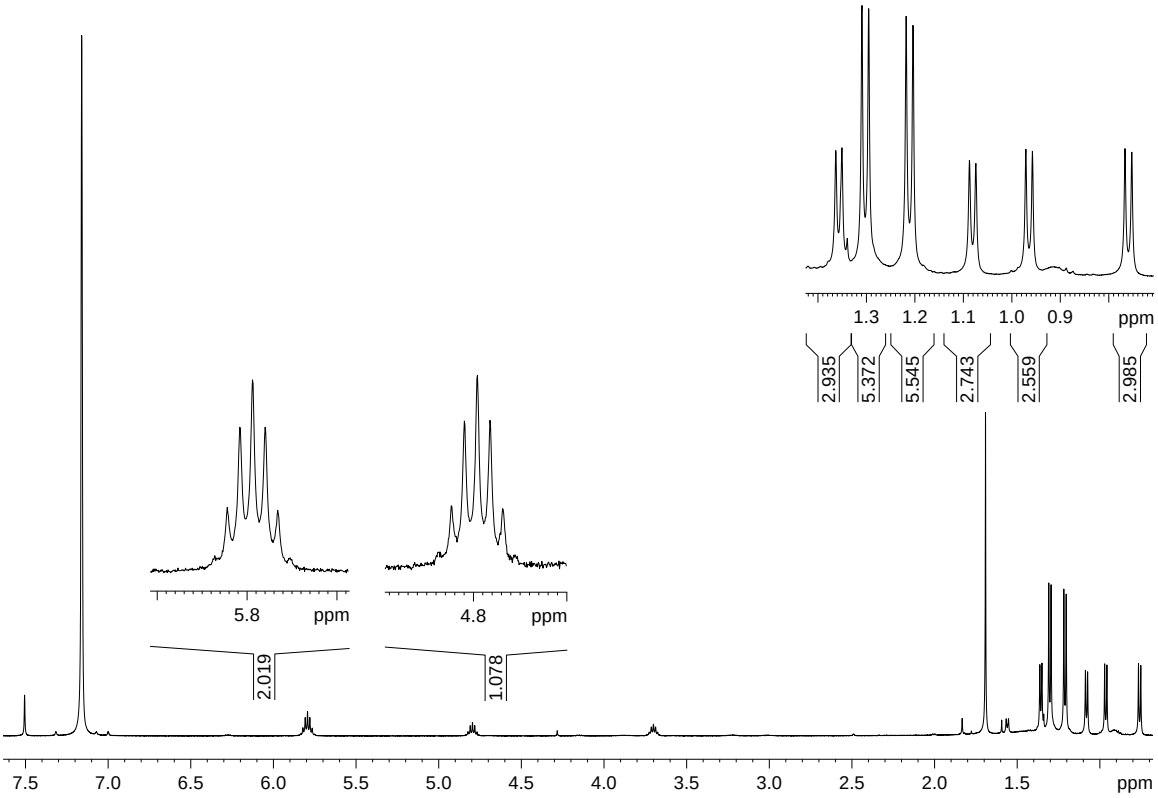

Figure 87: 500 MHz ^{1}H NMR spectrum of [Mn(l^{i}Pr$_2$Me$_2$)(O$_2$CO)(CO)$_3$][l^{i}Pr$_2$Me$_2$-H] (13) in C$_6$D$_6$ at 298 K.

Whilst monodentate carbonates and alkoxides of both Mn and Re(I) compounds exist, to the best of our knowledge this structure is the first non-bridging, bidentate carbonato complex of manganese(I).[15]

The route to **13** from reaction of EtOH with Mn(l^{i}Pr$_2$Me$_2$)$_2$(CO)$_3$Br is not immediately obvious. However, by comparison to similar transformations in the literature some possibilities can be discussed.[16,17] One such transformation, which may offer an insight into the mechanism involved here is metal alkoxide formation followed by CO_2 insertion, often seen for Lewis acidic metal centres. Johnson *et al* built upon this principle to design a one-pot synthesis for the formation of manganese and rhenium (I) alkylcarbonato complexes. The dimer, $Mn_2(CO)_{10}$, was reacted with DPPP in the presence of a 4:1 mixture of 1-pentanol:1-propanol.[18] Exposure to CO_2 gave approximately 1 equiv. of

$Mn(DPPP)(CO)_3(H)$ and $Mn(DPPP)(CO)_3(OC(O)OR)$ (R = $(CH_2)_2CH_3$ or $(CH_2)_4CH_3$) after 4 hours. When conducted under argon only the hydride was observed.

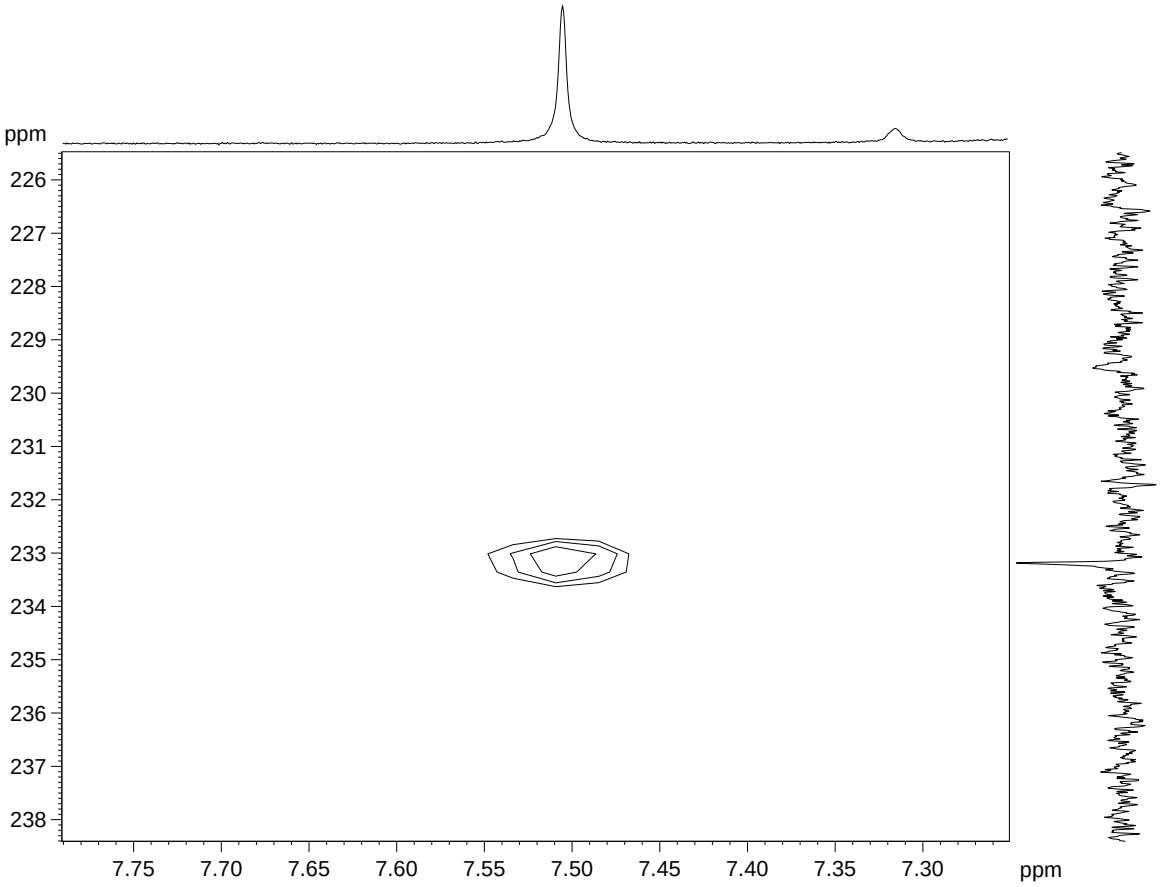

Figure 88: ^{1}H-^{13}C HMBC spectrum of (13) in C_6D_6, showing the cross peak for the strong hydrogen bond *J*-coupling between the imidazolium proton and carbonato carbon.

The reaction of $Mn(I^{i}Pr_2Me_2)_2(CO)_3Br$ and EtOH was carried out with rigorous exclusion of air and moisture to give *ca*. 63% of **13** from the yellow filtrate, and 6% of $Mn(I^{i}Pr_2Me_2)_2(CO)_3(H)$ (**14**) from recrystalisation of the green solid, along with imidazolium salt and other unidentified products. Even with such a low yield, it was possible to isolate small crystals of **14**, but unfortunately, the diffraction data obtained was less than ideal and inconclusive with regards to resolving the hydride ligand. However, the ^{1}H NMR spectrum of the reaction mixture did indicate the presence of a broad low frequency singlet at δ -4.83 ppm. The signals for the isopropyl C-H (6.73-6.12 ppm) and methyls (1.57-0.75 ppm) were very broad and the backbone methyl groups (1.76 ppm) were also broad at room temperature. Additionally, the solution IR spectrum of the crystals in C_6D_6 indicated a facial tricarbonyl species, with the appearance of three

bands at 1966 (s), 1876 (m) and 1845 (m) cm^{-1}. It was not possible to fully characterise **14** from this reaction, and an alternative route was sought by direct reaction of $Mn(I^iPr_2Me_2)_2(CO)_3Br$ and $NaBH_4$ in tetrahydrofuran. After 1 hour at 343 K the solution had turned from orange to green and the ^1H NMR spectrum indicated formation of **14** along with other unidentified products. It was not possible to isolate **14** from the reaction mixture. As such, the reaction was heated further in an effort to drive the formation of **14** to completion, but this led to precipitation of an off-white solid and formation of a red solution. At this stage of the reaction it was no longer possible to collect satisfactory NMR data or to isolate anything from the resultant solution. Unfortunately, despite all attempts it was not possible to conclusively prove the assignment of **14**.

Nonetheless, the presence of only very small amounts of **14** even with rigorous exclusion of air or moisture suggests two possibilities. Firstly, that the NHC complex is far more reactive than the phosphine system and able to react with trace amounts of adventitious CO_2. Secondly, an unanticipated process is responsible for formation of **13**, possibly deriving from activation of the ethanol solvent. The latter suggestion is probably more likely in this case as the relative concentration of atmospheric CO_2 is low and will be almost imperceptible inside a vessel under argon when handled with standard air sensitive procedures. Unfortunately, further experiments, such as reaction with ^{18}O labelled ethanol, would be required to confirm the involvement of the solvent in the formation of **13**, which is beyond the scope of this work.

However, if the formation of an intermediate monodentate alkylcarbonato species is assumed to occur (Figure 89), then the observation of the $^2J_{CH}$ correlation in the HMBC may suggest a possible mechanism for formation of **13**. The strong H-bond and the solution NMR data indicate that **13** exists as an intimate ion pair in benzene solution, like those described by Winstein.[19] Unfortunately, it is not clear how the NHC is lost as imidazolium salt or when the hydrogen bond is formed. However, the observation of the ion pair could be suggestive of NHC loss *via* an intramolecular protonation of the NHC. If that is indeed the case, it may be caused by conversion of the alkylcarbonato species to bicarbonate, where the subsequent dissociation reaction is ‘arrested’ prior to

complete imidazolium loss by the formation of the hydrogen bond (Figure 89). Despite the formation of a very strong hydrogen bond, this novel structure may arise, at least partly, due to the stabilisation afforded from the imidazolium, which effectively shields the polar carbonato group from the non-polar benzene solution.

Regrettably, this particular reaction leaves more questions than answers. The above discussion remains largely theoretical and highly speculative; it was not possible to identify any products other than **13**, and the tentatively assigned **14**, from the NMR.

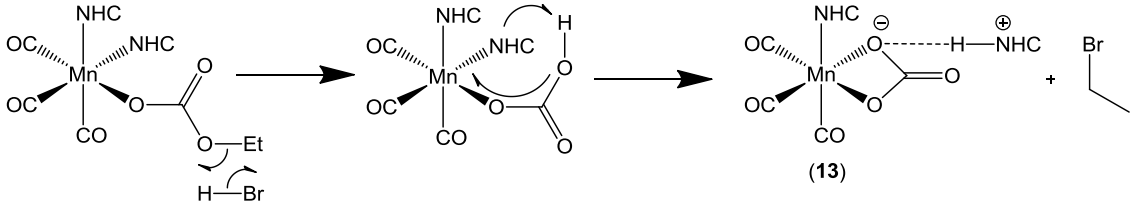

Figure 89: Proposed mechanism for the formation of bicarbonate and subsequent intramolecular protonation of NHC.

5.3 Synthesis of M(IPr)(CO)$_4$X (M = Mn, X = Br; M = Re, X = Cl).

When the reaction of the pentacarbonyl halides was repeated with IPr under the same conditions as used for I^{i}Pr$_2$Me$_2$, CO substitution for NHC was also observed. However, even in the presence of excess NHC only the monosubstituted products, Mn(IPr)(CO)$_4$Br (**15**) and Re(IPr)(CO)$_4$Cl (**16**), were obtained, due to the bulkier nature of IPr compared to I^{i}Pr$_2$Me$_2$. This is consistent with the work of Angelici *et al*, who observed monosubstitution in M(CO)$_5$X by bulky or inflexible phosphines and disubstitution for smaller phosphines or more flexible phosphites.[3,20] Complex **15** was isolated as an air-stable orange solid in 46% yield, while isolation of the rhenium analogue **16** as a white solid was achieved in 65% yield. As for reaction of I^{i}Pr$_2$Me$_2$ with Re(CO)$_5$Cl, more forcing conditions were necessary for preparation of **16** (Figure 90).

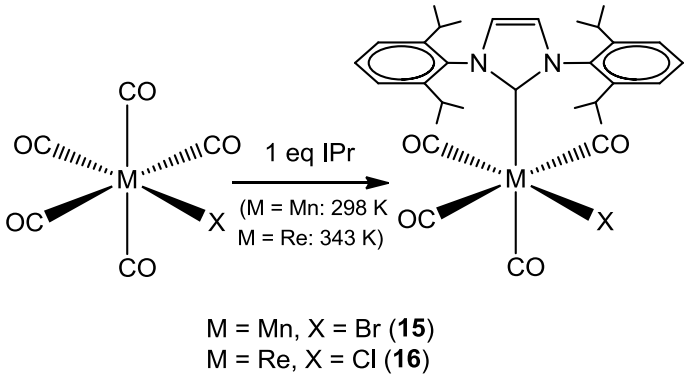

M = Mn, X = Br (**15**)
M = Re, X = Cl (**16**)

Figure 90: Reaction scheme for the formation of M(IPr)$(CO)_4$X (M = Mn, X = Br; M = Re, X = Cl).

The presence of three CO bands in the IR spectra of both **15** (2078, 1995, 1938 cm^{-1}) and **16** (2095, 1993, 1925 cm^{-1}) are consistent with a *cis*-configuration.[21] Crystals of both complexes were obtained by layering dichloromethane solutions with hexane. The corresponding structures are shown in Figure 91, with selected bond lengths and angles given in Tables 14 and 15 (pages 145 and 146).

In both structures, the M-CO distances *trans* to halide and NHC were the same and much shorter than those for the mutually *trans* CO ligands (Tables 14 and 15, pages 145 and 146). The M-C_{NHC} distances (**15:** 2.077(3) Å, **16:** 2.206(3) Å) were longer than those found in M(IH)$(CO)_4$X (IH = imidazol-2-ylidene; M = Mn, X = Br: 2.035(3)/2.040(2) Å, M = Re, X = Cl: 2.175(5) Å) reported by Hahn;[12] as expected, the M-C_{NHC} bond length for the Mn compound was shorter than for the Re analogue. It is noteworthy in these two structures that the IPr ligand results in negligible torsions between the plane of the imidazole ring and that subtended by the metal center, C1, C2, C2' and Br1. This arrangement minimizes steric repulsions between the isopropyl substituents on the bulky carbene ligand and the equatorial ligands in the complex, but not without cost. In particular, the M-C2-O2 and C2-M-C2' angles deviate significantly from linearity (168.96(19) and 166.21(13)^o in **15**, 170.0(2) and 170.37(13)^o in **16**) as a consequence of the ligand eclipsing.

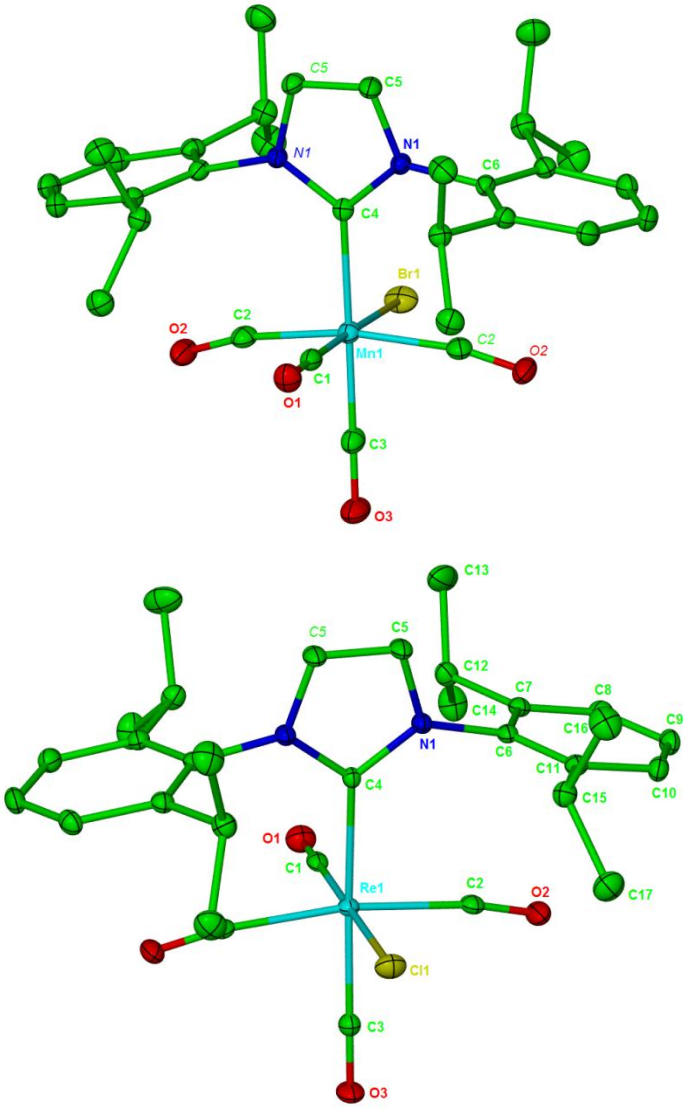

Figure 91: X-ray crystal structures of 15 (top) and 16 (bottom). Thermal ellipsoids shown at 30% level with all hydrogen atoms and minor disordered components omitted for clarity.

5.4 Halide abstraction from 11 and 12.

Treatment of **11** and **12** with $NaBAr_4^F$ in CH_2Cl_2 resulted in abstraction of the halide ligands and formation of the salts $[M(I^iPr_2Me_2)_2(CO)_3]BAr_4^F$ (M = Mn, **17**; Re, **18**) (Figure 92). At room temperature, both compounds displayed very broad NMR spectra (shown in the case of **18** in Figure 93), but upon cooling to 208 K, a low frequency isopropyl methyl doublet signal of integral 3 was resolved in their proton NMR spectra (**17**: δ -2.10; **18**: δ -0.24) suggestive of $M\cdots H_3C\text{-}CH(CH_3)$ agostic interactions (shown in the case of **18** in Figure 94).[22]

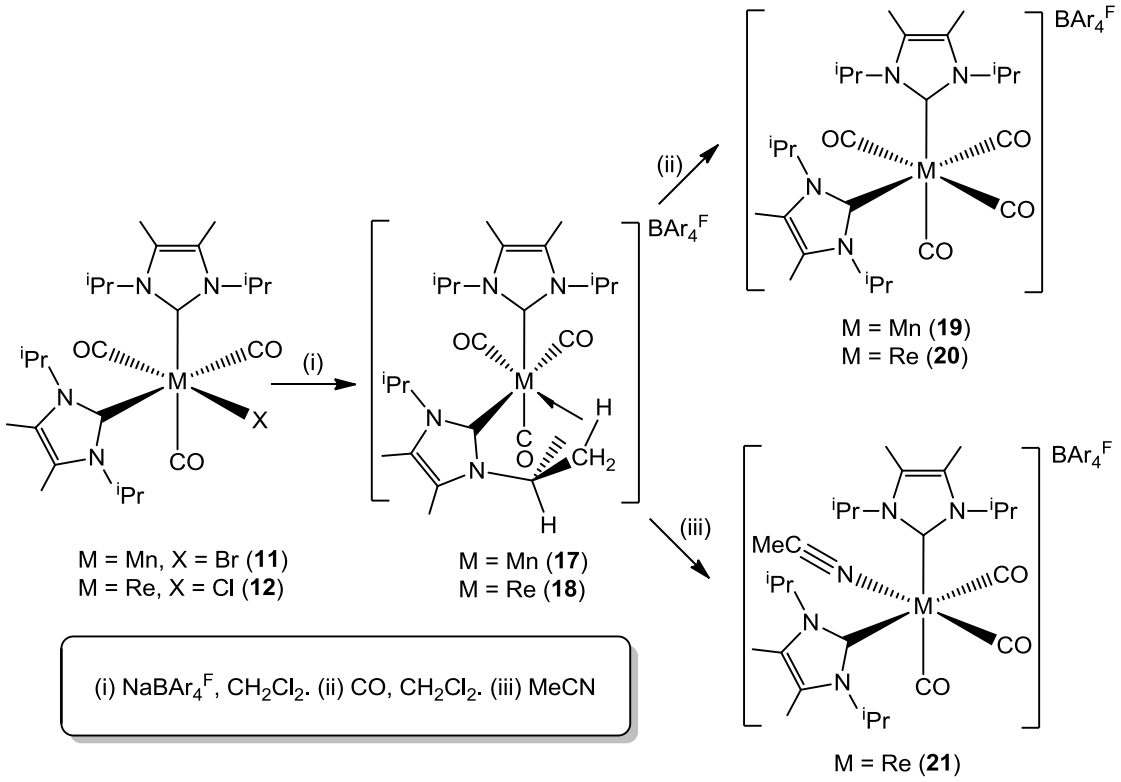

Figure 92: Reactions of M(I^{i}Pr$_2$Me$_2$)$_2$(CO)$_3$X (M = Mn, X = Br; M = Re, X = Cl).

Unfortunately, neither compound could be isolated. In case of **17**, the compound decomposed over a period of 2-3 hours upon warming to room temperature to afford a mixture of products, the major one being the tetracarbonyl species [Mn(I^{i}Pr$_2$Me$_2$)$_2$(CO)$_4$]BAr$_4^F$ (**19**). As the reaction was performed under an argon atmosphere, the source of the fourth CO ligand can only be a second molecule of **17**, although we were unable to observe any NMR signals arising from a leftover decarbonylated Mn-I^{i}Pr$_2$Me$_2$ species. Isolation and full characterization of **19** was achieved by addition of NaBAr$_4^F$ to **11** followed by the rapid introduction of a CO atmosphere.

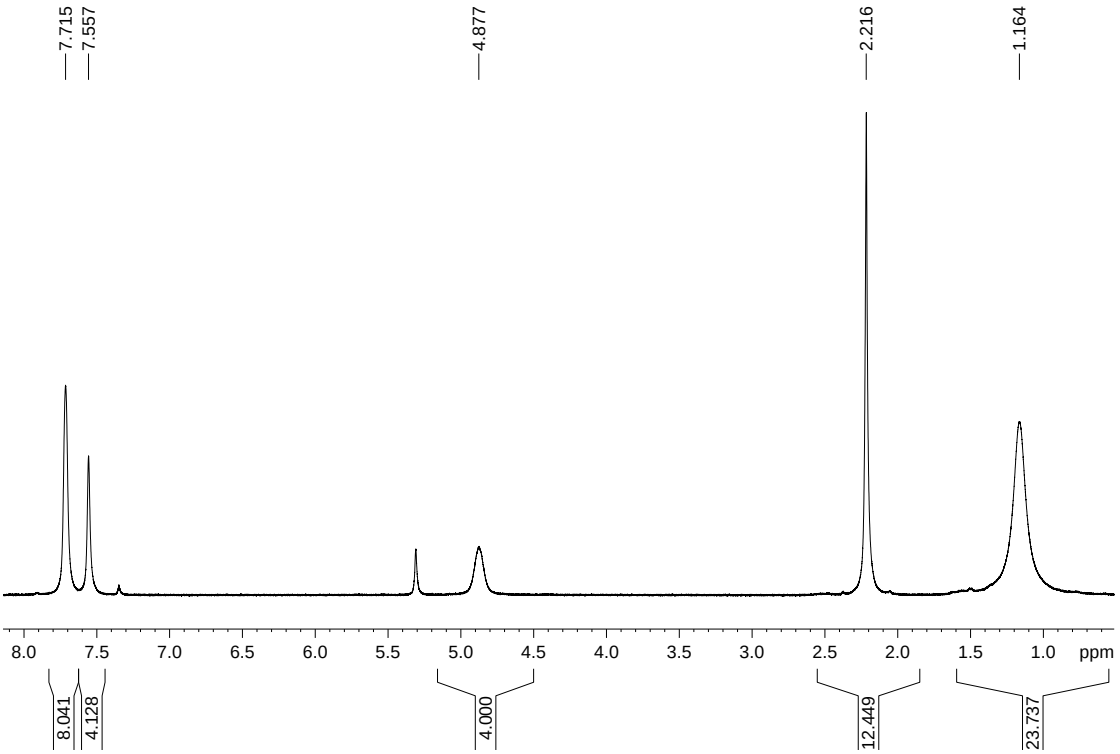

Figure 93: 500 MHz ^{1}H NMR spectrum of [Re(I^{i}Pr$_2$Me$_2$)$_2$(CO)$_3$]BAr$_4^F$ (18) in CD_2Cl_2 at 298 K.

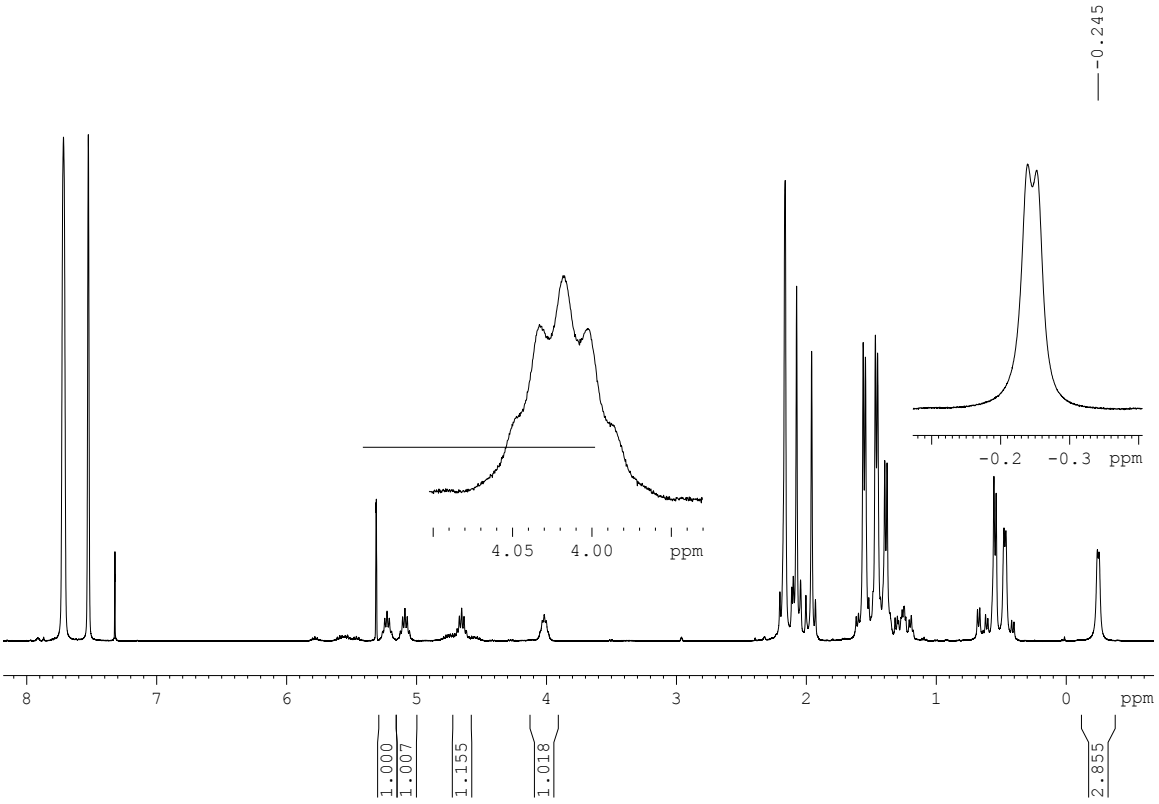

Figure 94: 500 MHz ^{1}H NMR spectrum of [Re(I^{i}Pr$_2$Me$_2$)$_2$(CO)$_3$]BAr$_4^F$ (18) in CD_2Cl_2 at 208 K.

Isolation of the agostic Re species **18** was thwarted by the appearance of a second Re carbonyl containing complex during the synthesis. An IR spectrum

recorded within 5 min of reacting **12** with $NaBAr_4^F$ in CH_2Cl_2 at room temperature showed strong carbonyl bands at 2036, 1945 and 1922 cm^{-1} assigned to **18**, alongside a much weaker absorption band from the second product at 2024 cm^{-1}. An increase in the intensity of this signal over the course of 2 hours made it apparent that this unidentified species also displayed two additional CO stretches at 1922 cm^{-1} and 1898 cm^{-1}. Traces of the tetracarbonyl complex $[Re(I^iPr_2Me_2)_2(CO)_4]BAr_4^F$ (**20**) were also apparent within hours at room temperature although in contrast to the reactivity of **17**, significant amounts of **20** only formed after several days.

Total conversion to **20** was achieved, as above, by addition of CO immediately after $NaBAr_4^F$ abstraction of chloride from **12**. Unlike the agostic interaction observed by Toupakadis *et al* in $[Mn(PCy_3)_2(CO)_3]BAr_4^F$,[22] addition of a dihydrogen atmosphere did not displace the agostic interaction in **18** by coordination of dihydrogen. This may indicate a stronger agostic interaction in the NHC complexes. However, other ligands such as CO (complex **20**) and MeCN, which gave $[Re(I^iPr_2Me_2)_2(CO)_3(MeCN)]BAr_4^F$ (**21**), both readily displace the agostic interaction in favour of coordination. Complex **21** also showed restricted rotation of the NHC and inequivalence in the ^1H NMR spectrum (Figure 95) alongside both bound (δ 2.46) and free (δ 1.99) MeCN. The NOESY spectrum (Figure 96) revealed that the NHC ligands were slowly exchanging positions in solution and that the MeCN ligand was exchanging with free MeCN. Presumably dissociation of MeCN allows the complex to ‘flip’ the positions of the NHC ligands before MeCN is once again re-coordinated.

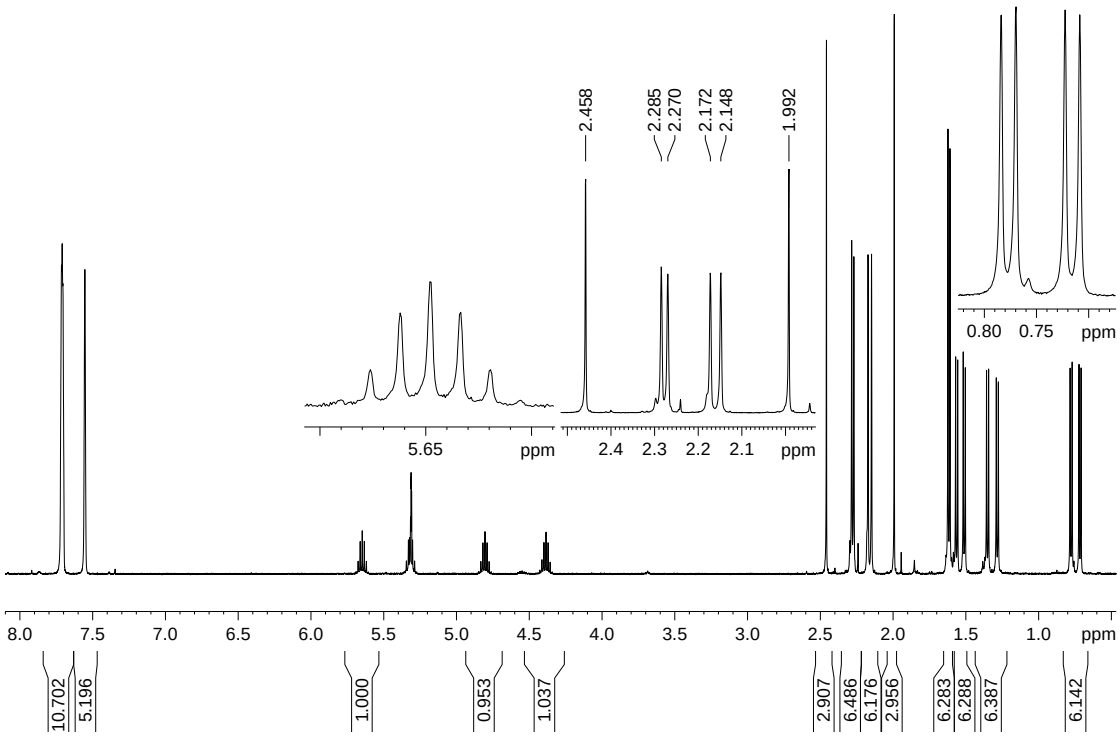

Figure 95: 500 MHz ^{1}H NMR spectra of [Re(I^{i}Pr$_2$Me$_2$)$_2$(CO)$_3$(MeCN)]BAr$_4^F$ (21) in CD_2Cl_2 at 298 K.

The IR spectra of both **19** and **20** contained four ν_{CO} bands consistent with *cis*-$[ML_2(CO)_4]^+$ (M = Mn or Re) structures, in contrast to the *trans*-isomers reported for L = PR_3.[23,24] The X-ray crystal structures of the two compounds (Figure 97) confirmed the presence of *cis*-I^{i}Pr$_2$Me$_2$ ligands.

Both geometries are somewhat distorted from regular octahedral, with M-NHC bond lengths that remain unchanged from those in the neutral precursors **11** and **12**. Selected bond lengths and angles are shown in Tables 14 and 15 (pages 145 and 146). While the Mn-CO distances also remain the same, those *trans* to NHC in the Re compound **20** (1.963(4), 1.967(4) Å) are significantly longer than the one in **12** (1.892(5) Å). Structurally, the disposition of the ligands about the metal centres in **19** and **20** is similar to that noted for **11** and **12**. Replacement of a halide ligand by a carbonyl appears to have little conformational affect other than to reduce the angles between the least square planes of the imidazole rings by *ca*. 5 and 6º (to 63.7 and 62.5º) in **19** and **20**, respectively, relative to **11** and **12.**

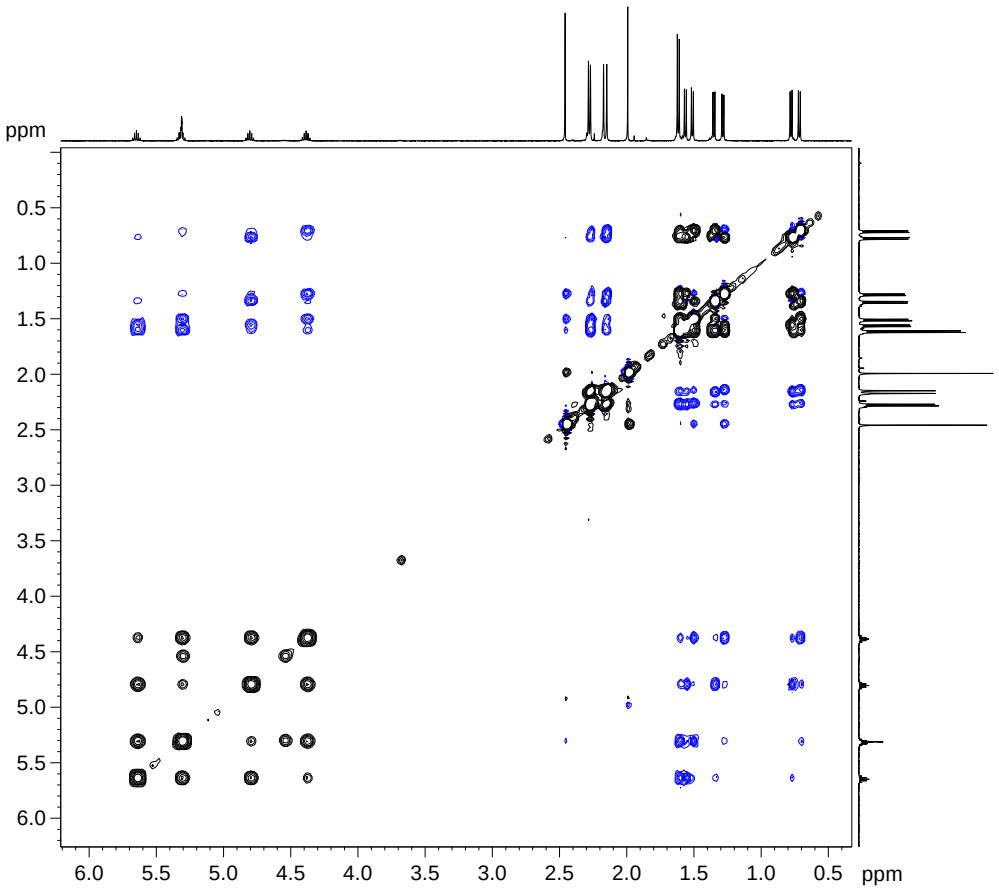

Figure 96: NOESY spectrum of $[Re(l^{i}Pr_2Me_2)_2(CO)_3(MeCN)]BAr_4^F$ (21) in CD_2Cl_2 at 298 K.

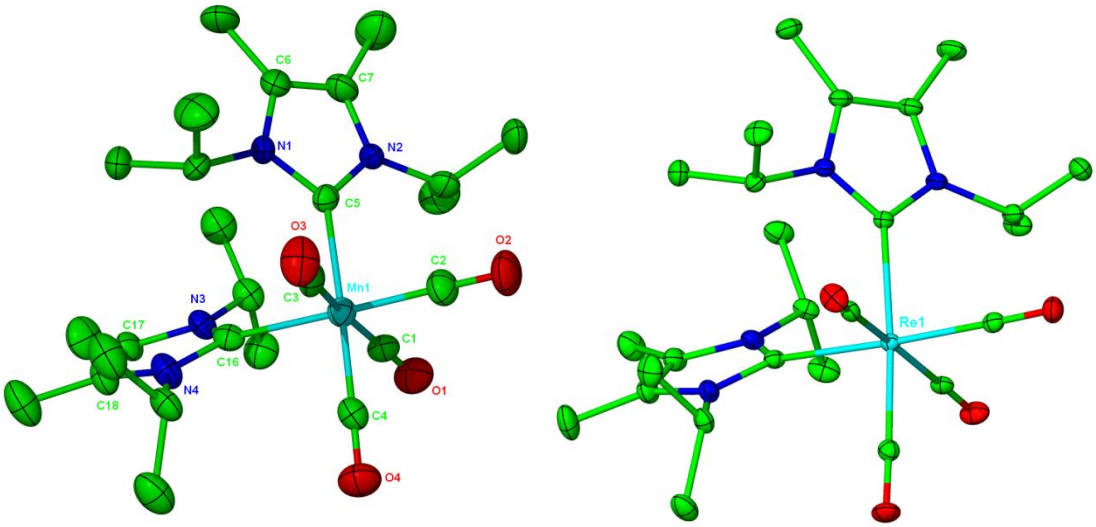

Figure 97: X-ray crystal structures of the cations in 19 (left) and 20 (right). Thermal ellipsoids are shown at 30% level with all hydrogen atoms removed for clarity.

5.5 Halide abstraction from 15 and 16.

In contrast to **11** and **12**, halide could not be removed from either **15** or **16** with $NaBAr_4^F$ alone. In the case of the Re species, halide abstraction was achieved upon addition of AgOTf followed by $NaBAr_4^F$ (Figure 98). The first step gave the neutral triflate complex $Re(IPr)(CO)_4OTf$ (**22**), which upon addition of $NaBAr_4^F$, precipitated NaOTf to afford the cationic dichloromethane complex $[Re(IPr)(CO)_4(ClCH_2Cl)]BAr_4^F$ (**23**). The coordination of very weakly basic solvents such as CH_2Cl_2 is known to require Lewis acidic metal centres;[25,26,27,28] the mono-carbene containing fragment $[Re(IPr)(CO)_4]^+$ will be more electrophilic than the bis-NHC species $[Re(I^iPr_2Me_2)_2(CO)_3]^+$, providing a rationale as to why the former binds solvent whereas the latter finds stabilization through the formation of an agostic bond to one of the NHC ligands.

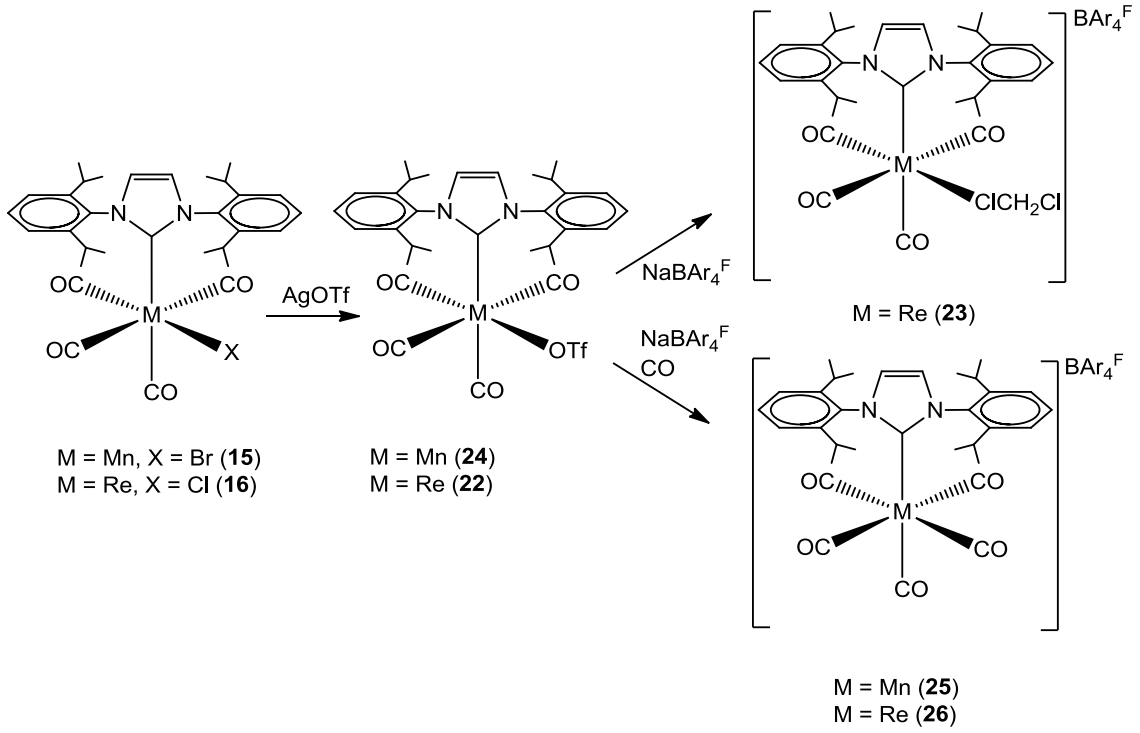

Figure 98: Reactions of $M(IPr)(CO)_4X$ (M = Mn, X = Br; M = Re, X = Cl).

It is worth noting that if the nucleophilicity of the L-type ligands is reduced, then $[ML_2(CO)_3]^+$ complexes will bind weakly coordinating solvents such as CH_2Cl_2 and Et_2O, as shown for the cationic phosphite species $[Re(P(OCH_2)_3CMe_3)_2(CO)_3]^+$.[9] However, it is likely in this case that the absence

of substituents on the phosphite that are capable of forming an agostic interaction consequently promotes solvent binding. Attempts to observe similar solvent coordination to $[Re(IMe_4)_2(CO)_3]^+$, in which the NHC is also unable to form agostic bonds, were thwarted by an inability to remove the chloride from *cis*-$Re(IMe_4)_2(CO)_3Cl$ with either $NaBAr_4^F$ or AgOTf.*

The dichloromethane ligand in **23** was tightly bound in the solid-state; IR spectra recorded before and after subjecting a solid sample of the compound to vacuum at room temperature for 48 hours were identical. X-ray quality crystals of the CD_2Cl_2 complex were isolated from CD_2Cl_2/hexane and the structure determined (Figure 99). The dichloromethane ligand is bound in a monodentate fashion and points down and away from the NHC ligand with the Re-Cl bond eclipsed by the two N-aryl substituents of the carbene. The Re-Cl bond distance of 2.596(3) Å is slightly longer than that reported for $[Re(P^iPr_3)(CO)_4(ClCH_2Cl)]BAr_4^F$ of 2.554(2) Å.[26] As seen in other structurally characterized η^1-CH_2Cl_2 complexes,[25,8,29] the C-Cl distance for the metal bound chlorine atom (1.727(15) Å) is considerably shorter than for the terminal one (1.860(12) Å). Selected bond lengths and angles are shown in Table 15 (page 146). The four Re-CO distances differ significantly; the one *trans* to the coordinated solvent molecule (1.894(9) Å) is shorter than the one *trans* to the NHC (1.960(8) Å), and these two in turn are both shorter than the two mutually trans-CO ligands (2.008(7), 2.012(7) Å).

* *cis*-$Re(IMe_4)_2(CO)_3Cl$ was synthesised with the same method used for **12**, although it proved impossible to isolate. The crude product was used for the attempted halide abstraction experiment.

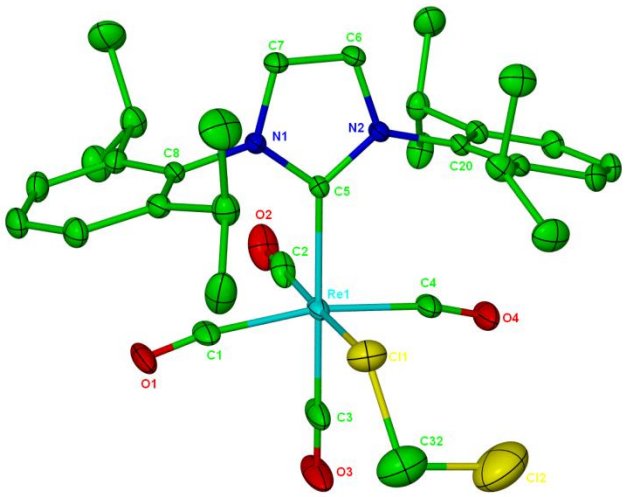

Figure 99: X-ray crystal structure of the cation in 23. Thermal ellipsoids are shown at the 30% level with all hydrogen atoms removed for clarity.

The donor strength of the IPr ligand accounts for the four CO stretching bands of **23** at 2115, 2016, 1984 and 1971 cm^{-1} being at much lower frequency than those of the P^iPr_3 analogue prepared by Kubas at 2124, 2044, 2026 and 1996 cm^{-1}.[26] The ^1H NMR spectrum for **23** in CD_2Cl_2 is shown in Figure 100. It was not possible to detect ^1H or ^{13}C NMR resonances for the bound dichloromethane ligand in solution, even upon cooling to 189 K. This may be due to rapid exchange with free CD_2Cl_2, but is then somewhat at odds with the inability to cleave the Re-CH_2Cl_2 interaction under vacuum in the solid-state. While this may simply reflect a difference between solution and solid-state reactivity, further work is required to fully reconcile these observations.

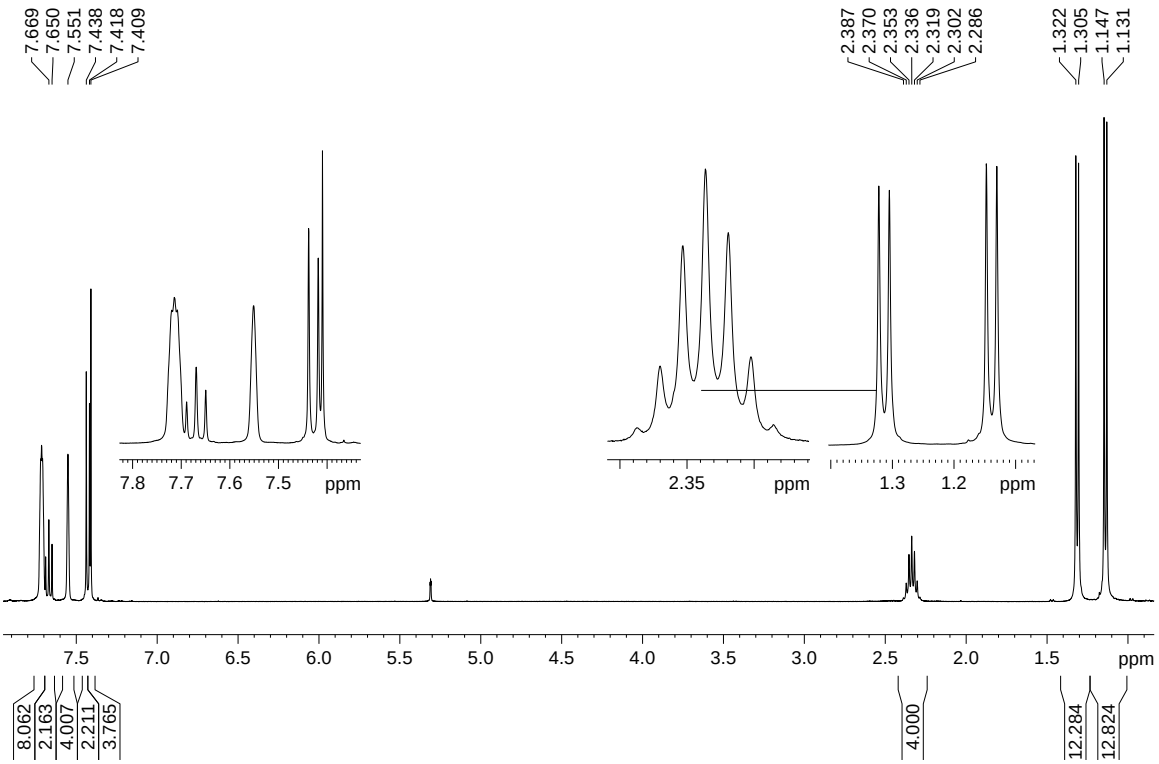

Figure 100: 400 MHz ^{1}H NMR spectrum of $[Re(I^{i}Pr_2Me_2)_2(CO)_3(CD_2Cl_2)]BAr_4^F$ (23) in CD_2Cl_2 at 298 K.

Solvent complexes have been employed as labile substrates for coordination of a variety of small molecules. Thus, complex **23** was placed under an atmosphere of hydrogen, although this did not produce any change in the NMR spectrum even upon cooling to low temperatures. Kubas *et al* have previously noted for $[Re(PPh_3)(CO)_4(CH_2Cl_2)]BAr_4^F$ that the bound dichloromethane is in rapid dynamic exchange with unbound solvent.[25] It is not immediately clear why rapid exchange appears to impede coordination of other weak ligands, such as H_2. One possible explanation is that the relative energies of $[Re(PPh_3)(CO)_4(CH_2Cl_2)]BAr_4^F$ and $[Re(PPh_3)(CO)_4(H_2)]BAr_4^F$ in CH_2Cl_2 are either very close or favour the former. In either case the CH_2Cl_2 complex would be favoured, energetically or due to much higher relative concentrations of CH_2Cl_2 *vs*. H_2.

Interestingly, Kubas *et al*. found that exposing $[Re(PPh_3)(CO)_4(CH_2Cl_2)]BAr_4^F$ to a hydrogen atmosphere in C_6H_5F, rather than CH_2Cl_2, afforded the dihydrogen complex $[Re(PPh_3)(CO)_4(H_2)]BAr_4^F$. Treatment of **22** with $NaBAr_4^F$ in C_6H_5F followed by addition of 1 atm. of hydrogen resulted in the observation of two

new species, on the basis of the IPr resonances in the ^{1}H NMR spectrum, which were in an approximate 1:1 ratio. The first of these was tentatively assigned as the dihydrogen complex $[Re(IPr)(CO)_4(H_2)]BAr_4^F$ (**27**) (Figure 101) due to the presence of a broad hydride signal at δ -4.90 that integrated to 2H. The second product was more difficult to assign. When **27** was left in C_6H_5F under hydrogen, trace amounts of other hydride signals grew in with time, possibly evidence of heterolytic activation of H_2 as seen for $[Re(PPh_3)(CO)_4(H_2)]BAr_4^F$ by Kubas *et al*.[25] In order to confirm the identity of **27** and quantify the extent of activation in this system, high pressure NMR experiments were conducted in collaboration with Dr. Jonathan Iggo (University of Liverpool). Again taking **22** and $NaBAr_4^F$ in C_6H_5F, but this time in a sapphire NMR tube, it was possible to pressurise the reaction to 20 atm. of hydrogen and observe almost complete conversion to **27** (Figure 102).

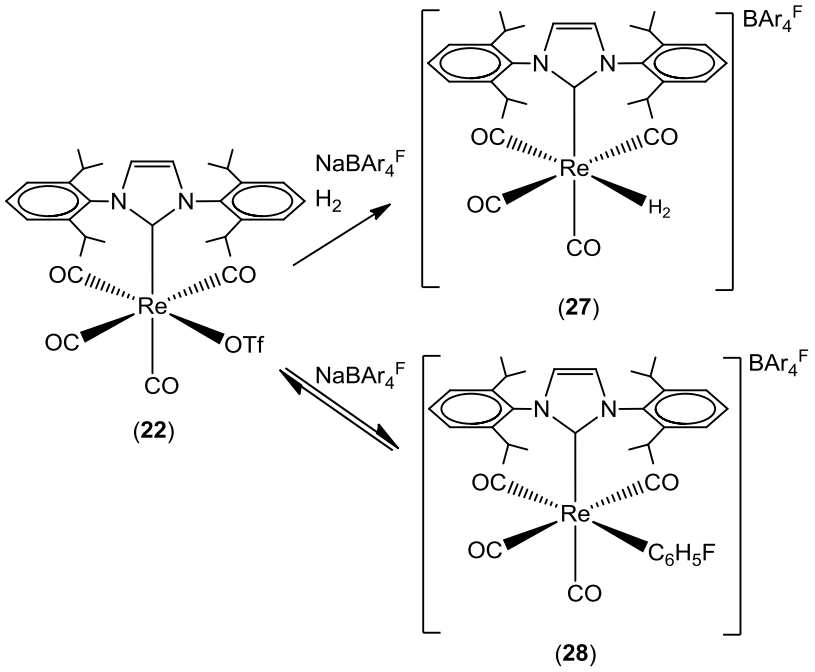

Figure 101: Reactions of Re(IPr)(CO)$_4$(OTf).

Under these conditions it was possible to take T_1 measurements on a 400 MHz spectrometer, which afforded a $T_{1(min)}$ of 13.2 ms at 252 K, this is keeping with other η^2-H_2 complexes.[30] During the course of the experiments traces of what appeared to be a dihydride species were detected. The reaction was warmed overnight to see if this species could be increased, but the distribution proved to

be largely insensitive to temperature. The pressure was increased up to 40 atm. of hydrogen, but this had no effect either. It is possible that ambient light could be responsible for the slow formation of the dihydride species, but further experiments are required to confirm this.

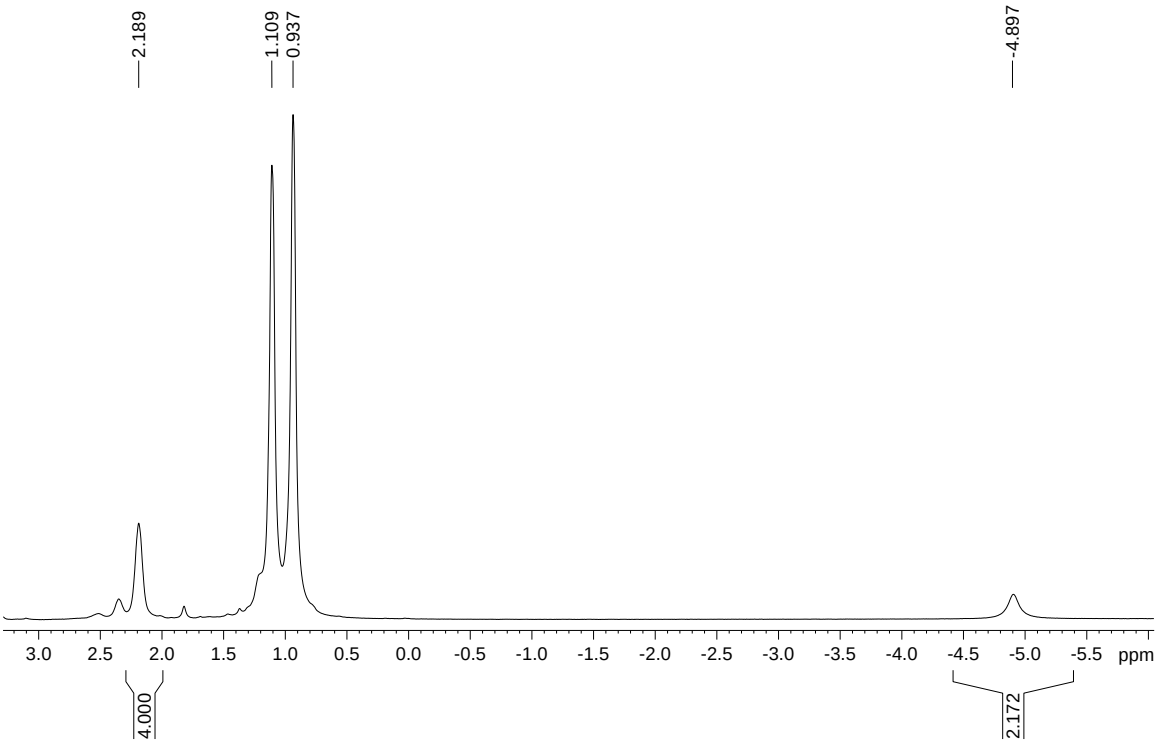

Figure 102: 400 MHz ^{1}H NMR spectrum of [Re(IPr)(CO)$_4$(H$_2$)]BAr$_4^F$ (27) in C_6H_5F under 20 atm. of hydrogen at 298 K.

Upon degassing the sample, the NMR signals for **27** reduced to zero intensity and the unidentified product was the sole species present. This was the first indication that the species could be a solvent complex of C_6H_5F, [Re(IPr)(CO)$_4$(C_6H_5F)]BAr$_4^F$ (**28**) (Figure 101), analogous to the dichloromethane adduct (**23**) isolated previously.[31] Unfortunately, due to the lack of NMR active nuclei in close proximity to the metal centre and the presumably (as for **23**) rapid dynamic exchange with solvent, it was hard to unambiguously characterise this species. The solution spectroscopy obtained, IR, ^{1}H, ^{13}C and ^{19}F NMR, were all suggestive of a species very similar to **23** (^{1}H NMR shown in Figure 103). However, it was not possible to confirm this due to a lack of direct spectroscopic evidence for bound C_6H_5F from any of the methods used, including ^{19}F{^{1}H} and ^{19}F-^{19}F COSY experiments. There are a

number of plausible reasons why this evidence may not be observable by solution spectroscopy. Primarily, it is very likely that this system is also in rapid dynamic exchange between bound and unbound C_6H_5F, this issue being compounded by the fact that the reactions were monitored in neat C_6H_5F, which would most likely mask any nearby signals in the NMR. As such, attempts were made to crystallise the product by layering a freshly, filtered solution of **28** with hexane. However, the crystals obtained were of a further product **29**, which appears to be an example of an 'arrested' metathesis prior to complete abstraction of triflate (Figure 104). In order to confirm that **29** was not in fact the same species as **28**, comparison of the solution spectroscopic data from the crystals was attempted. However, the crystals of **29** would not redissolve in C_6H_5F, so whilst it is unlikely that they are the same species it could not be conclusively proved either.

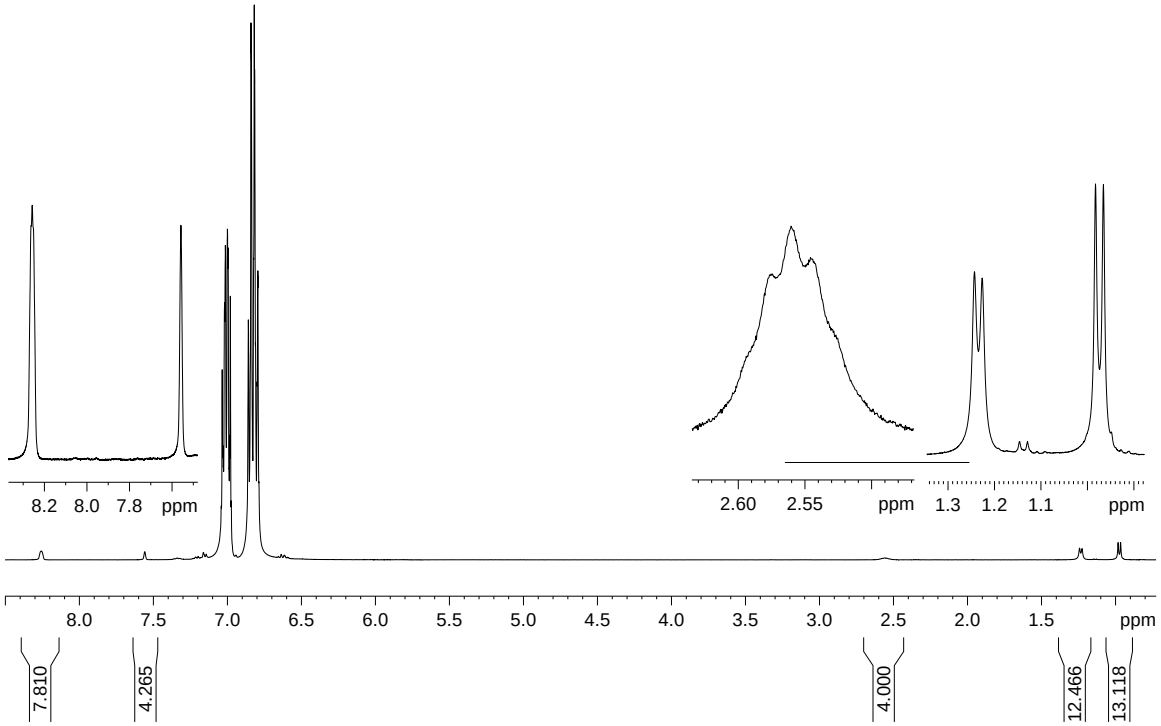

Figure 103: 400 MHz ^{1}H NMR spectrum of [Re(IPr)(CO)$_4$(C_6H_5F)]BAr_4^F (27) in C_6H_5F at 298 K.

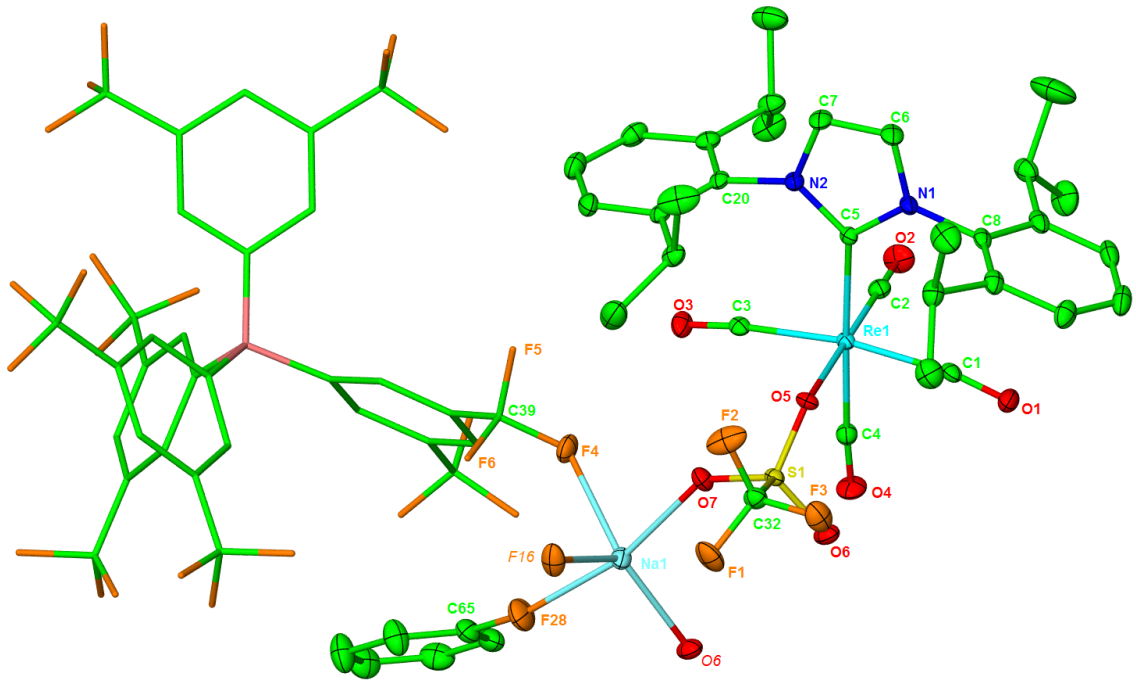

Figure 104: X-ray crystal structure for 29. Ellipsoids at 30% and all hydrogens omitted for clarity.

Several fresh solutions of **28** were prepared to examine the reactivity of the proposed solvent complex with other small molecules. There was no reaction under 1 atm. of CO_2 or N_2, even at low temperatures. This is unsurprising as both ligands require larger degrees of back bonding from the metal centre for stable binding than H_2. There was no binding for CO_2 or N_2 detected by Kubas *et al* for $[Re(PPh_3)(CO)_4(CH_2Cl_2)]BAr_4^F$ in C_6H_5F either.[25]

Efforts to prepare the manganese analogue of **23** were thwarted by the slow decomposition of the corresponding triflate precursor $Mn(IPr)(CO)_4OTf$ (**24**), which was apparent from the formation of a red precipitate in the yellow solution of the complex over a period of *ca*. 30 minutes at 298 K. Complex **24** could be prepared *in situ* as for **22**, by treatment of $Mn(IPr)(CO)_4Br$ with AgOTf, and was characterised by a combination of NMR and IR spectroscopy, as well as elemental analysis after rapid recrystallisation. When $NaBAr_4^F$ was reacted with freshly prepared dichloromethane solutions of **24** (as well as **22**), followed a short time later by the introduction of a CO atmosphere, the cationic pentacarbonyl complexes $[M(IPr)(CO)_5]BAr_4^F$ (M = Mn, **25**; M = Re, **26**) were formed in quantitative yields.

As expected, the strong σ donor ability of the IPr ligand has a marked impact on the IR spectra of **25** and **26**. The highest frequency CO stretches (**25**: 2134 cm^{-1}; **26**: 2148 cm^{-1}) are at lower energy than found in $[M(PR_3)(CO)_5]^+$ analogues containing even strongly donating phosphine ligands such as P^nBu_3 and PEt_3.[32] Two lower frequency vibrations were present for **25** at 2049 and 2045 cm^{-1}, while for **26**, only a single peak was observed at 2042 cm^{-1}, although the peak is quite broad and it is likely that the resolution was simply insufficient to distinguish two peaks.[33,34] The two complexes were crystallographically characterized (Figure 105). Selected bond lengths and angles for both compounds are shown in Tables 14 and 15 (pages 145 and 146). Comparison of the Re-CO bond lengths in **26** reveals only minor differences to those in the neutral chloride precursor **16**; this contrasts to what was noted earlier for the $I^iPr_2Me_2$ complexes **12** and **20**.

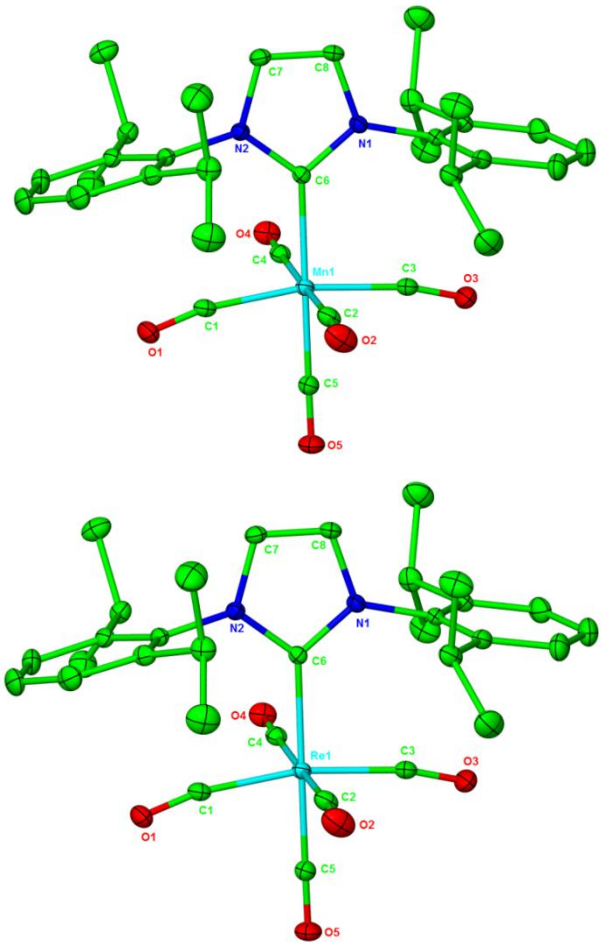

Figure 105: X-ray crystal structures of the cations in 25 (top) and 26 (bottom). Thermal ellipsoids are shown at the 30% level with all hydrogen atoms removed for clarity.

	11	**13**	**15**	**19**	**25**
Mn-NHC	2.093(4)	2.0775(14)	2.077(3)	2.120(3) 2.120(3)	2.090(2)
Mn-$CO_{trans\ to\ NHC}$	1.832(4)	1.8240(17)	1.821(6)	1.830(4) 1.823(4)	1.851(3)
Mn-$CO_{trans\ to\ CO}$			1.874(2)	1.862(4) 1.864(4)	1.883(3) 1.877(3) 1.892(3) 1.874(3)
Mn-$CO_{trans\ to\ halogen}$	1.850(4)		1.819(3)		
Mn-halogen	2.624(3)		2.5059(8)		
Mn-O		2.0386(10) 2.0478(10)			
Mn-$CO_{trans\ to}$ O_2CO		1.7830(15) 1.7933(17)			
NHC-Mn-CO	178.3(2)	172.30(7)	178.5(2)	177.72(15) 177.43(15)	176.28(10)
trans OC-Mn-CO				170.42(16)	168.98(11) 177.45(11)
OC-Mn-halogen	164.6(3)		178.14(10)		
cis OC-Mn-CO	88.4(3)	86.98(7) 87.34(7) 87.89(8)	93.14(7) 90.1(2)	88.46(15) 84.22(15) 84.61(15) 92.37(16) 89.44(16)	87.13(12) 92.83(11) 85.47(11) 90.48(12) 91.42(12) 90.03(12) 83.83(11) 91.12(11)

Table 14: Selected bond lengths (Å) and angles (°) in the manganese NHC complexes 11, 13, 15, 19 and 25.

	12	**16**	**20**	**23**	**26**
Re-NHC	2.224(4)	2.206(3)	2.235(4) 2.237(4)	2.200(6)	2.205(5)
Re-CO*trans* to NHC	1.892(5)	1.962(4)	1.967(4) 1.963(4)	1.960(8)	1.996(6)
Re-CO*trans* to CO		2.009(3)	1.995(4) 1.967(4)	2.008(7) 2.012(7)	2.028(6) 2.018(7) 2.053(7) 2.019(6)
Re-CO*trans* to halogen	1.873(15)	1.962(4)		1.894(9)	
Re-halogen	2.480(5)	2.479(8)		2.596(3)	
NHC-Re-CO	179.1(2)	173.39(12)	176.63(15) 176.16(15)		175.9 (2)
trans OC-Re-CO			170.76(16)	169.4(3)	170.7(2) 179.3(2)
OC-Re-halogen	171.8(7)				
cis OC-Re-CO	84.5(7)	89.62(6) 92.37(13)	87.51(16) 84.89(16) 85.79(16) 92.90(16) 89.10(16)	91.0(3) 85.1(3) 90.3(4) 91.1(3)	87.9(2) 92.8(2) 86.7(2) 89.9(2) 89.9(2) 89.4(2) 84.3(2) 90.2(2)

Table 15: Selected bond lengths (Å) and angles (°) in the rhenium NHC complexes 12, 16, 20, 23 and 26.

5.6 Conclusions.

A series of new Mn and Re NHC complexes have been synthesized and, in a number of cases, structurally characterized following treatment of the metal pentacarbonyl halide precursors with $I^iPr_2Me_2$ and IPr. Halide abstraction by $NaBAr_4^F$ leads to the formation of the cationic 16e species $[M(I^iPr_2Me_2)_2(CO)_3]^+$ and $[M(IPr)(CO)_4]^+$, which are stabilized through agostic bonding and solvent coordination respectively.

None of the $[ML_x(CO)_{(5-x)}]^+$ (x = 1, 2) species studied bound N_2 or CO_2, all are presumably too electrophilic to provide the necessary metal back bonding. However, whilst $[M(I^iPr_2Me_2)_2(CO)_3]^+$ did not bind H_2 either, which could be evidence for a stronger agostic interaction in the NHC complexes *vs.* their phosphine analogues, dihydrogen binding to $[M(IPr)(CO)_4]^+$ was observed with evidence for heterolytic activation of H_2. The $T_{1(min)}$ was determined and found to be in keeping with other dihydrogen species.[30]

The coordination of only two NHCs, $I^iPr_2Me_2$ and IPr, have brought about quite different chemistry not only to one another (bis *vs*. mono NHC products), but also to the analogous PR_3 substituted complexes (*cis* rather than *trans* $ML_2(CO)_3X$ products). Given the highly tunable stereoelectronic properties of NHCs, it is to be hoped that further studies will provide many other interesting observations in group 7 NHC chemistry.

5.7 References.

(1) Braband, H.; Kuckmann, T. I.; Abram, U.; *J. Organomet. Chem.* **2005**, *690*, 5421-5429.

(2) Hitchcock, P. B.; Lappert, M. F.; Pye, P. L.; *J. Chem. Soc., Dalton Trans.* **1977**, 2160-2172.

(3) Angelici, R. J.; Basolo, F.; Poe, A. J.; *Nature* **1962**, *195*, 993-994.

(4) Huhmann-Vincent, J.; Scott, B. L.; Kubas, G.; J. *Inorg. Chim. Acta* **1999**, *294*, 240-254.

(5) Chinn, M. S.; Heinekey, D. M.; Payne, N. G.; Sofield, C. D.; *Organometallics* **1989**, *8*, 1824-1826.

(6) Heinekey, D. M.; Schomber, B. M.; Radzewich, C. E.; *J. Am. Chem. Soc.* **1994**, *116*, 4515-4516.

(7) Heinekey, D. M.; Voges, M. H.; Barnhart, D. M.; *J. Am. Chem. Soc.* **1996**, *118*, 10792-10802.

(8) Fang, X.; Huhmann-Vincent, J.; Scott, B. L.; Kubas, G. J.; *J.Organomet. Chem.* **2000**, *609*, 95-103.

(9) Fang, X.; Scott, B. L.; John, K. D.; Kubas, G. J.; *Organometallics* **2000**, *19*, 4141-4149.

(10) Hiltner, O.; Boch, F. J.; Brewitz, L.; Härter, P.; Drees, M.; Herdtweck, E.; Herrmann, W. A.; Kühn, F. E.; *Eur. J. Inorg. Chem.* **2010**, *2010*, 5284-5293.

(11) Hiltner, O.; Herdtweck, E.; Drees, M.; Herrmann, W. A.; Kühn, F. E.; *Eur. J. Inorg. Chem.* **2009**, *2009*, 1825-1831.

(12) Kaufhold, O.; Stasch, A.; Pape, T.; Hepp, A.; Edwards, P. G.; Newman, P. D.; Hahn, F. E.; *J. Am. Chem. Soc.* **2009**, *131*, 306-317.

(13) Blake, P. R.; Lee, B.; Summers, M. F.; Adams, M. W. W.; Park, J.-B.; Zhou, Z. H.; Bax, A.; *J. Biomol. NMR* **1992**, *2*, 527-533.

(14) Blake, P. R.; Park, J. B.; Adams, M. W. W.; Summers, M. F.; *J. Am. Chem. Soc.* **1992**, *114*, 4931-4933.

(15) Sullivan, B. P.; Meyer, T. J.; *J. Chem. Soc., Chem. Commun.* **1984**, 1244-1245.

(16) Bo, C.; Dedieu, A.; *Inorg. Chem.* **1989**, *28*, 304-309.

(17) Darensbourg, D. J.; Mueller, B. L.; Bischoff, C. J.; Chojnacki, S. S.; Reibenspies, J. H. *Inorg. Chem.* **1991**, *30*, 2418–2424.

(18) Johnson, K.; Frazier, T.; Becker, T. M.; Miller, K.; Ho, D. M.; Krause-Bauer, J.; Mandal, S. K.; *Inorg. Chem. Commun.* **2001**, *4*, 602-605.

(19) Winstein, S.; Clippinger, E.; Fainberg, A. H.; Heck, R.; Robinson, G. C.; *J. Am. Chem. Soc.* **1956**, *78*, 328-335.

(20) Angelici, R. J.; Basolo, F.; *J. Am. Chem. Soc.* **1962**, *84*, 2495-2499.

(21) Liu, C.-Y.; Chen, D.-Y.; Lee, G.-H.; Peng, S.-M.; Liu, S.-T.; *Organometallics* **1996**, *15*, 1055-1061.

(22) Toupadakis, A.; Kubas, G. J.; King, W. A.; Scott, B. L.; Huhmann-Vincent, J.; *Organometallics* **1998**, *17*, 5315-5323.

(23) Brink, R. W.; Angelici, R. J. *Inorg. Chem.* **1973**, *12*, 1062-1066.

(24) Gibson, D. H.; Owens, K.; Mandal, S. K.; Sattich, W. E.; Franco, J. O.; *Organometallics* **1989**, *8*, 498-505.

(25) Huhmann-Vincent, J.; Scott, B. L.; Kubas, G. J.; *J. Am. Chem. Soc.* **1998**, *120*, 6808-6809.

(26) Huhmann-Vincent, J.; Scott, B. L.; Kubas, G. J.; *Inorg. Chem.* **1999**, *38*, 115-124.

(27) Arndtsen, B. A.; Bergman, R. G.; *Science* **1995**, *270*, 1970 -1973.

(28) Huang, D.; Huffman, J. C.; Bollinger, J. C.; Eisenstein, O.; Caulton, K. G.; *J. Am. Chem. Soc.* **1997**, *119*, 7398-7399.

(29) Butts, M. D.; Scott, B. L.; Kubas, G. J.; *J. Am. Chem. Soc.* **1996**, *118*, 11831-11843.

(30) Crabtree, R. H.; *Acc. Chem. Res.***1990**, *23*, 95-101.

(31) Bouwkamp, M. W.; de Wolf, J.; del Hierro Morales, I.; Gercama, J.; Meetsma, A.; Troyanov, S. I.; Hessen, B.; Teuben, J. H.; *J. Am. Chem. Soc.* **2002**, *124*, 12956-12957.

(32) Drew, D.; Darensbourg, D. J.; Darensbourg, M. Y.; *Inorg. Chem.* **1975**, *14*, 1579-1584.

(33) Lee, K. Y.; Kuchynka, D. J.; Kochi, J. K.; *Organometallics* **1987**, *6*, 1886-1897.

(34) Nitschke, J.; Schmidt, S. P.; Trogler, W. C.; *Inorg. Chem.* **1985**, *24*, 1972-1978.

Chapter 6 - Experimental

6.1 General procedures and analytical techniques.

All manipulations were carried out under argon using standard Schlenk, high vacuum and glovebox techniques using dried and degassed solvents. Cp'$Mn(CO)_3$, $Mn(CO)_5Br$ and $Re(CO)_5Cl$ were purchased from Strem and used as received. $I^iPr_2Me_2$, IEt_2Me_2, IMes, I^tBu, IMe_4, IPr and $NaBAr_4^F$ were prepared according to literature methods.[1,2,3] NMR spectra were recorded on Bruker Avance 400/500 MHz NMR spectrometers and referenced to $CFCl_3$ (δ 0.0) for ^{19}F and to residual solvent signals for ^1H and ^{13}C spectra for d_8-THF (δ 3.58, 25.4), C_6D_6 (δ 7.16, 128.4), CD_3CN (δ 1.94, 118.7) and CD_2Cl_2 (δ 5.32, 54.0). Resonances arising from both BAr_4^F and triflate have been omitted. IR spectra were recorded on a Nicolet Nexus FTIR spectrometer as CH_2Cl_2 solutions unless otherwise stated. Mass spectra were recorded using a microTOF electrospray time-of-flight (ESI-TOF) mass spectrometer (Bruker Daltonik GmbH) coupled to an Agilent 1200 LC system (Agilent Technologies). Elemental analyses were performed by Elemental Microanalysis Ltd, Okehampton, Devon, UK or the Elemental Analysis Service, London Metropolitan University, London, UK. Density functional theory calculations were run with Gaussian 03 and employed the BP86 functional.[4] Mn and P were described using SDD RECPs and basis sets with a polarisation function was added for P (ζ = 0.387).[5,6] 6-31G** basis sets were used for C, N, O, and H atoms.[7]

6.2 Preparation of Cp'$Mn(CO)_2(IEt_2Me_2)$ (1).

Cp′$Mn(CO)_3$ (0.223 g, 1.0 mmol) was combined with IEt_2Me_2 (0.152 g, 1.0 mmol) in hexane (100 mL) and photolysed for 40 min using a 125 W mercury arc lamp in a water-cooled immersion well with a slow flow of argon to expel released CO (see Chapter 2, section 2.2 for detailed setup). In this time, the solution darkened from pale yellow to a golden yellow-orange, with some orange precipitate formed. Conversion of starting material to product was

monitored by IR spectroscopy upon withdrawal of a sample of the solution, removal of hexane and dissolution of the residue in CH_2Cl_2. After the reaction was deemed to be complete, the hexane solution was transferred by cannula to a Schlenk tube, cannula filtered to a second Schlenk and reduced to dryness. The residue was redissolved in a minimum amount of hot hexane. Some insoluble, dark red material was typically present at this stage, but this can be removed by passing the hexane solution through a pad of celite. The solution was then left to crystallise upon cooling to room temperature. Yellow crystalline material was isolated, washed with cold hexane (10 mL) and dried to afford a yellow/orange solid. Yield 0.13 g (37 %). ^{1}H NMR (d_8-THF, 300 MHz, 298 K): δ 4.42 (q, 4H, J_{HH} = 7.1 Hz, NCH_2CH$_3$), 4.15 (s, 2H, Cp), 4.13 (s, 2H, Cp), 2.13 (s, 6H, NC(CH_3)=C(CH_3)N), 1.61 (s, 3H, Cp-CH_3), 1.29 (t, 6H, J_{HH} = 7.1 Hz, NCH$_2$CH_3). ^{13}C{^{1}H} NMR (d_8-THF, 125 MHz, 298 K): δ 235.6 (s, *C*O), 196.3 (s, N*C*N), 126.7 (s, N*C*(CH$_3$)=*C*(CH$_3$)N), 101.7 (s, C_{Cp}-CH$_3$), 82.8 (s, Cp), 81.1 (s, Cp), 44.2 (s, N*C*H$_2$CH$_3$), 16.8 (s, NCH$_2$*C*H$_3$), 14.0 (s, Cp-*C*H$_3$), 9.5 (s, NC(*C*H$_3$)=C(*C*H$_3$)N). IR (CH_2Cl_2, cm^{-1}): 1898 ν(CO), 1824 ν(CO). Elemental analysis calcd. (%) for $C_{17}H_{23}N_2O_2Mn$ (342.294): C 59.65, H 6.77, N 8.18; found C 59.68, H 6.90, N 8.38.

6.3 Preparation of Cp'Mn(CO)$_2$(IMes) (2).

As above (section 6.2), Cp′Mn(CO)$_3$ (0.223 g, 1.0 mmol) was combined with IMes (0.312 g, 1.0 mmol) in hexane (100 mL) and photolysed for 40 min under a slow flow of argon. In this time, the solution darkened from pale yellow to a golden yellow, with some red-orange precipitate formed which was removed by cannula filtration. Yellow crystalline material was isolated from a concentrated hexane solution, washed with cold hexane (10 mL) and dried to give a yellow/orange solid. Yield 0.21 g (42 %). ^{1}H NMR (C_6D_6, 500 MHz, 298 K): δ 7.00 (s, 4H, C_6H_2), 6.19 (s, 2H, NCH=NCH), 4.04 (s, 2H, Cp), 3.80 (s, 2H, Cp), 2.15 (s, 6H, *p*-CH$_3$), 2.09 (s, 12H, *o*-CH$_3$), 1.65 (s, 3H, Cp-CH$_3$). ^{13}C{^{1}H} (C_6D_6, 125 MHz, 298 K): δ 234.7 (s, *C*O), 205.8 (s, N*C*N), 138.6 (s, N-C_{ipso} or *C*-*o*-CH$_3$), 138.5 (s, *C*-*p*-CH$_3$), 136.2 (s, N-C_{ipso} or *C*-*o*-CH$_3$), 129.4 (s, m-*C*H), 123.7 (s, NC*H*=*C*HN), 96.0 (s, C_{Cp}-CH$_3$), 82.6 (s, Cp), 80.5 (s, Cp), 21.1 (s, *p*-CH$_3$),

19.4 (s, *o*-*C*H_3), 13.7 (s (Cp-*C*H_3). IR (CH_2Cl_2, cm^{-1}): 1905 ν(CO), 1832 ν(CO). Elemental analysis calcd. (%) for $C_{29}H_{31}N_2O_2Mn$ (494.478): C 70.44, H 6.32, N 5.66; found C 70.07, H 6.33, N 5.58.

6.4 Preparation of Cp'Mn(CO)$_2$(I^{i}Pr$_2$Me$_2$) (3).

As above (section 6.2), Cp'Mn(CO)$_3$ (0.223 g, 1.0 mmol) and I^{i}Pr$_2$Me$_2$ (0.180 g, 1.0 mmol) were combined in hexane (60 mL), photolysed for 30 min under a slow flow of CO. Most of the product crystallises on the walls of the immersion well as a yellow solid, and can easily be removed and washed with cold hexane (10 mL). Some insoluble, dark red material was also produced which was removed by passing the hexane solution through a pad of celite. Concentration of the solute afforded a further batch of yellow crystals. Total yield 0.19 g (51%). NB. The lower solvent volume used in comparison to **1**, **2** and **4** is crucial to keep the yield of **3** high. Larger amounts of the red precipitate by-product are formed under more dilute conditions. ^{1}H NMR (d_3-MeCN, 500 MHz, 298 K): δ 6.02 (sept., 2H, J_{HH} = 7.1 Hz, NC*H*(CH_3)$_2$), δ 4.30 (s, 2H, Cp), 4.25 (s, 2H, Cp), 2.20 (s, 6H, NC(C*H*$_3$)=C(C*H*$_3$)N), 1.77 (s, 3H, Cp-C*H*$_3$), 1.42 (d, 12H, J_{HH} = 7.1 Hz, NCH(C*H*$_3$)$_2$). ^{13}C{^{1}H} NMR (CD_3CN, 125 MHz, 298 K): δ 235.0 (s, *C*O), 194.6 (s, N*C*N), 127.6 (s, N*C*(CH_3)=*C*(CH_3)N), 101.5 (s, C_{Cp}-CH_3), 83.7 (s, Cp), 81.5 (s, Cp), 53.8 (s, N*C*H(CH_3)$_2$), 21.9 (s, NCH(*C*H$_3$)$_2$), 14.0 (s, Cp-*C*H_3), 10.8 (s, NC(*C*H_3)=C(*C*H_3)N). IR (CH_2Cl_2, cm^{-1}): 1898 ν(CO), 1824 ν(CO). Elemental analysis calcd. (%) for $C_{19}H_{27}N_2O_2Mn$ (370.37): C 61.62, H 7.35, N 7.56; found C 61.75, H 7.45, N 7.51.

6.5 Preparation of Cp'Mn(CO)$_2$(IPr) (4).

As above (section 6.2), Cp′Mn(CO)$_3$ (0.223 g, 1.0 mmol) was combined with IPr (0.389 g, 1.0 mmol) in hexane (100 mL) and photolysed for 40 min under a slow flow of argon. In this time, the solution darkened from pale yellow to a golden yellow, with some red-orange precipitate formed which was removed by cannula filtration. Yellow crystalline material was isolated from a concentrated hexane solution, washed with cold hexane (10 mL) and dried to give a

yellow/orange solid. Yield 0.27 g (47 %). ^{1}H NMR (d_8-THF, 500 MHz, 298 K): δ 7.43 (m, 2H, *p*-CH), 7.32 (m, 4H, *m*-CH), 7.18 (s, 2H, HC=CH), 3.84 (m, 2H, Cp), 3.47 (s, 2H, Cp), 2.87 (sept, 4H, $^{3}J_{HH}$ = 6.86 Hz, $(CH_3)_2C\underline{H}$), 1.56 (s, 3H, Cp-CH_3), 1.39 (d, 12H, $^{3}J_{HH}$ = 6.86 Hz, $(CH_3)_2$CH), 1.11 (d, 12H, $^{3}J_{HH}$ = 6.86 Hz, $(CH_3)_2$CH). ^{13}C{^{1}H} (d_8-THF, 125 MHz, 298 K): δ 234.5 (s, *C*O), 207.9 (s, N*C*N), 147.2 (s, *o*-*C*$(CH_3)_2$CH), 139.6 (s, Cp' *C*-CH_3), 130.2 (s, *p*-CH), 126.3 (s, H*C*=*C*H), 124.5 (s, *m*-CH), 82.8 (s, Cp), 80.2 (s, Cp), 29.3 (s, $(CH_3)_2$*C*H), 25.9 (s, $(CH_3)_2$CH), 22.8 (s, $(CH_3)_2$CH), 13.7 (s (Cp-CH_3). IR (CH_2Cl_2, cm^{-1}): 1906 ν(CO), 1834 ν(CO). Elemental analysis calcd. (%) for $C_{35}H_{43}N_2O_2Mn$ (578.27): C 72.63, H 7.49, N 4.84; found C 72.17, H 7.37, N 4.81.

6.6 Preparation of $[Re(IEt_2Me_2)(Bpy)(CO)_3]BAr_4^F$ (5).

Addition of dichloromethane (15 mL) to $Re(IEt_2Me_2)_2(CO)_3Cl$ (0.610 g, 1.0 mmol) and $NaBAr_4^F$ (0.886 g, 1.0 mmol) resulted in formation of a yellow solution and precipitation of NaCl. The mixture was stirred at room temperature for 1 h before addition of Bpy (0.312 g, 2.0 mmol) and refluxing overnight. A vivid yellow solution formed from which the product was isolated by column chromatography. The reaction mixture was loaded onto a column, packed with 60 Å silica in hexane, using the minimum amount of dichloromethane possible. The product was separated by elution with a 50:50 hexane/dichloromethane solvent mixture and collected as the first bright yellow band. This was then subjected to further purification by multiple fast recrystalisations from hexane/dichloromethane. Yellow crystals, suitable for X-ray diffraction, were obtained from a concentrated dichloromethane solution of the product layered with hexane at room temperature. Yield 0.519 g (36 %). ^{1}H NMR (CD_2Cl_2, 500 MHz, 298 K): δ 9.27 (m, 2H, Bpy), 8.14 (m, 2H, Bpy), 8.10 (m, 2H, Bpy), 7.67 (m, 2H, Bpy), 3.98 (q, 4H, $^{3}J_{HH}$ = 7.2 Hz, NC$H_2$$CH_3$), 1.97 (s, 6H, NC(C$H_3$)=C(C$H_3$)N), 0.65 (t, 6H, $^{3}J_{HH}$ = 7.2 Hz, $NCH_2C$$H_3$). ^{13}C{^{1}H} ($CD_2Cl_2$, 125 MHz, 298 K): δ 195.4 (s, CO), 190.2 (s, CO), 170.5 (s, NCN), 156.4 (s, Bpy), 154.1 (s, Bpy), 140.3 (s, Bpy), 128.3 (s, Bpy), 126.7 (s, N(CH_3)*C*=*C*(CH_3)N), 124.3 (s, Bpy), 43.4 (s, N*C*H_2CH_3), 15.9 (s, NCH_2*C*H_3), 8.9 (s, N(*C*H_3)C=C(*C*H_3)N). IR (CH_2Cl_2, cm^{-1}): 2029 ν(CO), 1934 ν(CO), 1915 ν(CO).

Anal. calcd. (%) for $C_{54}H_{36}BF_{24}N_4O_3Re.0.5C_6H_{14}$ (1484.96): C 46.10, H 2.92, N 3.77; found C 46.31, H 2.72, N 3.52.

6.7 Preparation of $[Re(I^iPr_2Me_2)(Bpy)(CO)_3]BAr_4^F$ (6).

As for **5**, but with $Re(I^iPr_2Me_2)_2(CO)_3Cl$ (0.666 g, 1.0 mmol) as the starting material. Yield 0.647 g (44 %). ^1H NMR (CD_2Cl_2, 500 MHz, 298 K): δ 9.21 (m, 2H, Bpy), 8.13 (m, 2H, Bpy), 8.11 (m, 2H, Bpy), 7.68 (m, 2H, Bpy), 4.93 (sept, 2H, $^3J_{HH}$ = 7.1 Hz, NC*H*$(CH_3)_2$), 2.04 (s, 6H, MeC=CMe), 1.08 (d, 12H, $^3J_{HH}$ = 7.1 Hz, NCH(C*H*$_3)_2$). $^{13}C\{^1H\}$ (CD_2Cl_2, 125 MHz, 298 K): δ 194.6 (s, CO), 189.9 (s, CO), 170.9 (s, NCN), 156.2 (s, Bpy), 153.8 (s, Bpy), 139.8 (s, Bpy), 127.9 (s, Bpy), 127.3 (s, CH_3C=*C*CH_3), 123.9 (s, Bpy), 52.9 (s, N*C*H$(CH_3)_2$), 21.6 (s, NCH(*C*$H_3)_2$), 10.6 (s, *C*H_3C=C*C*H_3). IR (CH_2Cl_2, cm^{-1}): 2029 ν(CO), 1934 ν(CO), 1916 ν(CO). Anal. calcd. (%) for $C_{56}H_{40}BF_{24}N_4O_3Re.0.5C_6H_{14}$ (1513.01): C 46.84, H 3.13, N 3.70; found C 47.33, H 3.00, N 3.33.

6.8 Preparation of $[Re(IEt_2Me_2)(Dppz)(CO)_3]BAr_4^F$ (8).

Addition of dichloroethane (15 mL) to $Re(IEt_2Me_2)_2(CO)_3Cl$ (0.610 g, 1.0 mmol) and $NaBAr_4^F$ (0.886 g, 1.0 mmol) resulted in formation of a yellow solution and precipitation of NaCl. The mixture was stirred at room temperature for 1 h before addition of Dppz (0.565 g, 2.0 mmol) and refluxing for 48 h. A vivid yellow solution formed from which the product was isolated by column chromatography. The reaction mixture was loaded onto a column, packed with 60 Å silica in hexane, using the minimum amount of dichloromethane possible. The product was separated by elution with a 50:50 hexane/dichloromethane solvent mixture and collected as the first bright yellow band. This was then subjected to further purification by multiple fast recrystalisations from hexane/dichloromethane. Yellow crystals, suitable for X-ray diffraction, were obtained from a concentrated dichloromethane solution of the product layered with hexane at room temperature. Yield 0.502 g (32 %). ^1H NMR (CD_2Cl_2, 500 MHz, 298 K): δ 9.92 (m, 2H, Dppz), 9.67 (m, 2H, Dppz), 8.45 (m, 2H, Dppz), 8.15 (m, 2H, Dppz), 8.09 (m, 2H, Dppz), 4.11 (q, 4H, $^3J_{HH}$ = 7.2 Hz, NC*H*$_2$CH$_3$),

1.91 (s, 6H, NC(C*H*$_3$)=C(C*H*$_3$)N), 0.69 (t, 6H, $^3J_{HH}$ = 7.2 Hz, NCH$_2$C*H*$_3$). ^{13}C{^{1}H} (CD_2Cl_2, 125 MHz, 298 K): δ 195.3 (s, CO), 190.1 (s, CO), 170.3 (s, NCN), 155.0 (s, Dppz), 149.6 (s, Dppz), 143.4 (s, Dppz), 138.7 (s, Dppz), 136.7 (s, Dppz), 133.0 (s, Dppz), 131.3 (s, Dppz), 129.8 (s, Dppz), 127.7 (s, Dppz), 126.8 (s, N(CH$_3$)*C*=*C*(CH$_3$)N), 43.4 (s, N*C*H$_2$CH$_3$), 16.2 (s, NCH$_2$*C*H$_3$), 8.8 (s, N(*C*H$_3$)C=C(*C*H$_3$)N). IR (CH_2Cl_2, cm^{-1}): 2031 ν(CO), 1936 ν(CO) and 1918 ν(CO). Anal. calcd. (%) for $C_{62}H_{38}BF_{24}N_6O_3Re$**.**$CH_2Cl_2$ (1652.91): C 45.78, H 2.44, N 5.08; found C 45.85, H 2.75, N 5.09.

6.9 Preparation of [Re(I^{i}Pr$_2$Me$_2$)(Dppz)(CO)$_3$]BAr$_4^F$ (9).

As for **8**, but with Re(I^{i}Pr$_2$Me$_2$)$_2$(CO)$_3$Cl (0.666 g, 1.0 mmol) as the starting material. Yield 0.654 g (41 %). ^{1}H NMR (CD_2Cl_2, 500 MHz, 298 K): δ 9.91 (m, 2H, Dppz), 9.61 (m, 2H, Dppz), 8.44 (m, 2H, Dppz), 8.16 (m, 2H, Dppz), 8.09 (m, 2H, Dppz), 5.17 (sept, 2H, $^3J_{HH}$ = 7.1 Hz, NC*H*(CH$_3$)$_2$), 1.95 (s, 6H, NC(C*H*$_3$)=C(C*H*$_3$)N), 1.13 (d, 12H, $^3J_{HH}$ = 7.1 Hz, NCH(C*H*$_3$)$_2$). ^{13}C{^{1}H} (CD_2Cl_2, 125 MHz, 298 K): δ 194.8 (s, CO), 190.1 (s, CO), 172.0 (s, NCN), 155.3 (s, Dppz), 150.0 (s, Dppz), 143.7 (s, Dppz), 139.0 (s, Dppz), 137.1 (s, Dppz), 133.4 (s, Dppz), 131.4 (s, Dppz), 130.2 (s, Dppz), 128.0 (s, Dppz), 127.6 (s, N*C*(CH$_3$)=*C*(CH$_3$)N), 53.3 (s, N*C*H(CH$_3$)$_2$), 22.1 (s, NCH(*C*H$_3$)$_2$), 10.4 (s, NC(*C*H$_3$)=C(*C*H$_3$)N). IR (CH_2Cl_2, cm^{-1}): 2031 ν(CO), 1937 ν(CO) and 1918 ν(CO). Anal. calcd. (%) for $C_{64}H_{42}BF_{24}N_6O_3Re$ (1596.04): C 48.16, H 2.65, N 5.27; found C 47.97, H 2.84, N 5.27.

6.10 Preparation of [Re(I^{i}Pr$_2$Me$_2$)(Dppz-F$_2$)(CO)$_3$]BAr$_4^F$ (10).

As for **8**, but with Re(I^{i}Pr$_2$Me$_2$)$_2$(CO)$_3$Cl (0.666 g, 1.0 mmol) as the starting material and Dppz-F_2 (0.637 g, 2.0 mmol) as the diimine ligand used. Yield 0.653 g (40 %). ^{1}H NMR (CD_2Cl_2, 500 MHz, 298 K): δ 9.84 (m, 2H, Dppz), 9.62 (m, 2H, Dppz), 8.18 (m, 4H, Dppz), 5.15 (sept, 2H, $^3J_{HH}$ = 7.1 Hz, NC*H*(CH$_3$)$_2$), 1.95 (s, 6H, NC(C*H*$_3$)=C(C*H*$_3$)N), 1.12 (d, 12H, $^3J_{HH}$ = 7.1 Hz, NCH(C*H*$_3$)$_2$). ^{13}C{^{1}H} (CD_2Cl_2, 125 MHz, 298 K): δ 195.0 (s, CO), 190.2 (s, CO), 172.1 (s, N*C*N), 155.8 (s, Dppz), 150.1 (s, Dppz), 141.8 (m, Dppz), 139.3 (s, Dppz),

137.2 (s, Dppz), 131.2 (s, Dppz), 128.4 (s, Dppz), 127.8 (s, N*C*(CH_3)=*C*(CH_3)N), 115.5 (m, Dppz), 53.5 (s, N*C*H(CH_3)$_2$), 22.1 (s, NCH(*C*H_3)$_2$), 10.5 (s, NC(*C*H_3)=C(*C*H_3)N). ^{19}F NMR (CD_2Cl_2, 400 MHz, 298 K): δ -123.3 (t, Dppz-F_2, J_{HF} = 9.0 Hz) IR (CH_2Cl_2, cm^{-1}): 2031 ν(CO), 1934 ν(CO) and 1918 ν(CO). Anal. calcd. (%) for $C_{64}H_{40}BF_{26}N_6O_3Re$ (1632.02): C 47.10, H 2.47, N 5.15; found C 47.09, H 2.58, N 5.14.

6.11 Preparation of Mn(I^{i}Pr$_2$Me$_2$)$_2$(CO)$_3$Br (11).

Addition of benzene (15 mL) to $Mn(CO)_5Br$ (0.275 g, 1.0 mmol) and I^iPr_2Me_2 (0.361 g, 2.0 mmol) resulted in immediate effervescence and the formation of a yellow/orange solution. The mixture was stirred at room temperature for 1 h and then left to stand. A yellow/orange precipitate formed, which was isolated by cannula filtration and washed with Et_2O (2 x 5 mL). Orange crystals, suitable for X-ray diffraction, were obtained from a concentrated benzene solution of the product at room temperature. Yield 0.30 g (52 %). ^{1}H NMR (THF-d_8, 500 MHz, 298 K): δ 6.89 (sept, 1H, $^3J_{HH}$ = 7.0 Hz, C*H*(CH_3)$_2$), 6.03 (sept, 1H, $^3J_{HH}$ = 7.0 Hz, C*H*(CH_3)$_2$), 5.23 (sept, 1H, $^3J_{HH}$ = 7.0 Hz, C*H*(CH_3)$_2$), 5.15 (sept, 1H, $^3J_{HH}$ = 7.0 Hz, C*H*(CH_3)$_2$), 2.34 (s, 3H, NC(C*H*$_3$)=C(C*H*$_3$)N), 2.32 (s, 3H, NC(C*H*$_3$)=C(C*H*$_3$)N), 2.22 (s, 3H, NC(C*H*$_3$)=C(C*H*$_3$)N), 2.18 (s, 3H, NC(C*H*$_3$)=C(C*H*$_3$)N), 1.67 (d, 3H, $^3J_{HH}$ = 7.0 Hz, CH(C*H*$_3$)$_2$), 1.59 (d, 6H, $^3J_{HH}$ = 7.0 Hz, CH(C*H*$_3$)$_2$), 1.43 (d, 3H, $^3J_{HH}$ = 7.0 Hz, CH(C*H*$_3$)$_2$), 1.34 (d, 3H, $^3J_{HH}$ = 7.0 Hz, CH(C*H*$_3$)$_2$), 1.25 (d, 3H, $^3J_{HH}$ = 7.0 Hz, CH(C*H*$_3$)$_2$), 0.79 (d, 3H, $^3J_{HH}$ = 7.0 Hz, CH(C*H*$_3$)$_2$), 0.58 (d, 3H, $^3J_{HH}$ = 7.0 Hz, CH(C*H*$_3$)$_2$). ^{13}C{^{1}H} (THF-d_8, 125 MHz, 298 K): δ 228.3 (s, CO), 222.2 (s, CO), 191.1 (s, NCN), 190.0 (s, NCN), 128.6 (s, N*C*(CH_3)=*C*(CH_3)N), 128.5 (s, N*C*(CH_3)=*C*(CH_3)N), 127.9 (s, N*C*(CH_3)=*C*(CH_3)N), 127.4 (s, N*C*(CH_3)=*C*(CH_3)N), 54.3 (s, *C*H(CH_3)$_2$), 55.0 (s, *C*H(CH_3)$_2$), 53.7 (s, *C*H(CH_3)$_2$), 53.4 (s, *C*H(CH_3)$_2$), 26.0 (s, CH(*C*H_3)$_2$), 23.2 (s, CH(*C*H_3)$_2$), 22.9 (s, CH(*C*H_3)$_2$), 22.6 (s, CH(*C*H_3)$_2$), 22.4 (s, CH(*C*H_3)$_2$), 21.9 (s, CH(*C*H_3)$_2$), 20.0 (s, CH(*C*H_3)$_2$), 19.8 (s, CH(*C*H_3)$_2$), 10.9 (s, NC(*C*H_3)=C(*C*H_3)N). IR (C_6D_6, cm^{-1}): 2004 ν(CO), 1926 ν(CO), 1864 ν(CO). Anal. calcd. (%) for $C_{25}H_{40}N_4O_3BrMn$ (579.46): C 51.82, H 6.96, N 9.67; found C 51.72, H 6.84, N 9.53.

6.12 Preparation of $Re(I^iPr_2Me_2)_2(CO)_3Cl$ (12).

$Re(CO)_5Cl$ (0.109 g, 0.3 mmol) was combined with $I^iPr_2Me_2$ (0.108 g, 0.6 mmol) in an ampoule fitted with a J. Young's resealable tap. Addition of benzene (15 mL) afforded a yellow solution and immediate effervescence. The solution was heated at 343 K for 2 h. After cooling, the solvent was removed under vacuum to yield an off-white solid, which was washed with EtOH (2 x 5 mL) and isolated by filtration. Colourless crystals, suitable for X-ray diffraction, were obtained from CH_2Cl_2/hexane. Yield 0.16 g (80 %). ^{1}H NMR (CD_2Cl_2, 400 MHz, 298 K): δ 6.57 (sept, 1H, $^3J_{HH}$ = 7.0 Hz, C*H*$(CH_3)_2$), 6.04 (sept, 1H, $^3J_{HH}$ = 7.1 Hz, C*H*$(CH_3)_2$), 5.50 (sept, 1H, $^3J_{HH}$ = 7.0 Hz, C*H*$(CH_3)_2$), 5.26 (sept, 1H, $^3J_{HH}$ = 7.1 Hz, C*H*$(CH_3)_2$), 2.31 (s, 3H, NC(C*H*$_3$)=C(C*H*$_3$)N), 2.29 (s, 3H, NC(C*H*$_3$)=C(C*H*$_3$)N), 2.20 (s, 3H, NC(C*H*$_3$)=C(C*H*$_3$)N), 2.17 (s, 3H, NC(C*H*$_3$)=C(C*H*$_3$)N), 1.61 (d, 3H, $^3J_{HH}$ = 7.0 Hz, CH(C*H*$_3)_2$), 1.58 (d, 3H, $^3J_{HH}$ = 7.0 Hz, CH(C*H*$_3)_2$), 1.51 (m, 6H, CH(C*H*$_3)_2$), 1.36 (d, 3H, $^3J_{HH}$ = 7.1 Hz, CH(C*H*$_3)_2$), 1.32 (d, 3H, $^3J_{HH}$ = 6.8 Hz, CH(C*H*$_3)_2$), 0.82 (d, 3H, $^3J_{HH}$ = 7.1 Hz, CH(C*H*$_3)_2$), 0.65 (d, 3H, $^3J_{HH}$ = 7.2 Hz, CH(C*H*$_3)_2$).^{13}C{^{1}H} (CD_2Cl_2, 100 MHz, 298 K): δ 197.1 (s, CO), 196.5 (s, CO), 193.6 (s, CO), 180.5 (s, NCN), 179.2 (s, NCN), 127.7 (s, NC(CH$_3$)=*C*(CH$_3$)N), 127.5 (s, NC(CH$_3$)=*C*(CH$_3$)N), 126.9 (s, NC(CH$_3$)=*C*(CH$_3$)N), 126.5 (s, NC(CH$_3$)=*C*(CH$_3$)N), 55.7 (s, *C*H$(CH_3)_2$), 55.0 (s, *C*H$(CH_3)_2$), 53.8 (s, *C*H$(CH_3)_2$), 53.6 (s, *C*H$(CH_3)_2$), 25.4 (s, CH(C*H*$_3)_2$), 23.6 (s, CH(C*H*$_3)_2$), 23.4 (s, CH(C*H*$_3)_2$), 22.5 (s, CH(C*H*$_3)_2$), 22.4 (s, CH(C*H*$_3)_2$), 22.1 (s, CH(C*H*$_3)_2$), 20.0 (s, CH(C*H*$_3)_2$), 19.9 (s, CH(C*H*$_3)_2$), 10.7 (m, NC(*C*H$_3$)=C(*C*H$_3$)N). IR (CH_2Cl_2, cm^{-1}): 2009 ν(CO), 1911 ν(CO), 1857 ν(CO). Anal. calcd. (%) for $C_{25}H_{40}N_4O_3ClRe$ (666.27): C 45.07, H 6.05, N 8.41; found C 44.66, H 5.98, N 8.19.

6.13 Preparation of $[Mn(I^iPr_2Me_2)(O_2CO)(CO)_3][I^iPr_2Me_2\text{-}H]$ (13).

Addition of benzene (15 mL) to $Mn(CO)_5Br$ (0.275 g, 1.0 mmol) and $I^iPr_2Me_2$ (0.361 g, 2.0 mmol) resulted in immediate effervescence and the formation of a yellow/orange solution. The mixture was stirred at room temperature for 1 h and then concentrated to *ca*. 5mL before addition of 10 mL of ethanol via cannula. A green precipitate formed, which was removed by cannula filtration and the

filtrate was concentrated and layered with hexane. Yellow crystals suitable for X-ray diffraction were obtained. Yield 0.58 g (57 %). ^{1}H NMR (C_6D_6, 500 MHz, 298 K): δ 7.51 (s, 1H, [I^{i}Pr$_2$Me$_2$-*H*]) 5.79 (sept, 2H, $^{3}J_{HH}$ = 7.0 Hz, C*H*(CH$_3$)$_2$), 4.80 (sept, 1H, $^{3}J_{HH}$ = 6.9 Hz, C*H*(CH$_3$)$_2$), 5.23 (sept, 1H, $^{3}J_{HH}$ = 6.5 Hz, C*H*(CH$_3$)$_2$), 1.69 (s, 6H, NC(C*H*$_3$)=C(C*H*$_3$)N), 1.36 (d, 3H, $^{3}J_{HH}$ = 6.9 Hz, CH(C*H*$_3$)$_2$), 1.30 (d, 6H, $^{3}J_{HH}$ = 7.0 Hz, CH(C*H*$_3$)$_2$), 1.21 (d, 6H, $^{3}J_{HH}$ = 7.0 Hz, CH(C*H*$_3$)$_2$), 1.08 (d, 3H, $^{3}J_{HH}$ = 6.9 Hz, CH(C*H*$_3$)$_2$), 0.97 (d, 3H, $^{3}J_{HH}$ = 6.5 Hz, CH(C*H*$_3$)$_2$), 0.76 (d, 3H, $^{3}J_{HH}$ = 6.5 Hz, CH(C*H*$_3$)$_2$). N.B. The backbone CH_3 groups for the NHC bound to the metal appear to be split into 6 1H singlets, but only 4 are visible with 2 presumably under other peaks (1.83, 1.60, 1.57, 1.56).^{13}C{^{1}H} (THF-d$_8$, 125 MHz, 298 K): δ 234.2 (s, O_2CO), 224.1 (s, CO), 221.3 (s, CO), 189.6 (s, NCN), 152.2 (s, NC(H)N), 126.8 (s, N*C*(CH$_3$)=*C*(CH$_3$)N), 57.6 (s, *C*H(CH$_3$)$_2$), 51.7 (s, *C*H(CH$_3$)$_2$), 40.4 (s, *C*H(CH$_3$)$_2$), 26.6 (s, CH(*C*H$_3$)$_2$), 23.6 (s, CH(*C*H$_3$)$_2$), 23.2 (s, CH(*C*H$_3$)$_2$), 22.7 (s, CH(*C*H$_3$)$_2$), 22.5 (s, CH(*C*H$_3$)$_2$), 10.9 (s, NC(*C*H$_3$)=C(*C*H$_3$)N). IR (C_6D_6, cm^{-1}): 2038 ν(CO), 2002 ν(CO), 1957 ν(CO), 1894 ν(CO), 1865 ν(CO).

6.14 Preparation of Mn(IPr)(CO)$_4$Br (15).

Mn(CO)$_5$Br (0.275 g, 1.0 mmol) was combined with IPr (0.389 g, 1.0 mmol) in an ampoule fitted with a J. Young's resealable tap. Addition of benzene (15 mL) resulted in rapid effervescence and formation of a yellow/orange solution. After stirring for 2 h at room temperature, the solvent was removed to leave a yellow/orange solid. This was extracted with hexane (2 x 20 mL), filtered and concentrated to ca.10 mL. Upon cooling to 196 K, a yellow precipitate formed, which was isolated by cannula filtration. Orange crystals of **15**, suitable for X-ray diffraction, were obtained from a concentrated hexane solution of the product at 243 K. Yield 0.29 g (46 %). ^{1}H NMR (CD_2Cl_2, 500 MHz, 298 K): δ 7.57 (t, 2H, $^{3}J_{HH}$ = 7.8 Hz, C$_6$^{i}Pr$_2$*H*$_3$), 7.38 (d, 4H, $^{3}J_{HH}$ = 7.8 Hz, C$_6$^{i}Pr$_2$*H*$_3$), 7.20 (s, 2H, NC*H*=C*H*N), 2.86 (sept, 4H, $^{3}J_{HH}$ = 6.8 Hz, C*H*(CH$_3$)$_2$), 1.35 (d, 12H, $^{3}J_{HH}$ = 6.8 Hz, CH(C*H*$_3$)$_2$), 1.11 (d, 12H, $^{3}J_{HH}$ = 6.8 Hz, CH(C*H*$_3$)$_2$). ^{13}C{^{1}H} (CD_2Cl_2, 125 MHz, 298 K): δ 219.3 (s, CO), 213.3 (s, CO), 209.2 (s, CO), 193.3 (s, NCN), 147.9 (s, *C*$_6$^{i}Pr$_2$H$_3$), 137.9 (s, *C*$_6$^{i}Pr$_2$H$_3$), 132.1 (s, *C*$_6$^{i}Pr$_2$H$_3$), 126.1 (s, NCH=*C*HN), 125.2 (s, *C*$_6$^{i}Pr$_2$H$_3$), 29.2 (s, *C*H(CH$_3$)$_2$), 26.6 (s, CH(*C*H$_3$)$_2$), 23.5

(s, CH(*C*H$_3$)$_2$). IR (CH_2Cl_2, cm^{-1}): 2078 ν(CO), 1995 ν(CO), 1938 ν(CO). Anal. calcd. (%) for $C_{31}H_{36}N_2O_4BrMn$ (635.48): C 58.59, H 5.71, N 4.41; found C 58.69, H 5.82, N 4.28.

6.15 Preparation of Re(IPr)(CO)$_4$Cl (16).

$Re(CO)_5Cl$ (0.109 g, 0.3 mmol) and 1 equiv. of IPr (0.117 g, 0.3 mmol) were combined in an ampoule fitted with a J. Young's resealable tap. The introduction of benzene (15 mL) resulted in the instant formation of an effervescent yellow solution, which was then heated at 343 K for 2 h. After cooling to room temperature, the solvent was removed to give an off-white precipitate. This was washed with 2 x 5 mL EtOH and dried under vacuum. Colourless crystals of **16** suitable for X-ray diffraction were obtained from CH_2Cl_2/hexane. Yield 0.14 g (65 %). ^{1}H NMR (CD_2Cl_2, 500 MHz, 298 K): δ 7.57 (t, 2H, $^3J_{HH}$ = 7.8 Hz, $C_6{}^{i}Pr_2H_3$), 7.37 (d, 4H, $^3J_{HH}$ = 7.8 Hz, $C_6{}^{i}Pr_2H_3$), 7.17 (s, 2H, NC*H*=C*H*N), 2.83 (sept, 4H, $^3J_{HH}$ = 6.6 Hz, C*H*(CH$_3$)$_2$), 1.33 (d, 12H, $^3J_{HH}$ = 6.7 Hz, CH(C*H*$_3$)$_2$), 1.11 (d, 12H, $^3J_{HH}$ = 6.9 Hz, CH(C*H*$_3$)$_2$). ^{13}C{^{1}H} (CD_2Cl_2, 125 MHz, 298 K): δ 186.7 (s, *C*O), 185.8 (s, *C*O), 184.4 (s, *C*O), 181.7 (s, N*C*N), 147.7 (s, $C_6{}^{i}Pr_2H_3$), 137.9 (s, $C_6{}^{i}Pr_2H_3$), 132.0 (s, $C_6{}^{i}Pr_2H_3$), 125.4 (s, N*C*H=*C*HN), 125.1 (s, $C_6{}^{i}Pr_2H_3$), 29.2 (s, *C*H(CH$_3$)$_2$), 26.3 (s, CH(*C*H$_3$)$_2$), 23.1 (s, CH(*C*H$_3$)$_2$). IR (CH_2Cl_2, cm^{-1}): 2095 ν(CO), 1993 ν(CO), 1925 ν(CO). Anal. calcd. (%) for $C_{31}H_{36}N_2O_4ClRe$ (722.30): C 51.55, H 5.02, N 3.88; found C 51.26, H 5.00, N 3.83.

6.16 Preparation of [Mn(I^{i}Pr$_2$Me$_2$)$_2$(CO)$_3$]BAr$_4^F$ (17).

A CD_2Cl_2 suspension of **11** (0.020 g, 0.03 mmol) and $NaBAr_4^F$ (0.027 g, 0.03 mmol) was prepared at 77 K in J. Young's resealable NMR tube. The sample was thawed to room temperature, shaken for 1-2 min, and then introduced into a pre-cooled NMR probe set at 208 K. Even under these conditions, traces of [Mn(I^{i}Pr$_2$Me$_2$)$_2$(CO)$_4$]BAr$_4^F$ (**19**) and imidazolium salt were present, which restricted definitive assignment of most of the resonances in the low frequency region of the proton NMR spectrum. As far as possible, the limited proton

assignments that were possible for **17** were confirmed by ^{1}H COSY and ^{1}H-^{13}C HMBC experiments. Selected ^{1}H NMR (CD_2Cl_2, 400 MHz, 208 K): δ 3.81 (br sept, 1H, C*H*$(CH_3)_2$), 0.28 (br s, 3H, CH(C*H*$_3$)(CH_3-agostic)), -2.21 (br s, 3H, CH(CH_3)(C*H*$_3$-agostic)). Selected ^{13}C{^{1}H} (CD_2Cl_2, 100 MHz, 208 K): δ 228.5 (s, *C*O), 214.4 (s, *C*O), 183.4 (s, N*C*N), 177.7 (s, NCN), 48.3 (s, *C*H(CH_3)(CH_3-agostic), 19.6 (s, CH(*C*H$_3$)(CH_3-agostic), 7.8 (s, CH(CH_3)(*C*H$_3$-agostic).

6.17 Preparation of $[Re(I^iPr_2Me_2)_2(CO)_3]BAr_4^F$ (18).

The rhenium carbene complex **12** (0.020 g, 0.03 mmol) was combined with $NaBAr_4^F$ (0.027 g, 0.03 mmol) in a J. Young's resealable NMR tube. CD_2Cl_2 was added by vacuum transfer. The sample was thawed to room temperature, shaken for 1-2 min, and then introduced into a pre-cooled NMR probe set at 208 K. ^{1}H NMR (CD_2Cl_2, 400 MHz, 208 K): δ 5.23 (sept, 1H, $^{3}J_{HH}$ = 6.5 Hz, C*H*$(CH_3)_2$), 5.10 (sept, 1H, $^{3}J_{HH}$ = 6.5 Hz, C*H*$(CH_3)_2$), 4.66 (sept, 1H, $^{3}J_{HH}$ = 6.9 Hz, C*H*$(CH_3)_2$), 4.03 (sept, 1H, $^{3}J_{HH}$ = 5.6 Hz, C*H*$(CH_3)_2$), 2.17 (s, 6H, NC(C*H*$_3$)=C(C*H*$_3$)N), 2.09 (s, 3H, NC(C*H*$_3$)=C(C*H*$_3$)N), 1.98 (s, 3H, NC(C*H*$_3$)=C(C*H*$_3$)N), 1.56 (d, 6H, $^{3}J_{HH}$ = 6.5 Hz, CH(C*H*$_3$)$_2$), 1.47 (d, 6H, $^{3}J_{HH}$ = 6.5 Hz, CH(C*H*$_3$)$_2$), 1.40 (d, 3H, $^{3}J_{HH}$ = 6.9 Hz, CH(C*H*$_3$)$_2$), 0.56 (d, 3H, $^{3}J_{HH}$ = 6.9 Hz, CH(C*H*$_3$)$_2$), 0.48 (d, 3H, $^{3}J_{HH}$ = 5.6 Hz, CH(C*H*$_3$)$_2$), -0.24 (d, 3H, $^{3}J_{HH}$ = 5.6 Hz, CH(C*H*$_3$)$_2$). ^{13}C{^{1}H} (CD_2Cl_2, 100 MHz, 208 K): δ 193.4 (s, *C*O), 193.2 (s, *C*O), 191.4 (s, *C*O), 179.5 (s, N*C*N), 172.3 (s, N*C*N), 128.1 (s, N*C*(CH_3)=*C*(CH_3)N), 126.6 (s, N*C*(CH_3)=*C*(CH_3)N), 126.1 (s, N*C*(CH_3)=*C*(CH_3)N), 120.2 (s, N*C*(CH_3)=*C*(CH_3)N), 56.4 (s, *C*H$(CH_3)_2$), 55.4 (s, *C*H$(CH_3)_2$), 54.5 (s, *C*H$(CH_3)_2$), 49.1 (s, *C*H$(CH_3)_2$), 22.1 (s, CH(*C*H$_3$)$_2$), 21.7 (s, CH(*C*H$_3$)$_2$), 20.9 (s, CH(*C*H$_3$)$_2$), 20.5 (s, CH(*C*H$_3$)$_2$), 20.4 (s, CH(*C*H$_3$)$_2$), 20.3 (s, CH(*C*H$_3$)$_2$), 19.6 (s, CH(*C*H$_3$)$_2$), 10.8 (s, NC(*C*H$_3$)=C(*C*H$_3$)N), 10.6 (s, NC(*C*H$_3$)=C(*C*H$_3$)N), 10.5 (s, NC(*C*H$_3$)=C(*C*H$_3$)N), 9.0 (s, NC(*C*H$_3$)=C(*C*H$_3$)N), 4.8 (s, CH(*C*H$_3$)$_2$). IR (CH_2Cl_2, cm^{-1}): 2036 ν(CO), 1945 ν(CO), 1921 ν(CO).

6.18 Preparation of $[Mn(I^iPr_2Me_2)_2(CO)_4]BAr_4^F$ (19).

The manganese precursor **11** (0.290 g, 0.5 mmol) was combined with $NaBAr_4^F$ (0.443 g, 0.5 mmol) in CH_2Cl_2 (20 mL) to yield a red solution and an off-white precipitate. The mixture was stirred at room temperature for 10 min before a slow stream of CO was introduced. The colour of the solution changed immediately to pale yellow. Treatment with CO was maintained for 1 h, after which, the solution was filtered and the filtrate reduced to a volume of ca. 5 mL. Layering with hexane generated X-ray quality, colourless crystals of **19**. Yield 0.19 g (28 %). ^{1}H NMR (CD_2Cl_2, 500 MHz, 298 K): δ 5.41 (sept, 2H, $^3J_{HH}$ = 6.9 Hz, C*H*(CH_3)$_2$), 4.51 (sept, 2H, $^3J_{HH}$ = 6.9 Hz, C*H*(CH_3)$_2$), 2.30 (s, 6H, NC(C*H*$_3$)=C(C*H*$_3$)N), 2.17 (s, 6H, NC(C*H*$_3$)=C(C*H*$_3$)N), 1.63 (m, 12H, CH(C*H*$_3$)$_2$), 1.38 (d, 6H, $^3J_{HH}$ = 6.9 Hz, CH(C*H*$_3$)$_2$), 0.73 (d, 6H, $^3J_{HH}$ = 6.9 Hz, CH(C*H*$_3$)$_2$). ^{13}C{^{1}H} (CD_2Cl_2, 125 MHz, 298 K): δ 130.2 (s, N*C*(CH_3)=*C*(CH_3)N), 130.0 (s, N*C*(CH_3)=*C*(CH_3)N), 55.2 (s, *C*H(CH_3)$_2$), 54.4 (s, *C*H(CH_3)$_2$), 22.6 (s, CH(*C*H$_3$)$_2$), 22.2 (s, CH(*C*H$_3$)$_2$), 21.5 (s, CH(*C*H$_3$)$_2$), 19.8 (s, CH(*C*H$_3$)$_2$), 11.2 (s, NC(*C*H$_3$)=C(*C*H$_3$)N). Mn-CO and Mn-NHC resonances could not be observed in the ^{13}C{^{1}H} spectra recorded either at room temperature or at 211 K. IR (CH_2Cl_2, cm^{-1}): 2077 ν(CO), 2000 ν(CO), 1980 ν(CO), 1971 ν(CO). Anal. calcd. (%) for $C_{58}H_{56}N_4O_4BF_{24}Mn$ (1394.80): C 49.94.44, H 4.05, N 4.02; found C 49.94, H 3.70, N 3.87.

6.19 Preparation of $[Re(I^iPr_2Me_2)_2(CO)_4]BAr_4^F$ (20).

A CH_2Cl_2 suspension (20 mL) of **12** (0.200 g, 0.3 mmol) and $NaBAr_4^F$ (0.266 g, 0.3 mmol) was stirred for 30 min at room temperature. A slow stream of CO was then bubbled through the yellow suspension, resulting in an instantaneous discharge of the colour. After 1 h, the suspension was filtered and concentrated to ca. 5 mL. Colourless crystals of **20** were obtained upon layering the solution with hexane. Yield 0.33 g (71 %). ^{1}H NMR (CD_2Cl_2, 400 MHz, 298 K): δ 5.31 (sept, 2H, $^3J_{HH}$ = 7.0 Hz, C*H*(CH_3)$_2$), 4.55 (sept, 2H, $^3J_{HH}$ = 7.0 Hz, C*H*(CH_3)$_2$), 2.29 (s, 6H, NC(C*H*$_3$)=C(C*H*$_3$)N), 2.18 (s, 6H, NC(C*H*$_3$)=C(C*H*$_3$)N), 1.63 (d, 6H, $^3J_{HH}$ = 7.0 Hz, CH(C*H*$_3$)$_2$), 1.59 (d, 6H, $^3J_{HH}$ = 7.0 Hz, CH(C*H*$_3$)$_2$), 1.37 (d, 6H,

$^{3}J_{HH}$ = 7.0 Hz, CH(CH_3)$_2$), 0.76 (d, 6H, $^{3}J_{HH}$ = 7.0 Hz, CH(CH_3)$_2$). $^{13}C\{^{1}H\}$ (CD_2Cl_2, 100 MHz, 298 K): δ 185.5 (s, *C*O), 185.3 (s, *C*O), 165.1 (s, N*C*N), 128.8 (s, N*C*(CH$_3$)=*C*(CH$_3$)N), 128.7 (s, N*C*(CH$_3$)=*C*(CH$_3$)N), 57.0 (s, *C*H(CH$_3$)$_2$), 55.9 (s, *C*H(CH$_3$)$_2$), 22.7 (s, CH(*C*H$_3$)$_2$), 22.2 (s, CH(*C*H$_3$)$_2$), 21.5 (s, CH(*C*H$_3$)$_2$), 19.8 (s, CH(*C*H$_3$)$_2$), 11.1 (s, NC(*C*H$_3$)=C(*C*H$_3$)N), 11.0 (s, NC(*C*H$_3$)=C(*C*H$_3$)N). IR (CH_2Cl_2, cm^{-1}): 2091 ν(CO), 1998 ν(CO), 1972 ν(CO). Anal. calcd. (%) for $C_{58}H_{56}N_2O_4BF_{24}Re$ (1526.07): C 45.65, H 3.70, N 3.67; found C 45.88, H 3.36, N 3.80. ESI-TOF MS: $[M]^+$ m/z = 659.2790 (theoretical 659.2602).

6.20 Preparation of [Re(I^{i}Pr$_2$Me$_2$)$_2$(CO)$_3$(MeCN)]BAr$_4^F$ (21).

To a rapidly stirring yellow suspension of **12** (0.133 g, 0.2 mmol) and $NaBAr_4^F$ (0.177 g, 0.2 mmol) in CH_2Cl_2 (20 mL), was added MeCN (3 mL), which instantaneously changed the colour of the suspension to pale pink. After stirring for 30 min, the reaction mixture was filtered and the filtrate concentrated to 5 mL. Layering with hexane gave **21** as an off-white precipitate. Yield 0.09 g (29 %). ^{1}H NMR (CD_2Cl_2, 400 MHz, 298 K): δ 5.65 (sept, 1H, $^{3}J_{HH}$ = 7.1 Hz, C*H*(CH$_3$)$_2$), 5.32 (sept, 1H, $^{3}J_{HH}$ = 7.1 Hz, C*H*(CH$_3$)$_2$), 4.80 (sept, 1H, $^{3}J_{HH}$ = 7.1 Hz, C*H*(CH$_3$)$_2$), 4.39 (sept, 1H, $^{3}J_{HH}$ = 7.1 Hz, C*H*(CH$_3$)$_2$), 2.46 (s, 3H, NCC*H*$_3$), 2.28 (s, 3H, NC(C*H*$_3$)=C(C*H*$_3$)N), 2.27 (s, 3H, NC(C*H*$_3$)=C(C*H*$_3$)N), 2.17 (s, 3H, NC(C*H*$_3$)=C(C*H*$_3$)N), 2.15 (s, 3H, NC(C*H*$_3$)=C(C*H*$_3$)N), 1.62 (d, 6H, $^{3}J_{HH}$ = 7.1 Hz, CH(C*H*$_3$)$_2$), 1.56 (d, 3H, $^{3}J_{HH}$ = 7.1 Hz, CH(C*H*$_3$)$_2$), 1.51 (d, 3H, $^{3}J_{HH}$ = 7.1 Hz, CH(C*H*$_3$)$_2$), 1.35 (d, 3H, $^{3}J_{HH}$ = 7.1 Hz, CH(C*H*$_3$)$_2$), 1.28 (d, 3H, $^{3}J_{HH}$ = 7.1 Hz, CH(C*H*$_3$)$_2$), 0.78 (d, 3H, $^{3}J_{HH}$ = 7.1 Hz, CH(C*H*$_3$)$_2$), 0.72 (d, 3H, $^{3}J_{HH}$ = 7.1 Hz, CH(C*H*$_3$)$_2$). $^{13}C\{^{1}H\}$ (CD_2Cl_2, 100 MHz, 298 K): δ 192.5 (s, CO), 192.4 (s, CO), 192.2 (s, CO), 174.4 (s, NCN), 173.7 (s, NCN), 128.2 (s, N*C*(CH$_3$)=*C*(CH$_3$)N), 127.9 (s, N*C*(CH$_3$)=*C*(CH$_3$)N), 127.8 (s, N*C*(CH$_3$)=*C*(CH$_3$)N), 127.6 (s, N*C*(CH$_3$)=*C*(CH$_3$)N), 123.5 (s, N*C*CH$_3$), 56.1 (s, *C*H(CH$_3$)$_2$), 55.1 (s, *C*H(CH$_3$)$_2$), 54.6 (s, *C*H(CH$_3$)$_2$), 53.5 (s, *C*H(CH$_3$)$_2$), 24.0 (s, CH(C*H*$_3$)$_2$), 23.2 (s, CH(C*H*$_3$)$_2$), 22.2 (s, CH(C*H*$_3$)$_2$), 21.8 (s, CH(C*H*$_3$)$_2$), 19.7 (s, CH(C*H*$_3$)$_2$), 19.6 (s, CH(C*H*$_3$)$_2$), 10.9 (s, NC(*C*H$_3$)=C(*C*H$_3$)N), 4.8 (s, NC*C*H$_3$). IR (CH_2Cl_2, cm^{-1}): 2025 ν(CO), 1931 ν(CO), 1910 ν(CO). Anal. calcd. (%) for

$C_{59}H_{58}N_5O_3BF_{24}Re$ (1538.10): C 46.07, H 3.80, N 4.55; found C 46.03, H 3.51, N 4.47.

6.21 Preparation of Re(IPr)(CO)$_4$(OTf) (22).

A CH_2Cl_2 (15 mL) solution of **16** (0.217 g, 0.3 mmol) and AgOTf (0.077 g, 0.3 mmol) was stirred for 16 h in the dark at room temperature. The suspension was then filtered and concentrated to *ca*. 5 mL. Slow addition of hexane precipitated a white solid, which was isolated by filtration and washed with 2 x 5 mL aliquots of hexane. Colourless crystals were obtained from CH_2Cl_2/hexane. Yield 0.211 g (84 %). ^{1}H NMR (CD_2Cl_2, 500 MHz, 298 K): δ 7.61 (t, 2H, $^3J_{HH}$ = 7.6 Hz, $C_6{}^iPr_2H_3$), 7.41 (d, 4H, $^3J_{HH}$ = 7.6 Hz, $C_6{}^iPr_2H_3$), 7.26 (s, 2H, NC*H*=C*H*N), 2.64 (sept, 4H, $^3J_{HH}$ = 6.8 Hz, C*H*$(CH_3)_2$), 1.33 (d, 12H, $^3J_{HH}$ = 6.8 Hz, CH(C*H*$_3)_2$), 1.13 (d, 12H, $^3J_{HH}$ = 6.8 Hz, CH(C*H*$_3)_2$). ^{13}C{^{1}H} (CD_2Cl_2, 125 MHz, 298 K): δ 187.2 (s, *C*O), 186.0 (s, *C*O), 185.2 (s, *C*O), 182.6 (s, NCN), 147.4 (s, $C_6{}^iPr_2H_3$), 137.5 (s, $C_6{}^iPr_2H_3$), 132.5 (s, $C_6{}^iPr_2H_3$), 126.2 (s, NCH=CHN), 125.4 (s, $C_6{}^iPr_2H_3$), 29.2 (s, *C*H$(CH_3)_2$), 26.3 (s, CH(*C*H$_3)_2$), 22.9 (s, CH(*C*H$_3)_2$). ^{19}F (CD_2Cl_2, 470 MHz, 298 K): δ -74.4 (s). IR (CH_2Cl_2, cm^{-1}): 2107 ν(CO), 2007 ν(CO), 1945 ν(CO). Anal. calcd. (%) for $C_{32}H_{36}F_3N_2O_7ReS$ (835.90): C 45.98, H 4.34, N 3.35; found C 46.08, H 4.40, N 3.27.

6.22 Preparation of [Re(IPr)(CO)$_4$(CD_2Cl_2)]BAr_4^F (23).

The triflate complex **22** (0.042 g, 0.05 mmol) was combined with $NaBAr_4^F$ (0.044 g, 0.05 mmol) and CD_2Cl_2 (0.5 mL) in a J. Young's resealable NMR tube. The mixture was left for 3 h at room temperature and then filtered. Colourless crystals of the product, suitable for X-ray diffraction, were obtained upon layering the filtrate with hexane. Yield 0.071 g (86 %). ^{1}H NMR (CD_2Cl_2, 400 MHz, 283 K): δ 7.67 (t, 2H, $^3J_{HH}$ = 7.6 Hz, $C_6{}^iPr_2H_3$), 7.44 (s, 2H, NC*H*=C*H*N), 7.41 (d, 4H, $^3J_{HH}$ = 7.6 Hz, $C_6{}^iPr_2H_3$), 2.34 (sept, 4H, $^3J_{HH}$ = 6.8 Hz, C*H*$(CH_3)_2$), 1.31 (d, 12H, $^3J_{HH}$ = 6.8 Hz, CH(C*H*$_3)_2$), 1.14 (d, 12H, $^3J_{HH}$ = 6.8 Hz, CH(C*H*$_3)_2$). ^{13}C{^{1}H} (CD_2Cl_2, 100 MHz, 283 K): δ 183.6 (s, *C*O), 181.9 (s, *C*O), 175.7 (s, NCN), 146.6 (s, $C_6{}^iPr_2H_3$), 136.2 (s, $C_6{}^iPr_2H_3$), 133.6 (s, $C_6{}^iPr_2H_3$), 127.5 (s,

NCH=CHN), 126.4 (s, $C_6^iPr_2H_3$), 29.5 (s, $CH(CH_3)_2$), 26.4 (s, $CH(CH_3)_2$), 22.7 (s, $CH(CH_3)_2$). IR (CD_2Cl_2, cm^{-1}): 2115 ν(CO), 2016 ν(CO), 1984 ν(CO), 1971 ν(CO). Anal. calcd. (%) for $C_{65}H_{48}D_2BCl_2F_{24}N_2O_4Re$ (1649.00): C 47.34, H 3.18, N 1.70; found C 47.42, H 3.09, N 1.64.

6.23 Preparation of Mn(IPr)(CO)$_4$(OTf) (24).

$Mn(IPr)(CO)_4Br$ (0.191 g, 0.3 mmol) was combined with AgOTf (0.077 g, 0.3 mmol) in CH_2Cl_2 (15 mL), producing a yellow solution and an off-white precipitate. The suspension was stirred in the dark at room temperature for 16 h, filtered and concentrated to ca. 5 mL. Addition of hexane precipitated **24** as a yellow solid, which was washed with 2 x 5 mL aliquots of hexane and dried under vacuum. Yield 0.167 g (79 %). The compound was stored as a solid, as it slowly decomposed in solution as shown by the appearance of a fine, red precipitate. ^{1}H NMR (C_6D_6, 500 MHz, 298 K): δ 7.25 (t, 2H, $^3J_{HH}$ = 7.8 Hz, $C_6^iPr_2H_3$), 7.10 (d, 4H, $^3J_{HH}$ = 7.8 Hz, $C_6^iPr_2H_3$), 6.56 (s, 2H, NC*H*=C*H*N), 2.73 (sept, 4H, $^3J_{HH}$ = 6.6 Hz, $CH(CH_3)_2$), 1.38 (d, 12H, $^3J_{HH}$ = 6.6 Hz, $CH(CH_3)_2$), 0.95 (d, 12H, $^3J_{HH}$ = 6.6 Hz, $CH(CH_3)_2$). $^{13}C\{^1H\}$ (C_6D_6, 125 MHz, 298 K): δ 218.7 (s, *C*O), 210.0 (s, *C*O), 207.0 (s, *C*O), 190.7 (s, N*C*N), 147.6 (s, $C_6^iPr_2H_3$), 137.6 (s, $C_6^iPr_2H_3$), 132.6 (s, $C_6^iPr_2H_3$), 126.7 (s, NCH=CHN), 125.4 (s, $C_6^iPr_2H_3$), 29.1 (s, $CH(CH_3)_2$), 26.5 (s, $CH(CH_3)_2$), 23.2 (s, $CH(CH_3)_2$). ^{19}F (C_6D_6, 470 MHz, 298 K): δ -74.0 (s). IR (CH_2Cl_2, cm^{-1}): 2099 ν(CO), 2020 ν(CO), 1959 ν(CO). Anal. calcd. (%) for $C_{32}H_{36}F_3N_2O_7MnS$ (704.64): C 54.54, H 5.15, N 3.98; found C 54.45, H 5.05, N 3.86.

6.24 Preparation of [Mn(IPr)(CO)$_5$]BAr$_4^F$ (25).

$Mn(IPr)(CO)_4Br$ (0.318 g, 0.5 mmol) was combined with AgOTf (0.128 g, 0.5 mmol) in CH_2Cl_2 (20 mL) to give a yellow suspension. After stirring for 16 h at room temperature, the mixture was filtered into a Schlenk tube containing $NaBAr_4^F$ (0.443 g, 0.5 mmol). This suspension was stirred for 30 min at room temperature and then subjected to a slow stream of CO for 1 h. During this time, the suspension became pale yellow. After cannula filtration, the filtrate

was concentrated to 5 mL and layered with hexane to afford colourless crystals of the product. Yield 0.61 g (83 %). ^{1}H NMR (CD_2Cl_2, 500 MHz, 298 K): δ 7.49 (s, 2H, NC*H*=C*H*N), 7.44 (m, 8H, $C_6{}^{i}Pr_2H_3$), 2.37 (sept, 4H, $^{3}J_{HH}$ = 6.8 Hz, C*H*$(CH_3)_2$), 1.37 (d, 12H, $^{3}J_{HH}$ = 6.8 Hz, CH(C*H*$_3)_2$), 1.18 (d, 12H, $^{3}J_{HH}$ = 6.8 Hz, CH(C*H*$_3)_2$).^{13}C{^{1}H} (CD_2Cl_2, 125 MHz, 298 K): δ 205.3 (s, *C*O), 203.7 (s, *C*O), 175.5 (s, N*C*N), 147.0 (s, $C_6{}^{i}Pr_2H_3$), 135.4 (s, $C_6{}^{i}Pr_2H_3$), 134.2 (s, $C_6{}^{i}Pr_2H_3$), 129.5 (s, N*C*H=*C*HN), 126.2 (s, $C_6{}^{i}Pr_2H_3$), 29.7 (s, *C*H$(CH_3)_2$), 26.5 (s, CH(*C*H$_3)_2$), 22.7 (s, CH(*C*H$_3)_2$). IR (CH_2Cl_2, cm^{-1}): 2134 ν(CO), 2047 ν(CO). Anal. calcd. (%) for $C_{64}H_{48}N_2O_5BF_{24}Mn$ (1446.77): C 53.13, H 3.34, N 1.93; found C 52.78, H 3.54, N 1.86.

6.25 Preparation of [Re(IPr)(CO)$_5$]BAr$_4^F$ (26).

Re(IPr)$(CO)_4$Cl (0.217 g, 0.3 mmol) was combined with AgOTf (0.077 g, 0.3 mmol) in CH_2Cl_2 (20 mL) to generate a light yellow solution and precipitate of AgCl. After stirring for 16 h in the dark at room temperature, the suspension was filtered by cannula into a Schlenk tube containing NaBAr$_4^F$ (0.266 g, 0.3 mmol). The resulting suspension was stirred at room temperature for 30 min before a slow stream of CO was introduced, which resulted in the instantaneous discharge of the yellow colour. After reaction with CO for 1 h, the suspension was filtered and the filtrate reduced under vacuum to ca. 5 mL. Colourless crystals of the product were obtained upon layering with hexane. Yield 0.26 g (55 %). ^{1}H NMR (CD_2Cl_2, 500 MHz, 298 K): δ 7.46 (s, 2H, NC*H*=C*H*N), 7.44 (m, 8H, $C_6{}^{i}Pr_2H_3$), 2.35 (sept, 4H, $^{3}J_{HH}$ = 6.8 Hz, C*H*$(CH_3)_2$), 1.35 (d, 12H, $^{3}J_{HH}$ = 6.8 Hz, CH(C*H*$_3)_2$), 1.18 (d, 12H, $^{3}J_{HH}$ = 6.8 Hz, CH(C*H*$_3)_2$). ^{13}C{^{1}H} (CD_2Cl_2, 125 MHz, 298 K): δ 177.1 (s, *C*O), 176.4 (s, *C*O), 164.4 (s, N*C*N), 146.6 (s, $C_6{}^{i}Pr_2H_3$), 136.0 (s, $C_6{}^{i}Pr_2H_3$), 134.0 (s, $C_6{}^{i}Pr_2H_3$), 127.9 (s, N*C*H=*C*HN), 126.2 (s, $C_6{}^{i}Pr_2H_3$), 29.8 (s, *C*H$(CH_3)_2$), 26.3 (s, CH(*C*H$_3)_2$), 22.8 (s, CH(*C*H$_3)_2$). IR (CH_2Cl_2, cm^{-1}): 2148 ν(CO), 2042 ν(CO). Anal. calcd. (%) for $C_{65}H_{48}N_2O_5F_{24}BrRe$ (1509.09): C 49.10, H 3.04, N 1.76; found C 49.01, H 3.05, N 1.87.

6.26 References.

(1) Kuhn, N.; Kratz, T.; *Synthesis,* **1993**, *6*, 561-562.

(2) Jafarpour, L.; Stevens, E. D.; Nolan, S. P.; *J. Organomet. Chem.* **2000**, *606*, 49-54.

(3) Yakelis, N. A.; Bergman, R. G.; *Organometallics* **2005**, *24*, 3579-3581.

(4) Gaussian 03, Revision C.02, M. J. Frisch, G. W. Trucks, H. B. Schlegel, G. E. Scuseria, M. A. Robb, J. R. Cheeseman, J. A. Montgomery, Jr., T. Vreven, K. N. Kudin, J. C. Burant, J. M. Millam, S. S. Iyengar, J. Tomasi, V. Barone, B. Mennucci, M. Cossi, G. Scalmani, N. Rega, G. A. Petersson, H. Nakatsuji, M. Hada, M. Ehara, K. Toyota, R. Fukuda, J. Hasegawa, M. Ishida, T. Nakajima, Y. Honda, O. Kitao, H. Nakai, M. Klene, X. Li, J. E. Knox, H. P. Hratchian, J. B. Cross, C. Adamo, J. Jaramillo, R. Gomperts, R. E. Stratmann, O. Yazyev, A. J. Austin, R. Cammi, C. Pomelli, J. W. Ochterski, P. Y. Ayala, K. Morokuma, G. A. Voth, P. Salvador, J. J. Dannenberg, V. G. Zakrzewski, S. Dapprich, A. D. Daniels, M. C. Strain, O. Farkas, D. K. Malick, A. D. Rabuck, K. Raghavachari, J. B. Foresman, J. V. Ortiz, Q. Cui, A. G. Baboul, S. Clifford, J. Cioslowski, B. B. Stefanov, G. Liu, A. Liashenko, P. Piskorz, I. Komaromi, R. L. Martin, D. J. Fox, T. Keith, M. A. Al-Laham, C. Y. Peng, A. Nanayakkara, M. Challacombe, P. M. W. Gill, B. Johnson, W. Chen, M. W. Wong, C. Gonzalez, and J. A. Pople, Gaussian, Inc., Wallingford CT, **2004**.

(5) Andrae, D.; Häusserman, U.; Dolg, M.; Stoll, H.; Preuss, *Theor. Chim. Acta*, **1990**, *77*, 123.

(6) Höllwarth, A.; Böhme, M.; Dapprich, S.; Ehlers, A. W.; Gobbi, A.; Jonas, V.; Köhler, K. F.; Stegmann, R.; Veldkamp, A.; Frenking, G., *Chem. Phys. Lett*. **1993**, *208*, 237.

(7) (a) Hehre, W. J.; Ditchfield, R.; Pople, J. A. *J. Chem. Phys*. **1972**, *56*, 2257. (b) Hariharan, P. C.; Pople, J. A. *Theor. Chim. Acta* **1973**, *28*, 213.

Appendices

Crystallographic data

Table 16. Crystal data and structure refinement for **1**.

Identification code	h07mkw03
Empirical formula	C17 H23 Mn N2 O2
Formula weight	342.31
Temperature	150(2) K
Wavelength	0.71073 Å
Crystal system	Monoclinic
Space group	P21/n
Unit cell dimensions	a = 13.2920(2)Å $\alpha = 90^{o}$
	b = 9.0680(2)Å $\beta = 97.209(1)^{o}$
	c = 14.0950(3)Å $\gamma = 90^{o}$
Volume	1685.47(6) $Å^3$
Z	4
Density (calculated)	1.349 Mg/m^3
Absorption coefficient	0.791 mm^{-1}
F(000)	720
Crystal size	0.25 x 0.20 x 0.20 mm
Theta range for data collection	3.82 to 27.10 ^{o}.
Index ranges	-16<=h<=15; -11<=k<=11; -18<=l<=17
Reflections collected	15484
Independent reflections	3665 [R(int) = 0.0500]
Reflections observed (>2σ)	2612
Data Completeness	0.987
Absorption correction	Semi-empirical from equivalents
Max. and min. transmission	0.87 and 0.84
Refinement method	Full-matrix least-squares on F^2
Data / restraints / parameters	3665 / 0 / 205
Goodness-of-fit on F^2	1.079
Final R indices [I>2σ(I)]	R1 = 0.0450 wR2 = 0.1174
R indices (all data)	R1 = 0.0774 wR2 = 0.1423
Largest diff. peak and hole	1.113 and -0.466 $eÅ^{-3}$

Table 17. Crystal data and structure refinement for **2**.

Identification code	k08mkw7
Empirical formula	C29 H31 Mn N2 O2
Formula weight	494.50
Temperature	150(2) K
Wavelength	0.71073 Å
Crystal system	Tetragonal
Space group	P41
Unit cell dimensions	a = 17.3820(1)Å $\alpha = 90^o$
	b = 17.3820(1)Å $\beta = 90^o$
	c = 33.1360(2)Å $\gamma = 90^o$
Volume	10011.51(10) $Å^3$
Z	16
Density (calculated)	1.312 Mg/m^3
Absorption coefficient	0.556 mm^{-1}
F(000)	4160
Crystal size	0.40 x 0.38 x 0.28 mm
Theta range for data collection	3.52 to 27.45 °.
Index ranges	-22<=h<=22; -22<=k<=22; -42<=l<=42
Reflections collected	136523
Independent reflections	22850 [R(int) = 0.0503]
Reflections observed (>2σ)	19964
Data Completeness	0.997
Absorption correction	Semi-empirical from equivalents
Max. and min. transmission	0.86 and 0.80
Refinement method	Full-matrix least-squares on F^2
Data / restraints / parameters	22850 / 1 / 1253
Goodness-of-fit on F^2	1.033
Final R indices [I>2σ(I)]	R^1 = 0.0351 wR2 = 0.0740
R indices (all data)	R^1 = 0.0463 wR2 = 0.0784
Absolute structure parameter	-0.009(7)
Largest diff. peak and hole	0.259 and -0.250 $eÅ^{-3}$

Table 18. Crystal data and structure refinement for **3**.

Identification code	k07mkw36
Empirical formula	C19 H27 Mn N2 O2
Formula weight	370.37
Temperature	150(2) K
Wavelength	0.71073 Å
Crystal system	Orthorhombic
Space group	Pbca
Unit cell dimensions	a = 9.2210 (1)Å $\alpha = 90^o$
	b = 15.2780(2)Å $\beta = 90^o$
	c = 26.0210(5)Å $\gamma = 90^o$
Volume	3665.80(9) $Å^3$
Z	8
Density (calculated)	1.342 Mg/m^3
Absorption coefficient	0.733 mm^{-1}
F(000)	1568
Crystal size	0.40 x 0.20 x 0.17 mm
Theta range for data collection	3.55 to 27.50^o
Index ranges	-11<=h<=11; -19<=k<=19; -33<=l<=33
Reflections collected	48267
Independent reflections	4182 [R(int) = 0.1234]
Reflections observed (>2σ)	2513
Data Completeness	0.997
Absorption correction	Semi-empirical from equivalents
Max. and min. transmission	0.88 and 0.80
Refinement method	Full-matrix least-squares on F^2
Data / restraints / parameters	4182 / 0 / 224
Goodness-of-fit on F^2	1.025
Final R indices [I>2σ(I)]	R1 = 0.0461 wR2 = 0.0987
R indices (all data)	R1 = 0.1079 wR2 = 0.1218
Largest diff. peak and hole	0.541 and -0.701 $eÅ^{-3}$

Table 19. Crystal data and structure refinement for **4**.

Identification code	k08mkw38
Empirical formula	C35 H43 Mn N2 O2
Formula weight	578.65
Temperature	150(2) K
Wavelength	0.71073 Å
Crystal system	Triclinic
Space group	P-1
Unit cell dimensions	a = 9.2500(2)Å α = 77.646(1)^{o}
	b = 10.3070(2)Å β = 86.996(1)^{o}
	c = 19.1900(5)Å γ = 64.279(1)^{o}
Volume	1608.42(6) Å^{3}
Z	2
Density (calculated)	1.195 Mg/m^{3}
Absorption coefficient	0.442 mm^{-1}
F(000)	616
Crystal size	0.30 x 0.25 x 0.25 mm
Theta range for data collection	3.55 to 27.74^{o}
Index ranges	-12<=h<=12; -13<=k<=13; -24<=l<=24
Reflections collected	24179
Independent reflections	7243 [R(int) = 0.1310]
Reflections observed (>2σ)	5666
Data Completeness	0.958
Absorption correction	Semi-empirical from equivalents
Max. and min. transmission	0.90 and 0.61
Refinement method	Full-matrix least-squares on F^{2}
Data / restraints / parameters	7243 / 0 / 371
Goodness-of-fit on F^{2}	1.048
Final R indices [I>2σ(I)]	R1 = 0.0493 wR2 = 0.1041
R indices (all data)	R1 = 0.0725 wR2 = 0.1215
Largest diff. peak and hole	0.384 and -0.671 eÅ^{-3}

Table 20. Crystal data and structure refinement for **[Re(IEt$_2$Me$_2$)(Bpy)(CO)$_3$]OTf**.

Identification code	k08mkw16
Empirical formula	C24 H26 Cl2 F3 N4 O6 Re S
Formula weight	812.65
Temperature	150(2) K
Wavelength	0.71073 Å
Crystal system	Monoclinic
Space group	C2/c
Unit cell dimensions	a = 34.5680(11)Å $\alpha = 90^o$
	b = 9.1070(3)Å $\beta = 104.071(1)^o$
	c = 17.9470(5)Å $\gamma = 90^o$
Volume	5480.4(3) Å^3
Z	8
Density (calculated)	1.970 Mg/m^3
Absorption coefficient	4.775 mm^{-1}
F(000)	3184
Crystal size	0.22 x 0.16 x 0.10 mm
Theta range for data collection	3.65 to 26.37^o
Index ranges	-43<=h<=43; -10<=k<=11; -22<=l<=22
Reflections collected	32818
Independent reflections	5592 [R(int) = 0.0954]
Reflections observed (>2σ)	4451
Data Completeness	0.996
Absorption correction	Semi-empirical from equivalents
Max. and min. transmission	0.64 and 0.45
Refinement method	Full-matrix least-squares on F^2
Data / restraints / parameters	5592 / 0 / 347
Goodness-of-fit on F^2	1.051
Final R indices [I>2σ(I)]	R^1 = 0.0400 wR2 = 0.0875
R indices (all data)	R^1 = 0.0587 wR2 = 0.0943
Largest diff. peak and hole	2.023 and -1.641 eÅ^{-3}

Notes: Asymmetric unit contains 1 molecule of the rhenium salt and a very disordered area of solvent (I've never seen anything like it!). Analysis of the latter using the Platon SQUEEZE function suggested that the unit cell contents should be augmented by one molecule of dichloromethane, and the final (post SQUEEZE) refinement has accounted for the inclusion of this solvent of recrystallisation.

Table 21. Crystal data and structure refinement for **6**.

Identification code	k08mkw45
Empirical formula	C56 H40 B F24 N4 O3 Re
Formula weight	1469.93
Temperature	150(2) K
Wavelength	0.71073 Å
Crystal system	Monoclinic
Space group	Cc
Unit cell dimensions	a = 12.2150(1)Å $\alpha = 90^{o}$
	b = 24.4320(2)Å $\beta = 104.080(1)^{o}$
	c = 20.5820(2)Å $\gamma = 90^{o}$
Volume	5957.89(9) $Å^3$
Z	4
Density (calculated)	1.639 Mg/m^3
Absorption coefficient	2.161 mm^{-1}
F(000)	2896
Crystal size	0.40 x 0.20 x 0.20 mm
Theta range for data collection	3.55 to 27.48 ^{o}.
Index ranges	-15<=h<=15; -31<=k<=31; -26<=l<=26
Reflections collected	58836
Independent reflections	13529 [R(int) = 0.0666]
Reflections observed (>2σ)	12104
Data Completeness	0.997
Absorption correction	Semi-empirical from equivalents
Max. and min. transmission	0.436 and 0.352
Refinement method	Full-matrix least-squares on F^2
Data / restraints / parameters	13529 / 92 / 868
Goodness-of-fit on F^2	1.022
Final R indices [I>2σ(I)]	R1 = 0.0346 wR2 = 0.0749
R indices (all data)	R1 = 0.0439 wR2 = 0.0792
Absolute structure parameter	-0.016(5)
Largest diff. peak and hole	1.445 and -1.337 $eÅ^{-3}$

Notes: Cation ordered, some of the CF_3 groups in the anion disordered. In particular, the moiety containing F1 exhibited 80:20 disorder, while those containing F7, F13, F16 and F19 bore 55:45 disorder. On major partial fluorines were treated anisotropically, but with restraints. Similarly, F…F and C-F distances were refined subject to restraints wherever disorder prevailed.

Table 22. Crystal data and structure refinement for **8**.

Identification code	k09mkw10
Empirical formula	C63 H40 B Cl2 F24 N6 O3 Re
Formula weight	1652.92
Temperature	150(2) K
Wavelength	0.71073 Å
Crystal system	Monoclinic
Space group	P21/n
Unit cell dimensions	a = 13.1530(1)Å $\alpha = 90^o$
	b = 13.0630(1)Å $\beta = 94.645(1)^o$
	c = 37.6690(3)Å $\gamma = 90^o$
Volume	6450.94(9) $Å^3$
Z	4
Density (calculated)	1.702 Mg/m^3
Absorption coefficient	2.087 mm^{-1}
F(000)	3256
Crystal size	0.25 x 0.25 x 0.15 mm
Theta range for data collection	3.59 to 27.49^o
Index ranges	-17<=h<=17; -16<=k<=16; -48<=l<=48
Reflections collected	77399
Independent reflections	14699 [R(int) = 0.0732]
Reflections observed (>2σ)	12222
Data Completeness	0.995
Max. and min. transmission	0.74, 0.66
Refinement method	Full-matrix least-squares on F^2
Data / restraints / parameters	14699 / 30 / 938
Goodness-of-fit on F^2	1.105
Final R indices [I>2σ(I)]	R1 = 0.0413 wR2 = 0.0878
R indices (all data)	R1 = 0.0591 wR2 = 0.0944
Largest diff. peak and hole	1.033 and -1.624 $eÅ^{-3}$

Notes: In addition to one formula unit of the salt, the asymmetric unit in k09mkw10 contains one molecule of dichloromethane, in which Cl1 exhibits 65:35 disorder. The fluorines attached to C47 and C54 also exhibit disorder (55:45 and 75:25 ratios respectively). Only fragment atoms with occupancy were refined anisotropically. C-F and F-F distances were refined subject to similarity restraints in the disordered functionalities.

Table 23. Crystal data and structure refinement for **9**.

Identification code	k09mkw22
Empirical formula	C65 H44 B Cl2 F24 N6 O3 Re
Formula weight	1680.97
Temperature	150(2) K
Wavelength	0.71073 Å
Crystal system	Triclinic
Space group	P-1
Unit cell dimensions	a = 13.0620(1)Å α = 70.069(1)^o
	b = 13.9410(2)Å β = 83.430(1)^o
	c = 19.4780(2)Å γ = 79.080(1)^o
Volume	3269.29(6) Å^3
Z	2
Density (calculated)	1.708 Mg/m^3
Absorption coefficient	2.061 mm^{-1}
F(000)	1660
Crystal size	0.30 x 0.25 x 0.25 mm
Theta range for data collection	3.62 to 27.47^o
Index ranges	-16<=h<=16; -18<=k<=18; -25<=l<=25
Reflections collected	59336
Independent reflections	14817 [R(int) = 0.0477]
Reflections observed (>2σ)	12593
Data Completeness	0.990
Absorption correction	Semi-empirical from equivalents
Max. and min. transmission	0.616 and 0.573
Refinement method	Full-matrix least-squares on F^2
Data / restraints / parameters	14817 / 90 / 976
Goodness-of-fit on F^2	1.050
Final R indices [I>2σ(I)]	R1 = 0.0363 wR2 = 0.0808
R indices (all data)	R1 = 0.0492 wR2 = 0.0865
Largest diff. peak and hole	0.878 and -1.362 eÅ^{-3}

Notes:

In addition to one molecule of the salt, the asymmetric unit in this structure contains 1 molecule of dichloromethane. Disorder was prevalent in some of the CF_3 groups present, with F4-6 disordered in a 50:50 ratio and F16-21 split over 2 sites in a 65:35 ratio. Fractional fluorines with 35% occupanct were treated isotropically, and convergence was assisted by constraint on C-F and F…F distances in disordered regions.

Table 24. Crystal data and structure refinement for **10**.

Identification code	h09mkw8
Empirical formula	C64 H40 B F26 N6 O3 Re
Formula weight	1632.03
Temperature	150(2) K
Wavelength	0.71073 Å
Crystal system	Triclinic
Space group	P-1
Unit cell dimensions	a = 12.9280(2)Å α = 93.768(1)^{o}
	b = 13.2450(2)Å β = 92.223(1)^{o}
	c = 18.7440(3)Å γ = 97.473(1)^{o}
Volume	3171.78(9) Å^{3}
Z	2
Density (calculated)	1.709 Mg/m^{3}
Absorption coefficient	2.044 mm^{-1}
F(000)	1608
Crystal size	0.20 x 0.20 x 0.10 mm
Theta range for data collection	3.54 to 27.53^{o}
Index ranges	-16<=h<=16; -17<=k<=17; -24<=l<=24
Reflections collected	62319
Independent reflections	14486 [R(int) = 0.0626]
Reflections observed (>2σ)	11489
Data Completeness	0.990
Absorption correction	Semi-empirical from equivalents
Max. and min. transmission	0.820 and 0.758
Refinement method	Full-matrix least-squares on F^{2}
Data / restraints / parameters	14486 / 246 / 1051
Goodness-of-fit on F^{2}	1.011
Final R indices [I>2σ(I)]	R1 = 0.0375 wR2 = 0.0731
R indices (all data)	R1 = 0.0599 wR2 = 0.0805
Largest diff. peak and hole	0.827 and -0.978 eÅ^{-3}

Table 25. Crystal data and structure refinement for **11**.

Identification code	bath1181
Empirical formula	C25 H40 Br Mn N4 O3
Formula weight	579.46
Temperature	100(2) K
Wavelength	0.68890 Å
Crystal system	Tetragonal
Space group	P41212
Unit cell dimensions	a = 11.795(6)Å $\alpha = 90^o$
	b = 11.795(6)Å $\beta = 90^o$
	c = 19.372(13)Å $\gamma = 90^o$
Volume	2695(3) $Å^3$
Z	4
Density (calculated)	1.428 Mg/m^3
Absorption coefficient	2.005 mm^{-1}
F(000)	1208
Crystal size	0.03 x 0.03 x 0.02 mm
Theta range for data collection	3.49 to 24.21^o
Index ranges	-14<=h<=13; -14<=k<=13; -23<=l<=23
Reflections collected	21749
Independent reflections	2361 [R(int) = 0.0786]
Reflections observed (>2σ)	2250
Data Completeness	0.992
Absorption correction	Semi-empirical from equivalents
Max. and min. transmission	0.98 and 0.92
Refinement method	Full-matrix least-squares on F^2
Data / restraints / parameters	2361 / 7 / 185
Goodness-of-fit on F^2	1.161
Final R indices [I>2σ(I)]	R1 = 0.0507 wR2 = 0.1086
R indices (all data)	R1 = 0.0536 wR2 = 0.1102
Absolute structure parameter	0.13(3)
Largest diff. peak and hole	0.232 and -0.303 $eÅ^{-3}$

Notes:

The manganese in this structure is located on a 2-fold rotation axis, implicit to the space group symmetry. The carbonyls based on C1 and C2 are disordered in 80:20 and 70:30 ratios with Br2 and Br1, respectively. The net overall result is that the metal:carbonyl:bromide ratio is 1:3:1 in the lattice as a whole.

Table 26. Crystal data and structure refinement for **12**.

Identification code	h08mkw8
Empirical formula	C25 H40 Cl N4 O3 Re
Formula weight	666.26
Temperature	293(2) K
Wavelength	0.71073 Å
Crystal system	Tetragonal
Space group	P43212
Unit cell dimensions	a = 12.0330(3)Å $\alpha = 90^o$
	b = 12.0330(3)Å $\beta = 90^o$
	c = 19.5880(5)Å $\gamma = 90^o$
Volume	2836.21(12) $Å^3$
Z	4
Density (calculated)	1.560 Mg/m^3
Absorption coefficient	4.410 mm^{-1}
F(000)	1336
Crystal size	0.20 x 0.20 x 0.15 mm
Theta range for data collection	3.93 to 27.55^o
Index ranges	-15<=h<=15; -15<=k<=15; -25<=l<=23
Reflections collected	33056
Independent reflections	3259 [R(int) = 0.0869]
Reflections observed (>2σ)	2913
Data Completeness	0.990
Absorption correction	Semi-empirical from equivalents
Max. and min. transmission	0.43 and 0.34
Refinement method	Full-matrix least-squares on F^2
Data / restraints / parameters	3259 / 0 / 175
Goodness-of-fit on F^2	1.113
Final R indices [I>2σ(I)]	R1 = 0.0299 wR2 = 0.0697
R indices (all data)	R1 = 0.0366 wR2 = 0.0724
Absolute structure parameter	-0.005(15)
Largest diff. peak and hole	1.120 and -0.711 $eÅ^{-3}$

Notes: Asymmetric unit consists of ½ of a molecule, with the central metal located on a crystallographic 2-fold axis. The chloride and carbonyl ligand (based on O1) are necessarily disordered in 1 50:50 ratio.

Table 27. Crystal data and structure refinement for **13**.

Identification code	h10mkw8
Empirical formula	C26 H41 Br0 Mn N4 O6
Formula weight	560.57
Temperature	150(2) K
Wavelength	0.71073 Å
Crystal system	Monoclinic
Space group	P21/a
Unit cell dimensions	a = 17.0400(4)Å $\alpha = 90^o$
	b = 10.1880(2)Å $\beta = 116.430(1)^o$
	c = 18.4610(4)Å $\gamma = 90^o$
Volume	2869.91(11) $Å^3$
Z	4
Density (calculated)	1.297 Mg/m^3
Absorption coefficient	0.504 mm^{-1}
F(000)	1192
Crystal size	0.25 x 0.20 x 0.20 mm
Theta range for data collection	4.00 to 29.97^o
Index ranges	-23<=h<=23; -14<=k<=14; -25<=l<=25
Reflections collected	58360
Independent reflections	8291 [R(int) = 0.0515]
Reflections observed (>2σ)	6310
Data Completeness	0.994
Absorption correction	Semi-empirical from equivalents
Max. and min. transmission	0.693 and 0.648
Refinement method	Full-matrix least-squares on F^2
Data / restraints / parameters	8291 / 0 / 348
Goodness-of-fit on F^2	1.035
Final R indices [I>2σ(I)]	R1 = 0.0372 wR2 = 0.0907
R indices (all data)	R1 = 0.0598 wR2 = 0.1018
Largest diff. peak and hole	0.314 and -0.396 $eÅ^{-3}$

Notes: The carbene ligand is tilted. C-H…O interactions shown in plot.

Table 28. Crystal data and structure refinement for **15**.

Identification code	k10mkw5
Empirical formula	C31 H36 Br Mn N2 O4
Formula weight	635.47
Temperature	150(2) K
Wavelength	0.71073 Å
Crystal system	Monoclinic
Space group	P21/m
Unit cell dimensions	a = 8.8080(2)Å $\alpha = 90^o$
	b = 19.7330(4)Å $\beta = 106.589(1)^o$
	c = 9.3240(2)Å $\gamma = 90^o$
Volume	1553.14(6) $Å^3$
Z	2
Density (calculated)	1.359 Mg/m^3
Absorption coefficient	1.747 mm^{-1}
F(000)	656
Crystal size	0.15 x 0.08 x 0.08 mm
Theta range for data collection	3.76 to 27.53^o
Index ranges	-11<=h<=11; -25<=k<=25; -12<=l<=12
Reflections collected	32262
Independent reflections	3661 [R(int) = 0.0588]
Reflections observed (>2σ)	2941
Data Completeness	0.995
Absorption correction	Semi-empirical from equivalents
Max. and min. transmission	0.882 and 0.818
Refinement method	Full-matrix least-squares on F^2
Data / restraints / parameters	3661 / 13 / 205
Goodness-of-fit on F^2	1.117
Final R indices [I>2σ(I)]	R1 = 0.0403 wR2 = 0.0938
R indices (all data)	R1 = 0.0560 wR2 = 0.1001
Largest diff. peak and hole	0.314 and -0.639 $eÅ^{-3}$

Notes:

Asymmetric unit consists of ½ of a molecule, with the manganese, bromine and carbonyls bases on O1 and O3 located on a mirror plane present in the space group.

The bromide is disordered in 1 40:10 ratio with the carbonyl containing O3. C-O, Mn-C and Mn…O distances are refined subject to ideal distance restraints in the disordered fragments.

Table 29. Crystal data and structure refinement for **16**.

Identification code	h09mkw4
Empirical formula	C31 H36 Cl N2 O4 Re
Formula weight	722.27
Temperature	150(2) K
Wavelength	0.71073 Å
Crystal system	Orthorhombic
Space group	Pbnm
Unit cell dimensions	a = 11.0430(2)Å $\alpha = 90^o$
	b = 14.0470(2)Å $\beta = 90^o$
	c = 19.8700(3)Å $\gamma = 90^o$
Volume	3082.25(8) $Å^3$
Z	4
Density (calculated)	1.556 Mg/m^3
Absorption coefficient	4.065 mm^{-1}
F(000)	1440
Crystal size	0.25 x 0.25 x 0.20 mm
Theta range for data collection	3.59 to 27.48^o
Index ranges	-14<=h<=13; -18<=k<=18; -25<=l<=25
Reflections collected	48498
Independent reflections	3628 [R(int) = 0.0481]
Reflections observed (>2σ)	2963
Data Completeness	0.996
Absorption correction	Semi-empirical from equivalents
Max. and min. transmission	0.452 and 0.385
Refinement method	Full-matrix least-squares on F^2
Data / restraints / parameters	3628 / 0 / 191
Goodness-of-fit on F^2	1.119
Final R indices [I>2σ(I)]	R1 = 0.0210 wR2 = 0.0438
R indices (all data)	R1 = 0.0315 wR2 = 0.0474
Largest diff. peak and hole	0.390 and -1.129 $eÅ^{-3}$

Notes: Asymmetric unit consists of ½ of a molecule, with atoms Re1, C3, O3 and C4 located on a crystallographic mirror plane.

Table 30. Crystal data and structure refinement for **19**.

Identification code	p10mkw11
Empirical formula	C58 H52 B F24 Mn N4 O4
Formula weight	1390.79
Temperature	150(2) K
Wavelength	0.71073 Å
Crystal system	Monoclinic
Space group	C2/c
Unit cell dimensions	a = 17.4842(3)Å $\alpha = 90^o$
	b = 19.9557(5)Å $\beta = 96.001(2)^o$
	c = 35.8042(9)Å $\gamma = 90^o$
Volume	12424.0(5) $Å^3$
Z	8
Density (calculated)	1.487 Mg/m^3
Absorption coefficient	0.333 mm^{-1}
F(000)	5648
Crystal size	0.23 x 0.20 x 0.18 mm
Theta range for data collection	3.10 to 27.48^o
Index ranges	-17<=h<=22; -25<=k<=25; -46<=l<=37
Reflections collected	45771
Independent reflections	14212 [R(int) = 0.0598]
Reflections observed (>2σ)	8848
Data Completeness	0.996
Absorption correction	Semi-empirical from equivalents
Max. and min. transmission	1.00000 and 0.94943
Refinement method	Full-matrix least-squares on F^2
Data / restraints / parameters	14212 / 351 / 973
Goodness-of-fit on F^2	1.015
Final R indices [I>2σ(I)]	R1 = 0.0649 wR2 = 0.1320
R indices (all data)	R1 = 0.1173 wR2 = 0.1578
Largest diff. peak and hole	0.850 and -0.530 $eÅ^{-3}$

Notes:

55:45 disorder prevalent in the CF_3 group fluorines attached to C41 and C49 while 50:50 disorder was present for those attached to C34, C42, C50 and C57.

C-F and F…F distances in disordered regions were refined subject to restraints to assist convergence. Similarly, a minimal number of ADP restraints were included – also to assist refinement.

Table 31. Crystal data and structure refinement for **20**.

Identification code	h10mkw22
Empirical formula	C58 H52 B F24 N4 O4 Re
Formula weight	1522.05
Temperature	150(2) K
Wavelength	0.71073 Å
Crystal system	Monoclinic
Space group	C2/c
Unit cell dimensions	a = 17.5070(2)Å $\alpha = 90^o$
	b = 20.0060(2)Å $\beta = 95.8920(10)^o$
	c = 35.9080(4)Å $\gamma = 90^o$
Volume	12510.2(2) $Å^3$
Z	8
Density (calculated)	1.616 Mg/m^3
Absorption coefficient	2.062 mm^{-1}
F(000)	6048
Crystal size	0.25 x 0.20 x 0.20 mm
Theta range for data collection	3.64 to 27.48^o
Index ranges	-22<=h<=22; -25<=k<=25; -46<=l<=44
Reflections collected	87010
Independent reflections	14298 [R(int) = 0.0725]
Reflections observed (>2σ)	11307
Data Completeness	0.996
Absorption correction	Semi-empirical from equivalents
Max. and min. transmission	0.738 and 0.558
Refinement method	Full-matrix least-squares on F^2
Data / restraints / parameters	14298 / 351 / 973
Goodness-of-fit on F^2	1.057
Final R indices [I>2σ(I)]	R1 = 0.0386 wR2 = 0.0762
R indices (all data)	R1 = 0.0573 wR2 = 0.0834
Largest diff. peak and hole	1.164 and -0.791 $eÅ^{-3}$

Notes:

55:45 disorder prevalent in the CF_3 group fluorines attached to C41 and C49 while 50:50 disorder was present for those attached to C34, C42, C50 and C57.

C-F and F…F distances in disordered regions were refined subject to restraints to assist convergence. Similarly, a minimal number of ADP restraints were included – also to assist refinement.

Table 32. Crystal data and structure refinement for **23**.

Identification code	k10mkw19
Empirical formula	C64 H50 B Cl2 F24 N2 O4 Re
Formula weight	1634.97
Temperature	150(2) K
Wavelength	0.71073 Å
Crystal system	Triclinic
Space group	P-1
Unit cell dimensions	a = 12.2710(1)Å α = 90.56^o
	b = 16.0840(1)Å β = 100.358(1)^o
	c = 17.8140(2)Å γ = 90.16^o
Volume	3458.39(5) Å^3
Z	2
Density (calculated)	1.570 Mg/m^3
Absorption coefficient	1.945 mm^{-1}
F(000)	1620
Crystal size	0.20 x 0.10 x 0.10 mm
Theta range for data collection	3.59 to 25.03^o
Index ranges	-14<=h<=14; -19<=k<=19; -21<=l<=21
Reflections collected	95411
Independent reflections	12180 [R(int) = 0.0472]
Reflections observed (>2σ)	11227
Data Completeness	0.997
Absorption correction	Semi-empirical from equivalents
Max. and min. transmission	0.827 and 0.718
Refinement method	Full-matrix least-squares on F^2
Data / restraints / parameters	12180 / 271 / 979
Goodness-of-fit on F^2	1.071
Final R indices [I>2σ(I)]	R1 = 0.0553 wR2 = 0.1373
R indices (all data)	R1 = 0.0604 wR2 = 0.1412
Largest diff. peak and hole	2.258 and -1.779 eÅ^{-3}

Notes:

55:45 disorder prevalent in the CF_3 group fluorines attached to C40, C47, C48, C55, C56 and C63 and C64. C64 is itself disordered over 2 sites – in the same ratio as that of the fluorine atoms bonded to same. This is not entirely 'crackers' [good scientific word!] as there is evidence for some disorder in the ligated CH_2Cl_2 moiety. Early efforts suggested that modelling of this disorder might be possible, but such endeavours were abandoned by the penultimate least-squares run. Analysis if the crystal packing however, revealed that this dichloromethane is proximate to the CF_3 based on C64.

Crystal size resulted is diffraction fall-off at higher Bragg angles. Hence, data were truncated to a theta of 25^o.

C-F and F…F distances in disordered regions were refined subject to restraints to assist convergence. Similarly, a minimal number of ADP restraints were included – also to assist refinement.

Table 33. Crystal data and structure refinement for **25**.

Identification code	h10mkw21
Empirical formula	C64.25 H48.50 B Cl0.50 F24 Mn N2 O5
Formula weight	1468.03
Temperature	150(2) K
Wavelength	0.71073 Å
Crystal system	Triclinic
Space group	P-1
Unit cell dimensions	a = 13.5510(2)Å α = 101.050(1)^o
	b = 15.5380(2)Å β = 104.266(1)^o
	c = 17.0200(2)Å γ = 99.296(1)^o
Volume	3325.64(8) Å^3
Z	2
Density (calculated)	1.466 Mg/m^3
Absorption coefficient	0.335 mm^{-1}
F(000)	1485
Crystal size	0.25 x 0.25 x 0.20 mm
Theta range for data collection	3.52 to 27.48^o
Index ranges	-17<=h<=17; -20<=k<=20; -22<=l<=22
Reflections collected	98121
Independent reflections	15211 [R(int) = 0.0512]
Reflections observed (>2σ)	11992
Data Completeness	0.997
Absorption correction	Semi-empirical from equivalents
Max. and min. transmission	0.908 and 0.795
Refinement method	Full-matrix least-squares on F^2
Data / restraints / parameters	15211 / 198 / 963
Goodness-of-fit on F^2	1.050
Final R indices [I>2σ(I)]	R1 = 0.0608 wR2 = 0.1641
R indices (all data)	R1 = 0.0773 wR2 = 0.1747
Largest diff. peak and hole	1.015 and -0.563 eÅ^{-3}

Notes:

The asymmetric unit contains 1 cation, 1 anion and a region of diffuse solvent that necessitated use of the PLATON SQUEEZE algorithm, which suggested the presence of approximately 0.25 of a molecule of dichloromethane. Presented data takes account of this solvent.

In addition, the CF_3 groups based on C47, c55 and c63 exhibited 62:38 disorder of the fluorines over 2 sites. C-F and F…F distances, in addition to the ADPs associated with these partial occupancy fluorines were restrained in the final least-squares to assist convergence.

Table 34. Crystal data and structure refinement for **26**.

Identification code	h09mkw22
Empirical formula	C64.50 H49 B Cl F24 N2 O5 Re
Formula weight	1620.52
Temperature	150(2) K
Wavelength	0.71073 Å
Crystal system	Triclinic
Space group	P-1
Unit cell dimensions	a = 13.6600(2)Å α = 101.088(1)^o
	b = 15.5040(2)Å β = 104.546(1)^o
	c = 17.0290(2)Å γ = 99.339(1)^o
Volume	3340.47(8) Å^3
Z	2
Density (calculated)	1.611 Mg/m^3
Absorption coefficient	1.975 mm^{-1}
F(000)	1606
Crystal size	0.25 x 0.25 x 0.20 mm
Theta range for data collection	3.67 to 26.37^o
Index ranges	-17<=h<=17; -19<=k<=19; -21<=l<=21
Reflections collected	63775
Independent reflections	13383 [R(int) = 0.0896]
Reflections observed (>2σ)	10077
Data Completeness	0.979
Absorption correction	Semi-empirical from equivalents
Max. and min. transmission	0.616 and 0.573
Refinement method	Full-matrix least-squares on F^2
Data / restraints / parameters	13383 / 198 / 963
Goodness-of-fit on F^2	1.031
Final R indices [I>2σ(I)]	R1 = 0.0519 wR2 = 0.1179
R indices (all data)	R1 = 0.0804 wR2 = 0.1272
Largest diff. peak and hole	1.025 and -0.716 eÅ^{-3}

Notes:

The asymmetric unit contains 1 cation, 1 anion and a region of diffuse solvent that necessitated use of the PLATON SQUEEZE algorithm, which suggested the presence of approximately 0.5 of a molecule of dichloromethane. Presented data takes account of this solvent.

In addition, the CF_3 groups based on C47, c55 and c63 exhibited 62:38 disorder of the fluorines over 2 sites. C-F and F…F distances, in addition to the ADPs associated with these partial occupancy fluorines were restrained in the final least-squares to assist convergence.

Table 35. Crystal data and structure refinement for **29**.

Identification code	k10mkw21
Empirical formula	C76 H58 B F29 N2 Na O7 Re S
Formula weight	1914.30
Temperature	150(2) K
Wavelength	0.71073 Å
Crystal system	Triclinic
Space group	P-1
Unit cell dimensions	a = 13.0030(1)Å α = 107.654(1)^o
	b = 16.9220(1)Å β = 104.721(1)^o
	c = 19.8310(2)Å γ = 93.222(1)^o
Volume	3979.29(6) Å^3
Z	2
Density (calculated)	1.598 Mg/m^3
Absorption coefficient	1.680 mm^{-1}
F(000)	1904
Crystal size	0.25 x 0.22 x 0.10 mm
Theta range for data collection	3.54 to 27.57^o
Index ranges	-16<=h<=16; -21<=k<=20; -25<=l<=25
Reflections collected	68249
Independent reflections	18133 [R(int) = 0.0501]
Reflections observed (>2σ)	15374
Data Completeness	0.985
Absorption correction	Semi-empirical from equivalents
Max. and min. transmission	0.736 and 0.682
Refinement method	Full-matrix least-squares on F^2
Data / restraints / parameters	18133 / 204 / 1152
Goodness-of-fit on F^2	1.022
Final R indices [I>2σ(I)]	R1 = 0.0347 wR2 = 0.0740
R indices (all data)	R1 = 0.0481 wR2 = 0.0796
Largest diff. peak and hole	0.947 and -1.379 eÅ^{-3}

Notes:
Asymmetric unit consists of one rhenium complex, one aanion, one cation (Na^+) and two fluorobenzene molecules.
80:20 disorder was modeled for fluorines attached to C48, C55 and C56
C-F and F…F distances restrained in final least squares cycles. ADP restraints for disordered fluorines – to assist convergence.

Table 36. Crystal data and structure refinement for **$CpRe(CO)_2(IEt_2Me_2)$**.

Identification code	k08mkw29
Empirical formula	C16 H21 N2 O2 Re
Formula weight	459.55
Temperature	150(2) K
Wavelength	0.71073 Å
Crystal system	Monoclinic
Space group	P21/n
Unit cell dimensions	a = 13.9240(2)Å $\alpha = 90^o$
	b = 8.1840(1)Å $\beta = 97.243(1)^o$
	c = 14.0824(3)Å $\gamma = 90^o$
Volume	1591.94(5) $Å^3$
Z	4
Density (calculated)	1.917 Mg/m^3
Absorption coefficient	7.639 mm^{-1}
F(000)	888
Crystal size	0.35 x 0.17 x 0.17 mm
Theta range for data collection	3.84 to 27.47 ^{o}.
Index ranges	-18<=h<=18; -10<=k<=10; -18<=l<=18
Reflections collected	29565
Independent reflections	3631 [R(int) = 0.0460]
Reflections observed (>2σ)	3222
Data Completeness	0.998
Absorption correction	Semi-empirical from equivalents
Max. and min. transmission	0.28 and 0.21
Refinement method	Full-matrix least-squares on F^2
Data / restraints / parameters	3631 / 0 / 194
Goodness-of-fit on F^2	1.106
Final R indices [I>2σ(I)]	R1 = 0.0221 wR2 = 0.0494
R indices (all data)	R1 = 0.0280 wR2 = 0.0517
Largest diff. peak and hole	1.576 and -1.206 $eÅ^{-3}$

Table 37. Crystal data and structure refinement for **[Re(I^{i}Pr$_2$Me$_2$)(PPh$_3$)(CO)$_3$]BAr$_4^F$**.

Identification code	k09mkw20
Empirical formula	C74.40 H57.80 B Cl2.80 F24 N4 O2 P Re
Formula weight	1823.09
Temperature	150(2) K
Wavelength	0.71073 Å
Crystal system	Triclinic
Space group	P-1
Unit cell dimensions	a = 13.8670(2)Å α = 84.287(1)^o
	b = 16.5980(3)Å β = 87.604(1)^o
	c = 17.1430(3)Å γ = 84.957(1)^o
Volume	3908.74(11) Å^3
Z	2
Density (calculated)	1.549 Mg/m^3
Absorption coefficient	1.775 mm^{-1}
F(000)	1814
Crystal size	0.20 x 0.20 x 0.10 mm
Theta range for data collection	3.60 to 27.47 ^{o}.
Index ranges	-17<=h<=17; -21<=k<=21; -22<=l<=22
Reflections collected	68018
Independent reflections	17604 [R(int) = 0.0582]
Reflections observed (>2σ)	14187
Data Completeness	0.983
Absorption correction	Semi-empirical from equivalents
Max. and min. transmission	0.851 and 0.817
Refinement method	Full-matrix least-squares on F^2
Data / restraints / parameters	17604 / 143 / 1062
Goodness-of-fit on F^2	1.094
Final R indices [I>2σ(I)]	R1 = 0.0693 wR2 = 0.1636
R indices (all data)	R1 = 0.0916 wR2 = 0.1753
Largest diff. peak and hole	4.506 and -2.386 eÅ^{-3}

Notes: **Asymmetric unit contains one cation, one anion, one full occupancy dichloromethane, and a additional 40% occupancy CH_2Cl_2. Disorder was prevalent in some of the CF_3 moieties. In particular, the group based on C48, C49, C65 and C72 exhibited fluorine disorder over two positions in 60:40, 65:3, 55:45 and 65:35 ratios respectively. C-F and F-F distances were restrained, and only fractional fluorines with occupancies greater than 50% were refined anisotropically.**

There is evidence of some disorder also in the region of the partial occupancy solvent, which could not be readily modeled. However, C-Cl bond distance restraints were applied in this region in addition to restrainst on the ADPs.

Additional disorder is also very likely in the carbene – not least due to the proximity of fractional occupancy solvent. However, this could not be modeled in any credible way, despite strenuous efforts.